AGARD-CP-484

AGARD-CP-484

AGARD

ADVISORY GROUP FOR AEROSPACE RESEARCH & DEVELOPMENT
7 RUE ANCELLE 92200 NEUILLY SUR SEINE FRANCE

AGARD CONFERENCE PROCEEDINGS 484

Landing Gear Design Loads

(Les Charges de Dimensionnement
dans des Attérrisseurs)

NORTH ATLANTIC TREATY ORGANIZATION

AGARD-CP-484

AGARD

ADVISORY GROUP FOR AEROSPACE RESEARCH & DEVELOPMENT
7 RUE ANCELLE 92200 NEUILLY SUR SEINE FRANCE

AGARD Conference Proceedings 484

Landing Gear Design Loads

(Les Charges de Dimensionnement
dans des Atterrisseurs)

Papers presented at the 71st Meeting of the AGARD
Structures and Materials Panel, held in Povoa de Varzim, Portugal
on 8th to 12th October 1990.

North Atlantic Treaty Organization
Organisation du Traité de l'Atlantique Nord

The Mission of AGARD

According to its Charter, the mission of AGARD is to bring together the leading personalities of the NATO nations in the fields of science and technology relating to aerospace for the following purposes:

- Recommending effective ways for the member nations to use their research and development capabilities for the common benefit of the NATO community;
- Providing scientific and technical advice and assistance to the Military Committee in the field of aerospace research and development (with particular regard to its military application);
- Continuously stimulating advances in the aerospace sciences relevant to strengthening the common defence posture;
- Improving the co-operation among member nations in aerospace research and development;
- Exchange of scientific and technical information;
- Providing assistance to member nations for the purpose of increasing their scientific and technical potential;
- Rendering scientific and technical assistance, as requested, to other NATO bodies and to member nations in connection with research and development problems in the aerospace field.

The highest authority within AGARD is the National Delegates Board consisting of officially appointed senior representatives from each member nation. The mission of AGARD is carried out through the Panels which are composed of experts appointed by the National Delegates, the Consultant and Exchange Programme and the Aerospace Applications Studies Programme. The results of AGARD work are reported to the member nations and the NATO Authorities through the AGARD series of publications of which this is one.

Participation in AGARD activities is by invitation only and is normally limited to citizens of the NATO nations.

Published June 1991

ISBN 92-835-0611-1

Printed by Specialised Printing Services Limited
40 Chigwell Lane, Loughton, Essex IG10 3TZ

Preface

Experience has shown that landing gears are often neglected in the early design process of an aircraft because interest is focussed mainly on flight performance aspects. However, the operational utility of an aircraft is strongly influenced by the landing gear. This importance is not adequately reflected in the available specifications. In addition, operation from bomb-damaged and repaired runways is not reflected in landing gear design requirements.

AGARD SMP decided to organize a Specialists' Meeting on landing gear design loads to provide a forum for the exchange of experiences between the NATO nations with the aim of advancing landing gear design criteria and methods of landing gear analyses. The Meeting was to review existing design practices and specifications, consider the various methods used for load measurement and data analysis and formulate guidelines for future design procedures.

The Meeting was well attended in terms of both number and quality of participants and was followed by a general discussion. The summary of this discussion is given at the end of this book.

Préface

L'expérience a montré que les atterrisseurs sont souvent négligés dans la phase de définition préliminaire des avions, parce que l'intérêt se porte surtout sur les aspects de performances de vol. Cependant, l'utilité operationnelle d'un avion est fortement influencée par les spécifications opérationnelles des atterrisseurs. Cette importance n'est pas bien reflétée dans les règlements disponibles. De plus, il ne figure rien dans les règlements sur les opérations à partir de pistes endommagées par bombes et réparées.

Le Panel Structures et Matériaux de l'AGARD a décidé de tenir une réunion de spécialistes sur les charges de conception des atterrisseurs afin d'offrir un forum à l'échange d'expériences entre pays de l'OTAN dans le but de faire progresser les critères et les méthodes de calcul des atterrisseurs.

Ce Meeting devait passer en revue les méthodes de conception et règlements, examiner les différentes pratiques quant aux mesures de charges en service et formuler des recommandations sur les procédures futures de conception.

Ce Meeting a regroupé une assistance nombreuse et de qualité et a été suivi d'une discussion générale. La synthèse de cette discussion est donnée à la fin de ce recueil.

D.Chaumette
Chairman, Sub-Committee on
Landing Gear Design Loads

Structures and Materials Panel

Chairman: Mr Samuel L.Venneri
Director, Materials & Structures
Division (Code RM)
Office of Aeronautics & Space
Technology
NASA Hq
Washington DC 20546
United States

Deputy Chairman: Mr Roger Labourdette
Directeur Scientifique des
Structures
ONERA
29 ave de la Division Leclerc
92320 Chatillon
France

SUB-COMMITTEE ON LANDING GEAR DESIGN LOADS

Chairman: Mr Daniel Chaumette
Chef Adjoint Nouvelles Technologies
Avions Marcel Dassault/BA
78 Quai Marcel Dassault
92214 St-Cloud
France

Members

A.Dimarogonas	GR
R.Freymann	LU
E.Fuente	SP
V.Giavotto	IT
J.J.Glaser	CA
G.Grüninger	GE
J.J.Kacprzynski	CA
R.F.O'Connell	US
H.H.Ottens	NL
C.L.Petrin	US
A.Salvetti	IT
O.Sari	TU
O.Sensburg	GE
A.F.Tovar de Lemos	PO
A.P.Ward	UK

PANEL EXECUTIVE

Mr Murray C. McConnell (UK)

Mail from Europe:
AGARD—OTAN
Attn: SMP Executive
7, rue Ancelle
92200 Neuilly-sur-Seine
France

Mail from US and Canada:
AGARD—NATO
Attn: SMP Executive
APO New York 09777

Tel: 33 (1) 47 38 57 90 & 57 92
Telex: 610176F
Telefax: 33 (1) 47 38 57 99

Contents

FAILURE ANALYSIS CASE HISTORIES OF CANADIAN FORCES AIRCRAFT LANDING GEAR COMPONENTS

by

Major P. Beaudet
Directorate Aerospace Support Engineering
National Defence Headquarters
Ottawa, Ontario, Canada, K1A 0K2

and

Dr. M. Roth
Quality Engineering Test Establishment
Department of National Defence
Ottawa, Ontario, Canada, K1A 0K2

SUMMARY

Despite the extensive landing gear design analyses and tests carried out by the designers and manufacturers, and the large number of trouble-free landings accumulated by the users, the Canadian Forces, as well as others, have experienced a range of problems or failures with landing gear components. Different data banks were surveyed and over 200 case histories on more than 20 aircraft types were reviewed in order to assess trends in failure mechanisms and their causes.

Fatigue and corrosion were found to be the main mechanisms. Fatigue occurred mainly in steel components while corrosion occurred mainly with aluminium alloy components and wheels. Very few overload failures were noted. Different failure causes were identified. Design deficiencies and manufacturing defects led mainly to fatigue failures while poor material selection and improper field maintenance were the principal origins of corrosion related failures. Hence, a series of preventive measures was either recommended or re-emphasized. While fatigue can best be addressed by improving the quality of manufacturing and by better characterizing in-service and manufacturing stresses, much work remains to be done on the time-dependant degradation processes and their synergism with fatigue, as corrosion has often been neglected in both the design and testing stages as well as in the maintenance domain.

LIST OF ACRONYMS

AA:	Aluminium Association
A/C:	Aircraft
ACAIRS:	Aircraft Accident/Incident Reporting System
AISI:	American Iron and Steel Institute
Al:	Aluminium
AMMIS:	Aircraft Maintenance Management Information System
ASIP:	Aircraft Structural Integrity Program
CF:	Canadian Forces
ENSTAFF:	Environmental Standard for Fatigue Evaluation
FALSTAFF:	Fighter Aircraft Loading Standard for Fatigue Evaluation
HSS:	High Strength Steel
IVD:	Ion Vapour Deposition
MECSIP:	Mechanical Equipment and Sub-Systems Integrity Program
NDT:	Non-Destructive Testing
SCC:	Stress Corrosion Cracking
TURBISTAN:	Standardized Fatigue Test Loading Sequence for Tactical Aircraft Cold Section Engine Discs
UTS:	Ultimate Tensile Strength

1 INTRODUCTION

Landing gears are designed to provide aircraft support and control when on the ground (steering and stopping) and to provide a method of absorbing the loads and stresses associated with landing and taxiing. Since they are not used in flight, landing gear components have traditionally been designed to meet design limit loads using high strength-to-weight materials in order to carry out their functions with minimum weight and use of space. From a design viewpoint, landing gear service life is assumed to be principally limited by fatigue considerations, the time-dependent degradation of the materials being addressed only by means of prevention.

Despite the extensive landing gear design analyses and tests carried out by the designers and manufacturers, and the large number of trouble-free landings accumulated by the users, the Canadian Forces (CF), as well as others, have experienced a range of problems or failures with landing gear systems. This paper provides an overview of the structural component failures as experienced by the

CF within the last two decades on more than 20 different aircraft. Table 1 describes the fleet and provides information on the number of landings, which range from 200 to 1,200 per year per aircraft; this information is not recorded for helicopters.

A/C MODEL NUMBER	A/C NAME	TYPE	MAX WEIGHT AT LANDING (lbs)	NUMBER OF A/C	ENTERED/ OUT OF SERVICE	AVERAGE No OF LANDINGS PER YEAR/PER A/C
CC 109	COSMOPOLITAN	CARGO	53000	7	1967	665
CC 115	BUFFALO	CARGO	43100	14	1967	573
CC 117	FALCON	CARGO	-	7	1967-1989	-
CC 129	DAKOTA	CARGO	-	180	1963-1989	-
CC 130	HERCULES	CARGO	155000	28	1960	583
CC 137	BOEING 707	CARGO	247000	5	1970	831
CC 138	TWIN OTTER	CARGO	12100	7	1971	846
CC 144	CHALLENGER	CARGO	-	16	1983	-
CC 142	DASH 8	CARGO	-	8	1987	-
CF 101	VOODOO	FIGHTER	-	133	1961-1985	-
CF 104	STARFIGHTER	FIGHTER	-	238	1961-1989	-
CF 116	FREEDOM FIGHTER	FIGHTER	15500	87	1968	214
CF 188	CF-18 HORNET	FIGHTER	51900	132	1983	197
CH 113	LABRADOR	HELICOPTER	-	14	1963	-
CH 118	IROQUOIS	HELICOPTER	-	9	1967	-
CH 124	SEA KING	HELICOPTER	-	34	1963	-
CH 135	TWIN HUEY	HELICOPTER	-	45	1971	-
CH 136	KIOWA	HELICOPTER	-	65	1971	-
CH 139	RANGER	HELICOPTER	-	16	1981	-
CH 147	CHINOOK	HELICOPTER	-	7	1975	-
CP 107	ARGUS	PATROL	-	45	1958-1981	-
CP 121	TRACKER	PATROL	-	29	1956-1990	-
[illegible]	[illegible]	[illegible]	[illegible]	18	90	[illegible]
CT 114	TUTOR	TRAINER	83000	191	1963	814
CT 133	SILVERSTAR	TRAINER	12200	63	1981	236
CT 134A	MUSKETEER II	TRAINER	2650	20	1982	1192

Table 1 - CF Aircraft Data

Following a brief review of landing gear design principles and material selection, the results of a variety of data bank surveys performed in order to assess trends in failure mechanisms and their causes will be reviewed and illustrated by a number of failure case histories. The findings will be analyzed in terms of current design concepts and maintenance practices to provide guidelines so that preventive or corrective measures can be developed and implemented during the life cycle management of the components and also provide guidance for future designs.

2 DESIGN CONSIDERATIONS

As mentioned, landing gears are designed to provide a method of absorbing the loads associated with landing and taxiing and to provide support and control of the aircraft on the ground for its life. In addition to their specific design requirements, landing gears create other challenges for their integration in the airframe: they necessitate openings in stressed components (e.g. skins) and strong attachment points in fracture critical parts of the structure (e.g. frames, longerons,...).

In order to absorb the landing loads, the landing gears are usually designed so that they can sustain specified sink speeds at landplane landing weight and at maximum landing weight without structural damage; typical values have been 3.05 and 1.83 meters/second (10 and 6 feet/second) respectively [1]. Once the airworthiness requirements for impact resistance have been demonstrated through drop testing, static strength tests are carried out to show that strength margins exist for all critical design cases. The safe-life design analyses are then validated by full scale fatigue tests simulating the loads associated with landing and taxiing. These tests, which are not standardized, may take a few years to be completed to take into account the large safety margin which is part of this design approach; often they are still in progress when aircraft production starts. In practice, the life of landing gear components is controlled by fatigue as well as corrosion. Both degradation mechanisms are being considered separately, the former through durability analysis and testing, and the latter by means of its prevention through the use of protective coatings and appropriate maintenance [2, 3].

Landing gears use valuable space and cause a severe weight penalty, making up approximately 3% of the total weight for transport aircraft and as much as 20% for those which are carrier based. Therefore, landing gears are usually designed to meet design limit loads using materials with high specific strengths. High

strength aluminium alloys and steels have most commonly been selected, with magnesium and titanium alloys used for special applications only. The requirements for high strength led to the widespread use of aluminium alloys from the 7xxx series heat treated to the peak strength T6 temper for structural components and 2014-T6 for wheels. A variety of high strength low alloy steels which could easily be heat treated to strength levels in excess of 1400 MPa (200 ksi) and up to 1930 MPa (280 ksi), were selected. AISI 4340 has been commonly specified and 300M selected more recently.

The current trend is to take a more balanced view in material selection considering, in addition to high strength, improved fracture toughness and corrosion/stress corrosion cracking (SCC) resistance. The fracture toughness requirements are becoming more stringent. The US Navy now requires that landing gear steels have a fracture toughness in excess of 110 MPa$\sqrt{m}$ (101 ksi$\sqrt{in}$) [4]. On the other hand, the SCC problems are being addressed by selecting the overaged T73 temper for the newer 7xxx aluminium alloys, by better characterizing materials with respect to their service environments and by using improved protective coatings.

3 SURVEY OF CANADIAN FORCES LANDING GEAR FAILURES

The CF have experienced many landing gear structural failures. Only by a proper understanding of the failure mechanisms and their causes can appropriate corrective action be taken. In order to obtain statistical and detailed information on landing gear failures, the following data banks were surveyed:

a. AMMIS: The Aircraft Maintenance Management Information System records all in-service maintenance actions per system, sub-system and individual components for all aircraft. It was surveyed to provide data on landing gear failures during the last five years for cargo, fighter and trainer aircraft.
b. ACAIRS: The Aircraft Accident/Incident Reporting System records all flight safety related accidents/incidents. It was surveyed to provide data on landing gear failures during the last 10 years per aircraft type (cargo, fighter, patrol, trainer and helicopter).
c. Failure Analysis Reports: The more than 200 landing gear failures on all aircraft investigated by the Quality Engineering Test Establishment over the last 25 years were reviewed. These reports were the only source of detailed information about mechanisms and causes.

3.1 Maintenance Reporting System - AMMIS

Only limited use of this system could be made because it provided general information without indication of cause or mechanism of failures, except that corrosion and cracking were used as generic terms to describe a failure.

The distribution of aircraft system failures (Fig. 1) and the distribution of those that resulted in a flight safety accident/incident (Fig. 2) indicated that landing gears are generally the second most important area of failure after engines. Furthermore, it appeared that there was more chance that a failure in landing gear systems resulted in a flight safety accident/incident, thereby indicating their criticality. No overload failures were reported for any of the hard landings recorded.

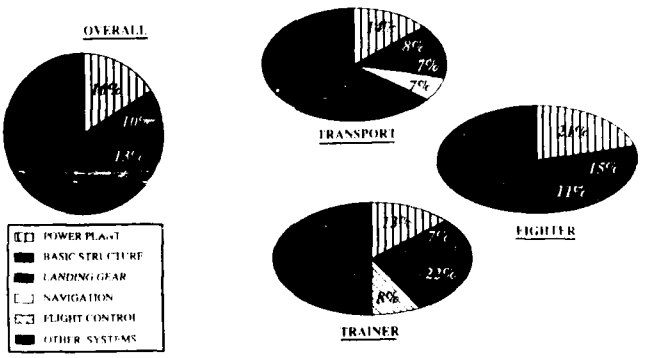

Fig. 1. Distribution of system failures by aircraft type.

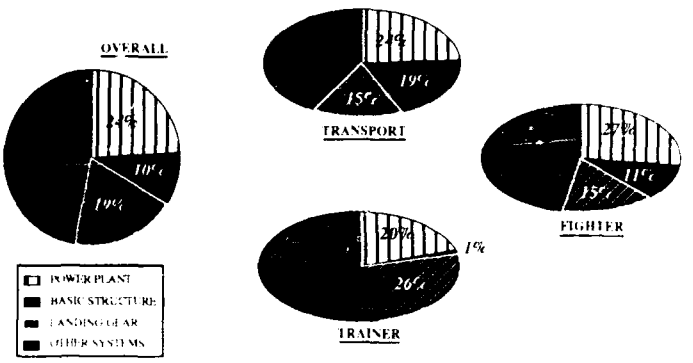

Fig. 2. Distribution of system failures resulting in a flight accident/incident by aircraft type.

3.2 Flight Safety Incident Report System - ACAIRS

This data bank was more precise than AMMIS because the description of the failures permitted identification of their causes in a number of cases, but there were no indications as to the failure mechanisms.

The distribution of landing gear structural component failures resulting in a flight safety accident/incident per aircraft type indicated that helicopters, followed by fighter and cargo (or transport) aircraft had the largest number of failures even though they did not necessarily represent the largest proportion of landings (Fig. 3). In order to normalize the results, the number of failures per million landings was calculated for each aircraft type and displayed in Fig. 4. Trainer aircraft showed the smallest figure although they sustain a larger number of hard landings due to pilot inexperience.

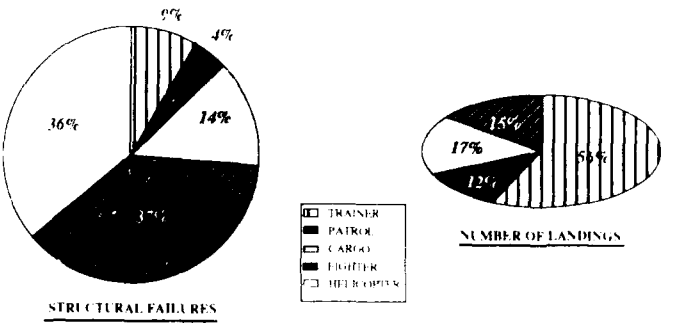

Fig. 3. Proportion of landing gear structural failures by aircraft type.

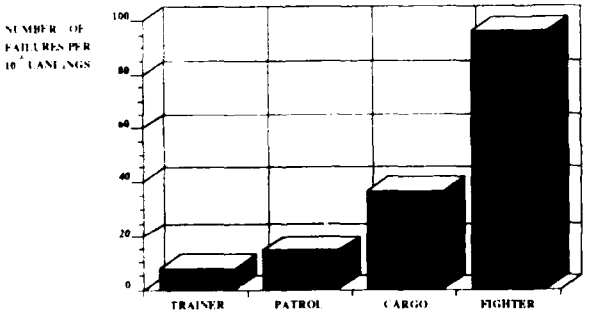

Fig. 4. Number of landing gear structural failures resulting in a flight safety accident/incident per million landings by aircraft type.

The distribution of structure related accident/incident causes per million landings for each aircraft type (Fig. 5) showed that, although many of the incidents could not be attributed to any particular cause due to the lack of information, some general observations could be made. Maintenance related failures were relatively important for each category of aircraft; accidents/incidents resulting from abnormal landings occurred mainly on patrol and fighter aircraft; and accidents/incidents resulting from towing operations were more important on trainer aircraft.

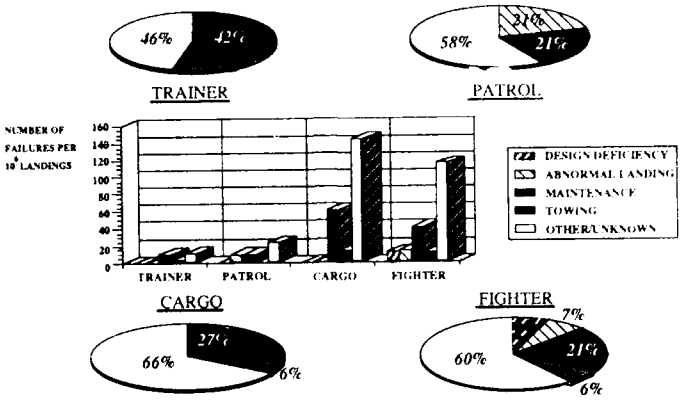

Fig. 5. Distribution of structure related accident/incident causes per million landings for each aircraft type.

3.3 Failure Analysis Reports

The results of the review and statistical analysis of more than 200 failures investigated by Quality Engineering Test Establishment will be presented in this section following the description of typical landing gear failure case histories.

3.3.1 Main landing gear cylinder of a fighter aircraft

Following a landing, the main landing gear shock strut was found deflated and fractured from top to bottom (Fig. 6a). This was the first and most dramatic manifestation of a subsequently widespread problem. The strut housings were forged from aluminium alloy 7079, heat treated to the T6 temper, shot peened and sulphuric acid anodized.

The fracture surface was flat, normal to the cylinder wall and coincided with the forging flash line. The failure of the part resulted from the presence of a nearly semicircular stress corrosion crack about 12 mm (0.5 in) in radius and centred in the eye-bolt bore surface (Fig. 6b). Its surface was only slightly damaged and did not show signs of corrosion pitting. Service loads were transmitted from the eye-bolt to the strut through press fit beryllium copper bushings which had been lubricated by a molybdenum disulphide type of grease.

The SCC failures occurred in parts made from a material now well known for its severe susceptibility to SCC. In this particular case, contributing factors were exposure of the end grains in the hole and possibly a galvanic couple between the aluminium forging and the beryllium copper bushings in the presence of an electrolyte formed by the grease contaminated with water. New parts were manufactured using aluminium alloy 7049 and heat treated to the T73 temper showing improved SCC resistance. The bushings are now cadmium plated on their outer surfaces and a multipurpose grease is used.

3.3.2 Main landing gear axle of a transport aircraft

During a training flight landing, one of the axles of the main landing gear of a light transport aircraft fractured in a complex helical manner around the lock pin hole at the bottom centre of the axle (Figs 7a and b). The 0.755 m long axle was made from AISI H11 tool steel tube and heat treated to an ultimate tensile strength (UTS) in the 1650-1790 MPa (240-260 ksi) range except for the ends which were in the 1240-1380 MPa (180-200 ksi) range. The outside surface was chromium plated to a thickness of 0.05 to 0.075 mm (0.002 to 0.003 in) and the lock pin hole flash chromium plated to a thickness of 0.0075 to 0.0125 mm

(0.0003 to 0.0005 in). The inside surface was coated with a corrosion preventive compound to MIL-C-16173 Grade 1 specification.

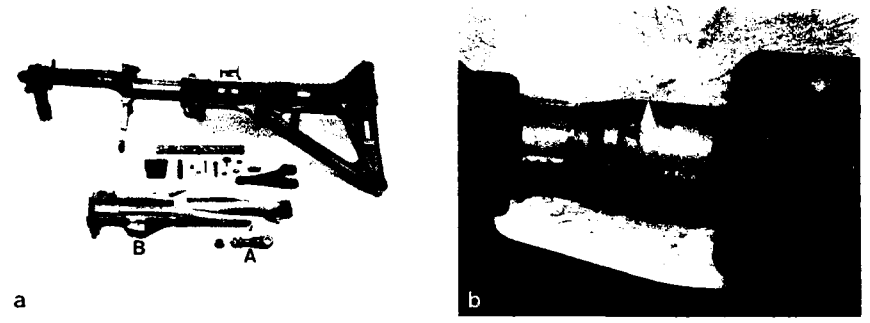

Fig. 6. a: Failed shock strut assembly: (A) indicates the eye-bolt with beryllium copper bushing and (B) the eye-bolt region on the strut housing.
b: The dotted line indicates the extent of the stress corrosion crack at the origin of the failure.

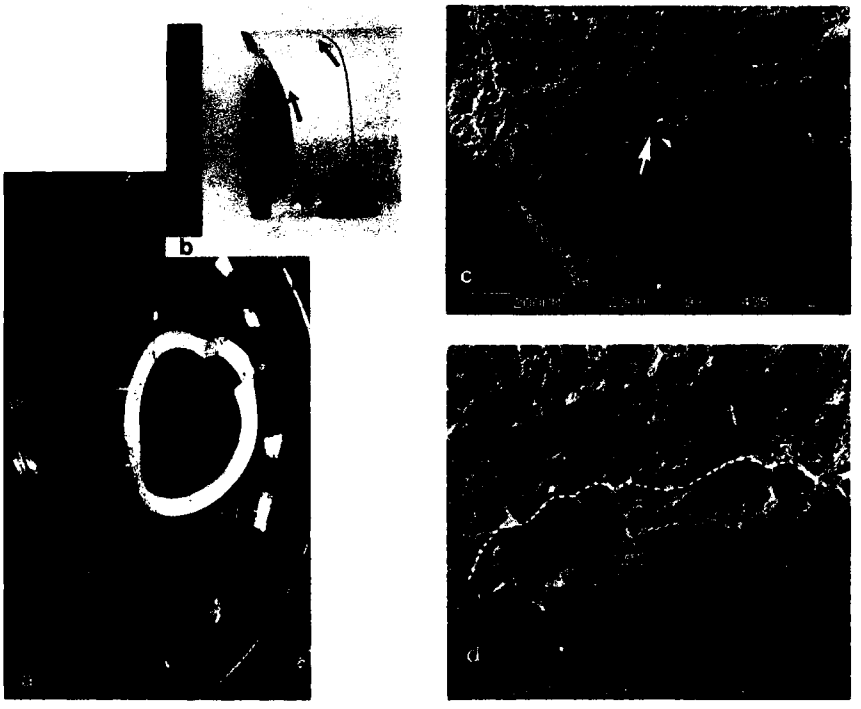

Fig. 7. a: Fractured axle half attached to one of the wheels.
b: Matching half, fracture started at the lock pin hole and propagated as indicated by the arrows.
c: Fracture surface in the vicinity of a corrosion pit in the lock pin hole, the arrow points to the location of the fatigue crack shown below (x40).
d: The dotted line outlines the extent of the fatigue crack (x 150).

Detailed examination of the broken axle revealed that the final fracture process had originated at a very small fatigue crack, 0.5 mm (0.020 in) long by 0.1 mm (0.004 in) deep spanning about half the width of a small and relatively shallow corrosion pit (Figs 7c and d). Other pits were present around the hole and they likely resulted from the ingress and accumulation of moisture at the axle locating hole and pin joint.

Fracture mechanics modelling showed that, because of the high operational stresses and poor damage tolerance properties of H11 steel with a mean room temperature fracture toughness around 37 MPa$\sqrt{m}$ (34 ksi$\sqrt{in}$) at the part strength level, very small crack-like discontinuities including corrosion pits, that cannot be reliably inspected, could cause catastrophic failure of the axle during normal operation. The criticality of these crack-like discontinuities is further aggravated by cold temperatures: a 10% reduction in room temperature toughness is expected at 40°F (5°C) and a 25% reduction at -40°F (-40°C) [5].

Replacement parts are being designed to provide larger margins of safety under ultimate and limit load conditions and infinite fatigue life using 300M steel heat treated to a UTS in the 1860-2070 MPa (270-300 ksi) range; the corresponding mean room temperature fracture toughness, 60 MPa$\sqrt{m}$ (55 ksi$\sqrt{in}$), would be slightly higher than that of the original material. Proper maintenance is imperative with this material to avoid situations where corrosion or SCC could occur. This will be discussed later in more detail.

3.3.3 Axle, crank lever and other components of fighter aircraft main landing gear

A main landing gear axle of a fighter aircraft failed catastrophically upon landing when the hub locating the axle in the hydraulic tube fractured circumferentially (Figs 8a and b). This failure damaged the aircraft but could have been more serious as it occurred on formation landing and the lead aircraft ditched off the runway following the failure. The axle assembly was made from 300M steel heat treated to a UTS in the 1800-1930 MPa (260-280 ksi) range. The part was shot peened. The outer contact surfaces were chromium plated, while the non-contact ones were coated with ion vapour deposited (IVD) aluminium. The inside of the hub, which had a polygon shape to accommodate a crank lever, was coated with electroless nickel.

The failure sequence was established. Flaking and cracking damage to the electroless nickel by the crank lever led to corrosion pitting of the exposed steel (Fig. 8c). A stress corrosion crack initiated at one of the pits and grew radially and longitudinally in the hub (Fig. 8c). When the crack had reached the critical size, 13 mm (0.5 in) long by 6 mm (0.25 in) deep, fast rupture occurred until the longitudinal crack stopped due to reduced stresses. Cracking resumed intergranularly, likely again by SCC, but mainly in a circumferential direction because of the different orientation of the principal tensile stress there, leading to catastrophic failure when it had reached a critical length of about 40 mm (1.57 in).

The crank lever of a similar aircraft was found with a 75 mm (2.95 in) long crack (Fig. 9). This part was also made from 300M steel, heat treated to a UTS in the 1930-2000 MPa (280-290 ksi) range and shot peened. The bearing surfaces were chromium plated and the non-bearing surfaces were IVD aluminium coated. A stress corrosion crack had initiated at one of many small corrosion pits in the radius where most of the IVD aluminium had disappeared from corrosion or occasional poor adhesion had left the steel unprotected (Fig. 9).

Many of the other landing gear components suffered from minor corrosion, usually in the form of degradation of the IVD aluminium coating, to more severe corrosion such as in the shock pins made from 300M steel with a UTS in the 1930-2070 MPa (280-300 ksi) range. The steel had started to corrode in areas where the chromium plating had cracked, likely from impact loads, and flaked away (Fig. 10). To prevent this type of damage and failure by SCC which was reported by another user, the shock pin was redesigned using a precipitation hardening PH 13-8 Mo stainless steel in the H1000 condition with a UTS around 1480 MPa (215 ksi), thus accepting a weight penalty.

These failures were promoted by a number of factors: poor seal design between the axle and the lever assembly which did not prevent water ingress, lack of sufficient lubrication points, and inherent low resistance to SCC of 300M steel in aqueous environments. The water/soap solution used under high pressure to wash the aircraft could also have contributed to corrosion by removing lubricant or filtering into sealed assemblies.

The main corrective steps taken have been to minimize water ingress by improving the seals, to use gentler washing procedures, to install lubrication points for periodic filling of the hub cavity with grease and to redesign parts.

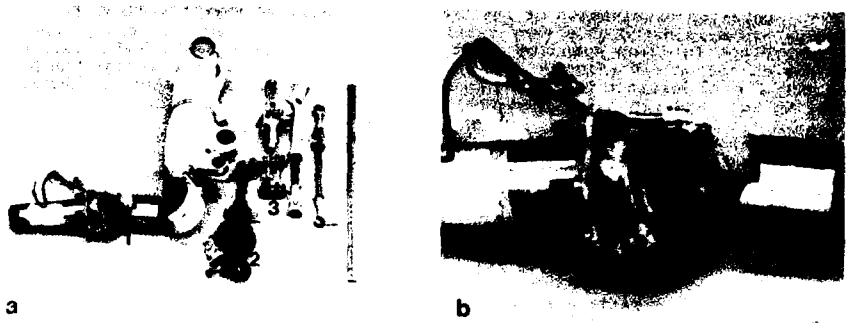

Fig. 8. a: Main landing gear components, broken axle (1) crank lever (2) and shock pin (3).
b: Details of the axle showing the longitudinal crack in the hub and the circumferential fracture.
c: Inside of the hub showing flaking (1) and damage (2) to the electroless nickel coating and corrosion pitting (3) at the origin of longitudinal/ radial stress corrosion crack (dotted line).

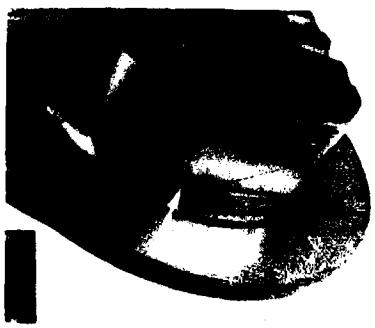

Fig. 9. The 75 mm (2.95 in) long stress corrosion crack in the lever initiated at a corrosion pit (arrow) in an area where the IVD aluminium coating had disappeared.

Fig. 10. Damage to the shock pin chromium plating and corrosion of the exposed steel.

3.3.4 Main landing gear truck beam of a large transport aircraft

A main landing gear truck beam from a large transport aircraft fractured on the ground just after refuelling as a result of circumferential crack located about 0.14 m (5.5 in) forward of the oleo attachment point (Fig. 11a). The part was made from 4340 steel heat treated to a UTS in the 1800-1930 MPa (260-280 ksi) range. The part had been treated with a manganese phosphate, primed and painted on both inner and outer surfaces. No sacrificial coating, such as cadmium, had been applied to minimize the occurrence of hydrogen embrittlement. A corrosion preventive compound (MIL-C-16173 Grade 1) was also applied to newly manufactured parts for additional protection.

Visual and microscopic examination of the fracture surface revealed that final failure had emanated from a small, nearly semicircular shaped area (12 mm long by 8 mm deep) (0.47 by 0.31 in) with intergranular features, most likely a manifestation of SCC (Figs 11b and c). The transition from intergranular to overload was abrupt. The stress corrosion crack had initiated at a corrosion pit which, at the time of failure, was quite broad but shallow (10 mm by 6 mm by 0.3 mm deep) (0.39 by 0.24 by 0.01 in) (Fig. 11c). Extensive corrosion in the form of shallow pits was observed in the forward portion of the beam in the vicinity of the fracture and particularly in an area at the inside top of the beam (Fig. 11b).

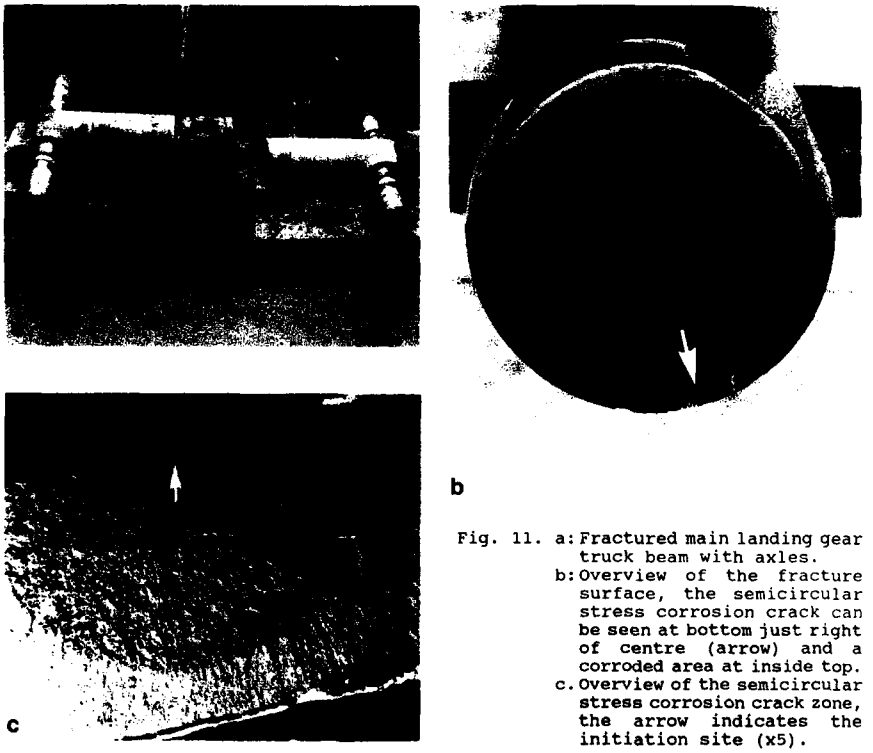

Fig. 11. a: Fractured main landing gear truck beam with axles.
b: Overview of the fracture surface, the semicircular stress corrosion crack can be seen at bottom just right of centre (arrow) and a corroded area at inside top.
c. Overview of the semicircular stress corrosion crack zone, the arrow indicates the initiation site (x5).

A fracture mechanics analysis of the failure was carried out. It confirmed that the actual stress corrosion crack corresponded to the theoretical critical crack size for the situation and that the stress intensity ahead of the corrosion pit, assuming that it behaved as a crack, corresponded to the K_{Iscc} value given in the literature: 20 MPa$\sqrt{m}$ (18 ksi$\sqrt{in}$). It also established that the critical crack size, assuming "worst case" design conditions (ground turn flat) would be about 3.2 mm (0.13 in) long by 1.6 mm (0.06 in) deep and located 90° from the bottom of the beam. However it is less likely that a stress corrosion crack would grow in that location. Limited data on stress corrosion crack growth for 4340 steel suggested that crack growth from a crack the depth of the corrosion pit could have occurred quite rapidly under full load conditions. These factors indicate that the part was not designed for damage tolerance.

To prevent a recurrence, the emphasis should therefore be placed on preventing or detecting and repairing any breaks in the protective coating. The manufacturer has addressed the widespread corrosion problem by recommending the reapplication of corrosion inhibitors at least annually or as part of the wash cycle. In this particular case, this measure had not yet been implemented and the aft of the beam was sealed by an "uncalled for" plug which prevented drainage and drying out of the inside of the beam. Also, since the phenomena of corrosion and SCC are not dependent on flying time, this criterion should not be used as the basis for inspection or maintenance intervals.

3.3.5 Nose-landing gear cylinder of a large transport aircraft

The nose-landing gear outer cylinder of a large transport aircraft failed catastrophically while landing (Fig. 12a). The part was machined from a 7079 aluminium alloy forging and heat treated to the T6 temper. It was shot peened and anodized. At a later stage, an interference fit steel sleeve was installed to line the inside of the bore.

The fracture at the top of the cylinder bore could visually be determined to have originated at a narrow fatigue band (2.5 mm (0.10 in) maximum depth by 70° arc) which had initiated at the inside radius at the top of the bore and was centered on the forward side. The fatigue zone consisted of a 2 mm (0.08 in) deep fatigue band followed by a narrow region of rapid crack extension and a very narrow fatigue band (Fig. 12b). The cylinder also contained a longitudinal crack through its wall 0.65 m (25.6 in) long from the bottom. That crack had propagated from a 35 mm (1.38 in) long elliptically shaped stress corrosion crack (Fig. 12c) which, along with some smaller ones, had initiated at the interface between the 7079 alloy and a flame sprayed aluminium-silicon coating which exhibited poor adhesion in some areas. The stress corrosion crack was about 40° away from the forging flash line.

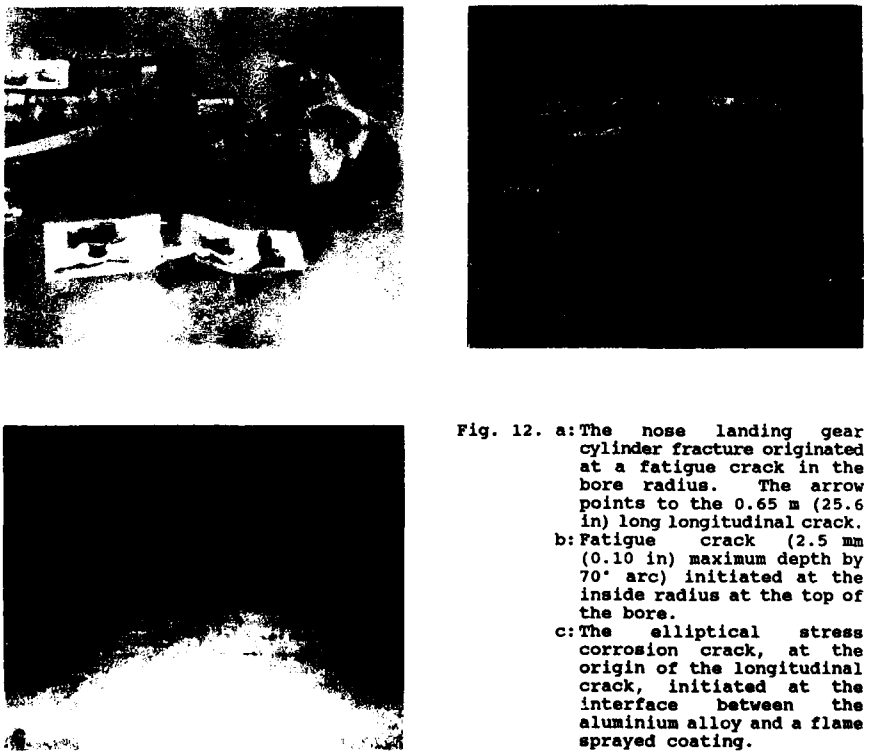

Fig. 12. a: The nose landing gear cylinder fracture originated at a fatigue crack in the bore radius. The arrow points to the 0.65 m (25.6 in) long longitudinal crack.
b: Fatigue crack (2.5 mm (0.10 in) maximum depth by 70° arc) initiated at the inside radius at the top of the bore.
c: The elliptical stress corrosion crack, at the origin of the longitudinal crack, initiated at the interface between the aluminium alloy and a flame sprayed coating.

Similar problems had been reported by the part manufacturer which attributed fatigue cracking to a too sharp radius at the top of the bore. In the present case the radius exceeded the minimum allowable dimensions required. Because evidence of SCC was found by non-destructive testing on all other cylinders in service, they were replaced with new ones made of 7049-T73 aluminium alloy. Changing the material will improve the SCC resistance properties significantly but not the fatigue properties to the same degree. In this respect, not much will be gained unless stress corrosion crack contributed significantly to the fatigue cracking.

3.3.6 Nose landing gear cylinder of a light transport aircraft

The trunnion area of the nose landing gear cylinder of a light transport aircraft fractured in a number of cases due to shimmying. In another instance, a long crack was observed in the trunnion area (Fig. 13a). The cylinder was made from 2014 aluminium alloy and heat treated to the T6 temper.

The 0.34 m (13.4 in) long crack had emanated from a small fatigue crack 32 mm (1.26 in) long by 2 mm (0.08 in) deep located in the trunnion radius (Fig. 13b). There was some evidence of fretting which could have facilitated fatigue initiation. Liquid penetrant inspection revealed an additional small crack diametrically opposite to the other one indicating reversed bending conditions on the trunnion where an assembly arm, linking the end of the steering actuator and the upper torque arm, fitted. The analysis of the failure showed that the crack size was critical for normal operating condition loads and that the trunnion area was underdesigned to carry the actuator limit load without local yielding. There were also some doubts that the ultimate design load was in fact the worst load case.

Modification to the actuator and redesign of the trunnion area by adding a reinforcement to the assembly arm to distribute the loads around the main cylinder eliminated further cracking and shimmying occurrences.

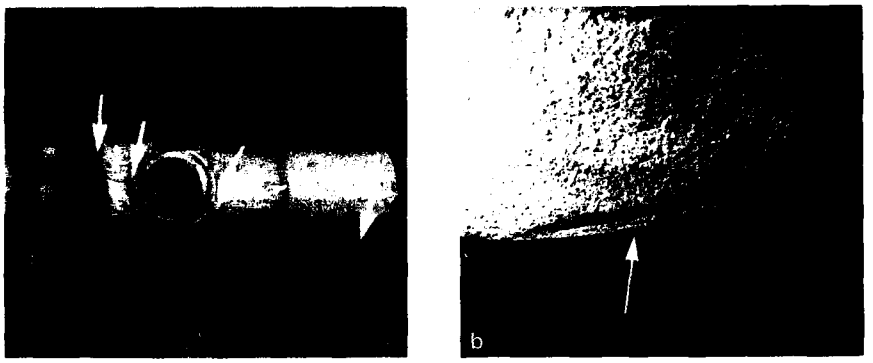

Fig. 13. a: The 0.34 m (13.4 in) long crack emanated from a fatigue crack in the trunnion radius.
b: 32 mm (1.26 in) long and 2 mm (0.08 in) deep critical fatigue crack.

3.3.7 Wheels

Over the years, a large number of wheels on all aircraft types have been found cracked and a few have failed catastrophically (Fig. 14a). The cracks have been discovered as a result of deflated tires and by NDT inspection. These failures occurred after a few years in service for some and much longer for others. Some of these wheels were made from magnesium alloys; all the others were forged from 2014 aluminium alloy, heat treated to the T6 temper, sulphuric acid anodized, and painted.

Many of these failures could be traced to corrosion pitting on the weather side of the wheels. Some of the pitting was promoted by fretting from parts such as heat shields which damaged the protective coatings. These pits, sometimes as small as 0.2 mm (0.008 in), were followed by intergranular cracking and then by fatigue (Fig. 14b to d). A number of other fatigue failures initiated on the inside, mainly in the tire bead seat area, again at pits although corrosion was less severe. In a few cases, manufacturing defects such as forging laps in the aluminium alloy wheels and porosity in the cast magnesium alloy wheels were at the origin of fatigue cracking.

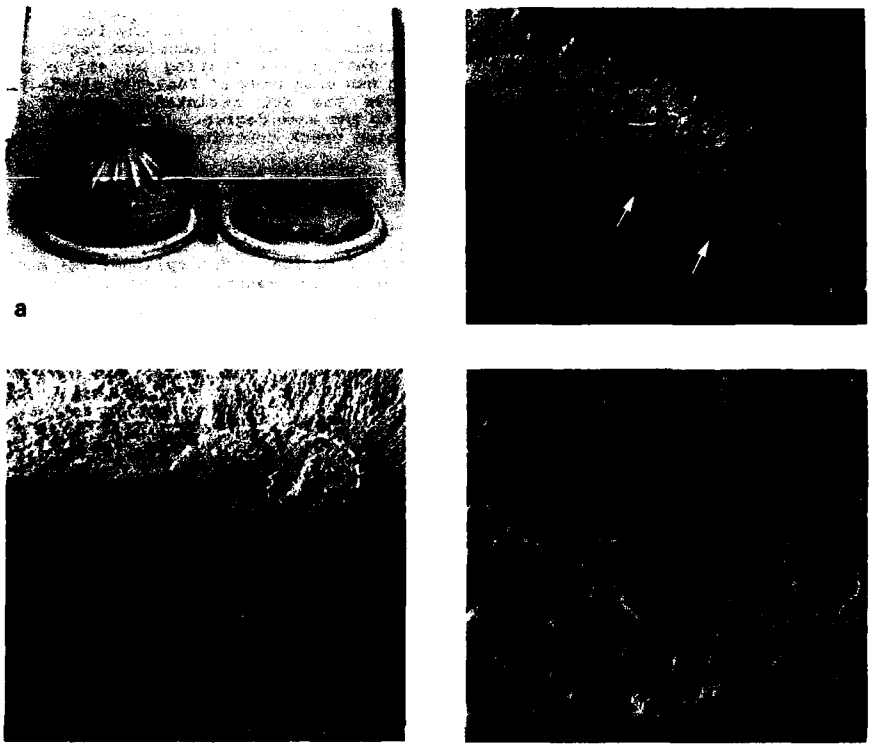

Fig. 14. a: Catastrophic wheel failure from a 0.14 m (5.5 in) long fatigue crack which had initiated on the weather side.
b: The arrows point to corrosion pits at the origin of a fatigue crack (x5).
c: Pitting followed by intergranular cracking, the dotted line marking its extent, and then fatigue (x40).
d. Transition from intergranular to fatigue cracking (x650).

Often wheels are lifed at the design stage in terms of roll distances. In practice, at least within the CF, wheels are not considered lifed, but rather are kept in service as long as possible and inspected periodically. In such a situation, proper maintenance to assure the integrity of the protective coatings, to remove corrosion and to reprotect the part becomes very important.

Cracking of a forged 2014-T6 aluminium alloy main landing gear wheel of a patrol aircraft has been a recurring problem. Fatigue cracking initiated all around the wheel hub bearing radius and propagated inwards (Fig. 15a to c). Both the design of the wheels and their maintenance contributed to these failures. Improper axle nut torquing procedures induced higher stresses than those for which the hub was designed, resulting in premature failure. Even when properly installed, the life of the wheels was short because the service loads were quite different than those used for the design. These wheels ended up being redesigned using a more realistic service roll spectrum and strengthened in the critical area.

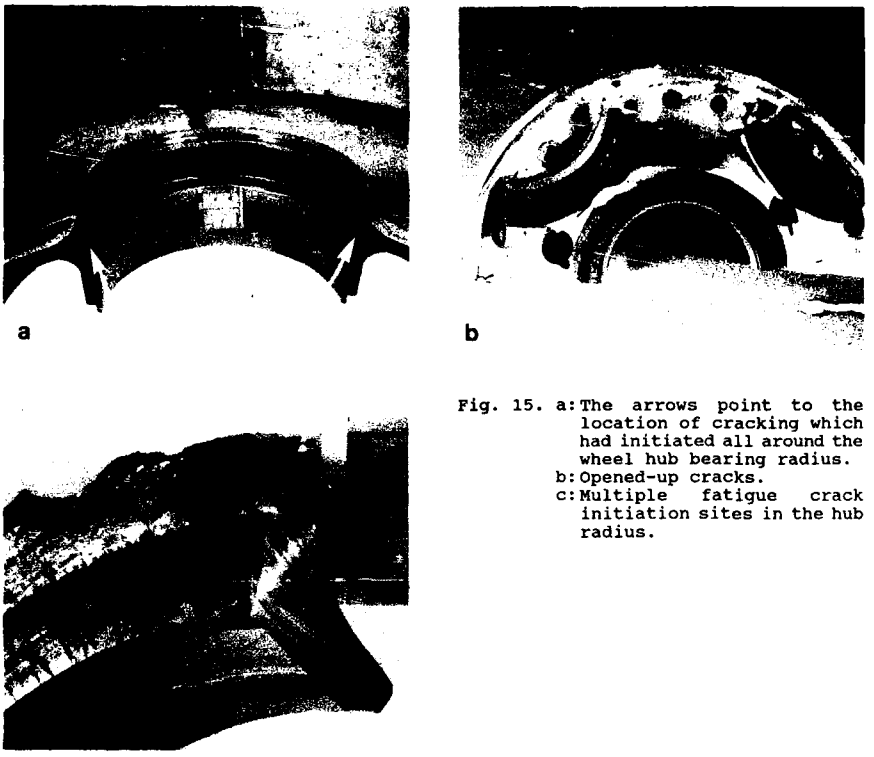

Fig. 15. a: The arrows point to the location of cracking which had initiated all around the wheel hub bearing radius.
b: Opened-up cracks.
c: Multiple fatigue crack initiation sites in the hub radius.

3.3.8 Statistical Analysis

The failure mechanisms used in this analysis were defined as one or a combination of the following:

a. overload
b. fatigue
c. pitting
d. stress corrosion cracking (including hydrogen embrittlement)
e. wear (including fretting)
f. false call, either an indication of a defect when in reality there was none, or an indication of a defect that could be tolerated and was usually inherent in the manufacturing process such as porosity in a casting, or flash line in a forging.

The following categories were used to classify the failure causes:

a. Design: obvious design deficiency (e.g. sharp corner), wrong assumption in the analysis (e.g. loads)
b. Material selection: an alloy which displayed a deficiency in one of its properties and should not have been used for such applications
c. Manufacturing: defects incurred during the process such as inclusions, forging laps, improper heat treatment, quench cracks, machining marks, grinding cracks, poor coatings, or hydrogen embrittlement
d. Field maintenance: inadequacies in the field such as shop malpractice, or procedures which were not followed
e. Maintenance directives: lack of proper instructions leading to a failure (e.g. corrosion preventive measures which were not addressed)
f. Abnormal landing.

About 10% of all components investigated were in the false call category mainly because of forging laps and porosity in castings. Those remaining were equally split between those which were found damaged or cracked and those which failed catastrophically. The distribution of these components by material types showed that slightly more than 50% were made of aluminium alloys, mainly 201x and 7xxx series alloys, but also 2024, 356.0 and 295.0. About 40% were made of steels, 4340 and 300M being the most common, the other high strength steel (HSS) being 4130, 8630, 8740, 9620, H11. The remaining were magnesium alloys (Fig. 16).

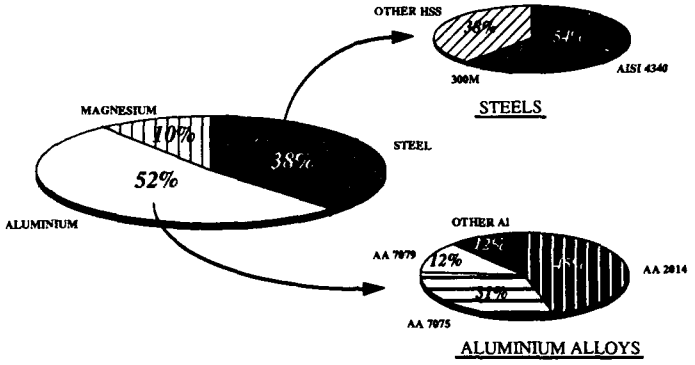

Fig. 16. Distribution of landing gear materials investigated.

The distribution of the mechanisms at the origin of the failures indicated that fatigue (42%) and corrosion (35%) were the most significant of the cases (Fig. 17). Within corrosion, pitting or pitting as the precursor to other failure mechanisms was a major source of problems. Comparing wheels and the other structural components, corrosion, mainly in the form of pitting, predominated in wheels, while fatigue was more prominent in the other structural components (Fig. 18).

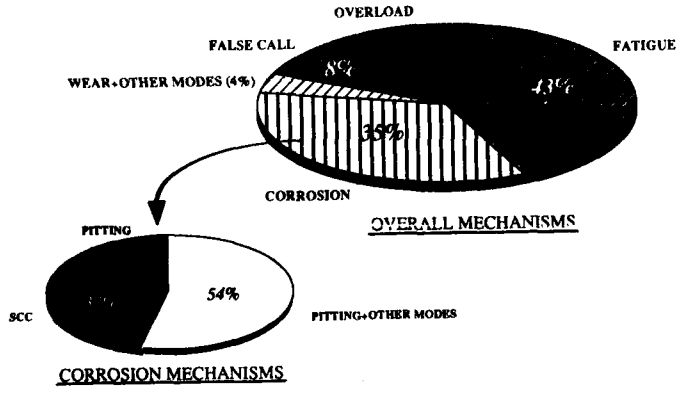

Fig. 17. Failure mechanism distribution.

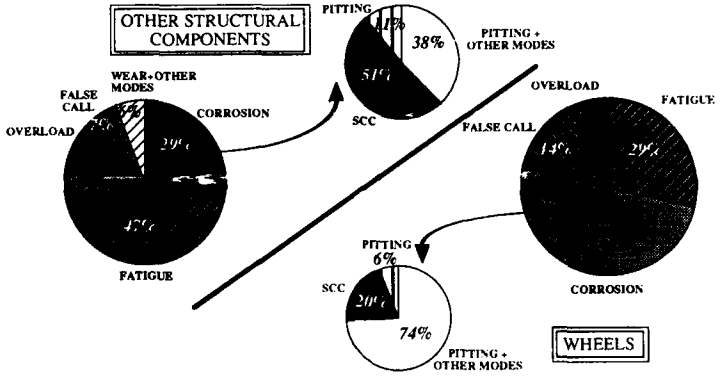

Fig. 18. Failure mechanism distribution for wheels and other structural components.

The distribution of failure mechanisms for steels, aluminium and magnesium alloys in general and for each statistically significant alloy type (Figs 19 to 21) indicated that:

a. Fatigue was the most important failure mechanism for all steels. However, for 300M, SCC and corrosion, often initiated by wear damage to coatings, were particularly significant
b. Corrosion was the most important failure mechanism for all aluminium alloys, pitting being relatively important for 2014 and SCC being the main failure mechanism for 7079-T6. Fatigue was also an important failure mechanism, especially in 7075
c. Corrosion and fatigue were equally important failure mechanisms in the magnesium alloys investigated; the large number of false calls resulted from porosity in cast wheels

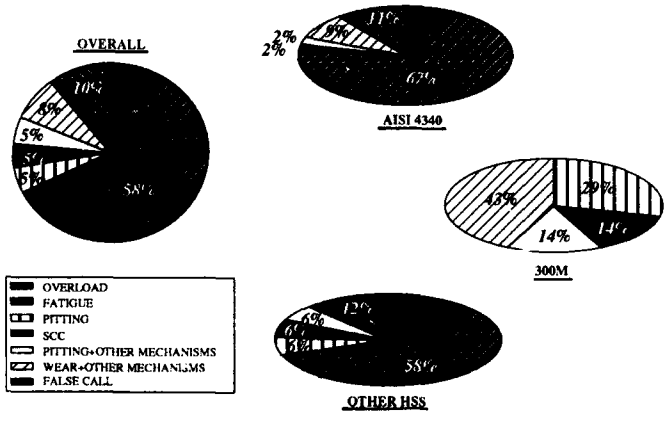

Fig. 19. Failure mechanism distribution for steel components by alloy type.

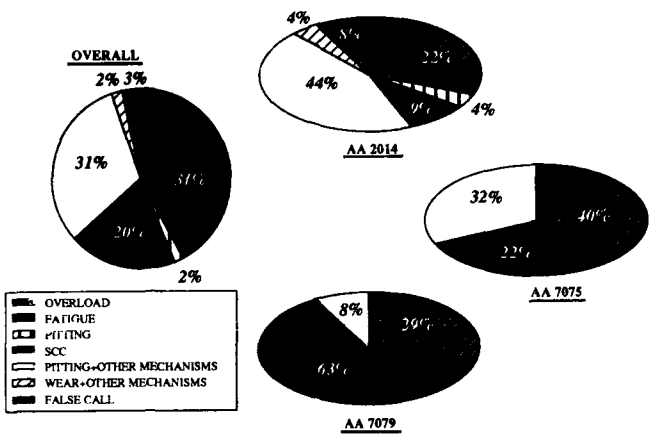

Fig. 20. Failure distribution for aluminium components by alloy type.

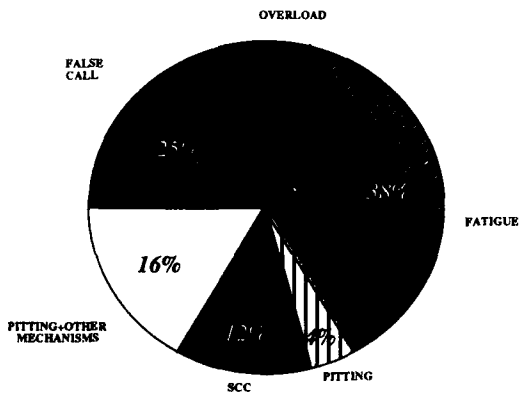

Fig. 21. Failure mechanism distribution for magnesium components.

The distribution of the causes of the failures indicated that they were attributed to manufacturing defects or problems in 30% of the cases (Fig. 22). Other causes such as design deficiencies, material selection and maintenance practices were also important for both wheels and the other structural components. Abnormal landings and improper directives for maintenance practices contributed only a small percentage.

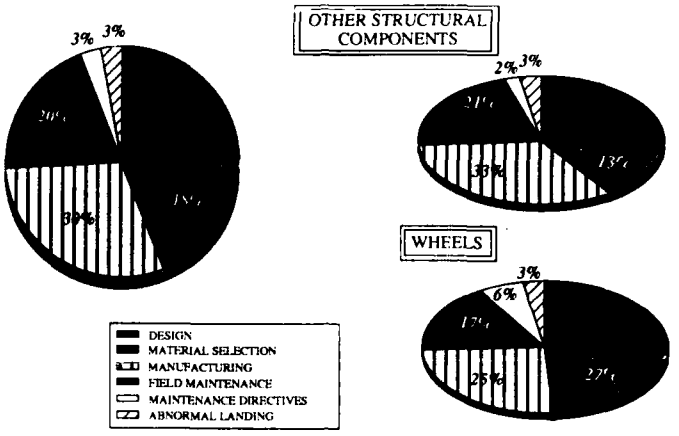

Fig. 22. Failure cause distribution.

The distribution of failure causes for steels, aluminium and magnesium alloys in general and for each statistically significant alloy type (Figs 23 to 25) indicated that:

a. Manufacturing defects were the most important failure cause for all steels in general. This figure also applies to 300M where poor performance and adhesion of coatings which were at the origin of many failures, were also considered to be a manufacturing problem. Field maintenance practices appear to be a very significant cause for the other high strength steels
b. Design deficiencies and field maintenance practices were the most significant failure causes for aluminium alloys in general, as well as for 2014 and 7075 alloys in particular, but not for the 7079 alloy where poor alloy selection was considered to be the prime cause
c. Material selection and manufacturing defects were the most important failure causes for the magnesium alloys

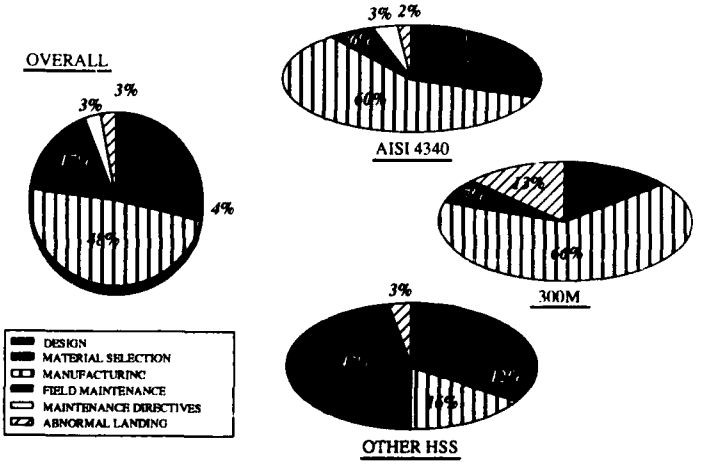

Fig. 23. Failure cause distribution for steel components by alloy type.

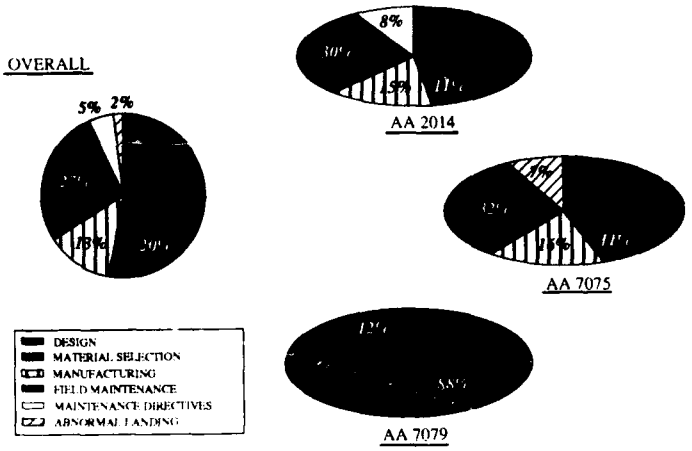

Fig. 24. Failure cause distribution for aluminium components by alloy type.

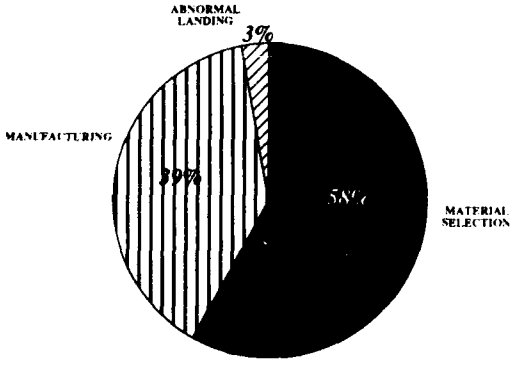

Fig. 25. Failure cause distribution for magnesium components.

The following observations were made from the distribution of failure causes for each particular failure mechanism (Fig. 26):

a. Fatigue resulted mainly from manufacturing defects or design deficiencies, as either can promote crack initiation
b. Pitting had many causes, principally poor material selection and inadequate maintenance practices in the field
c. SCC, a characteristic response of a material with a given environment, was mainly attributed to a poor selection of material

Similar conclusions were reached when the distribution of failure mechanisms resulting from the different failure causes was analyzed (Fig. 27), design deficiencies and manufacturing defects leading to fatigue, and poor material selection and improper field maintenance leading to corrosion.

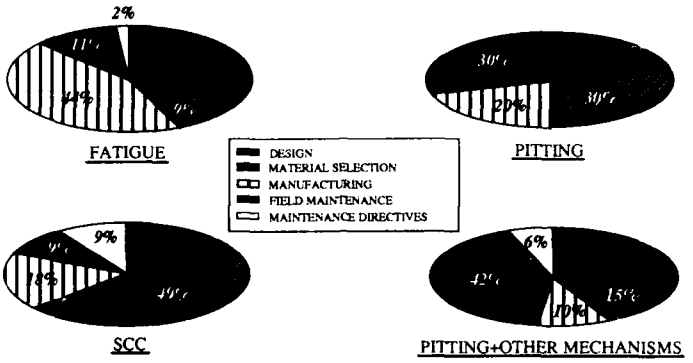

Fig. 26. Distribution of failure causes by failure mechanism.

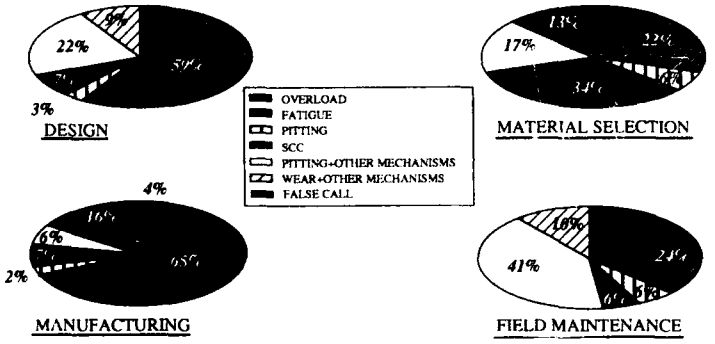

Fig. 27. Distribution of failure mechanisms by cause of failure.

4 DISCUSSION

The large percentage of aircraft maintenance activities on landing gears and associated high costs plus the criticality of these components from an airworthiness point of view indicate that efforts devoted to increase the structural integrity of these systems are well justified. These efforts should apply not only to the design stages and in the selection of materials, but also to proper manufacturing and in-service maintenance, as shortcomings in these areas contributed significantly to failures. Although somehow interrelated, each area will be considered in turn to see how improvements can be made in light of the findings presented in the survey.

4.1 Design

In our experience, landing gears have been quite successful in absorbing the loads associated with landings as hard landings have not been causal in the failures studied. Most of the overload failures noted in this survey occurred because of abnormal take-off or landing. Therefore, the energy absorption design features for impact loads and the design limit loads set for static strength appeared to be generally adequate for the landing gears investigated.

Although the design addresses the life of landing gear components in fatigue terms and the analysis is validated by tests, design related fatigue failure still occurred within the given life. The two main causes were poor design detail and improper assumption as far as loads and stresses were concerned. The poor design details include factors such as stress concentration and sharp radii. Possible explanations why these design deficiencies were not discovered through testing could be: statistical scattering of test data, difficulty of simulating actual loading conditions on all components through test articles with few loading points, test articles not fully representative of production parts and testing load not representative of actual in-service conditions.

Developing a realistic load spectrum is not an easy task. One must not only take into account the loads associated with landing as well as those associated with ground manoeuvers (steering, braking and taxiing) as they contribute significantly to fatigue damage [6], but also the stresses induced by manufacturing processes and assembly. Nevertheless, designers should be striving to achieve this goal [7]. In order to standardize the testing for comparison purposes, it might be appropriate to define realistic fatigue load spectra as they already exist for some aircraft structures (e.g. FALSTAFF) and some engine components (e.g. TURBISTAN). Further, in order to satisfy airworthiness authorities who have different interpretations of similar requirements, it would appear appropriate to establish a single, universally applicable set of fatigue design requirements.

Although fatigue failures have been attributed to design deficiencies in nearly 60% of the cases, corrosion as it accounted for nearly all of the remaining design related problems should not be neglected. The causes were many: no means of drainage, inadequate sealing from the environment, design allowing water entrapment, poor selection of protective coating, a design preventing access for corrosion inspection, the use of dissimilar metals in contact and assemblies promoting damage to the coatings. Although preventive measures can be taken for each of these examples, there is also a need to better understand how materials degrade with time in the chemical and physical environment in which the landing gear will be operating. The physical environment refers to the type of maintenance and possible types of damage (e.g. scratches, plating deterioration) that can be incurred during specific maintenance activities. As mentioned previously, actual design addresses fatigue through durability testing and corrosion through means of prevention but it would be wiser to consider the synergism of fatigue with the environment as many failures were caused by fatigue but promoted by corrosion pitting. The ENSTAFF spectrum, which is the FALSTAFF spectrum taking into account environmental effects for airframe, is, for example, a positive step in this direction. A similar approach could be followed for landing gears.

A landing gear system integrity program would probably be the most appropriate methodology to ensure the structural integrity of these components throughout their life cycle [6]. One such program could be a tailored version of MECSIP [8] and, as ASIP [3], it would be divided into five phases: design information, design analyses and development tests; component development and system functional tests, an integrity management data package and integrity management (Table 2). An alternative approach could be to include landing gears directly into the ASIP, so that the fracture and durability critical parts (specifically identified under the Damage Tolerance and Durability Control Plan [3]) of the landing gears would be designed, tested and inspected to ensure the structural integrity for their specific design applications.

However, the inherent poor damage tolerance and residual strength characteristics of traditional high strength landing gear materials made the use of the damage tolerant approach very difficult in most instances. The probability of detecting the required flaw size would have been low and the short inspection interval would have made the inspection unrealistic from an operational and economic point of view. In addition, the derivation of the fatigue crack growth rate from an analytical point of view would be difficult, but efforts are now being devoted to this area [10].

It is important to mention, however, that a few landing gear components analyzed showed large cracks before failing catastrophically. This was the case when cracks propagated longitudinally in components such as cylinder or struts, or when the load was relatively small such as in situations of load transfer through a different path. In these cases, the use of damage tolerance or the fail-safe approach could be appropriate and would allow the determination of the appropriate inspection interval. Although theoretically the same approach could be taken for corrosion related failures as SCC growth rate can to some extent be quantified, our knowledge of the time required for a pit to form and turn into a crack is very limited. In these cases, the prevention of corrosion is the only appropriate approach.

TASK I Design information	TASK II Design analyses and development tests	TASK III Component dev. & sys. functional tests	TASK IV Integrity mgt. data package	TASK V Integrity management
- Program strategy plan - System master plan - Method II brake energy analysis - Flotation analysis - Preliminary loads analysis -Trade studies - Critical component control plan - Component/subsystem development specs - M&P selection/charact. - Product integrity control plan - Corrosion prevention and control plan	- Final loads analyses - Design strem/environment spectra develop. - Thermal/environment analysis - Stress/strength analysis - Durability analysis - Damage tolerance analysis - Vibration/dynamics/acoustics analysis - Material characterization tests - Design development tests - Shimmy analysis	- Functional qual. tests - Strength tests - Durability tests - Full scale "Iron Horse" simulator tests - Ground vibration tests - Flight and ground operations tests - Integrated test plan - Interpretation and evaluation of tests results	- Provide revised reprocurement data packages - Finalize production control mgmt plan - Prepare tech order input data package - Maintenance plan and task development - Finalize materials specs & controls - Publish final strength & life summary rpt. - Establish landing gear tracking plan	- Operational usage - Maintenance records service reporting - Landing gear service times

Table 2 - Landing Gear System Integrity Program

The design of landing gear systems will continue to evolve. In the future weight minimization will remain an important requirement but factors such as the cost of material, manufacturing characteristics, environmental effects, repairability, survivability and crashworthiness should also be addressed. Some manufacturers are now looking at a new "jump strut" design which will "push" the nose of an aircraft up into the air, substantially reducing the ground roll required for take-off [10]. This would provide a tactical advantage for military aircraft and an increase in flexibility for commercial aircraft. However, this type of design would require a small increase in landing gear weight and volume, which is undesirable and would probably have to be offset by the use of new materials with higher specific strengths. Other manufacturers propose advanced integrated fault tolerant landing gear management systems providing complete braking, anti-skid, steering and sequencing for aircraft main wheels and nose gear [11]. In the future, we might expect on-line damage monitoring sensors hooked up to these advanced systems, especially in non-accessible/inspectable areas. It is believed that developments in landing gear configuration will be quite limited and that improvements in materials offer more potential benefits [6].

4.2 Material Selection

About 20% of the failures investigated could be traced back to the selection of materials which turned out to be less than adequate for the intended applications, leading mainly to many corrosion related problems.

As mentioned earlier, the requirements for minimum weight and use of space often led to trade-offs in material properties, high strength being selected over fracture toughness and corrosion resistance. For example, the H-11 steel selected for a main landing gear component of a CF transport aircraft is no longer used in the CF following a catastrophic failure because of its poor fracture toughness. Magnesium alloys have also been avoided by most manufacturers because of their inherent corrosion problems. Another good example, probably the most controversial, was the use of the 7079-T6 aluminium alloy in landing gears. This alloy was developed in the mid-50s and although its production ceased in the early 70s because of its poor resistance to SCC, it was, unfortunately, still used in the manufacture of landing gear components (struts, cylinders) for another decade. Major costs were incurred because of the numerous in-service SCC problems experienced and the need to replace landing gear components made of this alloy. Even with alloys developed and selected more recently, such as 300M, SCC is still occurring.

The need for materials with higher fracture toughness is now being addressed by more stringent requirements, but the concerns about corrosion and

SCC problems can only be addressed by a better characterization of materials with respect to their operating environments and by the use of appropriate protective coatings. While it is relatively simple to characterize a material for its fracture toughness and damage tolerance properties, it is much more difficult to address the time-dependent phenomena without even considering their synergism with cycle-dependent processes such as fatigue and fretting. Corrosion testing presents two major problems. Firstly, the reliability of the correlation between accelerated laboratory tests used to simulate long term exposure to the environment and in-service behaviour is still open to debate. Secondly, testing a material in all possible conditions and environments is a big challenge. Again the 7079-T6 alloy illustrates well this last concern. Comparing favourably with 7075-T6 from an SCC resistance point of view during its development stage, it was only later realized that the relatively "acceptable" SCC behaviour of this alloy when tested in 3.5% NaCl solution was much worse under normal atmospheric conditions, a case that was neglected in the original test matrix [12].

Some materials are being considered to replace the conventional 4340 and 300M steels and the 7xxx series aluminium alloys. A modified version of AF1410 is a potential candidate as it shows better fatigue life, fracture toughness and especially SCC resistance than 300M [4]. Powder metallurgy aluminium alloys and aluminium-lithium alloys could provide some improvements over the presently used aluminium alloy. Some researchers consider that composite structures such as a titanium matrix composite material may become a viable alternative to conventional materials for landing gear structures [4]. Development of new materials will require, in addition to their characterization in terms of their mechanical and corrosion properties, consideration of the life cycle of the component from manufacturing to service and the associated maintenance requirements.

4.3 Manufacturing

Nearly half of the fatigue problems surveyed originated from manufacturing defects. This indicates that efforts devoted to improving manufacturing are warranted, especially when considering that these problems can be easily prevented. While it may be appropriate to consider manufacturing defects during full scale qualification testing, efforts to improve the manufacturing quality should also be made. This can be accomplished two ways: by improving the manufacturing processes, and by ensuring that there is a reliable NDT technique for quality control.

Better manufacturing technique can be promoted by the use of new materials and processes (e.g. superplastic forming capability and better protective coatings). For example, a large landing gear manufacturer [8] has started a program to develop the largest ever built main fitting forging made of ultra high strength steel for the Airbus A320. This will minimize the number of components and eliminate many difficult problems associated with built-up structures. Concerning the protective coating aspects, new processes such as ion implantation and plasma arc spraying seem promising.

There is no doubt that better NDT techniques and more stringent inspection requirements could alleviate many fatigue failures from manufacturing defects and corrosion failures from poor protective coatings. The use of automated NDT inspection would also increase the probability of detecting a defect.

The other important manufacturing aspects to consider are the residual stresses induced by the manufacturing (e.g. heat treatment, forging, etc.) and the assembly stresses. These stresses should be considered with those induced in-service during the qualification tests. Efforts to reduce these stresses or at least to better characterize and quantify them should be made.

4.4 In-Service Maintenance

Maintenance at the field level, but also in terms of directives from headquarters, led to more than 20% of all the failures investigated. It is probably in this area that the greatest improvement is possible. Unsatisfactory field maintenance resulted in corrosion related failures in the majority of cases and to a lesser extent to fatigue in cases of improper torquing and adjustments of components such as links and actuators and sometimes in overload. Field technicians must be made aware of corrosion and how it can be prevented. Adherence to technical orders is one aspect, but this should be accompanied by an education program on proper preventive practices in terms of avoiding damage to coatings, application of inhibitors, grease, sealants, protective coatings and washing procedures. Detection of corrosion is an important part of any prevention program and efforts devoted to developing reliable NDT techniques to detect corrosion in the field should be pursued. These efforts should be undertaken in conjunction with the development of better protective coatings and a corrosion inspection/modelling and/or monitoring program.

Much effort is now being devoted in this area and the CF is presently sponsoring a research and development project to model corrosion processes. Hopefully, this program will permit better rationalization of the inspection process. The inspection cycle of many CF aircraft landing gears is presently based on the number of landing cycles. Although this may be appropriate only when the fatigue mechanism is considered, it is unfortunately irrelevant in preventing corrosion damage, since it is a time-dependent process. The use of corrosion probe monitoring may also be helpful in rationalizing the inspection cycles.

A corrosion prevention and control management program, in which there would be a dialogue between headquarters staff and field technicians, would be a definite asset. The directives imposed by headquarters and the corrective actions should be initiated in light of the failures experienced and feedback from field technicians. From such a program, the design and maintenance authorities could, for example:

a. Modify the inspection schemes, i.e. the interval of inspection (time versus number of landings or flying hours), the inspection location, the NDT technique and reporting methods
b. Redesign some components in order to avoid stress concentrations, introduce surface compressive residual stresses, use sacrificial coatings, prevent possible wear damage to the protective coatings, provide better drainage methods and sealants, prevent water entrapment and substitute better materials and/or processes
c. Modify the maintenance practices, by using dehumidifiers, corrosion inhibitors, proper drainage and wash procedures

Finally, as there is a worldwide trend to extend the life of aging aircraft, maintenance is expected to play an increasingly important role to ensure the integrity of landing gear systems.

5 CONCLUSIONS AND RECOMMENDATIONS

It is concluded that:

a. Landing gears are the second most important area of failures reported on aircraft and these have high safety implications
b. No reported overload failures resulted from hard landings. They occurred mainly during abnormal landings, such as skidding off the runway
c. Fatigue and corrosion were found to be the two main mechanisms of failure. Fatigue occurred mainly in steel components while corrosion related problems occurred mainly with aluminium alloys
d. Pitting or pitting as a precursor to other failure mechanisms was the major form of corrosion and particularly significant in wheels
e. Design deficiencies and manufacturing defects led primarily to fatigue failures, although they also promoted corrosion when protective coatings were involved
f. Poor material selection and improper field maintenance practices led principally to corrosion related failures and to a lesser extent to fatigue. Maintenance related failures were observed equally on all aircraft types
g. The penalty incurred by poor material selection in the design stage was very severe from an operational and economic point of view, requiring the replacement of landing gear components made with alternative materials
h. Manufacturing defects appeared to be the most important failure cause for steels, while design deficiencies, field maintenance practices and material selection were the most significant causes for failures in aluminium alloys
j. Although landing gears are not designed using a damage tolerance approach, there were many cases where it could have been used because large cracks were found

In light of the findings, it is recommended that:

a. Landing gear components be included into a structural integrity program. This would require proper characterization of the landing gear operational environment from both a fatigue and corrosion point of view
b. Realistic full scale qualification tests should not only consider inherent manufacturing defects but should also address the stresses induced during manufacture and assembly
c. Efforts be devoted into developing a single universally applicable set of fatigue design requirements
d. All new materials proposed for landing gear applications be fully characterized and evaluated in all applicable environmental conditions before being used

e. Efforts be pursued to improve protective finishes and coatings and manufacturing processes
f. Efforts be pursued to improve maintenance and inspection of defects
g. A corrosion program be developed in which a constant dialogue between maintainers and field technicians will highlight a series of preventive measures. More efforts should be put into the education of technicians about corrosion problems and preventive measures, and for its detection and monitoring through NDT
h. Efforts be devoted to corrosion modelling/monitoring and inspection methods development to enhance the landing gear inspection process
j. Landing gear components be designed to show some fail-safe and damage tolerant characteristics, thus avoiding catastrophic failures
k. The use of on-line fatigue and corrosion damage monitoring sensors be further investigated
m. Thorough failure analysis reports be made for each failed component discovered. Proper understanding of the failure mechanisms and assessment of the causes provide valuable feedback information to designers, operators and maintainers for the necessary corrective actions to be undertaken

REFERENCES

(1) Landing Gear Systems, MIL-L-87139(USAF), 13 July 1979.

(2) Materials and Processes for Corrosion Prevention and Control in Aerospace Systems, MIL-STD-1568A(USAF), 24 October 1979.

(3) Aircraft Structural Integrity Program (ASIP), MIL-STD-1530A, 11 Dec 1975.

(4) Advanced Material for Landing Gear, Aerospace Engineering Journal, vol. 10, no. 7, July 1990, pp. 17-21.

(5) Metallic Materials and Elements for Aerospace Vehicle Structures, MIL-HDBK-5D, May 1986.

(6) Davis, D.G.M., and Whitehead, M.R., "The Development of Landing Gear", Dowty Rotol United, Gloucester, England.

(7) Gustavsson, A.I., "In-Service Measurements of SAAB SF-340 Landing Gear Loads", FFA TN 1987-48, 1987 (ICAF Doc No 1638).

(8) Courtesy of The Technical Cooperation Program - Sub-Group P, Technical Panel No. 4.

(9) Mechanical Equipment and Sub-systems Integrity Program (MECSIP), MIL-STD-1798, 20 June 1988.

(10) Nagar, A., "Fatigue Crack Growth in Aircraft Main Landing Gear Wheels", Fracture Mechanics: Nineteenth Symposium, ASTM STP 969, T.A. Cruse Ed., American Society for Testing and Materials, Philadelphia, 1988, pp. 868-882.

(11) Forth, K.D., "Gearing Up for The Future", Aviation Equipment Maintenance Journal, January 1990, pp. 58-61.

(12) Lifka, B.W., and Sprawls, D.O., "Stress Corrosion Testing of 7079-T6 Aluminium Alloy in Various Environments", Stress Corrosion Testing, ASTM STP 425, American Society for Testing and Materials, 1967, p. 342.

ACKNOWLEDGEMENT

The authors would like to acknowledge the contribution of the Maintenance Analysis Branch of the Aircraft Maintenance Development Unit (AMDU) for their work in gathering AMMIS data and especially to 2Lt Gratton and Mr. St-Michel for their excellent work in the gathering of the ACAIRS and failure analysis reports data.

APPLICATION OF THE AIR FORCE GUIDE SPECIFICATION 87221A TO GROUND LOADS

by

Dan Sheets and Robert Gerami
ASD/YSX
Wright-Patterson AFB
OH 45433-6503
United States

1. It is well know that the U.S. Air Force has eliminated the use of rigid and mandatory structural design specifications. In their place a new approach has been instituted which requires every system structural specification be rationally tailored to the actual anticipated aircraft usage. In order to facilitate this approach, the Air Force Guide Specification (AFGS-87221A) contains an Appendix which can be used to form the basic framework of a unique, system specific, Aircraft Structural Specification. To use the Appendix, various blank areas in the specification must either be completed or marked as non-applicable. The completion of these blank areas may require only the insertion of a simple numerical value; while in other cases extensive data, direction, and analysis techniques must be described to fulfill the requirements. One cannot stress too strongly that the AFGS-87221A produces total system performance requirements as opposed to the old approach of meeting selected, isolated criteria. This new approach entails the conversion of operational requirements into the associated and anticipated loading environments. Since there is an interaction between the environments, structure, and resultant loads we will usually have a non-linear task in converting performance requirements to structural load levels. It must be well and fully understood that for this approach to work, all aspects of the operational requirements must be well defined. Admittedly, this new approach is not as easy to implement as the old arbitrary set of isolated criteria or requirements. The future operator of the aircraft and the engineers must work very closely to develop the system specification.

2. To compound the problem, aircraft ground activities have never generated the same excitement or enjoyed the same interest as flight operations. Some even look upon landing gear as a necessary evil, at best. Consequently, the development of ground loads analysis techniques and requirements, coupled with operational considerations and design trade-offs is not as advanced as other aspects of aircraft design. The result of this reduced level of interest need not be catastrophic structural failure. Normal ground operations rarely produce structural failures which kill people. A likely result of this reduced level of interest is an excessively conservative and over built design. While anyone can recognize structural failure, few can recognize the over designed, over weight structure. Therefore, most designers are reluctant to cease using historical factors, even when they are no longer appropriate.

3. This does not mean that the area of ground loads has been completely ignored. What this does mean is that due to an uneven amount of interest in different areas, some conditions are easier to tailor than others. In order to see the application of AFGS-87221A, let's consider a current USAF fighter that was designed before the specification tailoring concept. We will compare its actual requirements against AFGS-87221A and the current U.S. Navy document MIL-A-8863B(AS). No, not all of the requirements, just a selected few that pertain to landing gear: taxi, turns, pivot, landing and towing.

4. Let's first consider the actual taxi requirements for our sample aircraft, as shown below:

> 5.1.1.a Taxiing - The aircraft is in a three point attitude for three point and unsymmetrical braking and in a two point attitude for two point and reverse braking. The aircraft is in equilibrium with balancing gear and intertial loads. The coefficient of friction versus aircraft gross weight is shown on Figure 5.4.1.a-1.
>
> For operation from a paved surface, the aircraft shall be capable of withstanding loads from both a continuous runway profile and discrete 1.5 inch step and (1-cosine) bump and depression inputs. Figure 5.4.1.a-2 defines the paved runway step and bump and dip inputs.

5. We can immediately see that this references a coefficient of friction function and figure that defines a surface roughness requirement. Without reproducing the braking coefficient of friction figure, it varies from 0.7 to 0.8 as a function of aircraft weight. For the taxi way roughness the figure is reproduced here.

FIGURE 5.4.1.a-2
BUMP HEIGHT OR DIP DEPRESSION

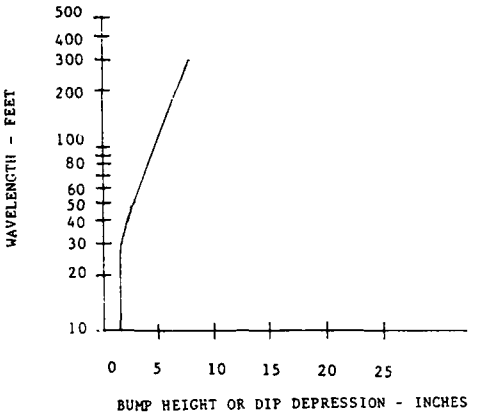

You can see that for a bump wave length between one landing gear separation to three times the landing gear spread, the bump height goes from 1½ inches to 3 inches. At twice the landing gear spread the bump height is only 2 inches. This does not suggest an aircraft intended for other than prepared bases.

5. Below is the U.S. Navy requirement from MIL-A-8863B(AS), which would have been imposed on the aircraft if it had been built for the Navy.

> 3.12.4 Taxiing. Applicable to all types of airplanes. The airplane shall be in the three-point attitude. The drag loads and side loads at each gear shall be zero. The sum of the vertical loads acting at the ground shall be equal to twice the weight of the airplane. Separately for the design of the nose gear, and its support structure only, the sum of the vertical loads, acting at the ground, shall be equal to three times the weight of the airplane.

6. Next, let's consider the taxi requirement as it is in AFGS-87221A. This is deceptively simple in appearance. While it no longer includes the braking criteria, it actually demands the engineer must have considerable amounts of information on various aspects of **aircraft taxi.**

> 3.4.2.1 Taxi
>
> a. Low speed taxi on taxiways and ramps of _____.
>
> b. High speed taxi on runways of _____.
>
> The purpose of this requirement is to establish structural requirements for straight ahead taxi without braking. Straight taxi typically produces maximum vertical loads on the landing gear and may produce significant loadings on other primary structure.
>
> REQUIREMENT GUIDANCE
>
> Define the taxi requirements in terms of general parameters 3.2 and any attainable combinations thereof. Taxiing loads shall be based on operational requirements such as taxiway, runway, and tire conditions. Taxi loads shall be established at appropriate speeds in accordance with 3.2.7. For example, low speed taxi on taxiways and ramps of paved and semiprepared airfields at speeds up to the taxi limit speed, V_T and high speed taxi on runways of paved and semiprepared airfields at speeds up to the lift-off limit speed, V_{LO}. The appropriate effects of weight, cg position, mass distribution, and landing gear characteristics shall be included. RTD-TDR-63-4139 Vol I and ASD-TDR-62-555 Vol I provide criteria and analysis techniques for establishing alighting gear dynamic loads. Power spectral density levels for paved, semiprepared, and unprepared airfields are presented in Figures 6 and 8. Discrete bumps and dips for slow and high speed taxi are presented in Figures 4 and 5.

Reading the Requirement Guidance you will realize that not only must the designer be cognizant of the proposed aircraft, but also the proposed operational bases and their taxiways and runways. This brings us back to the question of well defined operational requirements. Obviously, with a two inch bump for a wave length of twice the gear spacing, our example aircraft was never intended for semi-prepared field operations.

7. We shall now address turning. Below, is shown the actual turning requirement as it appears in the system specification for our sample aircraft.

> 6.5.2 Turning - The air vehicle in the three point attitude shall execute steady turns by the following means:
>
> a. Unsymmetrical thrust or nose gear steering.
>
> b. Unsymmetrical thrust or nose gear steering with symmetrical braking.
>
> c. Differential braking.
>
> The ratio of side load to vertical load shall be limited to 0.5 on any wheel and the sum of the side loads shall equal 0.5W at maximum design weight and 0.3W at maximum limit weight except that this value need not exceed a value which would result in overturning. For braked conditions, the drag load and side load on the braked wheels shall be such that the vector sum of the drag load and side load will not exceed 0.8 of the vertical load at maximum design weight and 0.65 of the vertical load at maximum limit weight with a linear variation between these weights. Requirement "b" above shall result in a side load factor of at least 0.3W at maximum design weight and 0.18W at 68,000 pounds and remain at 0.18W to maximum limit weight with a drag load on the braked wheels of at least 0.5 of the vertical load at maximum design weight and 0.4W at 68,000 pounds and above.

Next we have the MIL-A-8863B requirement for turning and steering.

> 3.12.2 Turning. Applicable to all types of airplanes. The airplane shall be in the static three-point attitude. The sum of the vertical ground loads on the landing gear shall be equal to the weight of the airplane. The drag loads shall be zero. The side loads on each landing gear shall act in the ground plane and in combination with the landing gear vertical loads, such that the total resultant load passes through the airplane CG. The ratio of the side load to the vertical load shall be the same at each landing gear. The sum of the side loads shall be 0.5 times the weight of the airplane, except that this sum need not exceed a value which would result in overturning.
>
> 3.12.6 Steering. Applicable to all types of airplanes. The airplane shall be in the statuc three-point attitude with the noise gear swiveled in all possible positions. A torque equal to the maximum available steering torque shall be applied to the nose gear.

What can we say about either or both of these? Obviously the actual requirement is noticeably more complicated than in MIL-A-8863B. But, does that tell us anything? No, neigher specification is a performance requirement! The coefficients of friction and the load factors tend to suggest they are the results of an analysis which converted performance to specific criteria. However, there is no ways to understand why the actual specification is more complex than MIL-A-8863B. What did this complexity buy us?

8. The application AFGS-87221A, as shown below, requires considerable knowledge.

> 3.4.2.2 Turns
>
> a. Turns on ramps at speeds up to _____.
>
> b. Turns on taxiways at speeds up to _____.
>
> c. Runway turn-offs at speeds up to _____.
>
> REQUIREMENT RATIONALE
>
> The purpose of this requirement is to provide structural requirements for unbraked steady turns.
>
> REQUIREMENT GUIDANCE
>
> *Define the turn requirements in terms of general parameters of 3.2 and any attainable* combinations thereof. Turning design loads shall be based on operational requirements such as taxiway, runway, and tire conditions. Turning requirements shall be established at appropriate speeds of 3.2.7. For example, turns on ramps at speeds of up to the taxi limit speed, V_T on paved and semiprepared surfaces. Turns on taxiways at speeds up to the taxi limit speeds, V_T on paved and semiprepared surfaces. Runway turn-offs at speeds up to the taxi limit speed, V_T, on paved and semiprepared surfaces. The effects of weight, cg position, mass distribution, and landing gear characteristics shall be accounted for.
>
> REQUIREMENT LESSONS LEARNED
>
> A technique for establishing lateral load factors during ground turning is presented in ASD-TR-79-5037.

Not only must the aircraft be well defined, but so must the taxiways and runways. In reality, it is probably more important to define the aircraft speeds besides the taxiways and runways, since in a first order analysis the mass of the aircraft is immaterial. Again, the implementation of AFGS-87221A requires more effort and insight than using either the U.S. Navy specification or the actual aircraft turning requirement.

9. Pivoting is in many ways just a very special type of turn. The actual specification requirement for our example aircraft is given below along with the plot which defines the tire coefficient of friction.

> 5.4.1.d Pivoting - The aircraft is pivoted about one wheel. The brakes are locked on the gear about which the aircraft is rotating. The tire coefficient of friction is defined by Figure 5.4.1.a-1.

FIGURE 5.4.1.a-1
FATIGUE BRAKING COEFFICIENT OF FRICTION

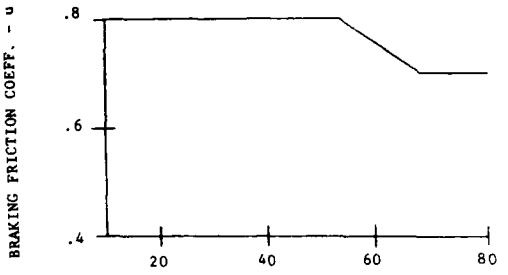

The requirement which MIL-A-8863B would have imposed on the development of this aircraft is given below.

> 3.12.3 Pivoting. Applicable to all types of airplanes except SKI airplanes. With brakes locked on the landing gear unit about which the airplane is rotating, the airplane shall pivot about one wheel, or in the base of multiple wheels, about the centroid of contact area of all wheels in the gear unit. The vertical load factor at the CG shall be 1.0 and the tire coefficient of friction shall be 0.8.

Obviously there is a great similarify between these two requirements. However, the Air Force allowed a linear reduction in the coefficient of friction beginning at 53,000 pounds and becoming 0.7 at 68,000 pounds. This means that this aircraft, designed to Air Force requirements, has slightly less pivoting capability at higher weights than it would have, had it been designed to MIL-A-8863B.

10. Now, let's see how AFGS-87221A addresses pivoting. Looking at the requirements as presented, there is a noticeable difference. We can see that the pivot points must be defined along with thrust levels. Both the sample Air Force requirement and the current U.S. Navy specification assume the point of pivot is known or obvious. Also, AFGS-87221A requests thrust levels when neither of the other two do. However, both the other two specifications give a tire coefficient of friction when the approach of AFGS-87221 does not. The AFGS-87221A simply presents a different approach, but this new approach does need power and thrust levels established by a rationale process.

> 3.4.2.3 Pivots. ( )
>
> a. The pivot points are _____.
>
> b. The power of thrust levels shall be _____.

REQUIREMENT RATIONALE (3.4.2.3)

> The purpose of this requirement is to establish maximum torsional load on the main landing gear.

REQUIREMENT GUIDANCE

> If the requirement is not applicable for pivots, insert N/A in all blanks including those blanks of the subparagraphs. If applicable, insert APP in the blank and define the extent of applicability. For each applicable subparagraph define the pivoting requirements in terms of the general parameters of 3.2 and any appropriate combination thereof. For example, the pivot points are about one main landing gear wheel with brakes locked, or in the case of multiple wheel gear units, about the centroid of contact area of all wheels in the gear unit. The power and thrust levels shall be based on a rational analysis to determine power required to perform the maneuver. The coefficient of friction between the tires and ground shall be 0.8 and the vertical load factor at the c.g. shall be 1.0.

Some aircraft configurations, such as a very large transport, preclude true pivot turns, in which cases a minimum radius turn should be defined in 3.4.2.2 instead of pivoting.

11. Landing as a loading condition requires extensive definition. Additionally the U.S. Navy has a requirement to be able to land on aircraft carriers. This adds at least an order of magnitude to the complexity of their specifications and makes any real attempt to compare requirements difficult. Therefore, let's just consider landing sink rates in order to get some feeling of the difference. The figure below is the actual landing sink rate requirement for our sample aircraft.

ALLOWABLE LANDING SINK SPEED
VERSUS
AIRCRAFT WEIGHT

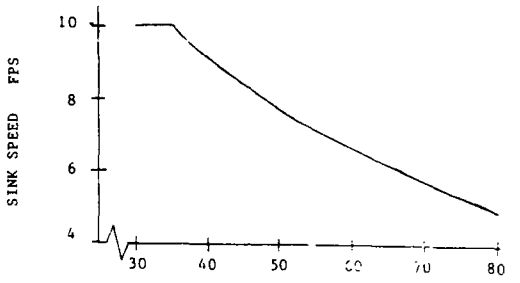

Below 35,000 pounds the aircraft can land with a vertical sink rate of 10 feet per second. About 35,000 pounds the sink rate is gradually reduced in order to account for the energy increase due to the added weight of the aircraft. It is important to remember that this aircraft's maximum sink rate is 10 feet per second since the same aircraft when designed by the U.S. Navy would have a sink rate of over 20 feet per second.

12. The requirement from AFGS-87221A, as shown below, is intended to be tailored to any operational requirement. It can be made to cover all operational landing conditions, while accepting that not all aircraft need have all landing capabilities.

3.4.2.6 Landings

a. Hard surface runways ( ). Landings on _____.

b. Semiprepared runways ( ). Landings on _____.

c. Unprepared surfaces ( ). Landings on _____.

d. Arrestment ( ). _____.

e. Declerating devices ( ). _____.

f. Other landing conditions ( ). _____.

REQUIREMENT RATIONALE

The purpose of this requirement is to establish structural requirements for landing operations on specified surfaces.

Following the conceptof a rationally tailored system specific structured specification, the Air Force Guide Specification approach allows the selection of appropriate conditions. However, what are appropriate conditions? Sink rates in excess of twenty feet per second might be appropriate for carrier landings or air assault situations, but what is appropriate for a fighter using a main operating base? I don't know. Not until the intended user and the design engineers review the proposed operational requirements and all the trade-offs and interactive design impacts can the totality of the landing requirement be established. Not only must numerous aircraft parameters be defined, but so must the runway be defined in great detail.

13. The new AFGS-87221A recommends that towing conditions be tailored as it does all other structural loadings. However, it does suggest as a safe selection the very requirements that have been used for years and are still current in MIL-A-8863B(AS). These are the very towing requirements that our sample aircraft used. I don't know how old these towing requirements are, but they have been found in a 1940

document. Much the same can be said for jacking and hoisting. These requirements are historical, and their basis or supporting justification has been lost over time. It is especially true in the area of towing besides jacking and hoisting that we lack research to assist in developing the well tailored, system specific, structural specification.

14. With the advent of AFGS-87221A there is a commitment to tailoring the actual system specific structural specification. However, those of us who use this document must increase our depth of activity in several areas. First, we must work very closely with the final user of our product. Second, those of us who use AFGS-87221A must realize that specification development is going to be more complicated than it has been in the past. Due to conflicting operational requirements, it may be necessary to perform trade studies which appear to be very close to preliminary design concept studies, in order to convert performance requirements. The comfort and supposed safety of the old, rigid specifications is over. Besides, the old approach may have been safe with respect to contracting laws, but they often fail the laws of physics. Therefore, our old criteria was not as uniformly conservative as we thought.

ETUDE COMPARATIVE DES NORMES FRANCAISES AIR 2004 ET AMERICAINES MIL-SPEC RELATIVES AUX CHARGES SUR LES ATTERRISSEURS

par

J.M. DAUPHANT
DGA/DCAé/Service Technique des Programmes Aéronautiques
4 avenue de la Porte d'Issy
75015 PARIS
FRANCE

RESUME

L'étude comparative des normes françaises (AIR 2004 D / AIR 2004 E) et américaines (MIL-A-8862A / MIL-A-8863A) dont fait l'objet cette présentation montre, à partir d'un avion embarqué (SUPER ETENDARD) et d'un avion terrestre (MIRAGE 2000), l'influence de ces normes et les répercussions liées à l'application de celles-ci sur les cas de charges, sur les efforts au sol et sur le dimensionnement des trains d'atterrissage.

INTRODUCTION

L'évolution des normes militaires relatives aux charges sur atterrisseurs est continue depuis un demi-siècle.

Elle résulte principalement de l'exploitation et de l'analyse des problèmes et des accidents rencontrés ainsi que de l'apparition de moyens d'essai, de calcul et de simulation plus performants.

L'ensemble de ces éléments, associé à l'élargissement des compétences technologiques des industriels, permet aujourd'hui d'appréhender plus finement les cas d'atterrissage, de décollage et d'évolution au sol et de prendre en compte plus fidèlement les phénomènes liés aux interactions "avion/sol".

L'étude des règlements étrangers est également un facteur d'évolution important. L'adoption par les Services Officiels étrangers de concepts nouveaux, l'introduction d'approches plus ou moins novatrices sont suivies avec intérêt et donnent lieu à des travaux d'analyse dont la finalité est double: mesurer le degré de pertinence de ces concepts et noter, en cas d'application de ceux-ci, leur influence sur la définition et le dimensionnement des avions et plus particulièrement sur ceux des atterrisseurs.

C'est dans cette optique que le STPA (Service Technique des Programmes Aéronautiques), organisme de la DGA (Délégation Générale pour l'Armement) au sein du Ministère de la Défense français, a commandé à la société MESSIER-BUGATTI, avec le concours de la société DASSAULT-AVIATION, une étude comparative des normes françaises et américaines récentes.

L'étude demandée s'inscrit dans le cadre d'une réflexion globale en vue d'une possible révision de la norme actuelle AIR 2004 E.
Cette norme nécessite en effet des modifications pour prendre en compte les caractéristiques des avions de combat dits de nouvelle génération (en particulier à cause des commandes de vols électriques).

Les normes retenues pour cette étude sont les normes françaises AIR 2004 D, AIR 2004 E et les normes américaines MIL-A-8862A, MIL-A-8863A.

Deux avions - un avion marin: le SUPER ETENDARD et un avion terrestre: le MIRAGE 2000 - ont servi à évaluer l'influence des différentes normes sur les cas de charges, sur les efforts au sol et sur le dimensionnement des atterrisseurs.

I PRESENTATION DES NORMES

Une rapide présentation chronologique permet de mieux comprendre l'évolution des normes au cours des dernières années.

I-1 NORMES FRANCAISES

I-1.1 Historique

De manière relativement rudimentaire, la norme **AIR 2004 B** prend en compte des 1947 les cas d'atterrissage classiques (atterrissage en ligne de vol, atterrissage plané, atterrissage en ripé, atterrissage trois points) ainsi que les conditions de décollage, de freinage et de giration au sol.

En 1947 lui succède la norme **AIR 2004 C** qui est plus complète et qui traite des principaux cas d'atterrissage, de décollage et d'évolution au sol (freinage, manoeuvre au sol, remorquage, hissage, amarrage, transport,...) nécessaires à la conception et au dimensionnement des atterrisseurs.

C'est en 1960 que la norme **AIR 2004 D** entre en application. Celle-ci aborde des phénomènes autres que les phénomènes statiques jusqu'alors abordés, comme les vibrations et la fatigue. Le changement est radical puisque le titre de la norme AIR 2004 C "Conditions Générales de Résistance Statique des Avions et Hydravions" est abandonnée au profit de "Résistance des Avions".

La norme AIR 2004 D impose l'étude d'un certain nombre de cas nouveaux comme :

- l'abatée sur l'atterrisseur auxiliaire (train tricycle)
- le franchissement des obstacles de piste au roulement

et reexamine les conditions de ripé, de mise en rotation, de retour élastique et d'atterrissage dissymétrique.

La norme **AIR 2004 E** (1972) emprunte globalement le schéma de la norme AIR 2004 D tout en redéfinissant la vitesse de chute limite (*Fig.1*), en exigeant la prise en compte de cas supplémentaires:

- vitesse d'atterrissage extrême
- cas d'atterrissage à trois composantes
- cas de freinage au point fixe
- cas de la détente et de l'extension brutale de l'amortisseur faisant suite à un rebond

et en faisant disparaître notamment la notion désuète de charges de base (ou charges sûres).

NORME AIR 2004 E

VITESSE DE CHUTE LIMITE en m/s	Configuration normale d'atterrissage	3
	Configuration exceptionnelle d'atterrissage	2
	Configuration Ecole	3,6
VITESSE DE CHUTE EXTREME en m/s	$\sqrt{1,3}$ V	

NORME AIR 2004 D

VITESSE LIMITE en m/s	Pa	Pae	Pa	Pae
Atterrissage Symétrique	2,8	2	3,6	2,8
Atterrissage dissymétrique	2	1,4	2,8	2
	Bonnes pistes		Terrains courts	

Pa : poids d'atterrissage normal maximal
Pae : poids d'atterrissage exceptionnel

Figure 1

I-1.2 Réflexions sur la norme actuelle

a) Conditions d'élaboration

L'élaboration de la norme AIR 2004 E est dûe à la conjonction de plusieurs facteurs :

- les mutations technologiques et le développement amorcé dès le début des années 1960 des moyens de calcul et de modélisation tels que les éléments finis, ainsi que le développement des moyens de simulation et d'essai,

- l'expérience acquise par les Services Officiels et les industriels au travers des accidents et des problèmes survenus en service,
- les enseignements tirés des programmes nationaux et internationaux ainsi que des travaux de coopération,
- la parution en 1960, 1971 et 1974 des nouvelles éditions des règlements militaires américains,
- la volonté de parvenir à une norme suffisamment claire et exploitable exprimée conjointement par les Autorités compétentes et les industriels,
- le souci d'aboutir à une certaine homogénéité au niveau des règlements militaires (en vue d'éventuelles nouvelles coopérations) et des règlements civils (en vue de possibles développements).

Ainsi, l'exemple fourni par la vitesse de chute limite définie dans la norme française est frappant. Cette vitesse de chute limite tend à se rapprocher de celle préconisée par la norme MIL-A-8862A (*Fig.2*) et de celle recommandée par les règlements civils FAR 25/JAR 25.

NORME MIL-A 8862A			
		Poids normal d'atterrissage	Poids maximal d'atterrissage
VITESSE DE CHUTE LIMITE en m/s	Ecole et Entraînement	3,96	2,6
	Classique	3,05	[illegible]
VITESSE DE CHUTE EXTREME en m/s	1,25 x	au poids d'atterrissage	

Figure 2

Il est intéressant de rappeler à ce propos que le règlement JAR 25 impose une vitesse limite de descente de 3,05 m/s (10 fps) à la masse de calcul à l'atterrissage et une vitesse limite de descente de 1,83 m/s (6 fps) à la masse de calcul au décollage. En outre, ce règlement prend en compte les cas d'atterrissage en ligne de vol, les cas de ripé, de mise en rotation, de retour élastique, de rebonds à l'atterrissage, de roulement au décollage, de manoeuvres au sol, de virage, de freinage, d'amarrage, de levage, de hissage abordés dans la norme AIR 2004 E.

Bien entendu, le rapprochement entre normes n'est pas total; des différences existent et subsistent malgré tout. Une illustration est donnée par le tableau présenté en *Fig.3* relatif aux normes AIR 2004 E et MIL-A-8862A.

NORMES	AIR 2004E	MIL-A-8862A
Coefficient de sécurité CE = e CL	1,3	1,5
Atterrissage trois composantes	oui	non
Variation du conditionnement nominal de l'atterrisseur	pneu	amortisseur pneu
Remorquage	0,2 Md g	0,3 Md g
Levage	Rv = 1,2 R Rh = 0,3 R	Rv = 1,35 R Rh = 1,4 R
Freinage	cas différents	

Figure 3

b) Evolutions envisageables

Il serait aujourd'hui nécessaire de faire évoluer la norme AIR 2004 E qui date de 1974 afin qu'elle réponde aux exigences nouvelles des avions de combat modernes.

Un certain nombre de points peuvent être d'ores et déjà soulevés dans le domaine des charges au sol :

- réévaluation de la vitesse normale d'atterrissage,
- redéfinition du cas de décollage en configuration normale (cas de rotation au décollage où le coefficient 1,7 donnant la charge verticale à appliquer en statique sur chaque atterrisseur (1,7 Zs) est à revoir à la hausse),
- prise en compte éventuelle des évolutions au sol (notamment sur pistes sommairement réparées),
- prise en compte du cas des avions marins par un règlement national adapté.

I-2 NORMES AMÉRICAINES

L'évolution des règlements aux U.S.A. est importante tant dans le nombre des normes rédigées que dans les changements apportés.

La norme **MIL-A-8862 A** relative aux avions terrestres succède par exemple en 1971 à la norme **MIL A-8862 ASG**; elle se distingue de celle-ci par l'expression d'une valeur de vitesse de chute extrême et une approche plus complète des cas de virage et de roulement au sol.

Toutefois, c'est la norme **MIL-A-8863 ASG** datant de 1960 et relative aux avions embarqués qui illustre avec plus de netteté l'importance des changements enregistrés.

C'est avec elle en effet qu'est introduit le concept de combinaison multivariable. Grâce à ce concept, les cas de calcul à l'atterrissage ne sont plus définis de manière figée mais sont selectionnés sur la base de distributions statistiques de différents paramètres d'atterrissage.

Ainsi la norme MIL-A-8863 ASG présente les conditions initiales d'impact sous la forme d'une combinaison de la vitesse de chute, de l'angle de roulis et de la vitesse d'engagement satisfaisant l'équation d'un ellipsoïde :

$$a(V_V - V_{Vm})^2 + b(TETA - 2)^2 + c(V_E - V_{Em})^2 = 1 \quad .$$

(fps) (degrees) (fps)

La norme **MIL-A-8863A** (1974) conserve le principe de combinaison multivariable; elle l'étend d'ailleurs à huit paramètres qui sont les paramètres suivants :

vitesse d'approche, vitesse d'engagement, vitesse de chute, angle de roulis, angle de tangage, angle de lacet, taux de roulis, distance d'excentrement par rapport à l'axe de la piste.

Ces paramètres sont rassemblés et explicités le tableau (*Fig.4*) extrait de la norme.

VARIATION OF LANDING IMPACT CONDITIONS

Symbol	Variable	Type Landing	See Paragraph 3.11.2(a)	See Paragraph 3.11.2(b)(c)	See Paragraph 3.11.2(d)(e)(f)	See Paragraph 3.11.2(g)	See Paragraph 3.11.2(h)
		Type Airplane	CB	CB	CB, LB, SKI, STOL	LBT	VTOL/STOL
V_A	Approach Speed (KIAS)	$\bar{V}_A$	$1.05V_{P_{Amin}}$	$1.05V_{P_{Amin}}$	$1.05V_{P_{Amin}}$	$1.05V_{P_{Amin}}$	$1.05V_{P_{Amin}}$
		σ_{V_A}	4.0	8.0	8.0	8.0	8.0
V_E	Engaging horizontal ground speed, (KIAS)	$\bar{V}_E$	$\bar{V}_A - 20$	$\bar{V}_A$	$\bar{V}_A$	$\bar{V}_A$	$\bar{V}_A$
		σ_{V_E}	5.0	8.0	8.0	8.0	8.0
V_V	Sinking speed, (FPS)	$\bar{V}_V$	$0.139\bar{V}_E$ but not < 11.5	$0.0833\bar{V}_E$ but not < 6.0	3.0	8.5	$0.044\bar{V}_E + 7.5$
		σ_{V_V}	$0.018\bar{V}_E + 1.667$ but not < 3.0	2.0	1.33	2.0	$0.006\bar{V}_E + 2.5$
		α_3	0	0	-0.5	0	0
θ_P	Airplane Pitch angle, (DEG)	$\bar{\theta}_P$	See note (b)	See note (b)	See note (b)	See note (b)	See note (b)
		σ_{θ_P}	2.25	2.25	2.25	2.25	2.25
θ_R	Airplane roll angle, (DEG)	$\bar{\theta}_R$	2.0	2.0	2.0	2.0	2.0
		σ_{θ_R}	2.5	2.5	2.5	2.5	2.5
$\dot{\theta}_R$	Airplane roll rate (DEG/SEC)	$\bar{\dot{\theta}}_R$	0	0	0	0	0
		$\sigma_{\dot{\theta}_R}$	3.0	3.0	3.0	3.0	3.0
θ_Y	Airplane yaw angle, (DEG)	$\bar{\theta}_Y$	0	0	0	0	0
		σ_{θ_Y}	3.0	3.0	3.0	3.0	3.0
d	CG-Center engagement distance (FT)	$\bar{d}$	0	0	----	----	----
		σ_d	6	0	----	----	----
		P_R	1×10^{-3}	1×10^{-3}	1×10^{-4}	1×10^{-3}	1×10^{-3}
		P_T	7.0135×10^{-6}	7.0135×10^{-6}	1.0486×10^{-6}	1.0434×10^{-6}	1.0425×10^{-6}

Figure 4

La norme **MIL-A-8863B** qui remplace en 1987 la norme MIL-A-8863A emprunte la structure de cette dernière. Les modifications majeures qui sont faites ont trait au cas d'"atterrissage arrondi avec arrêt dans les brins" pour lequel la valeur moyenne, l'écart-type et le coefficient d'inclinaison (loi de Pearson) de la vitesse de chute sont redéfinis avec les probabilités associées correspondantes.

II COMPARAISON

Les normes AIR 2004 D, AIR 2004 E, MIL-A-8862A et MIL-A-8863A présentées succinctement dans le paragraphe précédent sont appliquées au SUPER ETENDARD et au MIRAGE 2000 afin d'évaluer leur influence sur les cas de charges, les efforts résultants et sur le dimensionnement et la masse des atterrisseurs.

L'accent est mis plus spécialement dans cette étude sur le MIRAGE 2000 et sur le concept multivariable développé dans la norme MIL-A-8863A.

II-1 CAS DE CHARGES POUR UN AVION EMBARQUE APPLICATION AU SUPER ETENDARD

La norme MIL-A-8863A examine la résistance d'un avion embarqué pour les types d'atterrissages ci-après :

I Posé-décollé et arrêt dans les brins sur porte-avions
II Posé-décollé et arrêt dans les brins sur terrains courts ou semi-préparés
Entraînement à l'appontage sur pistes préparées
III Atterrissage arrondi avec arrêt dans les brins sur pistes préparées
Atterrissage arrondi sur piste préparées
IV Atterrissage simulé par essais en laboratoire

L'analyse des cas de présentation (cas multivariable et cas forfaitaires d'atterrissage trois points, d'atterrissage cabré et d'engagement avant impact) est instructive.

Elle permet de balayer un grand nombre de cas et d'isoler ceux susceptibles d'être à l'origine de problèmes structuraux.

L'atterrissage "Posé-décollé et arrêt dans les brins sur porte-avions" conduit pour les cas les plus sévères à une valeur de vitesse de chute maximale de 7,64 m/s dans des configurations d'atterrissage cabré (centrage arrière), d'atterrissage trois points (centrage avant et angle de roulis égal à 0° et 2°) et pour un des cas multivariables.

En revanche, les cas de charges en ce qui concerne les atterrissages de type II et III sont moins sévères puisque les vitesses de chute maximales obtenues sont égales respectivement à 5,50 m/s et 3,05 m/s.

L'analyse des cas de présentation fait donc ressortir une différence importante (30%) entre la valeur de vitesse de chute la plus élevée obtenue avec la norme MIL-A-8863A (7,64 m/s) et la valeur retenue dans les Clauses Techniques pour le dimensionnement des atterrisseurs du Super-Etendard qui est de 5,50 m/s [1].

Il est probable qu'un tel écart se traduise par des efforts importants au niveau du train principal pour l'atterrissage cabré (centrage arrière) et des efforts importants au niveau du train auxiliaire pour l'atterrissage trois points (centrage avant).

Bien qu'aucun calcul d'efforts au sol suivant la norme MIL-A-8863A n'ait en fait été mené avec ces cas de charges, il est raisonnable de penser que l'application de cette norme remette en cause le dimensionnement des trains d'atterrissage du SUPER ETENDARD.

II-2 AVION TERRESTRE APPLICATION AU MIRAGE 2000

II-2.1 Cas de charges

La norme MIL-A-8862A impose l'étude des atterrissages pour une vitesse de chute limite de 3,05 m/s.

La norme MIL-A-8863A prend également en compte la résistance d'un avion de type avion terrestre. Les atterrissages définis dans la norme sont les atterrissages arrondis sur pistes préparées et atterrissages simulés par essais en laboratoire.

Une analyse des cas de présentation, analogue à celle faite pour le SUPER ETENDARD, est réalisée pour le MIRAGE 2000 et donne les résultats suivants.

---

[1] cette valeur est issue d'un compromis entre la norme anglaise Av.P.970 (Design Requirements for Aircraft for the ROYAL AIR FORCE and ROYAL NAVY) et la norme AIR 2004 D.

Les cas dimensionnants sont les suivants : appontage trois points, portance équilibrant les deux-tiers du poids pour le train d'atterrissage auxiliaire / appontage sur les atterrisseurs principaux queue basse et queue haute pour le train d'atterrissage principal)

Les cas de présentation à l'atterrissage (cas multivariable et cas forfaitaires d'atterrissage cabré) conduisent pour certains d'entre eux, c'est-à-dire pour les cas les plus sévères, à une vitesse de chute maximale de 3,05 m/s. Cette vitesse de chute est légèrement supérieure à la vitesse normale d'atterrissage définie dans la norme AIR 2004 D (2,8 m/s) qui a été prise comme valeur de référence pour le dimensionnement des atterriseurs du MIRAGE 2000.

II-2.2 Réponse de l'avion

Les cas de charges permettent de calculer les efforts et notamment :

- l'effort vertical au sol correspondant à l'instant où le coefficient de frottement pneu/sol atteint sa valeur maximale (sensiblement égal à l'effort au sol en cours d'enfoncement)
- l'effort vertical au sol maximal
- les efforts relatifs aux cas de ripé (intérieur et extérieur), de mise en rotation et de retour élastique.

La comparaison des efforts issus de l'application des différentes normes suggère des commentaires différents suivant qu'il s'agisse du train d'atterrissage principal ou du train d'atterrissage auxiliaire.

a) Train principal

Les tableaux et les graphiques présentés en *Fig.5.*, *Fig.6a/6b* et *Fig.7* relatifs au train principal du MIRAGE 2000 amènent diverses remarques.

La norme MIL-A-8863A donne un effort en cours d'enfoncement et des efforts de mise en rotation et de retour élastique comparables à ceux obtenus avec la norme AIR 2004 D. La différence la plus significative concerne l'effort au sol maximal (9%), l'effort latéral dans le cas de ripé intérieur (21%) et l'effort vertical dans le cas de ripé extérieur (11%)

La norme MIL-A-8862A est globalement légèrement plus sévère que les normes AIR 2004 D et MIL-A-8863A, cas de ripé mis à part.

La norme AIR 2004 E est la plus sévère des normes. Dans le cas du retour élastique et de la mise en rotation, les efforts au sol dépassent de 29 % les efforts correspondants, calculés à partir de la norme AIR 2004 D; dans le cas de ripé extérieur, l'écart est considérable puisqu'il est de 68%.

	ATTERRISSEUR PRINCIPAL
Effort en cours d'enfoncement suivant la norme MIL-A-8863A (atterrissage cabré) (en kN)	82,0
Effort en cours d'enfoncement retenu pour le dimensionnement (norme AIR 2004 D) (en kN)	79,8
Différence en %	3
Effort au sol maximal suivant la norme MIL-A-8863A (atterrissage cabré) (en kN)	135,0
Effort au sol maximal retenu pour le dimensionnement (norme AIR 2004 D) (en kN)	124,0
Différence en %	9

Effort au sol maximal suivant la norme MIL-A-8862A : 130,8 KN

Figure 5

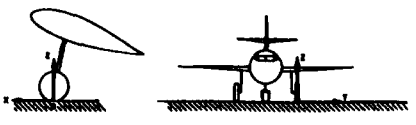

ATTERRISSEUR PRINCIPAL DU MIRAGE 2000

			NORMES APPLIQUEES			
			AIR 2004 D	AIR 2004 E	MIL-A-8862A	MIL-A-8863A
EFFORTS AU SOL en kN	MISE EN ROTATION	Fx	-63,8	-82,0	-71,3	-65,6
		Fy	0	0	0	0
		Fz	79,8	102,5	87,1	82,0
	RETOUR ELASTIQUE	Fx	51,8	66,6	57,2	55,3
		Fy	0	0	0	0
		Fz	79,8	102,5	105,0	85,0
	RIPE intérieur	Fx	0	0	0	0
		Fy	-42,3	-42,3	-35,7	-51,2
		Fz	90,4	108,4	44,6	64,0
	RIPE extérieur	Fy	42,3	42,3	26,8	38,4
		Fz	57,5	96,4	44,6	64,0

légende : Fx, Fy et Fz sont respectivement les efforts au sol suivant les axes X, Y et Z

Figure 6a

ATTERRISSEUR PRINCIPAL DU MIRAGE 2000

			AIR 2004 E	MIL-A-8862A	MIL-A-8863A
Efforts au sol : ECARTS PAR RAPPORT A LA NORME AIR 2004 D en %	MISE EN ROTATION	Fx	29	12	3
		Fy	/	/	/
		Fz	29	9	3
	RETOUR ELASTIQUE	Fx	29	10	7
		Fy	/	/	/
		Fz	29	32	7
	RIPE intérieur	Fx	/	/	/
		Fy	0	-16	21
		Fz	20	-51	-29
	RIPE extérieur	Fy	0	-37	-9
		Fz	68	-22	11

légende : Fx, Fy et Fz sont respectivement les efforts au sol suivant les axes X, Y et Z

Figure 7

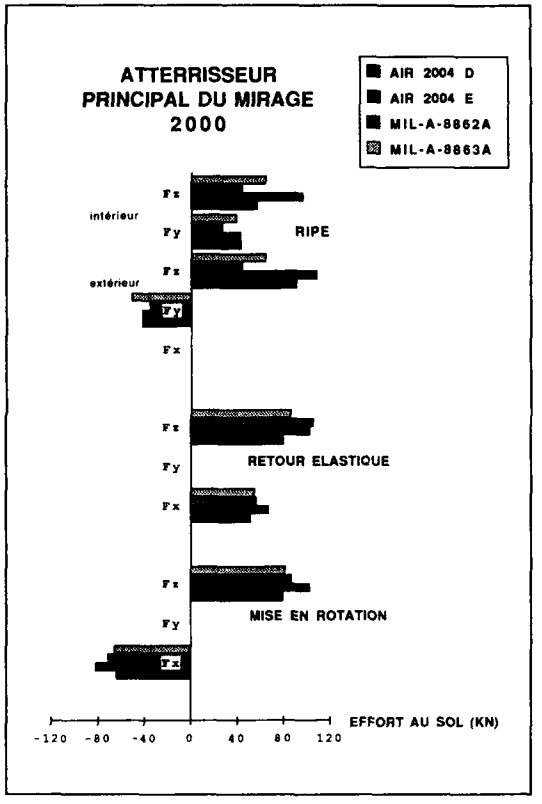

Figure 6b

b) Train auxiliaire

Les calculs ont trait dans cette partie au train auxiliaire du MIRAGE 2000 avec application des normes AIR 2004D et MIL-A-8863A. Les résultats sont intéressants.

L'effort en cours d'enfoncement (*Fig.8*) et les efforts de mise en rotation et de retour élastique (*Fig.9a/9b*) déterminés à partir de la norme MIL-A-8863A sont élevés.

Les cas de ripé sont très sévères; ils se distinguent par des efforts trois fois plus importants que ceux définis à partir de la norme AIR 2004 D.

	ATTERRISSEUR AUXILIAIRE
Effort en cours d'enfoncement suivant la norme MIL-A-8863A (atterrissage cabré) (en kN)	46,0
Effort en cours d'enfoncement retenu pour le dimensionnement (norme AIR 2004 D) (en kN)	37,2
Différence en %	24
Effort au sol maximal suivant la norme MIL-A-8863A (atterrissage cabré) (en kN)	77,0
Effort au sol maximal retenu pour le dimensionnement (norme AIR 2004 D) (en kN)	68,7
Différence en %	12

Figure 8

ATTERRISSEUR AUXILIAIRE DU MIRAGE 2000

			NORMES APPLIQUEES AIR 2004 D	NORMES APPLIQUEES MIL-A-8863A	Différence en %
EFFORTS AU SOL en kN	MISE EN ROTATION	Fx	-28,3	-36,8	30
		Fy	0	0	/
		Fz	35,4	46,0	30
	RETOUR ELASTIQUE	Fx	23,0	30,6	33
		Fy	0	0	/
		Fz	37,2	47,0	26
	RIPE intérieur	Fx	0	0	/
		Fy	-15,3	-15,4	0,01
		Fz	10,2	38,5	> 100
	RIPE extérieur	Fy	15,3	15,4	0,01
		Fz	10,2	38,5	> 100

légende : Fx, Fy et Fz sont respectivement les efforts au sol suivant les axes X, Y et Z

Figure 9a

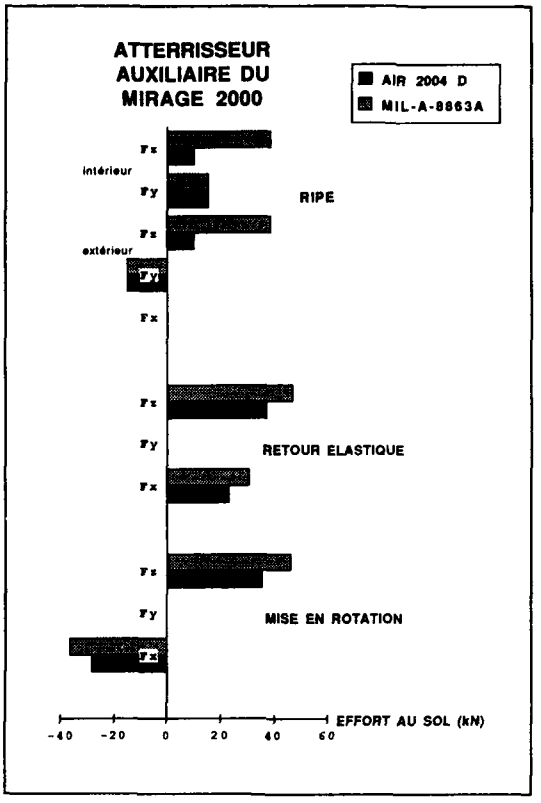

Figure 9b

II-2.3 Dimensionnement

Le dimensionnement de l'atterrisseur principal du MIRAGE 2000 a été réalisé vis à vis des charges obtenues par application des normes AIR 2004 D et MIL-A-8862A. Ce dimensionnement n'a pas tenu compte du cas "hors norme" de pointe d'effort au décollage.

Le bilan de masse résultant de ce dimensionnement fait apparaître un écart relativement faible entre l'atterrisseur principal du MIRAGE 2000 dimensionné suivant la norme AIR 2004 D et l'atterrisseur principal du MIRAGE 2000 dimensionné suivant la norme MIL-A-8862A *(Fig.10)*.

ATTERRISSEUR PRINCIPAL DU MIRAGE 2000

NORME APPLIQUEE	AIR 2004 D	MIL-A-8862A
MASSE DE L'ATTERRISEUR en kg	90,258	90,939
	0,80%	

Figure 10

Le bilan de masse global qui met en évidence une augmentation de poids de l'atterrisseur de 0,8% en "défaveur" de la norme MIL-A-8862A (i.e. cette norme conduit à un train plus lourd) est complété par une analyse pour chaque élément constituant le train d'atterrissage. Celui-ci révèle des différences sensibles en fonction de la partie considérée (*Fig.11*).

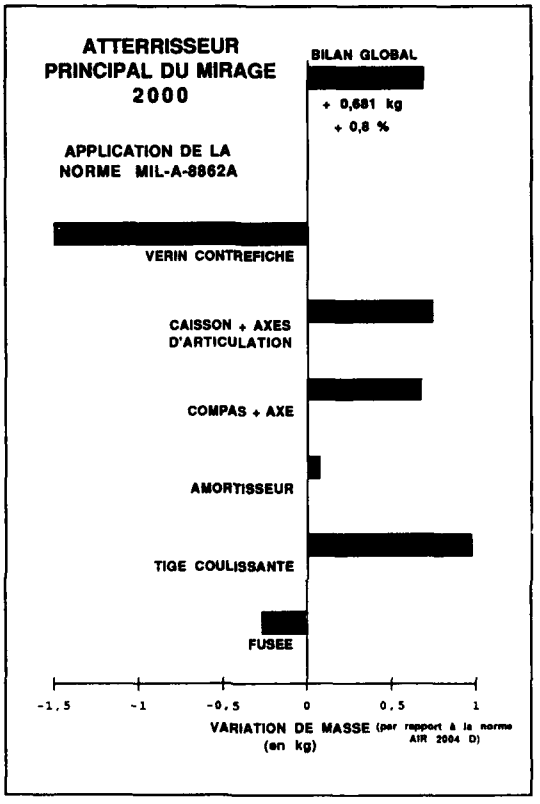

Figure 11

Compte-tenu de ce bilan de masse, et dans la mesure où les efforts déterminés à partir des normes MIL-A-8863A et AIR 2004 D sont proches, il est raisonnable de penser que le dimensionnement actuel du train d'atterrissage principal du MIRAGE 2000 ne devrait pas subir de modifications majeures par application de la norme MIL-A-8863A, et ceci même en cas de variation de conditionnement nominal de l'atterrisseur (pression d'air et volume d'huile de l'amortisseur, pression des pneumatiques) qu'impose la norme américaine.

En revanche, il est clair, à la vue des résultats présentés au paragraphe II-2.2, que le dimensionnement actuel du train d'atterrissage auxiliaire du MIRAGE 2000 serait remis en cause par l'application de la norme MIL-A-8863A.

CONCLUSION

L'étude comparative commandée par le Service Technique des Programmes Aéronautiques, dont rendait compte cette présentation, permet de mettre en évidence un certain nombre de points importants.

Le premier d'entre eux concerne les conclusions auxquelles conduit l'application de la norme MIL-A-8863A. Ces conclusions sont différentes suivant la nature de l'avion considéré (avion marin: SUPER ETENDARD et avion terrestre: MIRAGE 2000).

En effet, les exigences de la norme MIL-A-8863A se traduisent par une remise en cause du dimensionnement de l'atterrisseur auxiliaire et de l'atterrisseur principal du SUPER ETENDARD alors qu'elles n'affectent pas significativement le dimensionnement de l'atterrisseur principal du MIRAGE 2000.

Le second point intéressant porte sur les normes MIL-A-8862A et AIR 2004 D et concerne plus particulièrement l'influence de ces normes sur le bilan de masse total de l'atterrisseur principal du MIRAGE 2000.

L'écart de poids entre l'atterrisseur principal du MIRAGE 2000 dimensionné d'après la norme AIR 2004 D et le même atterrisseur dimensionné d'après la norme MIL-A-8862A est faible. Les répercussions sont donc relativement peu importantes du point de vue du bilan de masse total.

L'intérêt que revêt le concept multivariable contenu dans la norme MIL-A-8863A et conservé dans la norme MIL-A-8863B doit être souligné. Il constitue le troisième point clef de l'étude.

Ce concept permet une description plus souple des cas d'atterrissage puisque les conditions initiales d'impacts ne sont plus figées mais sont données sous la forme d'une combinaison multivariable de plusieurs paramètres. En fait, il offre surtout l'avantage de définir les cas d'atterrissages de façon plus rationnelle et plus proche des situations réelles.

L'étude montre toutefois la nécessité de choisir correctement les valeurs de base du concept multivariable (la vitesse d'approche minimale en atmosphère tropicale par exemple) et l'obligation pour cela d'avoir recours à des campagnes d'essais ou à des informations suffisamment fiables et représentatives.

ANNEXE

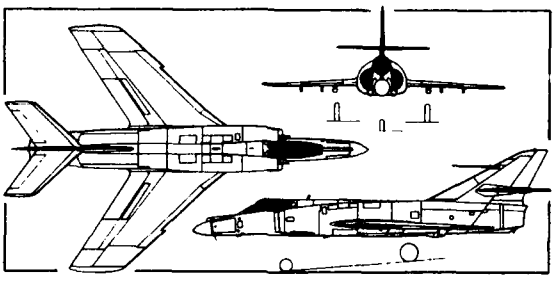

Dassault-Breguet Super Etendard

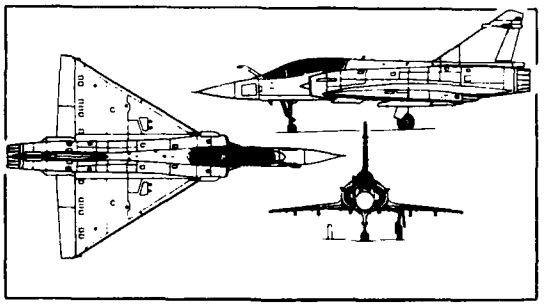

Dassault Aviation Mirage 2000

DEVELOPMENT OF UNDERCARRIAGE DESIGN LOADS

by
G Kempf
MBB-UF
Munich
Germany
and
G H Haines
Manager Product Development & Research
DOWTY AEROSPACE GLOUCESTER
Cheltenham Road
Gloucester GL2 9QH
UK

SUMMARY

During the different phases of development from feasibility studies to the final design, the landing gear designer applies increasingly refined methods of analysis to derive the loads to which the system is designed. Future design procedures should reflect such a staged approach leading to designs which are fully optimised with the aid of rational methods of analysis to meet the complete range of aircraft operating conditions.

Based on experience gathered from various projects the design process is described. Comparisons are made of design load cases obtained using current landing gear requirements and those derived by rational analysis. These comparisons are made for the critical phases of landing touchdown, derotation onto the nosegear, landing roll out, repaired runway operation, etc. The application of the rational method of analysis to determining aircraft operating envelopes under asymmetric landing conditions is also discussed.

Finally areas of work are identified which need addressing further, in order that a staged approach can be adopted completely in the future military landing gear design procedures.

1. INTRODUCTION

A staged approach for landing gear design, which runs in parallel and in phase with that used for the aircraft is required in order to achieve an optimum design for the complete system. In the Feasibility Stage, the aircraft design criteria must be formulated, the basic design data for the landing gear determined, and possible configurations of the landing gear studied. At this stage a rapid method of deriving initial design loads on an empirical and an arbitrary basis is required. The second stage, or Initial Design, requires firmed up data and should utilise a 'rational' form of analysis to examine in detail the design load conditions which are critical for the landing gear and aircraft attachment structure. Rational analysis enables actual optimisation of the shock absorber characteristics to be made at this time. In the third stage, or Final Design phase, the structural design and shock absorber characteristics are fully optimised using a refined rational analysis taking account of the full range of design, fatigue and extreme conditions for the landing gear as well as the realistic operating requirements of the aircraft.

Experience gained from applying such an approach in a number of recent projects is used to illustrate where the results of the rational method differ from the current 'arbitrary' conditions of existing design requirements. The examples considered show sufficient differences in some basic design cases to recommend a review of current arbitrary requirements and the need for consideration of a more formal requirement for rational analysis.

2. DESIGN PROCESS

A staged design process for the landing gear in parallel and in phase with that used for the aircraft is required to achieve an optimum total system design. The design process breaks down into three discrete stages, Feasibility Studies, Initial Design and Final Design.

2.1 Feasibility Studies

In the first stage of the design process the following areas of activity must be addressed:-

- compilation of Design Criteria consistent with the operational requirements of the Aircraft (short field, repaired runway etc.)

- identification of devices which may influence landing gear design loads (arrestor system, take-off assistance etc.)

- evaluation of proposed landing gear layouts (track, wheelbase, height etc.)

- compilation of initial design loads using 'arbitrary' cases of current requirements

- initial estimation of landing gear system characteristics (shock absorber spring and damping, tyre size etc.).

During this Feasibility Design phase many configuration options need to be considered for both the aircraft and landing gear design, therefore it is important that a rapid but realistic assessment of design loads can be made. Even at this stage it may be feasible with today's computing facilities to determine basic design loads by dynamic analysis in order to provide better accuracy in configurational studies.

2.2 Initial Design Phase

The initial design phase includes the following activities:-

- Finalisation of design configurations of aircraft, landing gears etc.

- Update of design criteria

- Update of design data for the aircraft (mass, centre of gravity, aerodynamics etc.) and for the landing gear (mass, stiffness, wheel tyre and brake data etc.).

- Use of dynamic analysis to derive design loads by rational rather than arbitrary methods especially for conditions leading to critical design loads for landing gear or aircraft structure.

- Definition of rational conditions in terms of steady state pre-conditions and dynamic transients for each of the possible critical cases including landing impact, dynamic braking, retardation by arrester device, traversing runway obstacle or repair.

- Optimisation of landing gear shock absorber characteristics and structural stiffness to produce a balanced set of design loadings for the gear and aircraft attachment structure including both limit and ultimate conditions.

- Determination of fatigue loads.

During this phase the envelope of design conditions is arrived at using the 'firmed up' information for aircraft and landing gear configuration. A 'rational' analysis method is used rather than an arbitrary approach particularly for those conditions which lead to critical design cases for the landing gear or aircraft structure.

2.3 Final Design Phase

The last phase of the design process includes the following activities:-

- Refinement of the defined rational conditions and final optimisation of the landing gear shock absorber damping and stiffness characteristics to achieve:-

  - the required operational envelope for the aircraft

  - optimum balance of the various design loads

  - minimum weight of the landing gear and attachment structure

- Determination of the aircraft operational envelopes within the limits set by landing gear strength:

  - for landing, permissible combinations of aircraft weight, sink rate roll, yaw, etc.

  - for taxiing on repaired runways, permissible combinations of weight, speed, repair height, repair spacing, etc.

- Determination of final design loads including limit, fatigue and ultimate.

- Consideration of deviations from traditional design methods (eg. reduction in ultimate factor 1.5).

- Finalisation of fatigue operating conditions (aircraft weight, sink rate and pitch rate distribution, etc.).

In this final phase of design, in addition to ensuring that the design is fully optimised to best meet the requirements, the aircraft operational envelope should be fully explored theoretically prior to subsequent practical demonstration by rig, ground and flight testing as hardware becomes available.

3. DEVELOPMENT OF IMPROVED METHODS OF CALCULATION OF DESIGN LOADS

To illustrate the extent to which improved 'rational' methods for the calculation of landing gear design loads may be applied and to make comparisons with the 'arbitrary' cases of current requirements, a number of examples are considered below which relate to typical fighter type aircraft and reflect experience gathered from a number of recent projects. The examples cover the range of arbitrary design conditions such as landing, taxiing, braking, etc. and where possible direct comparisons are made between the arbitrary and rational approaches.

3.1 Landing Touchdown

This is the condition applying to maingear impact. To make possible the calculation of landing touchdown loads it is first necessary to transform aircraft operational performance requirements into landing touchdown conditions. This means expressing such things as aircraft configuration, approach path, field length, crosswind and runway condition in terms of touchdown parameters like aircraft mass and inertia, lift ratio, sink rate, landing speed, pitch roll and yaw angles, etc.

This can be done by modelling the complete aircraft as a six degree of freedom system, with fully representative aerodynamics and setting up the appropriate touchdown condition as a trimmed or balanced condition with lift equal to weight, zero pitch moment etc. The complete aircraft model can then be used to generate in a 'rational' manner the conditions corresponding to specific 'arbitrary' cases. The landing gear system must also be modelled with proper representation of the shock absorber spring, damping and friction components, the flexible structure of the gear and attachments, the wheel and tyre assembly dynamics and the wheel spin-up process under the influence of a slip dependent tyre/ground friction coefficient which gives rise to drag and spring-back forces usually critical for the design of the complete system.

A number of features emerge from using the rational approach for the landing touchdown which should be taken into account in reviewing the validity of current arbitrary design conditions.

i) Today's fighter aircraft touchdown at relatively high nose-up angles and the 'three-point' attitude of the arbitrary cases is an abnormal condition.

ii) Time varying lift forces due to the sudden decrease in the angle of incidence caused by rapid sink rate reduction, to aircraft pitch rotation and to lift dumping devices during the impact phase can significantly increase the energy to be absorbed by the landing gear compared with the arbitrary consideration of lift equal to aircraft weight during the whole landing impact phase. (See Figure 1)

iii) Spin-up and spring-back forces should be derived using a representative model of the flexible gear and support structure together with a slip dependent tyre to ground friction relationship with a maximum value of 0.8. (See Figures 2 and 3).

iv) Tyre side forces induced by side slip due to aircraft yaw, roll or lateral velocity or by deflection of the landing gear can lead to design load combinations more severe than those derived from the arbitrary design conditions. These are often more severe on the second gear to touchdown in an asymmetric landing. (See Figures 4, 5 and 6).

v) Asymmetric landings involving relatively small amounts of roll or yaw can significantly reduce the sink rate capability where the gear has been designed to a symmetric landing only. Consideration should therefore be given to the inclusion in landing gear design requirements of an asymmetric condition with specified values of sink rate and roll and yaw angles.

vi) Final optimisation of shock absorber characteristics and possibly structural stiffnesses should aim at producing a 'balanced' set of landing gear design loads, ie. of relatively equal severity. These should include typical (fatigue), design (limit) and extreme (ultimate) conditions.

3.2 Landing De-Rotation

This is the condition applying at nosegear impact with the ground. As already indicated the normal condition for most modern fighter aircraft is for the main gears to touchdown with the aircraft in a nose-up attitude, this is followed by a period during which the aircraft pitches under the influence of aerodynamic and ground forces until the nosegear impacts the ground. This period of pitching onto the nosegear can be long compared with that of maingear energy absorption and the influences of the changing pitch attitude and aircraft lift are therefore correspondingly greater on the nosegear energy absorption requirements. Additionally during this interim period between maingear and nosegear impact landing procedures such as pilot selected or

automatic de-rotation, drag chute deployment or reverse thrust selectors can play an even more influential role. All these events must be properly modelled to arrive at the initial conditions and time varying forces and moments required to rationally predict nosegear design loads.

From the use of a rational approach to the analysis of the nosegear impact the following points emerge which are considered relevant to a review of the arbitrary defined requirements.

i) The 'vertical' velocity at nose landing gear impact is made up of translational and rotational components, the translational component bears little relationship to the design sink rate for the aircraft and the rotational component is largely due to automatic and pilot induced landing procedures which can depend upon the particular type of landing being performed (eg. short field). (See Figure 7).

ii) The lift at nose landing gear impact is probably near to zero through a combination of the instantaneous aircraft attitude and the fully deployed lift dumping devices.

iii) Spin-up and spring-back forces should be derived using a representative model of the landing gear and support structure together with a slip dependent tyre to ground friction relationship with a maximum value of 0.8.

iv) For nosegear design asymmetric landing conditions are generally of much less significance than the effect of de-rotation procedures referred to above.

v) Optimisation of the shock absorber characteristics should be made using both the most critical of the rationally derived de-rotation conditions and the typical fatigue conditions and should aim to produce a balanced set of design cases, principally for vertical and drag loads in typical, design and extreme landings.

3.3 Landing Roll-out

This is the condition covering the decelerating transition from landing touchdown and de-rotation to steady taxiing and is likely to affect nosegear loads particularly. Any retardation devices such as drag chutes, thrust reversers or mainwheel brakes need to be included in a rational analysis of this phase with particular attention paid to their time dependence, both their sequence and rate of application. (See Figure 8).

The following are likely to be of significant influence to the landing gear loads.

. Aircraft configuration (particularly weight and centre of gravity position) which will determine the base level load on the gear.

. Steady incremental loads (associated with retardation devices)

. Rate of application of retardation devices which will influence the dynamic magnification factor associated with application of the incremental load.

Operational procedures for the aircraft will lead to definition of typical, design and extreme conditions for this phase and the optimisation of shock absorber characteristics, particularly recoil damping and nosegear compression damping should take these fully into account. Indications obtained from adopting a rational approach are that the arbitrary braking cases of present requirements do not always adequately cover loads resulting from realistic combinations of thrust reversers, wheel brakes, etc.

3.4 Take-off Run

This condition represents the accelerating take-off run and should include the sequence of events from brake release to take-off rotation.

The phase of the take-off run most likely to benefit from use of a rational analysis approach seems to be at the point of aircraft rotation, where aerodynamic forces can lead to significant incremental maingear loads being developed. These could become critical for landing gear design if taken in combination with runway obstacle traversing considered in section 3.6 below.

3.5 Ground Manoeuvres and Handling

The various existing landing gear requirements include design cases for a range of ground manoeuvring and handling conditions which evolve from a vast amount of experience and have been shown to be realistic by application on many different types of aircraft. Of the many conditions covered two are worthy of further consideration in the context of a rational method of analysis.

Firstly, the condition of sudden braking which needs not necessarily occur in the landing roll out phase (3.3 above) but could be associated with very slow taxi speeds. Adverse phasing of the aircraft pitch frequency and the time to develop peak brake torque can lead to transient loads on the nosegear in excess of those derived from the

arbitrary approach. However, by including a rational analysis of the condition in the shock absorber damping optimisation process, it is usually possible to keep the loads arising from this case within the envelope of other design cases.

Secondly, for the turning condition arbitrary requirements are based on a lateral acceleration level of 0.5 g which can lead to landing gear design conditions particularly for multi-wheel configuration maingears on large aircraft. It is suggested that use of an analysis which properly accounts for the taxiing manoeuvres and the rational distribution of tyre forces on multi-wheeled gears consistent with the associated roll and yaw, could lead to a reduction in severity of design loads for this case.

3.6 Repaired Runway Operations

The inclusion of repaired runway operations is a relatively recent addition to most landing gear design requirements. There is therefore little or no background of arbitrary approach against which to evaluate the advantages of rational analysis. Further it is the one area to which some form of rational analysis has been employed from the outset probably because the complexity of the problem makes it difficult to break down into equivalent arbitrary conditions.

Care is needed when defining the aircraft operational requirements on repaired runways since the super-position of runway repairs and the most severe of the design cases discussed above will obviously produce design cases of increased severity. Consideration needs to be given therefore to which, if any, of the above operating phases needs to be associated with damaged or repaired runways and whether some combinations of repaired runway crossing and certain of the above manoeuvres could be treated as extreme cases subject to reduced design strength factors.

The use of rational analysis is essential to determine the influence of runway repairs on landing gear design loads. In addition to the modelling requirements already described the repair profile and tyre model must be fully representative and the integration procedure must be capable of retaining sufficient accuracy of solution during the very rapid discontinuities associated with crossing repairs at high speed.

A design load investigation should include the following conditions in order to determine their influence on landing gear design.

- Single and multiple repairs with realistic variations of repair height, repair spacing and aircraft speed. (See Figure 9).
- Super-position of single and adversely spaced repairs with steady state conditions such as braking or reverse thrust.
- Super-position of single and adversely spaced repairs with landing and de-rotation phases using typical values of significant parameters such as sink rate and pitch rate. (See Figure 10).
- Super-position of single and multiple repairs with the extreme cases from the various phases in 3.1 to 3.5 above.

Experience to date suggests:-

i) By including repair capability from the outset in the design optimisation of landing gear shock absorbers a good capability can be achieved with relatively small penalty to the design especially when ultimate obstacle heights are considered.

ii) Superimposing repair capability on top of every existing design condition will severely penalise the landing gear design.

iii) The most damaging design conditions result from the super-position of repair requirements and landing, de-rotation, or take-off rotation phases which produce particularly severe increments in vertical and drag (spin-up and spring-back) load combinations.

4. FURTHER APPLICATIONS OF THE RATIONAL APPROACH

The preceding section 3. shows that existing methods of rational analysis can be applied to the various design conditions of the arbitrary method of deriving landing gear design loads to illustrate the differences between the two procedures. A further extension to the use of the rational approach is to examine the basis of the typical, design and extreme conditions used to determine fatigue, limit and ultimate loads respectively.

Existing requirements typically specify the landing gear design conditions in terms of sink rate (typically 12 fps or 3.7 m/s) pitch angle range, aircraft lift equal to weight and zero angles of roll and yaw. These specified conditions define the energy to be absorbed, from which design loads (limit) can be generated. These design loads include drag loads due to wheel spin-up and sideloads from an arbitrarily defined

lateral drift case derived from the maximum vertical load. Together with other non-landing conditions covering braking and turning these loads determine the landing gear basic strength level.

In a rational analysis values of parameters other than those specified for the design conditions can be examined to determine their influence on gear loads and maybe for their restrictive influence on aircraft performance, where the rationally derived loads exceed gear strength capability. Such use of rational analysis has identified at least two areas where further examination is suggested.

First is the case for inclusion of asymmetric landing conditions in current design requirements. It has been found that introducing typical values of roll and yaw into a rational analysis of the landing condition, which already includes effects such as lift reduction due to aircraft rotation, etc., can lead to sideloads in excess of the arbitrary design levels. Further the reduction in sink rate required to compensate for these asymmetries can be quite restrictive on the aircraft's operating envelope (sink rate reduction 3.7 m/s to 3.2 m/s).

Increasing the roll and yaw values to correspond to maximum crosswind landing levels can lead to even greater restrictions on the operating envelope (typically 3.2 m/s to 2.6 m/s), a level which may be incompatible with aircraft short field approach procedures.

Secondly, it can be shown that the loads resulting from rational analysis with parameter values appropriate to extreme (or ultimate) conditions are generally below the level of the 1.5 ultimate factor specified in some requirements. This suggests that ultimate strength factors could be reduced where it can be shown that predicted loads for extreme conditions are less than 1.5 times limit loads.

Any such approach should give due consideration to the following:-

- Extreme conditions need to be defined in terms of agreed combinations of all relevant parameters including roll, yaw and crosswinds in addition to sink rate, lift ratio, etc.
- The sensitivity of predicted extreme loads to effects such as bottoming or impaired functioning of shock absorbers or tyres should be fully explored. Since the probability of occurrence of such effects is increased near to the boundaries of design performance.
- The benefits of a design approach involving reduced ultimate strength factors and the consequent increased risk of structural failure should be assessed against the alternative of designing to ensure continued functioning of the shock absorber at extreme conditions as in some helicopter requirements.

5. CONCLUSIONS

5.1 The need for a rapid method of deriving initial design loads on an 'arbitrary' basis will continue to exist and consideration should therefore be given to the validity of the currently defined landing gear design cases of some requirements.

5.2 The comparisons made in section 3 highlight some differences in landing gear design loads derived from the 'arbitrary' method of existing requirements and a 'rational' analysis method taking account of all the relevant parameters for the various design conditions.

5.3 The value of a 'rational' method of analysis is very clear both determining landing gear design loads and aircraft operating envelopes, and consideration should be given to making this a more formal requirement for landing gear design.

5.4 Further work in the areas listed below is considered necessary in order to apply completely the staged approach to future military landing gear design procedures.

- Asymmetric landing cases for the landing gear design
- Realistic operating envelopes for the aircraft landing conditions
- Operational requirements relating to damaged or repaired runways
- Designing for extreme or ultimate conditions

5.5 Future undercarriage design work should be based on the so called staged design approach with increasingly refined methods of calculation dependent on the design phase. Arbitrary cases should be refined by rational cases. Single design conditions should be refined by super-position and sequences of steady and transient conditions simulated by means of rational methods.

LIFT DECAY DURING MAINGEAR IMPACT

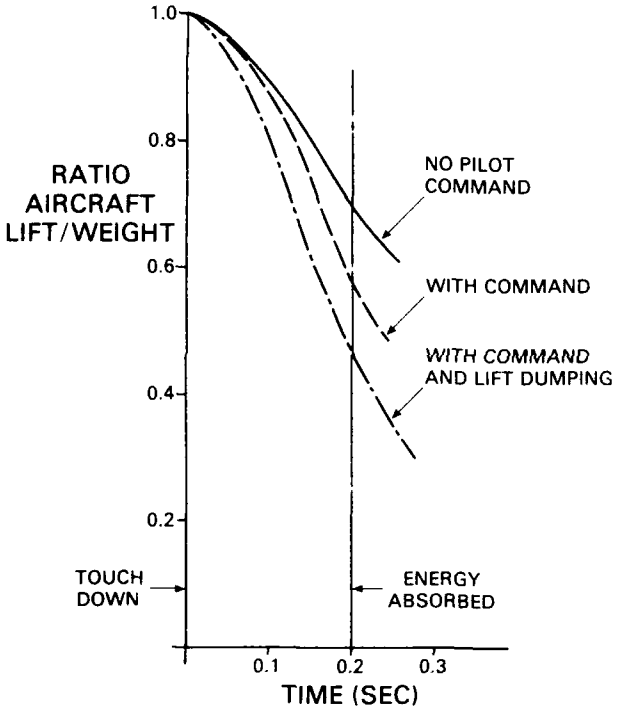

FIGURE 1

SIMPLIFIED SLIP DEPENDENT TRACTION COEFF. OF FRICTION

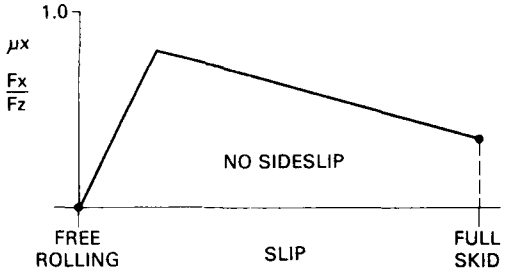

LATERAL VERSUS TRACTION COEFF. OF FRICTION

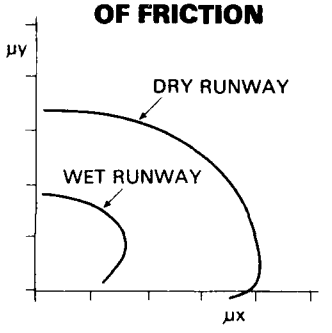

LATERAL VERSUS TRACTION COEFF. OF FRICTION AND TYRE SIDESLIP ANGLE

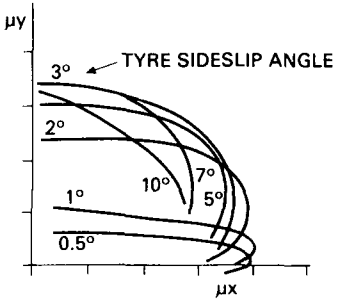

FIGURE 2

SYMMETRIC LANDING RATIONAL ANALYSIS

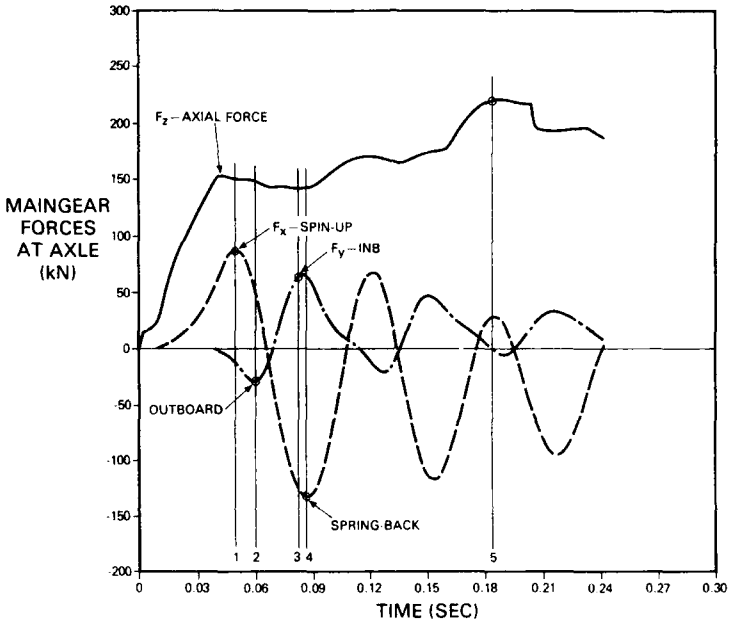

DESIGN LOAD CONDITION	ARBITRARY (kN)	RATIONAL (kN)
1. SPIN-UP	84	86
2. OUTBOARD SIDE FORCE	66	55
3. INBOARD SIDEFORCE	88	67
4. SPRING-BACK	135	135
5. VERTICAL	220	220

FIGURE 3

RATIONAL ANALYSIS
ASYMMETRIC LANDING TIME HISTORY

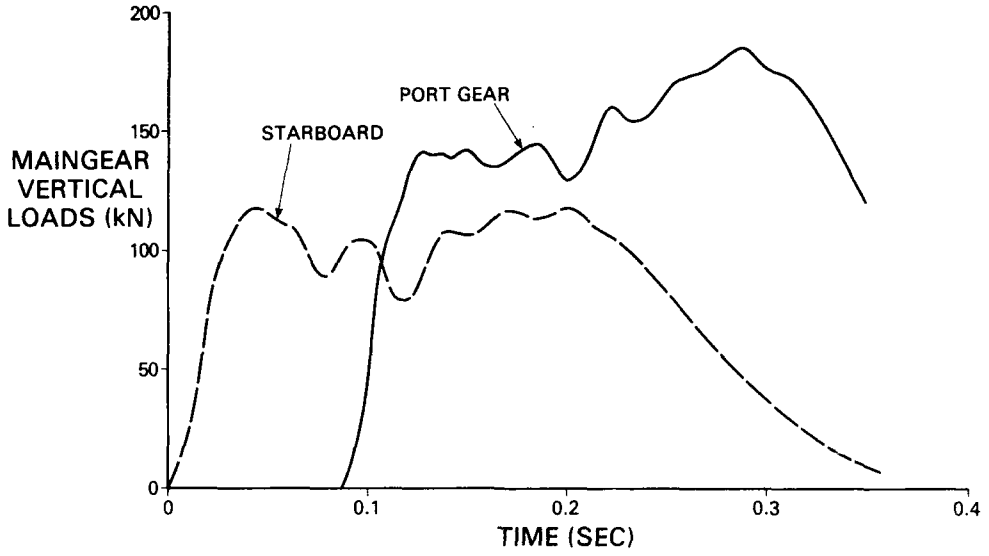

FIGURE 4

RATIONAL ANALYSIS
ASYMMETRIC LANDING TIME HISTORY

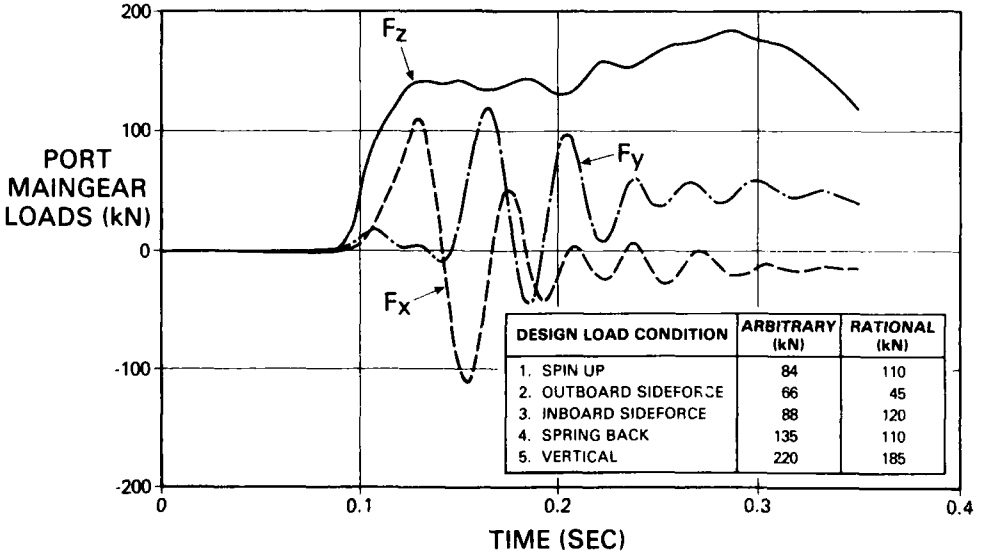

DESIGN LOAD CONDITION	ARBITRARY (kN)	RATIONAL (kN)
1. SPIN UP	84	110
2. OUTBOARD SIDEFORCE	66	45
3. INBOARD SIDEFORCE	88	120
4. SPRING BACK	135	110
5. VERTICAL	220	185

FIGURE 5

RATIONAL ANALYSIS
ASYMMETRIC LANDING MAINGEAR LOAD SIGNATURE

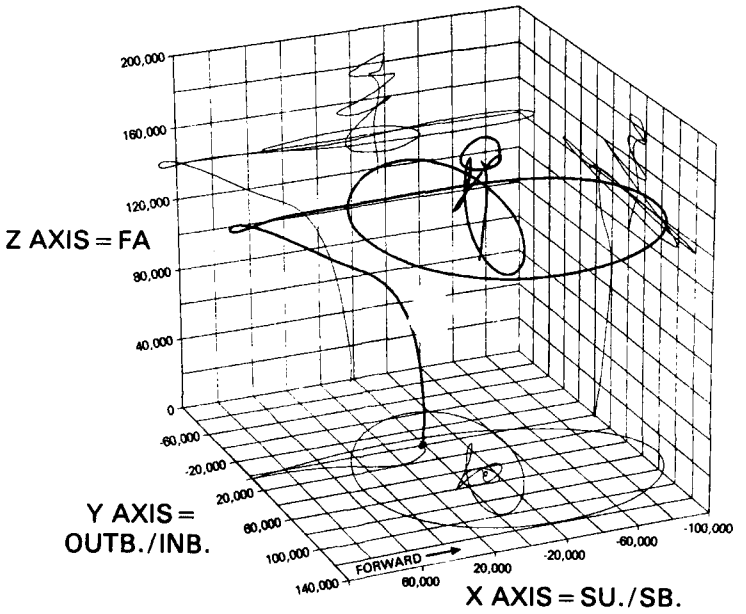

PORT GEAR COMBINED X,Y,Z LOADS (N)

FIGURE 6

RATIONAL ANALYSIS LANDING DEROTATION

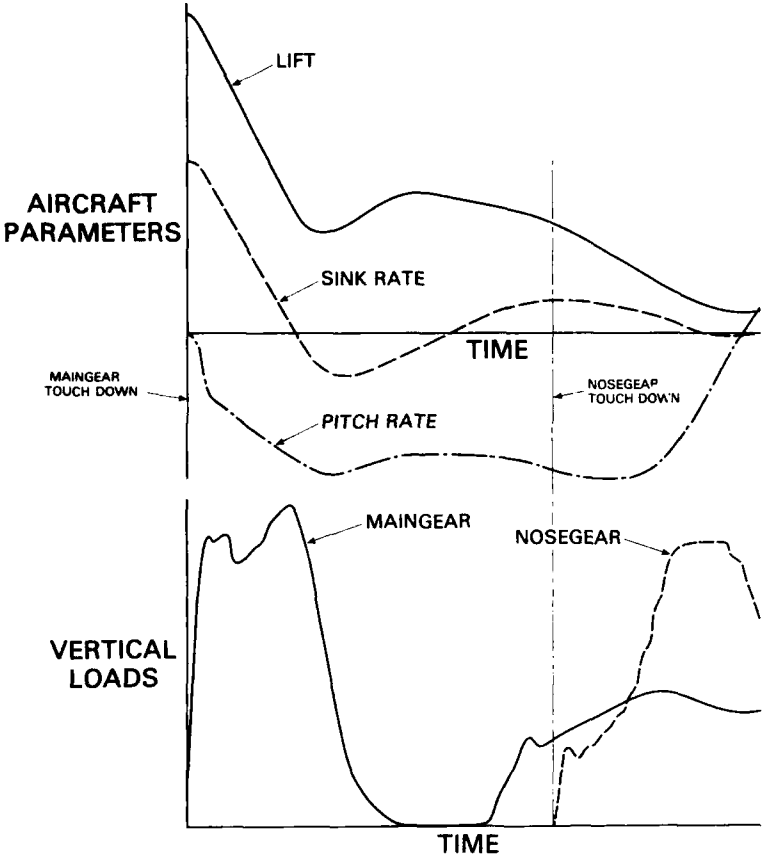

FIGURE 7

RATIONAL ANALYSIS OF LANDING WITH THRUST REVERSAL AND MAINWHEEL BRAKING

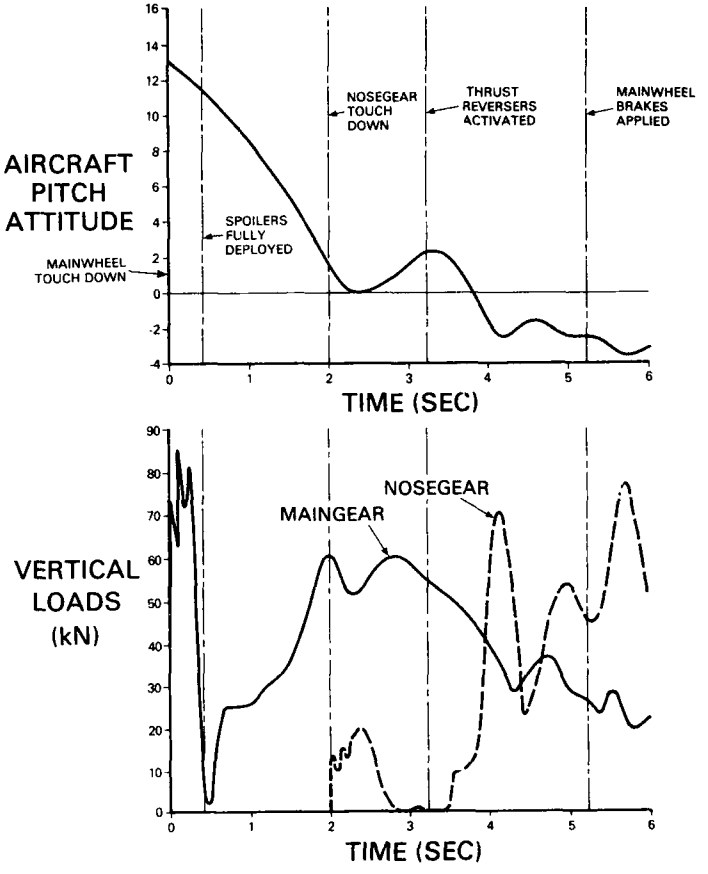

FIGURE 8

TAKE-OFF RUN ADVERSE REPAIR SPACING

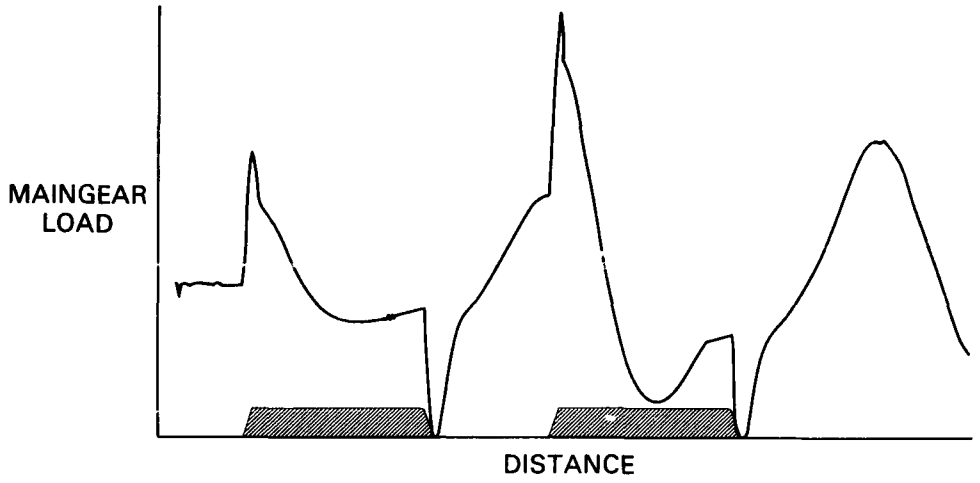

FIGURE 9

LANDING DEROTATION AND TRAVERSE OF RUNWAY REPAIR

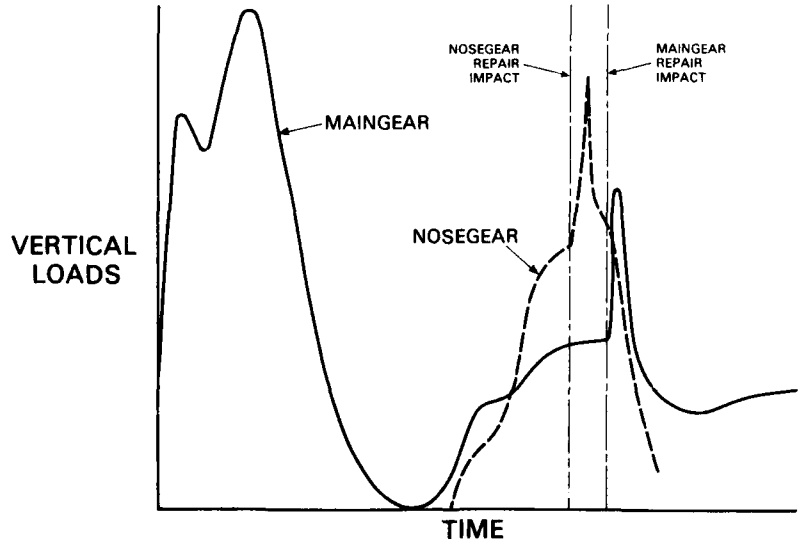

FIGURE 10

RECENT DEVELOPMENTS IN THE AREA OF AIRCRAFT ROUGH FIELD PERFORMANCE

David Morris, Senior Project Engineer
WRDC/FIVM
Tony Gerardi, Chief Engineer
WRDC/FIBE
Wright Research and Development Center
Wright-Patterson AFB OH 45433

SUMMARY

Under Project "Have Bounce" (HB), the USAF successfully determined the level of surface roughness that could be tolerated by most aircraft in the inventory. The runway roughness capability of each aircraft was determined by developing a sophisticated computer model of each aircraft. In most cases these computer models were validated with aircraft tests on rapidly repaired runways. This multimillion dollar effort has resulted in the definition of surface roughness criteria (repair criteria) for each aircraft. The knowledge gained as a result of all of the testing and computer modeling has led to a much more thorough understanding of the complex interaction between the flexible structure, landing gear, and rough pavement.

The first part of this paper discusses the development, laboratory qualification testing, and taxi testing of an improved F-15 rough field landing gear which provides a significant improvement in rough field and sink rate performance over the existing F-15 landing gear. This landing gear design utilizes passive, internal strut modifications to achieve this performance without any effect on reliability and maintainability. The second part of the paper discusses the advantages of an automated Personal Computer (PC) based process for selecting the minimum operating strip (MOS) and for determining the minimum level of runway repair required. As backup to this automated approach, a novel technique for quantifying the ability of a given aircraft to traverse rough surfaces is also discussed. This method assigns a "Vulnerability Index" (VI) to each aircraft. The VI is a reflection of the aircraft's ability to absorb the energy that is transmitted from the pavement to the struts and the airframe. This method will give the base commander a tool for making good "intuitive" decisions in the event that the automated process cannot be used. It can also be used as a validation technique for the automated method.

F-15 ROUGH FIELD LANDING GEAR

Landing gear designs of the past 40 years have stressed efficiency in weight and volume, and performance with respect to landing impact loads. While landing impact performance has been adequately addressed in landing gear designs to date, load alleviation following landing impact and during taxi and takeoff has received much less emphasis. Some production landing gear designs have been developed which provide a rough pavement capability, but these typically resulted in an adverse effect on weight and volume. Several rough pavement landing gear designs have been laboratory tested, but most of these either provided minimal improvement or were not easily incorporated without affecting weight, volume or reliability/maintainability.

Enhancements in the area of computer modeling, particularly the change in overall aircraft response to rough pavement due to changes in landing gear characteristics, have resulted in a significant improvement in the ability to balance a landing gear design to provide both excellent landing impact and rough pavement characteristics. In addition, an improvement in laboratory testing capability through the utilization of a computer driven hydraulic shaker has greatly improved both the speed and accuracy of computer model validation. Exact rough runway profile shapes at various simulated forward speeds can be input directly to the landing gear in a drop tower and the resulting landing gear response measured. The combination of enhanced computer modeling techniques and laboratory testing capability coupled with extensive landing gear design experience has resulted in the development, fabrication and very successful laboratory and flight testing of an improved high sink rate rough field landing gear system for the F-15 aircraft.

Development of this particular landing gear design was initiated by the Cleveland Pneumatic Company (CPC) in response to Air Force interest and efforts in this area. CPC's approach was to utilize passive design concepts in order to minimize any adverse complexity, and resulting effect on reliability and maintainability. They utilized their experience in oleo relief valves and multiple stage air curves along with an extensive landing gear dynamic response model to arrive at designs for both the main and nose landing gears with essentially the same predicted reliability as the existing F-15 landing gears. All modifications to the landing gears were internal and consisted of replacement of several internal components without requiring any modifications to either the outer cylinder or piston. In the 1984/85 time period, the improved main and nose designs were subjected to a series of simulated rough runway tests at the Air Force's Landing Gear Development Facility (LGDF) which verified the enhanced performance offered by the new designs.

The STOL and Maneuver Technology Demonstration Program (STOL/MTD) contract was awarded to McDonnell Douglas in October 1984 with the F-15 aircraft selected as the

demonstrator vehicle. In addition to demonstration of 2-dimensional thrust vectoring/reversing nozzles, integrated flight/propulsion control, and advanced pilot vehicle interface, the demonstrator was to have a landing gear capable of both rough field (multiple 4.5 inch bumps at 80 foot minimum spacing as well as a 5 inch 1-cosine shaped dip of 50 foot length) and increased sink rate (12 ft/sec) operation. The CPC landing gear design was chosen for this program in March 1986, having already demonstrated the bump capability and requiring only minor modifications to achieve the increased sink rate performance.

LABORATORY QUALIFICATION TESTING

The nose landing gear was successfully qualification tested at the LGDF in September 1986. The test weights were based upon a STOL/MTD aircraft takeoff weight of 50,000 pounds and a landing weight of 35,000 pounds. While the takeoff weight was less than that of an F-15 C/D (68,000 pounds), the landing weight was the same as an F-15 C/D. Drop tests were conducted utilizing both wheel spin-up and simulated wing lift. Even at a 14.1 ft/sec sink rate, the loads were well below limit values as can be seen in Figure 1. The energy absorbed at this sink rate was twice that to which the landing gear was designed as the energy absorbed is proportional to the sink rate velocity squared.

Rough runway laboratory testing was conducted in a drop tower with a hydraulic shaker providing a simulation of ground profile traversal at simulated forward speeds of 30, 50, 70, 90, 110, 120, and 146 knots. Ground profiles that were simulated included a 5 inch 1-cosine shaped dip of 50 foot length, multiple 3 and 4.5 inch bumps with an 80 foot spacing, and a single 7 inch bump. These profiles are shown in Figure 2. As can be seen in Figure 3, the peak gear loads for all of the rough runway tests were significantly below the design limit load for the nose landing gear. Although testing of the nose landing gear to the limit load would have provided an assessment of the maximum allowable bump height, the fact that this particular landing gear was to be utilized on the STOL/MTD flight test aircraft precluded such tests. A final test for the nose landing gear was a sudden free extension test which verified the improved rebound damping. Post test inspection revealed that no damage or deformation of either external or internal components resulted from the qualification testing.

The main landing gear was then successfully qualification tested in the January/February 1987 time period. The nine inch stroke of the main landing gear constrained the improvement in landing impact sink rate as compared to the sixteen inch stroke of the nose landing gear, but a 12.5 ft/sec vertical sink rate was obtained in testing nonetheless. Both the nose and main landing gears were designed for a 10 ft/sec vertical sink rate. As in the nose landing gear drop tests, wheel spin-up and simulated wing lift were utilized to enhance the simulation of landing impact. For the tail down attitude drop tests of the main landing gear, a 12.5 degree wedge shaped platform was placed under the drop tower. The 12.5 ft/sec sink rate tail down drop test data is shown in Figure 4.

Rough runway testing of the main landing gear was conducted in the same manner as for the nose gear with the same bump and dip profiles being utilized. As can be seen in Figure 5, the main landing gear performed very well when subjected to the simulated rough runway profiles. In the case of the single 7 inch bump, predicted loads close to the limit precluded testing of the 120 and 146 knot cases, especially considering that this bump height was in excess of program requirements. A key aspect of the performance of the rough field design that was verified in these tests was the fact that the largest improvement over the production F-15 C/D landing gears occurred during the highest load test cases. This was expected as the designs were optimized to 'chop off' the load peaks that occur during repair traversal. The main landing gear tests also verified the improved rebound damping characteristics designed to minimize aircraft bounce at the higher landing sink rates.

STOL/MTD AIRCRAFT TAXI TESTING

Actual taxi testing of the F-15 STOL/MTD aircraft was conducted in the summer of 1989 at the Air Force Flight Test Center at Edwards AFB. For these initial rough runway taxi tests, two 4.5 inch bumps with an 80 foot spacing were installed on the runway using a combination of AM-2 aluminum matting and plywood to achieve an approximation of the shape of the 4.5 inch repair as tested in the laboratory. In order to determine the predicted loads for the taxi tests, a computer model of the landing gear dynamic response characteristics was validated with the laboratory test data and then incorporated into an F-15 aircraft response computer model. The aircraft response model had been previously validated with taxi data from the Have Bounce Program. This computer model was then utilized to generate all of the predicted loads for the upcoming taxi tests to ensure that no limits would be exceeded.

Aircraft gross weights of 40,000 and 50,000 pounds were tested over the two 4.5 inch bumps. An upper limit of 90 knots resulted from the location of the repairs on the runway and the need for overrun area in case of an abort. The results for the 40,000 pound gross weight testing are shown in Figure 6. As can be seen from this data, the loads were quite low relative to the landing gear limits and the resulting improvement was minimal. For the 50,000 pound testing, the improvement relative to the F-15 C/D aircraft with the current landing gear was significant, especially for

the speeds in which the current landing gears generated loads near their limits. This data can be seen in Figure 7.

Future testing that will be conducted over the 4.5 inch repairs will include the effects of hard braking, landing gear performance during engine thrust reversing, and two point attitude testing. Although the F-15 STOL/MTD aircraft will be limited to 50,000 pounds, the performance of the improved landing gears at the 68,000 pound F-15 C/D maximum gross weight has been verified during the earlier laboratory testing. Significant improvements relative to the current landing gears resulted from the higher loads that were generated by the high gross weight.

In summary, a significant improvement in rough runway performance has been demonstrated by the CPC rough runway landing gear designs. This capability was achieved with a minimal weight increase (less than 30 pounds for the shipset) and no projected effect on reliability and maintainability. These designs can be applied to other landing gears with the amount of improvement dependent on the landing gear and aircraft configuration and available strut stroke.

'PC BASED' RUNWAY REPAIR CRITERIA

The primary purpose for developing the computer models under the HB program was to establish rapid runway repair Surface Roughness Criteria (SRC) for each aircraft. The intent is to deliver the SRC to the Operational Commands through technical manuals and in the form of 'overlay' charts depicting the allowable bump heights and spacings versus distance down the runway. This is done for each aircraft at a cross spectrum of gross weights, density ratios, headwind components, etc. Although these SRC are accurate, they are also complex and become conservative when multiple aircraft types operate on the same MOS. Repair crews must be trained to use the SRC and MOS procedures. Another drawback of this approach is that the addition of future aircraft or even derivatives of the existing aircraft to the fleet requires Tech Order revision and the addition of numerous overlays and perhaps more training. It is not an ideal system.

Another method could be to automate the process. Figure 8 depicts an approach that would solve many of the deficiencies of the current technique. The approach is to modify the mainframe computer programs developed under the HB program to run on-site using readily available PCs. The primary benefits of an on-site computing capability are as follows:

* MORE ACCURATE; Using a menu driven on-site computer program to simulate the actual aircraft and conditions will be more accurate. Important aircraft parameters such as gross weight and center of gravity and ambient conditions such as density ratio and headwind component can completely alter the repair criteria. This approach also reduces the conservatism built into the present 'static' system that is induced when multiple aircraft are superimposed on the same MOS.
* RETALIATE FASTER; If actual aircraft and ambient conditions are used in the computer simulations, quicker repair times will result because less conservative repairs will be identified.
* FLEXIBILITY; An on-site simulation capability will provide the flexibility needed to allow gross weight and other aircraft changes. Using the current method, this would have to be approximated through interpolation.
* PROVIDES OPTIONS; One of the highest payoffs of this method is that it provides the base commander with a tool for answering important 'what if' questions and getting accurate answers in a short response time. For example, if the runway repair crews could not maintain the quality of runway repair specified, the commander may want to reduce the aircraft gross weight to a point where a safe takeoff can be made. Assessment of the effect of relocation of the runway threshold to permit successful takeoffs is another option. The ability to quickly assess options is a powerful benefit of this capability.
* UPDATE; As new aircraft or derivatives of existing aircraft enter the inventory, updating the SRC will be a simple matter of mailing a floppy disk containing the new computer model to each main operating base.
* MORE EFFICIENT; On-site, menu driven computer programs designed to select the MOS and specify the required level of repair will be much easier to use than the current technique. Consequently much less training will be required and since the process is simpler, there is less chance for error in a wartime situation. Also, the computerized technique would do away with the requirement for tech orders, overlay charts, and subsequent revisions.
* MONITOR REPAIRS; Repeated aircraft operations will result in degradation of the repaired runway surface. Measured runway profile data can be fed into the PC based computer programs to determine if rework is required and to what extent.

The benefits obtained by going to a PC based on-site technique for determining the MOS location and required repair quality are obvious. The negatives are:

* ADDITIONAL DEVELOPMENT; The computer programs that were developed under the HB program were designed to run on 'mainframe' computers. Each of these programs would require modification in order to run on a PC. This could however, prove to be more efficient than the current proposal when you consider the reduced training requirements and ease of updating for future systems. The feasibility of running these computer programs on a 'PC' has already been demonstrated. Run times and

memory requirements are not a problem.

* BACKUP SYSTEM REQUIRED: Since our ability to retaliate in a reasonable length of time would be hinged to the use of this on-site capability, a manual backup technique would be required. One promising approach for providing an easy to use backup technique is called the Vulnerability Index.

VULNERABILITY INDEX (VI)

The VI number of an aircraft reflects that aircraft's ability to absorb the energy of a specific bump at all velocities. All aircraft VI's will be calculated using the same bump so that the runway roughness capability of each aircraft will be directly comparable.

The VI is calculated using the complex computer programs developed under the HB program. Consequently the VI very accurately reflects the ability of each aircraft to 'absorb' the bump. Although the VI is complex from the standpoint of how it is calculated, it is simple to use, because it boils down the effects of speed, resonant frequencies, spacing, etc. into one number. It will introduce some conservatism, which unfortunately, is the penalty that must be paid for not having the fully operational on-site PC based capability.

Ideally, it is desirable to define the 'bump energy' on a comparable scale to the aircraft's vulnerability index. This 'bump energy' would have to be a function of the bump profile, spacing and location on the runway. Work is currently underway to define a method for quantifying bump energy in a form that is mathematically relatable to aircraft vulnerability index. Until this method is developed, however, it will be necessary to use rule of thumb guidelines based on lessons learned in the Have Bounce project. Once the initial MOS is repaired using these guidelines, the roughness effect of the MOS from one aircraft to another can be determined using the Vulnerability Index.

GUIDELINES FOR MOS REPAIR

The following are 'rule of thumb' guidelines for repairing and operating on an MOS based on the lessons learned in the Have Bounce project. These guidelines are intended to be used in the event that the PC based system is not available or as a validation check to the PC based system results.

* The grade of any repair will not exceed 4 percent.
* Step bumps will not exceed .75 inches.
* Any repair in the first 500 feet (landing touchdown zone) of the MOS will not exceed 1.5 inches from the undamaged grade. All other repairs will not exceed 3.0 inches from the undamaged grade except for the following spacing requirements.
* Bump spacing requirement is directly proportional to aircraft velocity. Consequently the spacing between 3 inch bumps will be no less than:

$$S = V \times 2.5$$

Where S is the spacing in feet from the trailing edge of the previous bump and V is the aircraft velocity in feet per second. Aircraft speed can be obtained from the flight manual and should include density ratio effect and headwind component.

* Any bump closer than the calculated S above will not exceed 1.5 inches from the undamaged grade.
* Use 'soft field' takeoff and landing procedures. The purpose is to unload the nose landing gear as much as possible and unload the main landing gear with wing lift as soon as possible.
* Minimizing aircraft weight will result in maximum runway roughness capability.

CALCULATION OF VI

The VI is a reflection of the ability of an aircraft to 'absorb' the energy of a bump rather than transmit that energy to the airframe. It is based on the computed response (using TAXI) of an aircraft traversing a 'standard' bump at all possible velocities. Figure 9 is a typical plotted time history response predicted by TAXI. For a given velocity, both the nose and main landing gear loads will reach a peak at some point in time. Figure 10 is a plot of landing gear peak loads predicted by TAXI for all velocities up to the takeoff speed. If the design limit load for both landing gears were included on this velocity plot, the VI for that aircraft would be the sum of the shaded areas as shown in Figure 10. The value of the VI can be mathematically represented as illustrated in Figure 11.

If the VI for all aircraft are calculated for the same bump for the entire takeoff range of speeds, then the VI can be used to directly compare the 'goodness' of an aircraft's ability to absorb roughness. Consequently once the VI for an aircraft is determined it can be 'ranked' using this single number. This would tell the Operations Commander that an aircraft having a smaller VI than aircraft currently using the MOS could also use this same MOS. This could be his only data for making a go/no-go decision, particularly for non-USAF aircraft.

CONCLUSIONS

In summary, both the technology of landing gear strut design and the understanding and analysis of aircraft response to runway roughness have evolved dramatically during the past decade. The benefits which would be provided by incorporating this knowledge far outweigh the small costs involved. Increased aircraft capability coupled with accurate and timely assessment of aircraft/repaired runway compatibility would significantly enhance post-attack sortie generation. It is recommended that the knowledge gained be incorporated into design handbooks, military specifications, and operational procedures.

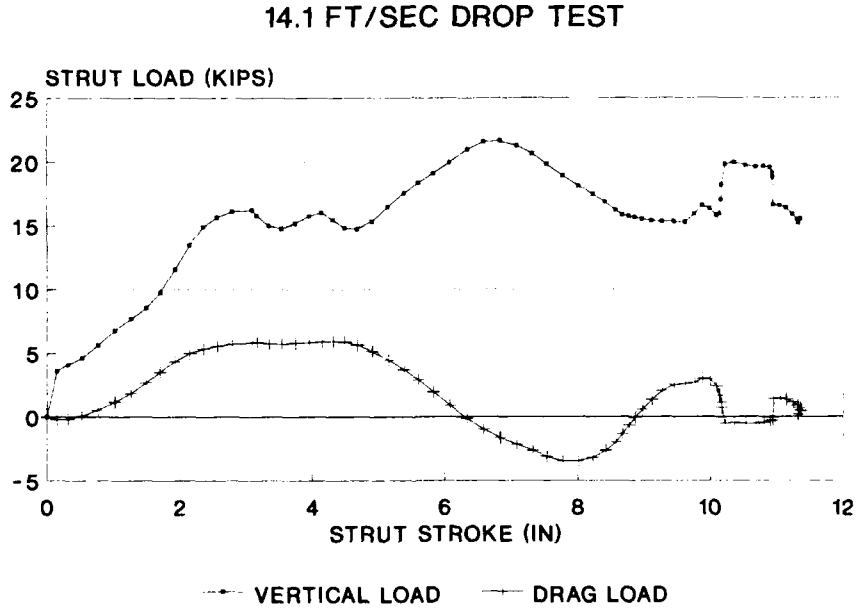

FIGURE 1. F-15 STOL/MTD NOSE GEAR DATA

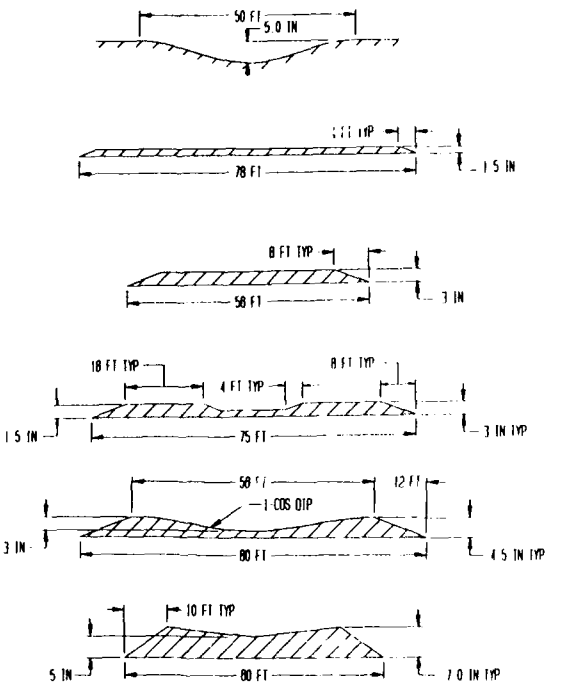

FIGURE 2. REPAIRED RUNWAY PROFILES

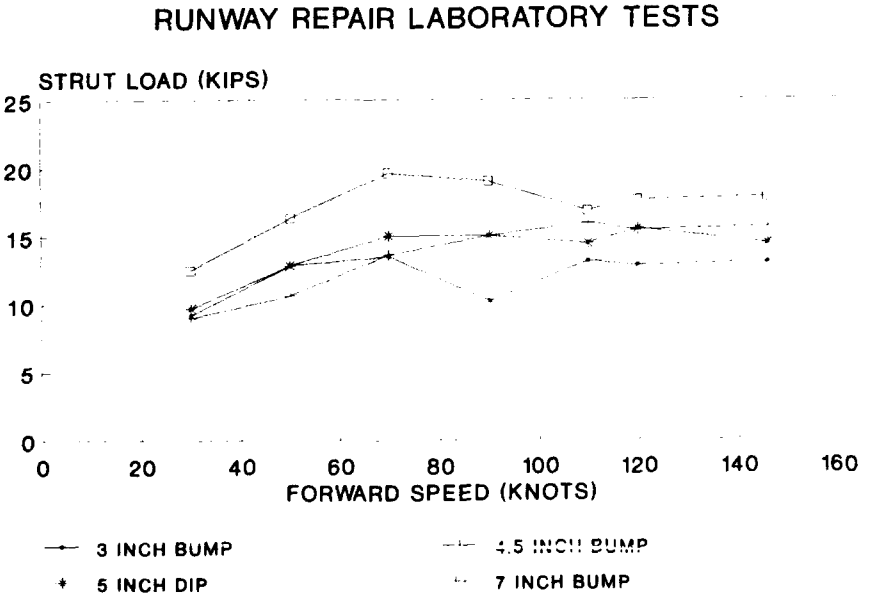

FIGURE 3. F-15 STOL/MTD NOSE GEAR DATA

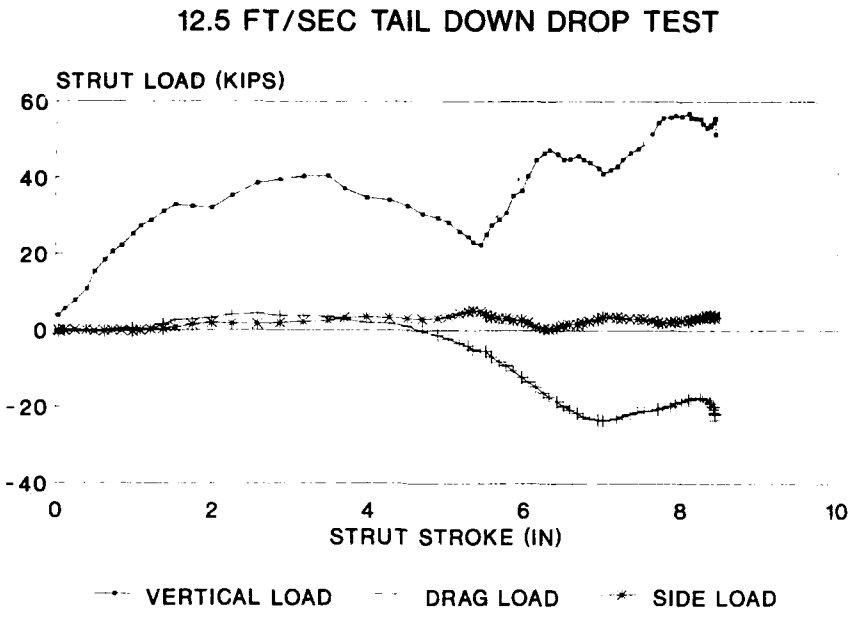

FIGURE 4. F-15 STOL/MTD MAIN GEAR DATA

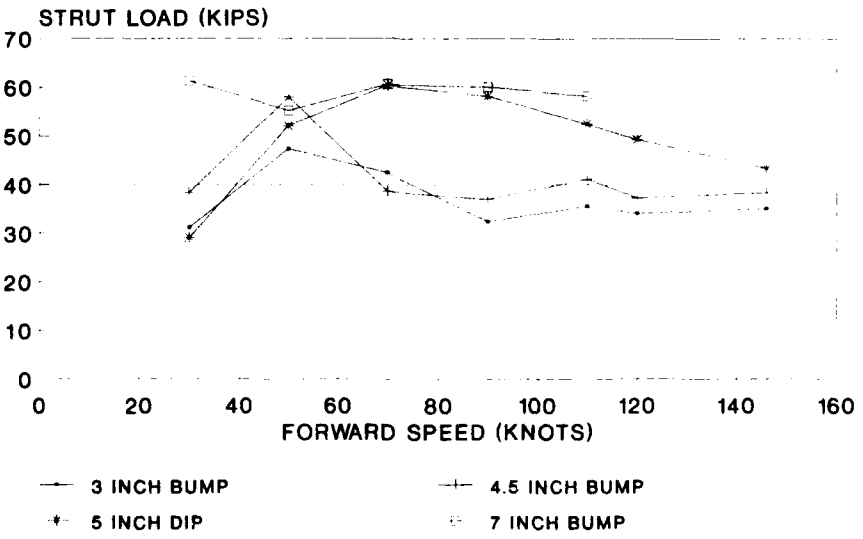

FIGURE 5. F-15 STOL/MTD MAIN GEAR DATA

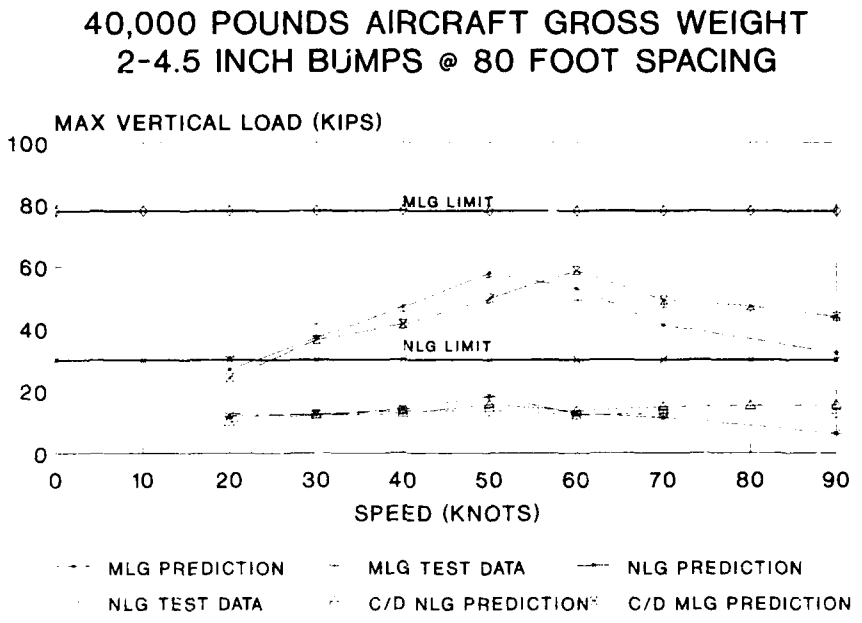

FIGURE 6. F-15 STOL/MTD TAXI TEST DATA

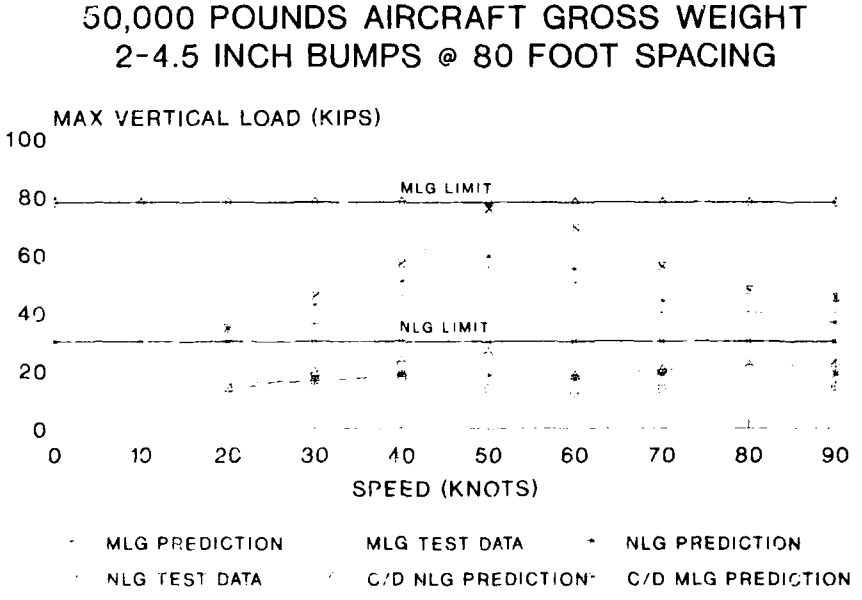

FIGURE 7 F-15 STOL/MTD TAXI TEST DATA

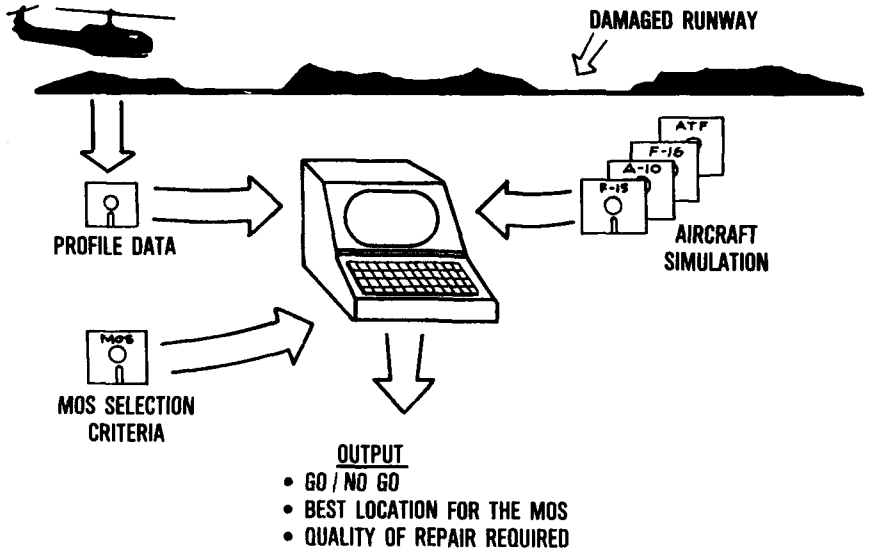

FIGURE 8. "ON SITE" PC APPROACH TO RAPID RUNWAY REPAIR PROCESS

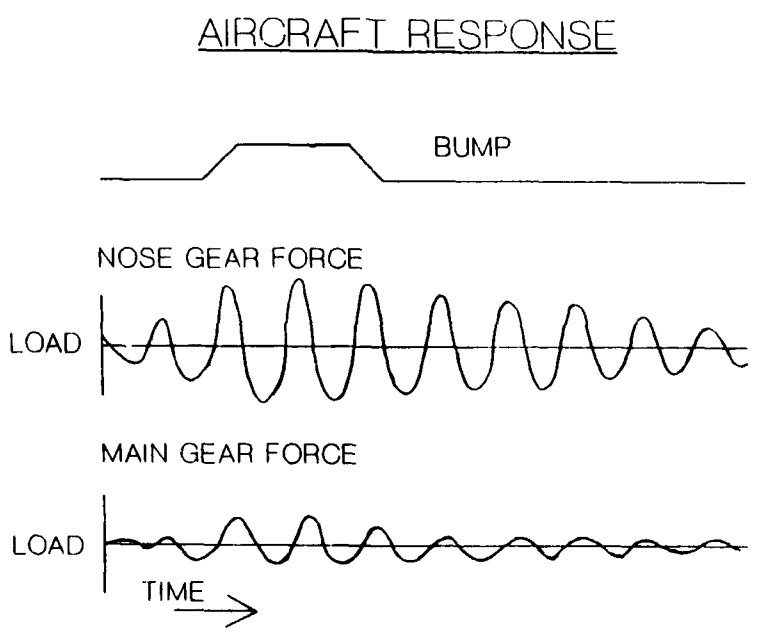

FIGURE 9. TYPICAL TIME HISTORY PLOT GENERATED BY "TAXI"

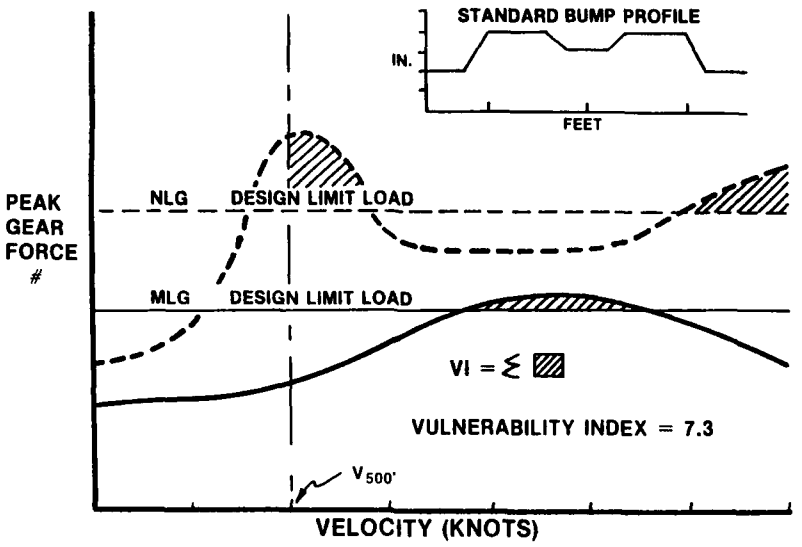

FIGURE 10. PLOT OF "VELOCITY SWEEP" SHOWING TYPICAL VULNERABILITY INDEX

VULNERABILITY INDEX (VI)

$$VI = \sum_{V=V_I}^{V_{TO}} \frac{(FSN}{DLLN} + \frac{FSM)}{DLLN}$$

WHERE:

FSN	= NOSE GEAR PEAK STRUT FORCE
FSM	= MAIN GEAR STRUT FORCE
DLL	= DESIGN LIMIT LOAD
V	= AIRCRAFT VELOCITY
V_I	= VELOCITY AT 500 FT DOWN RUNWAY
V_{TO}	= VELOCITY AT TAKEOFF

FIGURE 11. METHOD FOR COMPUTING THE VULNERABILITY INDEX

THE SPECIAL REQUIREMENTS OF A VSTOL AIRCRAFT

by
D.C.Thorby
J.Johnson
A.B.K.Auld
H.T.Newman
M.J.Brooker

Dynamics Group
Aerodynamics Department
British Aerospace (Military Aircraft) Ltd.
Richmond Road
Kingston-upon-Thames
Surrey KT2 5QS
United Kingdom

SUMMARY

The paper describes the special landing gear requirements of the Harrier family of aircraft, and is based on modelling and testing experience over a considerable period of time. Only topics peculiar to the VSTOL (Vertical and Short Take Off and Landing) aspects of this aircraft are addressed.

Of the four possible modes of take-off, ramp-assisted (the "ski-jump") presents unique landing gear problems. This is described, covering the design of ramp profiles and the procedures used to establish service operating limits for the landing gear, including the effects of ship motion.

The particular problems associated with vertical landing are next discussed. This mode of landing can produce landing gear side loads potentially much higher than are normally possible in a conventional landing with forward speed. Clearance procedures using a multivariate approach are described.

The Harrier has also been cleared for operation on unprepared rough fields. The Monte Carlo method, applied to the results of numerical modelling using computer-generated surfaces, is described.

Other topics discussed are: runway directional stability, and the load and directional stability implications of converting to radial tyres.

1. INTRODUCTION

The original Harrier concept has been described in many publications. Several marks have been produced, but as far as the landing gear is concerned there are essentially two versions: the Harrier I produced by British Aerospace, and the Harrier II produced jointly by BAe and the McDonnell-Douglas Corporation. Dowty Rotol Ltd. are the main contractors for the landing gear. The gear units for the two aircraft (except for the outriggers) are geometrically similar, but the Harrier II units are stronger with stiffer strut spring curves designed for a sink speed of 15 ft/s (4.6 m/s) at higher weight rather than the 12 ft/s (3.7 m/s) used for Harrier I. Figure 1 shows the very similar landing gear layouts for the two aircraft, and figure 2 sketches the Harrier II units.

All Harriers have four possible modes of take-off: vertical, short, conventional and ramp-assisted, and three landing modes: vertical, slow and conventional. In addition, some versions of both Harrier I and Harrier II have been cleared for operation from unprepared fields. This normally means grass fields, but interlocking metal strips over grass are also used. The vertical landing requirement particularly has dictated the use of an unusual landing gear arrangement, essentially a bicycle with outriggers for roll stability. The nose and main gears carry roughly equal static loads, each about 45% of the weight, while the outriggers together take the remaining 10%. The unique rotating "vectoring" nozzles of the Rolls-Royce Pegasus engine mean that the total engine jet force may be used for forward thrust, jet lift or to give a combination of these, as in "partially jet-borne flight".

Many aspects of Harrier operations involving the landing gear are perfectly conventional, and are not discussed in this paper. Operations standing out as unusual are firstly, ramp-assisted take-off, or the "ski-jump". This produces a normal acceleration in the order of 3g, virtually all reacted by the landing gear. Secondly, vertical landing gives a landing gear side loading mechanism quite different from conventional landing. Rough field operations are not unique to Harriers, but the methods used to clear the GR Mk 5 version of the Harrier II may be of interest. Finally some remarks on the often neglected area of directional stability on the runway, and the related question of changing to radial-ply tyres, are included.

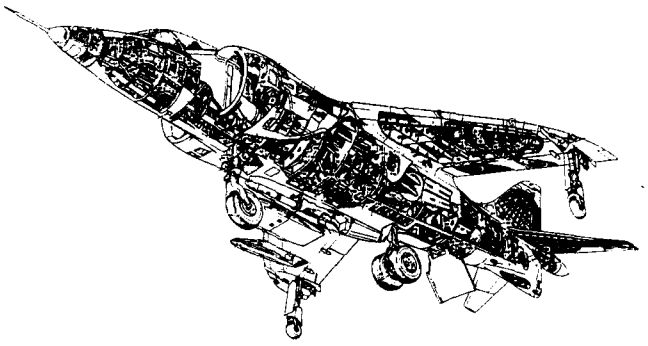

HARRIER I

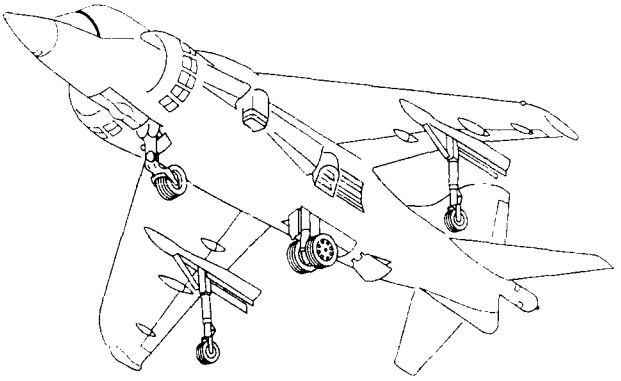

HARRIER II

FIGURE 1. LANDING GEAR LAYOUT FOR HARRIER I AND HARRIER II

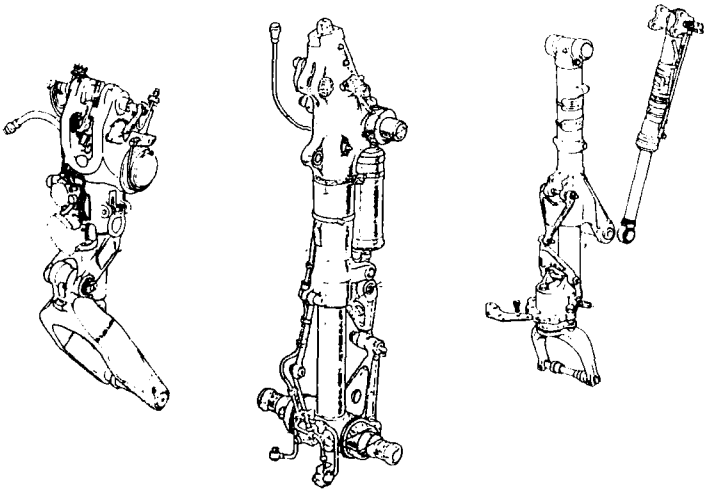

NOSE GEAR MAIN GEAR OUTRIGGER GEAR

FIGURE 2. HARRIER II LANDING GEAR UNITS

2. RAMP-ASSISTED TAKE-OFF

This is now the conventional mode of take-off from the ships of several navies. The corresponding landing on to the ship is always vertical. For those unfamiliar with the "ski-jump", Appendix 1 gives a brief explanation of this interesting topic together with an outline of the method used to establish the optimum exit angle for a particular application. Ramp-assisted take-off may be from land, as demonstrated at the Farnborough and Le Bourget salons some years ago, but it is in naval applications where the technique shows dramatic advantages.

2.1 OPTIMISING THE RAMP SHAPE

Devising the best shape for the ramp is an interesting problem. If the landing gear were rigid and the speed constant, a circular arc would clearly be the correct shape, since the aim is to impart the maximum possible vertical momentum to the aircraft, while at the same time minimising the applied load. Figure 3 shows what happens in practice if a circular arc profile is used. Because the centrifugal load is applied suddenly, an oscillation is set up. This has two adverse effects: it increases the peak gear loads, requiring a reduction in endspeed to avoid full strut closure, and it could make the launch pitch rate somewhat variable.

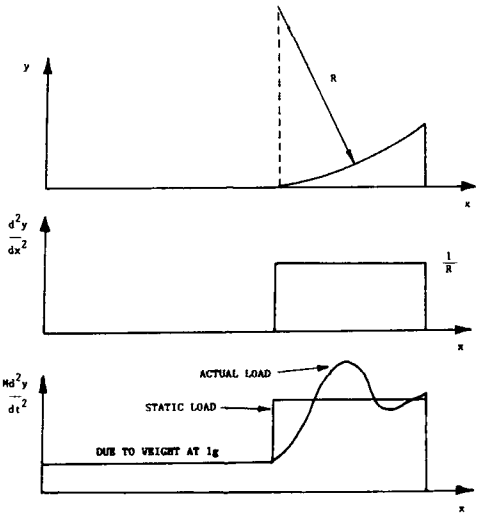

FIGURE 3. CIRCULAR ARC RAMP PROFILE

An analogous problem was known to the early railway builders, who found that a straight length of rail followed by a curve of constant radius caused trains to oscillate in roll. Their solution was to insert a "cubic transition", so that curvature and hence load increased more gradually. The same cure works with the ramp, as illustrated in figure 4.

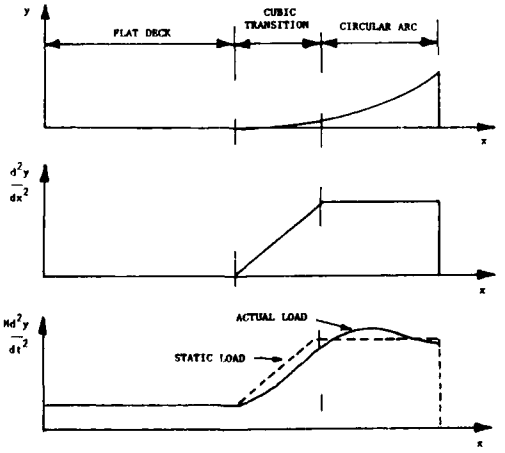

FIGURE 4. CIRCULAR ARC RAMP PROFILE WITH CUBIC TRANSITION

Later, an alternative way of preventing the heave and pitch oscillations, avoiding the additional ramp length caused by the transition curve, was found. This is described in the patent application (reference 1), and figure 5 gives a brief explanation of the method. It consists, essentially, of adding a correction profile equal to the closure history of the landing gear strut under constant load to the circular arc, or whatever profile is required "statically". This has been made to work with the Harrier, in spite of there being two landing gears with differing characteristics on the same track.

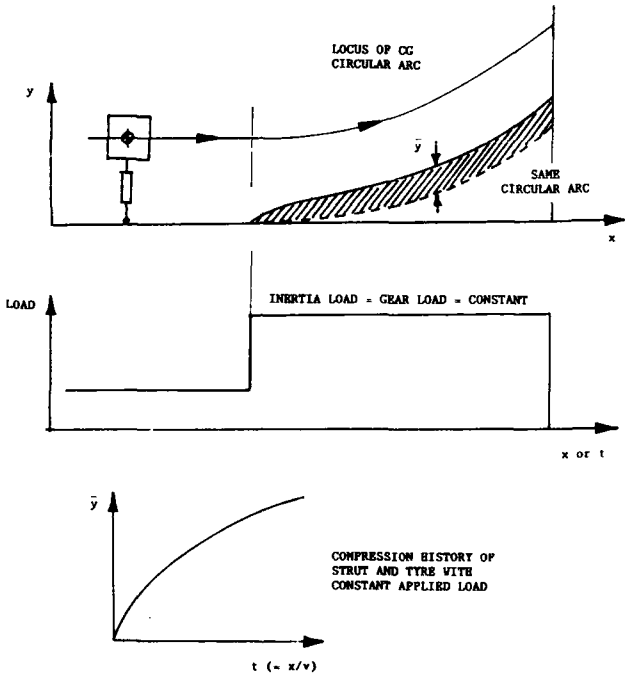

1. INERTIA FORCE = LANDING GEAR LOAD
2. BOTH MUST BE CONSTANT ON CURVE
3. LOCUS OF CG MUST BE A CIRCULAR ARC
4. FOR DESIRED CONSTANT GEAR LOAD THE STRUT MUST COMPRESS IN A PRECISE WAY
5. THE CORRECTION TO THE CIRCULAR ARC IS THE STRUT COMPRESSION HISTORY WITH CONSTANT LOAD

FIGURE 5. ALTERNATIVE RAMP PROFILE DESIGN METHOD

The process of optimising a profile for a given application is in practice iterative, using a mathematical model fully simulating the launch process. The criterion currently used is that no strut or tyre should fully close during the launch. Load might be thought to be a more appropriate criterion but, because strut closure velocities and hence damping forces are very low on the ramp, load and closure are virtually interchangeable and related by the strut spring curve. Full strut closure would imply large indeterminate loads, and this is currently avoided.

2.2 CONTROL OF LAUNCH PITCH RATE

Since a typical ramp reaching 12° may be traversed in much less than a second, the launch pitch rates could reach very high nose-up values. Fortunately this does not actually occur with the Harrier, as shown in figure 6. The nose-down moment produced during the short time that only the main gear and outriggers are on the ramp provides an almost perfect correction leaving a desirable, slightly nose-up, pitch rate at launch. This permits the optimum angle of attack for the semi-ballistic, partially jet-borne, phase to be obtained quickly, and earlier than from a flat short take-off (STO). Thus an important secondary advantage of ramp take-off is that it allows aircraft rotation earlier than would otherwise be possible.

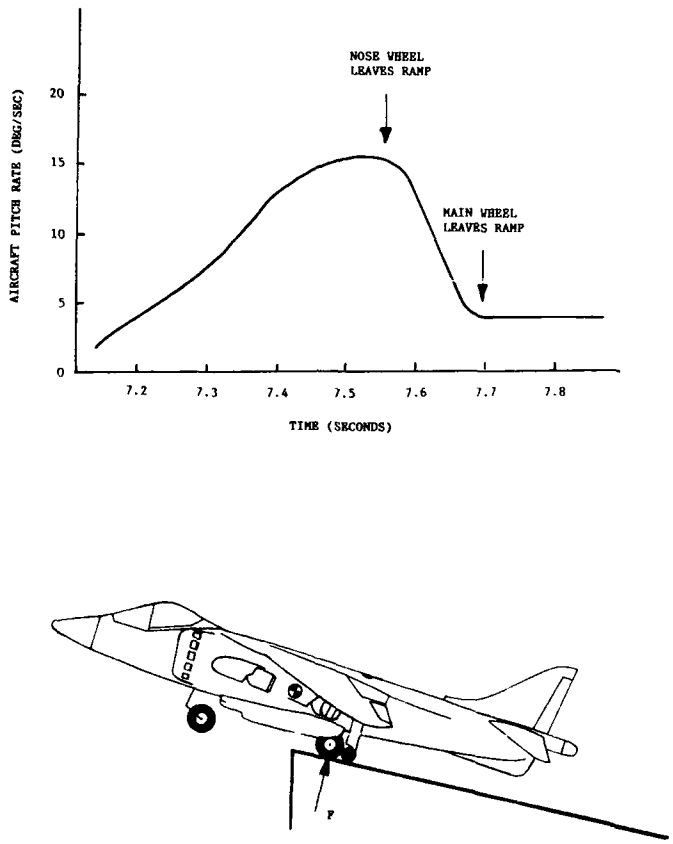

FIGURE 6. AIRCRAFT PITCH RATE AT RAMP EXIT

2.3 SERVICE OPERATING LIMITS

The service user must be provided with safe limits for ramp take-off. These involve performance limits, which are beyond the scope of this paper, and landing gear limits. In practice the latter are produced by computer simulation, validated by ship trials. As far as the landing gear is concerned it is normally only necessary to measure strut closures in these trials.

2.4 SHIP MOTION EFFECTS

The rolling motion of the ship has potential aircraft stability implications, although no problems have been found in practice. It is the pitching motion of the ship which is more important since it may have a favourable or unfavourable effect on both performance and landing gear operating limits, depending upon the point in the pitch cycle at which launch takes place. Controlling the moment of launch to improve the statistics is theoretically possible, but is inherently more difficult than with a catapult launch due to the longer time interval (typically ten seconds) between the start of launch, on the flat deck behind the ramp, and free flight. An allowance based on ship pitch amplitude, assuming random timing, is currently made. The loading effect on the landing gear due to ship motion is appreciable and is found to be caused by Coriolis force (a function of ship pitch velocity and aircraft speed) as much as by the direct vertical acceleration. Figure 7 illustrates this and shows the predicted RMS total normal acceleration per RMS degree of pitch for a cruiser-sized ship. Modelling of ship motion takes advantage of the large frequency ratio between the ship pitching motion and the rigid modes of the aircraft on its landing gear, and the short time taken to traverse the actual ramp. During this time the total aircraft normal acceleration can be regarded as constant, at values typically between 0.5 and 1.5 g, i.e. the effect of the motion can be as much as 0.5 g either way in addition to the usual gravitational 1 g. The simulations are carried out at fixed values of "gravity" (e.g. 1.0, 1.1, 1.2, etc.). Each of these can be interpreted as a range of ship pitch and aircraft speed combinations, giving considerable economy of computation.

Landing gear operating limits are kept entirely separate from aircraft performance considerations.

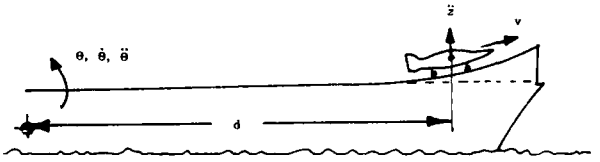

$$\ddot{z} = d\ddot{\theta} + 2v\dot{\theta}$$

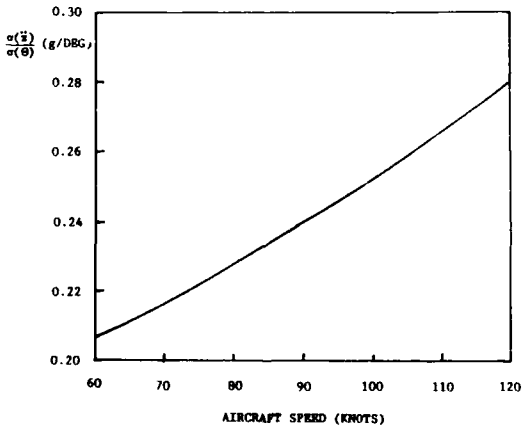

FIGURE 7. VERTICAL FORCES DUE TO SHIP PITCH

2.5 SUDDEN RELEASE LOADS

While these can be important in a catapult launch they are even more so in a ramp launch where the landing gear is certain to be highly compressed for the majority of launches. Although the usual hydraulic pulsing problem associated with sudden release had to be considered in the main gear, it was the sudden release of bending moment from the nose gear that caused difficulty in early development. In its fully compressed state the nose gear has about 400 mm of trail. Since the wheel load is very high at the end of the ramp, it can be seen that a bending oscillation is inevitable when this is suddenly released (figure 8).

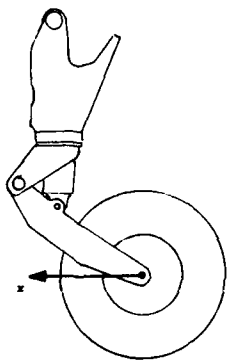

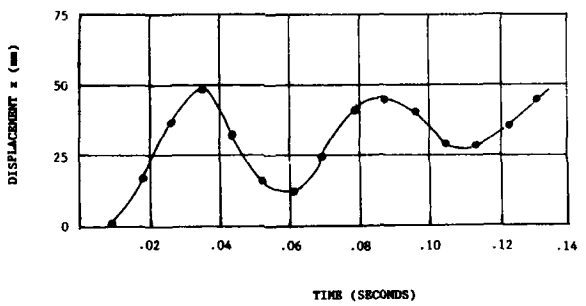

FIGURE 8. NOSE GEAR "OVERSWING" AFTER SUDDEN LOAD RELEASE AT RAMP EXIT

The cure for this was extremely simple, consisting of a run-down section designed to unload the nose gear in one natural period of the oscillation, or about 0.044 s, (figure 9).

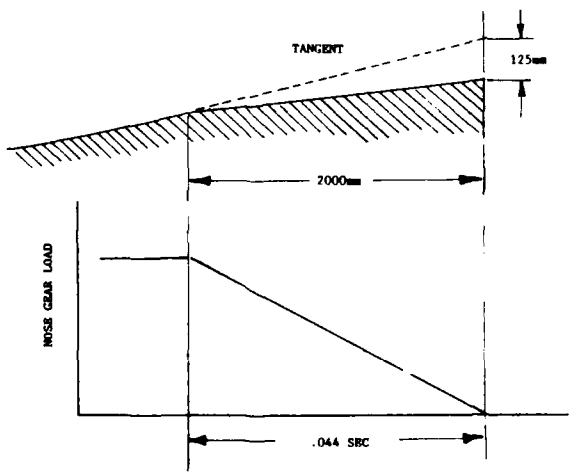

FIGURE 9. "RUN-DOWN" TO REDUCE NOSE GEAR OVERSWING AT RAMP EXIT

Figure 10 shows that the overswing is zero if this is achieved, and can be kept small for the practical range of transition times. This time varies, of course, with exit speed. All Harrier ramps must be fitted with the run-down section, which in practice may be straight, about 2 m long, and tilted down about 125 mm (about 3.5°) from the ramp exit angle.

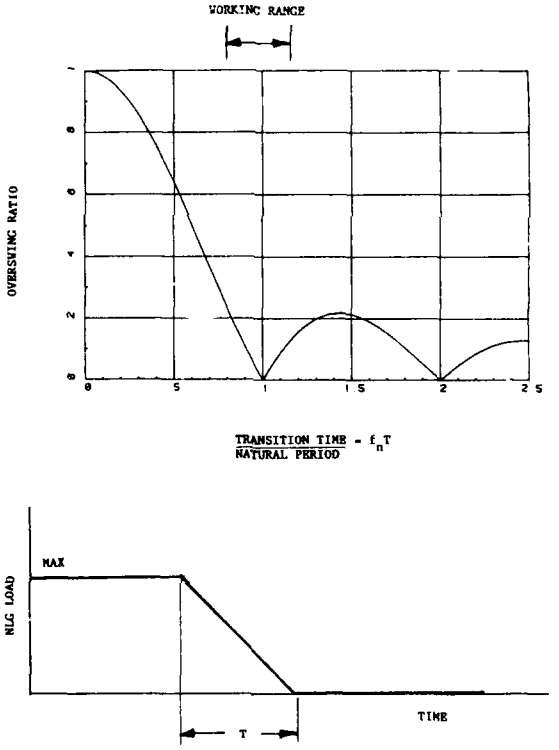

FIGURE 10. REDUCTION IN OVERSWING AGAINST TIME FOR LOAD REDUCTION

3. VERTICAL LANDING

Of the three landing modes, only vertical landing will be discussed here. The multivariate approach to limit and fatigue loads (based on MIL-A-8863A), described below, was also used for the slow and conventional landing modes.

Whether a tyre is rotating or not at touch-down makes a fundamental difference to the way side load is developed, and side loads are potentially much higher in a vertical landing than in a conventional landing. In the latter, if the aircraft is yawed relative to the runway, each tyre has a slip angle and this gives rise to a side force. The rotating tyre however acts as an efficient damper and the side force developed rarely exceeds a small fraction of the vertical load. This is reflected in current specifications where the design side force is typically between 25% and 40% of the maximum vertical load on the tyre. No such mechanism operates in a nominally-vertical landing, particularly in a case where there is lateral velocity but absolutely zero forward velocity. When there is no laterally-acting shock absorber the lateral energy must be absorbed by the elasticity of the tyres and possibly that of the landing gear in lateral bending. These have an effective "stroke" of only 50mm or so and are practically undamped. Very large side forces are thus possible, but an ultimate limit is set by the coefficient of friction between the tyre and the runway. Under dry conditions this can be as high as 1.0, so the side load is potentially as large as the maximum vertical load on the tyre.

3.1 TYRE SIDE FORCE MODELLING

The landing gear side forces determined from a mathematical model are only as accurate as the basic data used. The empirical relationships developed by Smiley and Horne in reference 2 still appear to be the best basis for modelling tyre side forces when specific measurements are not available, and for extrapolating measurements to conditions not tested. Figure 11 illustrates the empirical model applied to a rotating tyre of a particular size. "Cornering power" is the slope of the side force versus slip angle curve at low slip angles where it is nearly linear. Steady state forces are given by the expressions presented in reference 2, and it is stated that the side force builds up exponentially with distance, with a "time constant" in the order of one footprint length. In the case of conventional landing, this is rapid enough to regard as instantaneous, but can be taken into account in the case of nominally-vertical landings with some forward (or rearward) velocity.

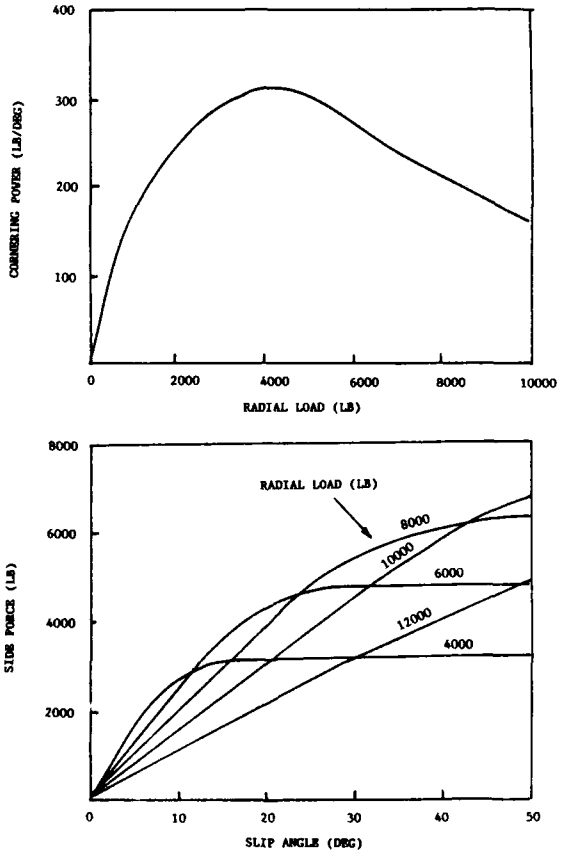

FIGURE 11. TYRE SIDE-FORCE CHARACTERISTICS PLOTTED FROM NACA 4110

Reference 2 appears to predict steady-state side forces of cross-ply (bias) tyres due to yawed rolling with remarkable accuracy. Figure 12, for example, shows the "cornering power" of cross-ply tyres measured by two different suppliers; the curves fall each side of the Smiley and Horne prediction for this size. Radial tyres have, in our experience, somewhat higher cornering power as shown in figure 13 which is based on data from the same two suppliers. It is worth noting that a third supplier claims that side-force characteristics can be "tailored" to requirements, and that the cornering power of a radial tyre can actually be lower than that of the corresponding cross-ply tyre.

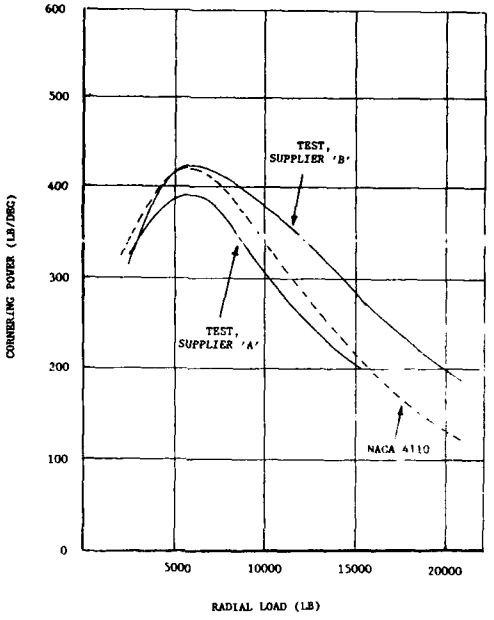

FIGURE 12. CORNERING POWER OF TWO MAKES OF CROSSPLY TYRE COMPARED WITH NACA 4110 PREDICTION

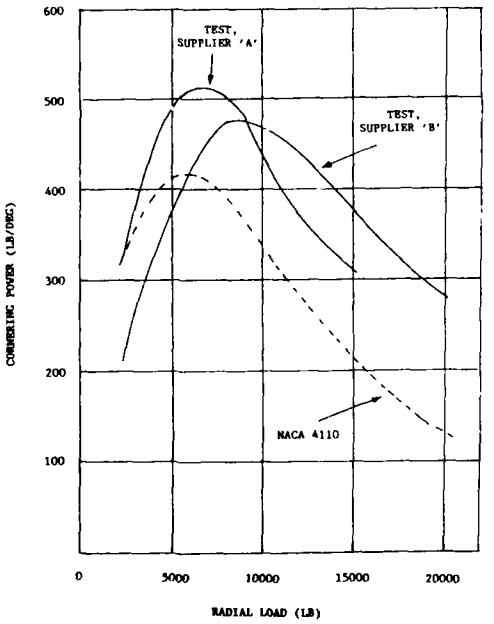

FIGURE 13. CORNERING POWER OF TWO MAKES OF RADIAL TYRE COMPARED WITH NACA 4110 PREDICTION

Reference 2 also predicts lateral static (non-rotating) tyre stiffness and, based on one supplier's data, the predictions are in the order of half the measured values for cross-ply tyres as shown in the following table. The table also shows the static lateral stiffness of the same supplier's radial tyres which, as would be expected, are less stiff than the corresponding cross-ply tyres.

LATERAL STATIC STIFFNESS (kN/m)
(HARRIER MAINWHEEL TYRE)

	RADIAL LOAD	
	30 kN	75 kN
CROSS-PLY (BIAS), MEASURED (SUPPLIER B)	475	404
RADIAL, MEASURED (SUPPLIER B)	336	281
REFERENCE 2 PREDICTION	264	199

These figures suggest that some caution is necessary in using reference 2 to predict static lateral stiffness, and measurements are required in critical applications.

3.2 COMPLIANCE WITH MIL-A-8863A

MIL-A-8863A, which is the specification applicable for ground loads on the AV-8B version of the Harrier II, requires a multivariate analysis for landing limit loads. Table 1 of the Specification lists the variates to be investigated, their mean and standard deviation values etc., and the range to be covered both individually and in combination.

Individually, each variate need only be considered within the range giving 0.001 probability of exceedance each way, or about 3.1 standard deviations each way for an unskewed normal distribution. For combinations of variates, the joint exceedance probability P_T need only be considered up to the value given by one variate at 0.001 probability with all the others at mean value, i.e. 0.5 probability of exceedance. Thus:

$$P_T = P_0 \times 0.5^{n-1}$$

where P_0 is the individual minimum probability of each variate, and n is the number of variates.

Figure 14 shows these limits for two variates V_A and V_B with the other variates at fixed values. C is a constant, determined by the fixed values chosen for the other variates.

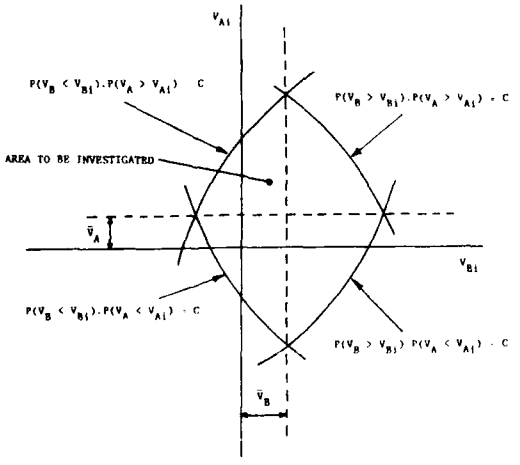

$$C = \left[\frac{P_T}{P(V_C \gtrless V_{C1}).P(V_D \lessgtr V_{D1})}\right]$$

Suffix 1 denotes initial condition

FIGURE 14. RANGE OF V_A AND V_B TO BE INVESTIGATED WITH V_C AND V_D FIXED

The VTOL (Vertical Take-Off and Landing) column of Table 1 of MIL-A-8863A does not really address vertical landing, since it requires variation of yaw angle (which has no effect in a VL), but omits lateral velocity. Substitution of yaw by lateral velocity was agreed with the procuring authority for vertical landing, and it was further shown that only the following four variates need be considered in detail:

(i) SINK SPEED
(ii) PITCH ANGLE
(iii) ROLL ANGLE
(iv) LATERAL VELOCITY

All combinations of these variates can be covered by a series of load contour plots like figures 15 and 16. Here sink speed and pitch angle are temporarily fixed, and load contours etc. are plotted on a graph of roll angle against lateral velocity.

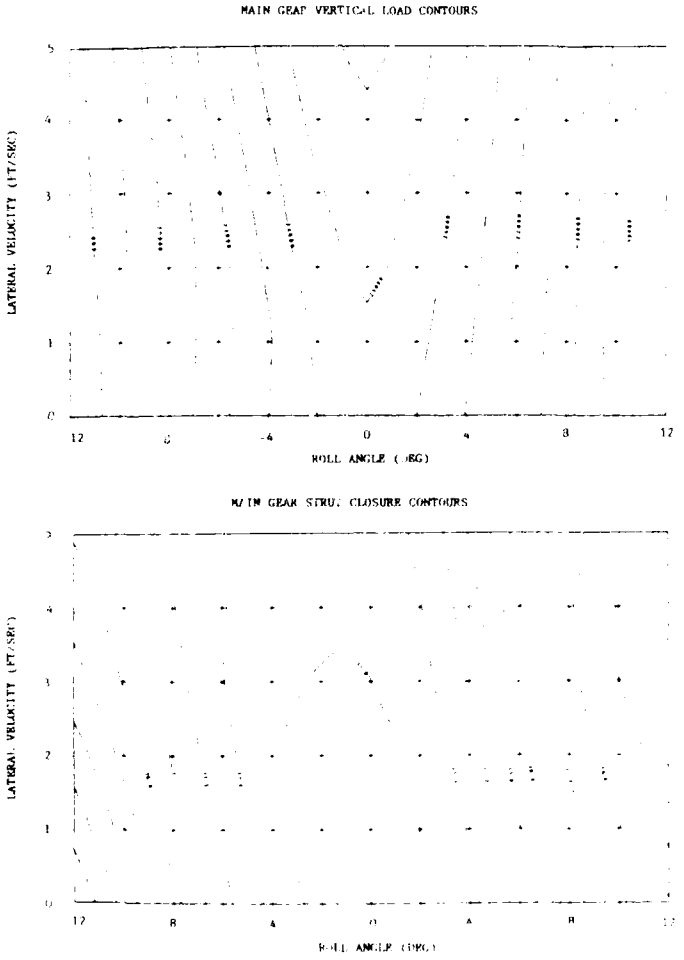

FIGURE 15. MAIN GEAR VERTICAL LOAD AND CLOSURE CONTOURS SINK SPEED OF 12 FT/SEC AND PITCH ANGLE OF 8°

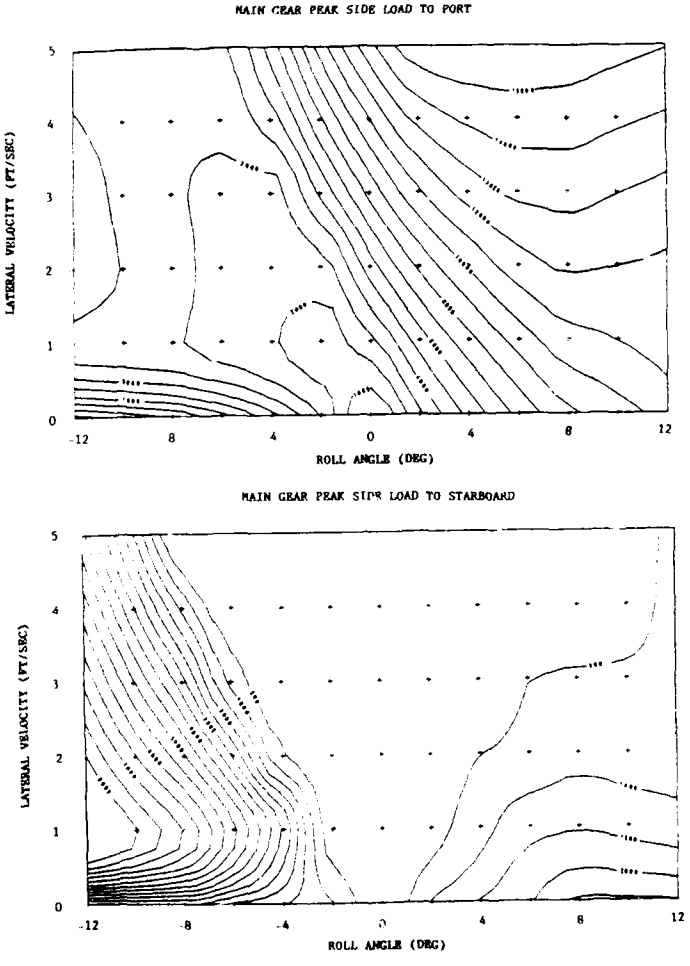

FIGURE 16. MAIN GEAR SIDE LOAD WITH SINK SPEED OF 12 FT/SEC AND PITCH ANGLE OF 8°

Figure 17 shows roll and lateral velocity combinations producing limit load boundaries for the various gear units at fixed sink speed and pitch angle, in relation to the probability boundary required in this case. For four variates the value of P_T as defined above is 0.000125.

Mention should be made of a series of landing impact parameters measured on the AV-8A version of the Harrier I by MADC. These were invaluable in defining the multivariate parameters for the later AV-8B. All relevant impact quantities were extracted from 70 mm film and expressed in statistical terms: mean, standard deviation, skew and kurtosis were listed for statistically significant numbers of landings. A similar exercise was carried out by the Royal Navy and the RAE, but using a smaller film size. Data of this kind gives landing load prediction a sound statistical basis and should be gathered whenever possible.

Fatigue loads, applied by the supplier to the landing gear and by the airframe manufacturer to the airframe abutments, can be generated in a similar way. In order to limit the loadings to a reasonable number, the probability density curve of each variate must be "lumped" as shown in figure 18, in this case to five discrete values. The overall pattern of cases to be run to produce the fatigue loading schedule, for a particular landing mode, can then be built up from all combinations of such discrete values.

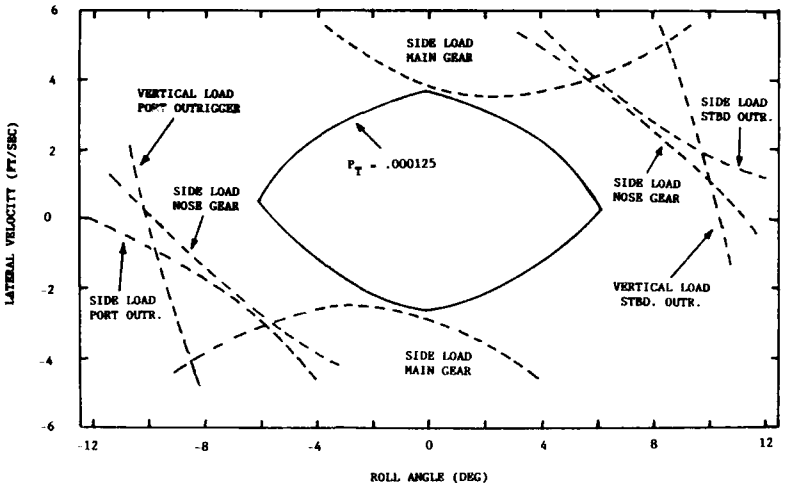

FIGURE 17. LIMIT LOADS AND MULTIVARIATE REQUIREMENT - VERTICAL LANDING

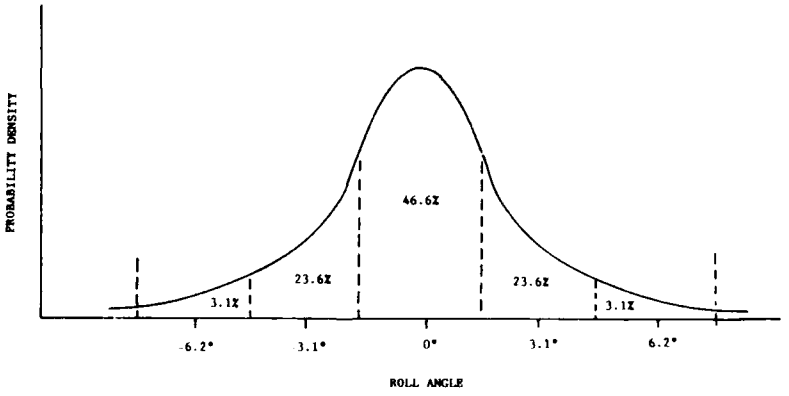

FIGURE 18. LUMPING A VARIATE INTO FIVE DISCRETE VALUES FOR FATIGUE

3.3 SHIP MOTION EFFECTS

Ship motion can change the statistical parameters for vertical landing. In order to arrive at a reasonable rationale, it is necessary to consider how a vertical landing is performed with a Harrier. This is accomplished by first hovering over the deck station upon which it is desired to land. The vertical position is fixed in space, rather than relative to the ship. A constant rate of descent is then set up by reducing the throttle setting slightly, then returning it to the hover position. Given this procedure, it is seen that the statistical variation of impact parameters should be a combination of two uncorrelated distributions, one due to the aircraft (similar to operation from land) the other due to the ship, which can be defined from ship data, independently of the aircraft.

4. ROUGH FIELD OPERATIONS

4.1 THE BUMP SPECTRUM

Some versions of Harrier I and Harrier II have been cleared for operation from unprepared fields. This generally means grass fields with or without an interlocking metal strip covering. The ground roughness is quantified by a method believed to be unique to the Royal Air Force and known as the "Bump Spectrum". Production of the bump spectrum for a particular rough surface is illustrated in figure 19, and figure 20 shows a typical result produced by computer although the process is simple enough to implement by hand. The method works very well in practice and the bump spectrum plots can be related to the more fundamental Power Spectrum method.

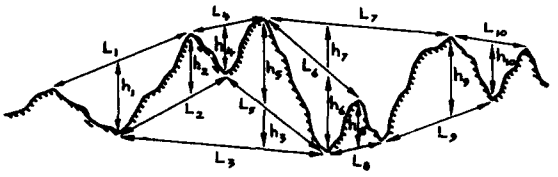

POINTS (L_1,h_1), (L_2,h_2) ETC ARE PLOTTED ON A BUMP SPECTRUM DIAGRAM

FIGURE 19. DERIVATION OF BUMP SPECTRUM

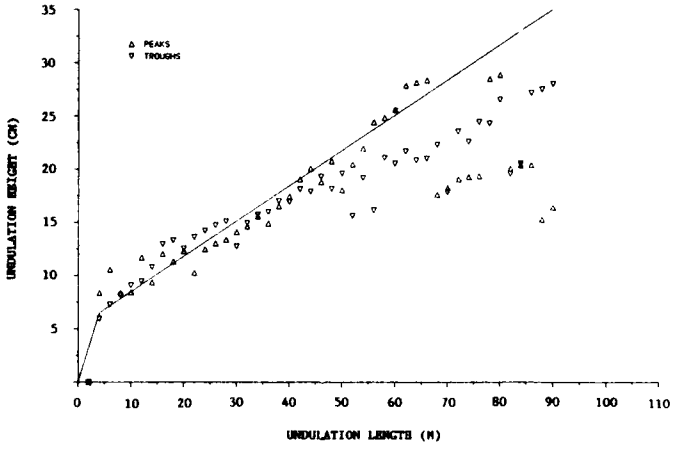

FIGURE 20. TYPICAL BUMP SPECTRUM

4.2 TEST PHILOSOPHY

Rough ground clearance of a particular aircraft presents a statistical difficulty even when, as in the case of Harrier GR Mk 5, fully instrumented trials were carried out. During such trials it is practical and reasonable to use five or maybe six different operating sites. Each strip, however, can only be expected to contain a few significant bumps and a clearance based this would always be open to the objection that another strip meeting the bump spectrum requirements could fully close the landing gear. In order to overcome such objections it would be necessary operate from a very large number of strips. With a well-validated model this should be possible by computer simulation. Pursuing this line of thought, the following rationale was developed:

1) The trials were only used to validate the model. The surfaces used were:

   (a) A **smooth runway** to check aerodynamic loads in ground effect by using the landing gear load instrumentation to measure the lift and pitching moment directly at various speeds.

   (b) An accurately known **discrete bump**, similar to a standard runway repair bump.

   (c) **Grass and metal-covered grass** surfaces with increasing roughness as measured by the bump spectrum and progressively increasing aircraft weight.

2) Having validated the model, long lengths of computer-generated "rough ground" were produced based on Gaussian white noise. It was found that a single integration with respect to distance produced surfaces indistinguishable from samples of real ground, as judged by the following criteria:

   (a) Similar Power Spectra. This follows from the way the surfaces were generated: single integration of white noise.

   (b) Similar Bump Spectra.

   (c) Using the model it was also demonstrated that the ratio of RMS load to RMS closure for each strut was similar for simulated and real surfaces.

3) In principle a large number of take-offs and landings should then be simulated. It was, however, demonstrated that a series of constant-speed runs could be substituted, provided the model was adjusted to include the vertical forces and pitching moments due to thrust and, during landing, braking. Thus acceleration or deceleration has no effect, in itself, on response, but the associated steady forces must be included in the model. The use of constant speed runs had the advantage of making the time histories of loads and strut closures etc., stationary and therefore more amenable to statistical processing. It should be noted that the model was not linearised in any way.

4.3 RESULTS

4.3.1 Model Validation

Some adjustments to the model were required to achieve good correlation with tests. These were:

(a) Friction forces, which had been based on static friction measurements had to be considerably reduced. This is reasonable, since friction tends to reduce with increasing rubbing velocity.

(b) In common with other workers it was found that a single gas spring curve would not give satisfactory results over the range of closure velocities experienced on rough ground, and it was necessary to represent the thermodynamic behaviour of the gas in the struts.

With these adjustments there was generally very good agreement between model predictions and test results, as shown in figures 21A and 21B. In these plots the solid line is the computed response using the measured surface profile in all cases, and the broken line is the measured aircraft response. The computer model was provided with measured aircraft velocity and engine fan speed time histories as part of its input data.

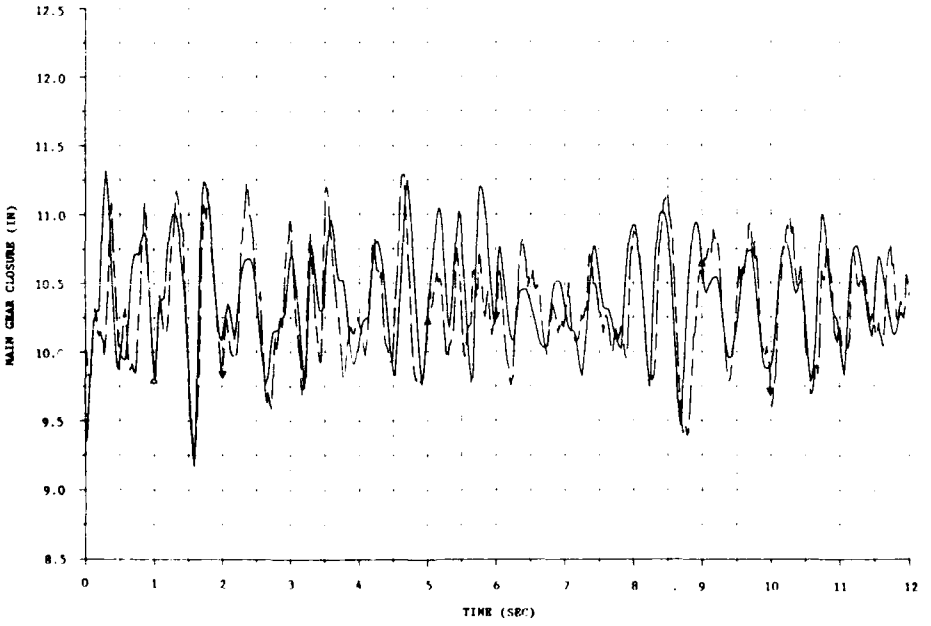

FIGURE 21A. MEASURED AND PREDICTED MAIN GEAR CLOSURE 40 KNOT TAXI OVER GRASS STRIP

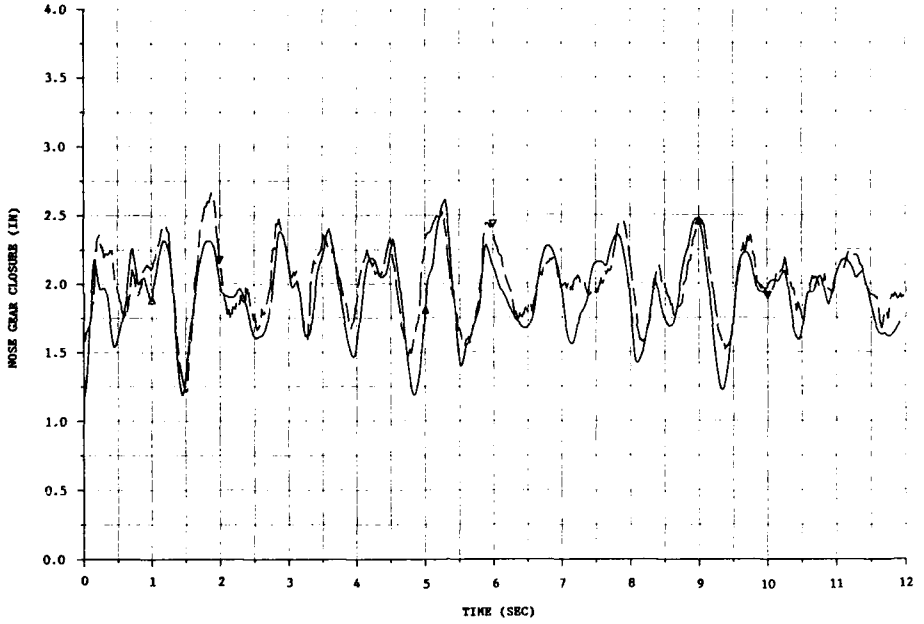

FIGURE 21B. MEASURED AND PREDICTED NOSE GEAR CLOSURE 40 KNOT TAXI OVER GRASS STRIP

4.3.2 Monte Carlo Method

Having accepted that computer-generated surface profiles could be used and that accelerating and decelerating ground runs could be replaced by a series of constant speed runs, the clearance procedure was reduced to one of time series analysis. The simulated ground surface (figure 22 for example) when "traversed" by the model at 50 knots produced the main gear closure time history shown in figure 23.

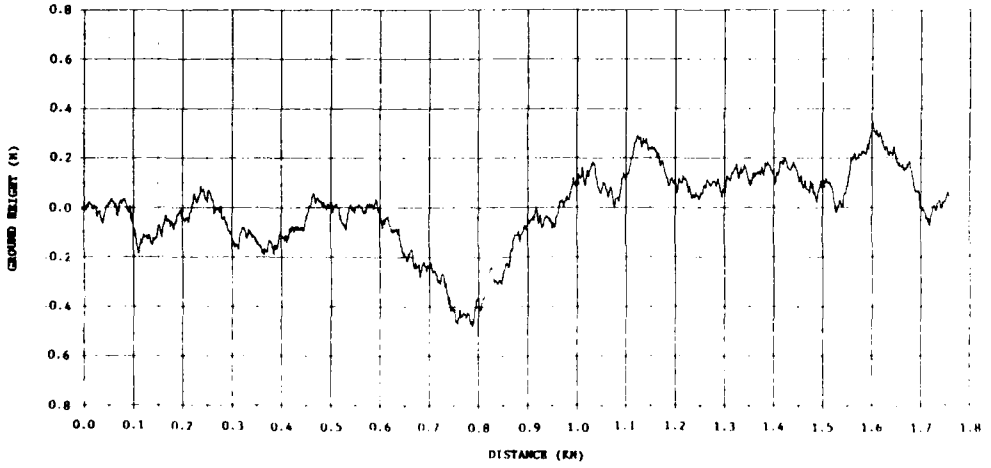

FIGURE 22. TYPICAL COMPUTER GENERATED ROUGH GROUND PROFILE

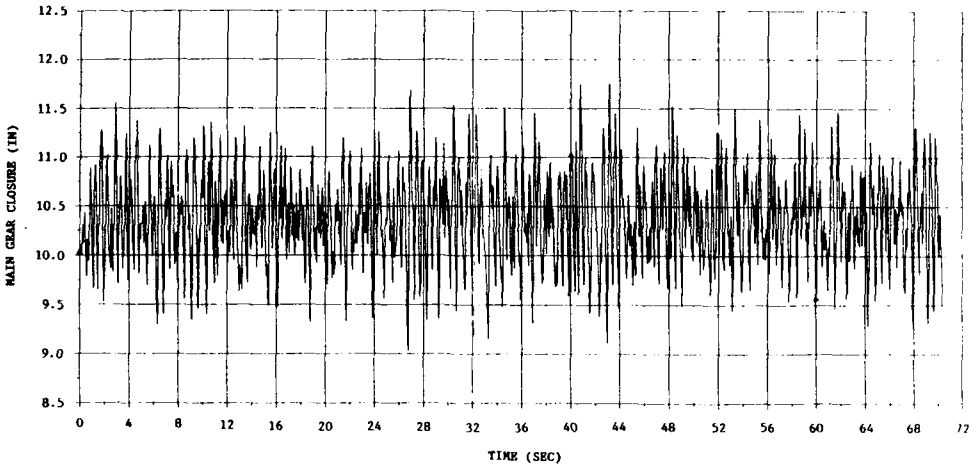

FIGURE 23. MAIN GEAR CLOSURE ON COMPUTER GENERATED PROFILE

These time histories could be processed in any desired way, the most obvious being to determine amplitude or peak probability distributions. Both were tried and, although peak distributions are theoretically desirable, amplitude distributions worked better in practice. Figure 24 is a plot of occurrences in narrow amplitude bands for main strut closure, the most critical quantity in the case of the Harrier at the critical speed. Figure 25 is a cumulative amplitude plot of the same quantity on a grid such that a Gaussian distribution of amplitudes would produce a straight line. It will be seen that the main gear closure plot is not straight, reflecting the nonlinearity of the spring curves since the "ground" surface input was Gaussian.

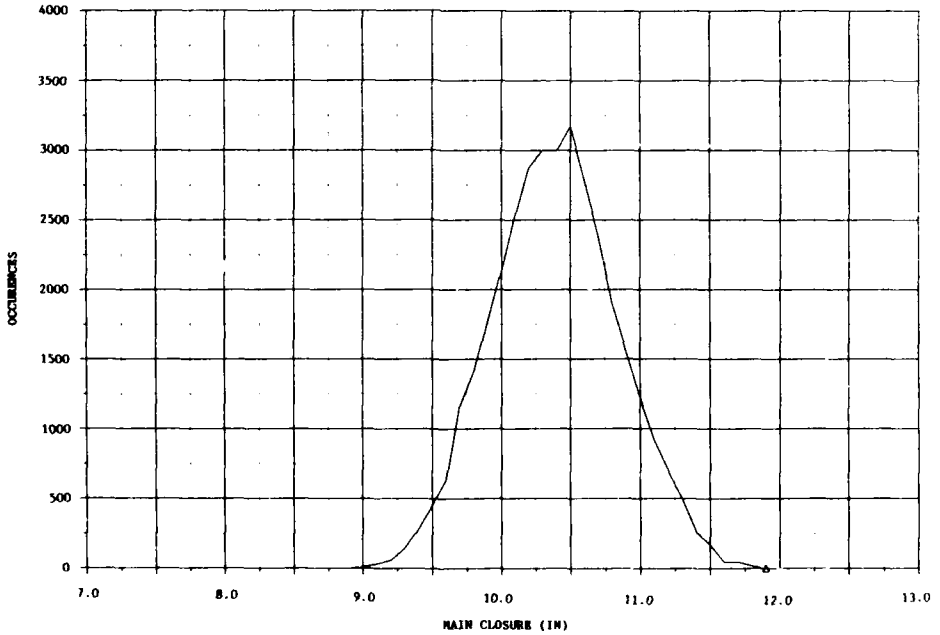

FIGURE 24. MAIN GEAR CLOSURE AMPLITUDE DISTRIBUTION

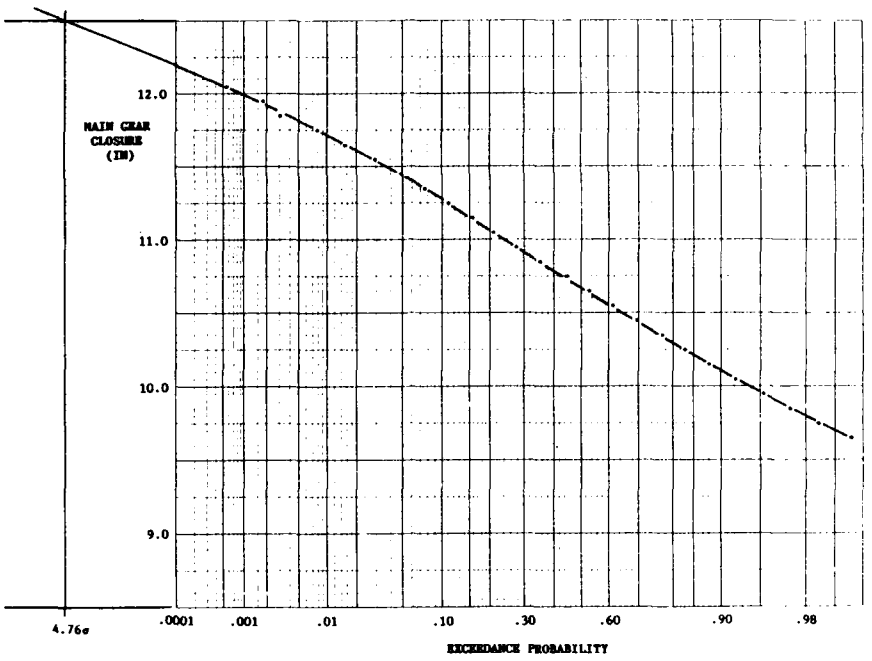

FIGURE 25. MAIN GEAR CLOSURE CUMULATIVE AMPLITUDE DISTRIBUTION WITH EXTRAPOLATION TO CLOSURE LIMIT

Various methods were tried to relate the probability plots to service conditions. All gave similar results; the most satisfactory appeared to be the following:

(a) It was first decided that an acceptable probability of full strut closure would be once per 1000 operations, equivalent to 4000 seconds in the critical speed range.

(b) A fictitious Gaussian distribution is fitted to the upper tail of the cumulative closure amplitude plot. This is represented by the straight line extrapolation in figure 25. Only the upper extremity of the distribution is of importance, of course.

(c) Since the main gear response is essentially narrow-band, with a mean frequency of 1.8 Hz, we may say that the extrapolated Gaussian amplitude distribution corresponds to a Rayleigh peak distribution, and that this may reach full closure once in 7200 peaks (i.e. 1.8x4000). This sets a limit to the standard deviation of strut closure that can be permitted at any particular aircraft weight. Typically, 4.8 standard deviations must be alloved between mean and full closure.

5. RUNWAY DIRECTIONAL STABILITY

The unusual landing gear arrangement of the Harrier has made us conscious of the importance of the directional stability of aircraft on runways, a phase of operation often overlooked, since the usual tricycle arrangement tends to be inherently stable. It is well known, however, that the aircraft of fifty years ago having castering tail wheels, were directionally unstable at low speeds.

Directional stability on the runway can be assessed by relatively simple modelling, but simulator work, with a pilot in the loop, seems necessary for good results. Reference 2 appears to predict tyre cornering power (the dominant effect) with reasonable accuracy, as discussed in section 3.1.

An interesting example of a runway stability problem, from the Harrier (Kestrel) prototype days may be mentioned. Following a very light landing, it was possible for the aircraft to roll over slightly, producing the main gear loading situation shown (exaggerated) in figure 26.

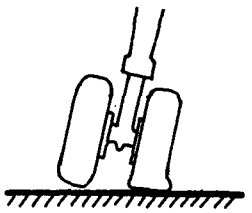

FIGURE 26. MAIN GEAR IN ROLLED ATTITUDE FOLLOWING A LIGHT LANDING

This resulted not only in the loss of (stabilising) side force from one tyre, but also the cornering power of the remaining tyre was reduced by overloading. As shown in figure 27, instead of two tyres operating at point A on the cornering power curve, there was only one tyre at point B. The problem was solved by introducing a main gear modification permitting the strut to compress with almost no load until both outriggers had made contact with the ground, thus avoiding the rolled attitude.

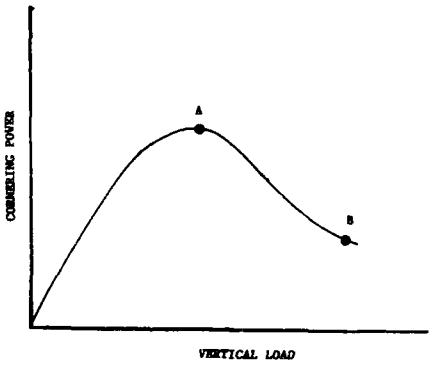

FIGURE 27. REDUCED CORNERING POWER DUE TO ONE TYRE OPERATING AT POINT B INSTEAD OF TWO TYRES OPERATING AT POINT A

6. CONVERTING TO RADIAL TYRES

All marks of Harrier are in the process of converting to radial ply tyres. These tyres have several advantages over cross-ply or bias tyres, as demonstrated in the automotive field. When converting an existing aircraft to radials, load and directional stability implications need to be considered.

6.1 LANDING GEAR LOADS

Instances of increased landing gear loads due to changing to radial tyres can be predicted theoretically. The most obvious is in a conventional or slow landing with appreciable yaw at touchdown where increased "cornering power" (i.e. side force per unit slip angle) can be expected to increase wheel side forces. Also wheel side loads in low-speed turns can be expected to be redistributed. Conversely, the reduced lateral static stiffness of radial tyres would be expected to reduce side loads in vertical landings with lateral velocity, possibly throwing more load on to other wheels, when these are not fitted with radials.

Although the mass of a radial tyre tends to be lower than the equivalent cross-ply tyre, the moment of inertia is generally higher, with implications for spin-up drag.

6.2 DIRECTIONAL STABILITY

The increased cornering pover of radial tyres can theoretically have an effect on runway directional stability, particularly on an aircraft such as the Harrier where not only is there an unusual distribution of static load between nose and main gears (close to 50/50), but also tyre forces generally are large in relation to aerodynamic forces. As with road vehicles radial tyres at the rear are stabilising and at the front destabilizing (assuming an increase in cornering power). At the very least aircraft converted to radial tyres should be assessed by an experienced test pilot. It is also necessary to establish clear rules about the mixing of tyre types.

7. CONCLUDING REMARKS

Ramp-assisted take-off with the Harrier created a new loading action for the landing gear. The resulting loads are readily predictable and no difficulties have been encountered using gear units not originally designed for the purpose.

Vertical landing differs fundamentally from conventional landing in that landing gear side loads, produced by a different mechanism, are potentially as large as the corresponding vertical loads.

The Monte Carlo approach to rough ground clearance on Harrier II resulted in some economies, since it permitted the number of test flights to be reduced without loss of confidence. A similar approach could probably be used for the more common requirement of clearance for operation on repaired runways which might be regarded as random surfaces not necessarily having Gaussian amplitude properties.

Runway directional stability calculations, at their simplest, are relatively easy to carry out and it is surprising that they do not receive as much attention as flight cases. They are indispensable in the case of unconventional landing gear layouts and can be useful also in predicting the effect of burst tyres, steering system failures, etc.

The effects of fitting radial tyres to established aircraft types must be considered seriously, taking into account possible load increases and changes in runway directional stability.

8. REFERENCES

1. British Patent No. 7933885 (US Patent No. 4441671)

2. Smiley, R.F. and Horne, W.B. (Langley Research Center)
"Mechanical Properties of Pneumatic Tires with Special Reference to Modern Aircraft Tires"
1958, RAE Technical Report R-64 (NACA 4110).

9. ACKNOWLEDGEMENTS

The authors are grateful to British Aerospace for permission to publish this paper and for the support of the Procurement Executive, UK Ministry of Defence. Any views expressed are those of the authors and not necessarily those of British Aerospace.

APPENDIX 1

A SIMPLIFIED EXPLANATION OF RAMP-ASSISTED TAKE-OFF

First consider the take-off of a conventional aircraft (figure A1). The runway is used to accelerate the aircraft to flying speed on the ground. Aircraft rotation then produces enough wing lift for unstick.

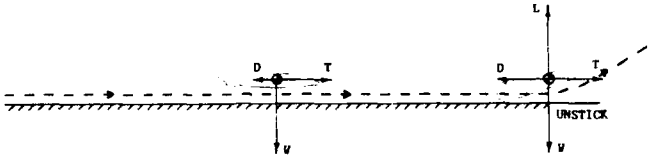

FIGURE A1. TAKE-OFF OF CONVENTIONAL AIRCRAFT

Figure A2 shows a Harrier "short take-off". This aircraft does not rotate in the usual sense; instead the engine nozzles are partially rotated so that the combined upward components of engine thrust and wing lift produces unstick, even though the wing lift is much less than the weight.

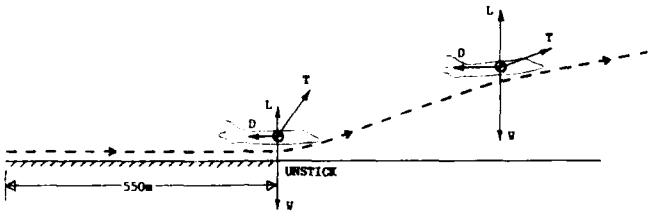

FIGURE A2. HARRIER SHORT-TAKE-OFF (STO) FROM GROUND OR FLAT DECK

Introduce a ramp, as shown in figure A3, with the end 150m from the start of the ground run. First consider the **hypothetical** case of no forward acceleration or lift increase after leaving the ramp. In this case, the aircraft would describe a ballistic, parabolic, trajectory and re-land approximately 1000m from the start point. This in itself is of little use but note that a "runway" 1000m long has been created.

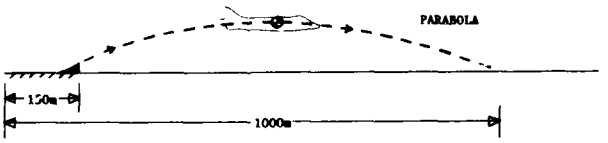

FIGURE A3. BALLISTIC BEHAVIOUR IF AIRCRAFT DID NOT ACCELERATE AFTER RAMP LAUNCH

Actually, as shown in figure A4, the aircraft does accelerate considerably during the ballistic phase and flies out of the parabola because of the build up of wing lift combined with the vertical component of engine thrust. It is using an effective "runway" much longer than the real runway and the ramp-assisted take-off run can be less than one-quarter of that required for a flat STO, explaining the expression "the *runway in the sky*". *It is thus feasible to launch heavy aircraft from very small ships.*

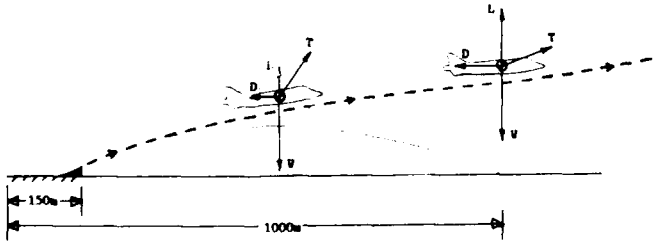

FIGURE A4. ACTUAL BEHAVIOUR WITH AIRCRAFT ACCELERATING

Conventional aircraft have used the ski-jump technique but, in comparison with the Harrier, the reduction in take-off run is considerably less because engine thrust cannot be vectored.

DETERMINATION OF OPTIMUM ANGLE

For a given mark of Harrier, it is possible to produce charts like figures A5, A6 and A7. Figure A5 shows the **minimum** speed at the end of the ramp to give a safe launch as a function of weight and launch angle. This chart would be unaffected by the method of launch: for example it would apply equally well to an aircraft catapulted at that speed and angle. Figure A6 shows the **maximum** launch speed from the viewpoint of the landing gear strut closure as a function of weight and ramp radius. Figure A7 shows the achievable endspeed as a function of weight and deck run.

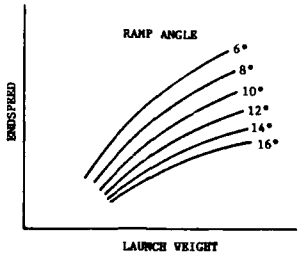

FIGURE A5. MINIMUM ENDSPEED FOR SATISFACTORY TRAJECTORY

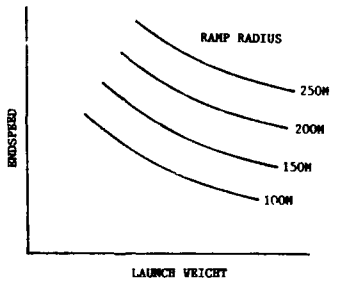

FIGURE A6. MAXIMUM ENDSPEED DUE TO LANDING GEAR LIMITATION

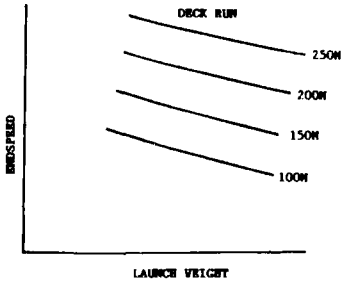

FIGURE A7. ACHIEVABLE ENDSPEED

Deck run is the most fundamental limitation and it is also clear that exit angle and radius are related by:

$$H = R(1 - \cos\alpha)$$

for any given ramp height or length, the other main limitations (see Figure A8).

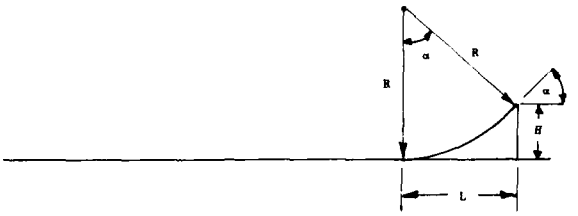

FIGURE A8. RAMP GEOMETRY

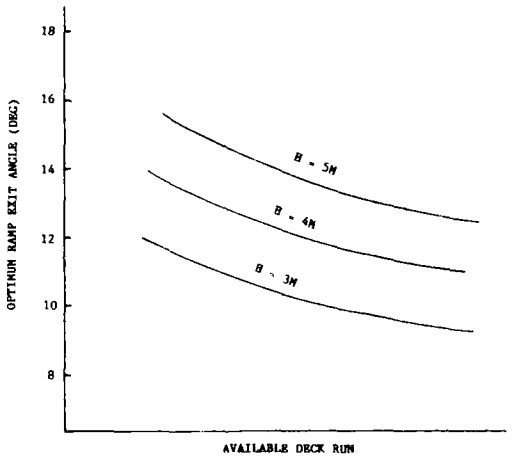

FIGURE A9. OPTIMUM RAMP ANGLE AS A FUNCTION OF RAMP HEIGHT AND AVAILABLE DECK RUN

It is easy to show that an optimum ramp angle exists, defined as that which will permit the maximum aircraft weight to be launched, and is the angle where all three limitations listed below coincide:

(i) PERFORMANCE (Flight)
(ii) LANDING GEAR LOAD/CLOSURE
(iii) DECK RUN.

The optimum angle may be plotted, as a function of available deck run and permissible ramp height as shown in figure A9.

Having determined an approximate optimum angle, simulation methods are used to refine the estimate, taking into account further variables such as wind over deck, ship motion, etc. Although useful as an approximation., having simple geometry, purely circular arc ramps are not recommended for the reasons given in 2.1.

CONSIDERATIONS ON OPTIMALITY OF LANDING GEAR ARRANGEMENT AND DESIGN

A.J.Krauss

MBB-Deutsche Aerospace, Military Airplane Division
Postfach 80 11 60, 8000 Muenchen 80

Germany

1. INTRODUCTION

Much effort has been spent and is still being spent on development and improvement of optimization procedures and computer codes.

The formal task of optimization is to quantify that set of design variables which both satisfies a set of constraints and yields the absolute maximum or minimum of an objective function. One of the intrinsic problems of optimization is that the objective must be expressed as a numerical quantity, which often leads to conversion problems (in which way can one convert a quality into a nonnegative real number?). An other even more serious problem is that formal optimization requires that the dependence of the objective on the design variables must be analytically defined. In relation to these problems it appears of secondary importance that in most cases the optimization process will stop at the local "optimum" which is closest to the starting design, albeit there might exist better optimum solutions across the surrounding ridges of the objective function. Before formal ("automatic") optimization methods are called in, the design must therefore be developed to a starting point in reasonable vicinity to the real optimum.

A retractable landing gear is complex, requires a lot of internal space on the airplane, features a variety of doors, spoils the cleanliness of the structure by large cutouts and local introduction of large loads, and adds weight. Unquestionably the landing gear impairs flight performance proper of an airplane. However, operational benefit from a landing gear apparently is big enough to outweigh said disadvantages. It appears that the primary objective of airplane design is operational usefulness.

Now, having accepted the landing gear as a basically useful subsystem the aircraft designer should proceed by integrating the landing gear into the overall functional optimization of the system. Based on a functionally sound general arrangement of the landing gear, specialists for aircraft-integrated landing gear loads evaluation teamed with landing gear design specialists should provide for optimum detail characteristics fulfilling a variety of design criteria. At that point, the climax of the landing gear related design process could be structural weight optimization which then yields the optimum, i.e. the system integrated optimum function at minimum weight.

The primary aim of present paper is to provide combat aircraft designers with information on landing gears such that they are enabled to treat design conflicts on a rational basis and to solve them with a keen sense of overall optimum.

2. LANDING GEAR FUNCTIONS

The author does not intend to weigh the importance of the various functions of landing gears. Rather there will be the attempt to proceed from "simple" functions to more complex functions while keeping in mind that all these functions cannot truly be separated from each other nor from the aircraft and its characteristics.

2.1 PROTECTION AGAINST UNDUE GROUND CONTACT

This function should be provided in all phases of taxi-out, take-off, landing, taxi-in, and ground operations such as reverse braking. Deficiencies w.r.t. protective function detrimentally affect total weapon system effectiveness and life cycle cost by e.g. increased aircraft downtime due to more frequent structural damage.

2.1.1 Straight Ground Roll

The protective function requires a minimum clearance between the lowest point of the aircraft (including external stores) and the plane ground beneath an "all flat" landing gear. The residual ground clearance is recommended to be at least 0.15 m (6", Ref.1) against fixed and movable parts in their most critical position. Under normal operating conditions, this clearance is deemed sufficient to cope for elastic deflections of landing gear and aircraft as well as for arrestor cables bouncing up behind nose and main landing gear. If the "all flat" condition was caused by a failure, then this clearance leaves the operator with a fair chance to remove external stores from the aircraft before jacking or hoisting. This ground clearance requirement determines the least possible lengths (hence least weight, approximately) of the landing gear legs with a given wheel size.

2.1.2 Landing Touch-Down

Para 2.1.1 has dealt with protection in a virtually ground-parallel attitude when the only requirement w.r.t. main landing gear position is that the effective point of ground contact must not be farther forward than the aircrafts most rear C.G. position with landing gear extended.

Unless the aircraft is equipped with a tail bumper the extreme landing pitch attitude, on an "all flat" main landing gear, sets the requirement. Ref.1 sees that extreme attitude at 90% of the maximum lift coefficient; however, with computerized flight controls and vectorized thrust this may well be exceeded. There should also be consideration of failure cases such as flaps-up landings.

Although, on paper, landing pitch attitudes could be limited by limited pilots' view the designer should not hastily soften up landing gear position requirements on this ground. It might prove relatively easy to improve pilots' ability to compensate poor view (e.g. by electronic means) while cost for repositioning of the landing gear could be prohibitive. Thus considerable landing performance potential can be lost due to an early mistake.

Aspects of protection treated so far are summarized in Figure 1: Acceptable ground clearance in symmetric ground roll and landing is provided by a main landing gear, if the wheel axle or, with a bogie, the bogie pivot in the "all flat" condition is positioned on or below the solid line angle shown in Fig.1.

Ground clearance aspects could be treated without referring to the aircraft's C.G. position. However, fulfilment of the following protective function requires consideration of C.G. position both longitudinally and vertically.

2.1.3 Reversal of Landing Gear Pitching Moment

The ground clearance consideration of para 2.1.2 does not allow for pitch up motion of the landing aircraft. Therefore a straight line normal to the ground line at extreme pitch attitude through the most adverse C.G. position should lie ahead of the main wheel axle in its fully extended position (Fig.2).

This requirement is not only based on protection against ground contact but also on aspects of flight safety and flight performance. Flight safety is enhanced if at all permitted landing touch-down attitudes regardless of runway friction the ground forces on main landing gear induce a pitch-down moment. Flight performance is enhanced if pilots may land their aircraft at high pitch attitude and correspondingly low approach speed without having to expect reversal of landing gear pitching moment.

Fig.3 illustrates that a limitation of landing pitch attitude may lead to considerable increase in landing speed and consequently loss of A/C landing performance.
This loss could eventually be expressed by an analytical function and be included in a formal optimization procedure.

2.1.4 Reverse Braking (Tail-Tipping)

Aircraft handling by ground crew includes coarse brake application while rolling backwards. Operational experience w.r.t. A/C handling by ground crew appears to be cast into a requirement of MIL-A-8862.
Reverse braking at an initial speed of 5 mph (approximately twice pedestrian speed) must not lead to tail-tipping, unless a suitable tail-bumper is provided.

If any possible a tail-bumper should be avoided on a combat aircraft due to various reasons:

- Potential conflicts with arrestor hook.
- Added weight and system complexity.
- With a tail-bumper there is either a modified landing ground clearance requirement eventually leading to a longer and heavier landing gear or design of the tail-bumper and its supporting structure must cope for landing loads.

With C.G. in its most adverse position (rear and high) relative to the main wheel ground contact point in static position, the angle κ (see insert on Fig. 4) could be determined to not less than 39 deg by the simple requirement that a braking ground drag coefficient of $\mu = 0.8$ should not completely unload the nose LG.
However, detailed dynamic analysis of reverse braking yields much less restrictive values for κ.
Results for a combat aircraft (Fig.4) show that in this case a tail-bumper can be avoided if $\kappa \geq 17$ deg.
The geometry of this boundary condition is shown on Fig.5. The dependence of affordable reverse speed on the angle κ could also be cast into a penalty function and be used in a formal optimization procedure.

Cautionary note: The angle κ is measured in the earth-fixed coordinate system. Static pitch attitude of the aircraft must be taken into account to arrive at the appropriate angle in the aircraft-fixed design coordinate system.

2.2 NOSE WHEEL LIFT-OFF

Strictly speaking, only special landing gear designs such as a "Jump Strut" may enhance nose wheel lift-off. However, this function is antithetical to para 2.1.4 Reverse Braking and is therefore due to be discussed here.

An aircraft can be lifted off the runway as soon as Lift exceeds Weight. For conventional HTOL aircraft lift is basically a function of airspeed and angle of incidence. In order to achieve shortest possible take-off ground roll distance maximum allowable incidence should be attained at the time when minimum lift-off speed is reached. To attain the incidence in general requires rotation of the aircraft from a by and large horizontal position. However, this rotation can only take place if and when the aerodynamic moment about the pitch axis overcomes the opposing moment produced by vertical and drag ground forces on the landing gear. Nose wheel lift-off speed must be less than main wheel lift-off speed. Since rotation takes finite time, the required difference between nose wheel lift-off (NWLO) speed and Main Wheel Lift-off (MWLO) speed becomes larger with larger A/C thrust to weight ratio.

The following equation yields the nose wheel lift-off speed with two simplifying assumptions, viz. that the aircraft is rigidly supported on the ground and that lifting forces and pitching moments are produced aerodynamically.

$$V_{NWLO} = \left[\frac{2}{\rho} \cdot \frac{W}{A} \cdot \frac{1}{C_{Maero} \cdot \underline{c}/(l_{main} + \mu_{Roll} \cdot h_{CG}) + C_{Laero}} \right]^{1/2} \qquad (2.2\text{-}1)$$

It is apparent that the easiest way to achieve any desired nose wheel lift-off speed is manipulation of the longitudinal distance from C.G. to main LG ground contact, L_{main}. However, this may lead to operationally unfit LG configurations (e.g. with respect ot reverse braking). To avoid this it is urgently recommended to perform dynamic simulations which include the *flexibility of LG and tyres. This is much closer* to reality than the assumption of rigid support and yields larger affordable L_{main} than eq. 2.2-1.

With modern aerodynamically unstable aircraft designs $dc_K/dc_{\cdot}$ is positive for controls fixed. With regards to V_{NWLO} it would therefore be beneficial to engage artificial stabilization only after nose-wheel lift-off.
If the design of the aircraft features powered lift and/or powered moment (e.g. by thrust vectoring) there should be no problem with V_{NWLO}, as can be seen from Eq. 2.2-2:

$$V_{NWLO} = \left[\frac{2}{\rho} \cdot \frac{1}{A} \cdot \frac{W\text{-LIFTP} - \text{MOMENTP} / (l_{main} + \mu_{Roll} \cdot h_{CG})}{C_{Maero} \cdot \underline{c}/(l_{main} + \mu_{Roll} \cdot h_{CG}) + C_{Laero}} \right]^{1/2} \qquad (2.2\text{-}2)$$

It is certainly possible to derive a formal optimality criterion based on the ratio of V_{NWLO} achieved to desired, but definition of the weighting factor should cope for the fact that LG is not the only contributor to an eventually unsatisfactory V_{NWLO}.

Fig.6 and Fig.7 show that there might be no free choice between a levered and a telescopic main LG design. Whilst at moderate touchdown attitude all requirements of para 2.1 could be met by both designs (Fig.6), an increased touchdown attitude enhances a telescopic design. Telescopic design provides for a static wheel position which is close to the most forward position limit and thus is least detrimental to V_{NWLO}.

2.3 MISCELLANEOUS FUNCTIONS

The following is an incomplete collection of functions which contribute to the rating of a landing gear.

2.3.1 Turning Responsiveness

In adverse conditions (e.g. gusty sidewind, low ground friction coefficient) a good aircraft response to nose wheel steering input is desirable to keep the aircraft on track, especially if this track is a narrow Minimum Operating Strip on a repaired runway.

The performance criterion proposed here is "yaw acceleration per lateral friction coefficient at nose LG". This ratio can be shown to be

$$\dot{\omega}_z/\mu_{lat} = \frac{W}{I_z} \cdot \frac{l_{main} \cdot l_{nose}}{\text{WHEELBASE}} \quad . \qquad (2.3\text{-}1)$$

Eq. 2.3-1 can be rearranged by substituting the distribution of static load on nose and main LG:

$$l_{main}/WB = F_{static\ nose}/W = FPROP_{nose}$$

$$l_{nose}/WB = F_{static\ main}/W = 1\text{-}FPROP_{nose}$$

Eq. 2.3-1 becomes

$$\dot{\omega}_z/\mu_{lat} = \frac{W}{I_z} \cdot WB \cdot FPROP_{nose} \cdot (1\text{-}FPROP_{nose}) \qquad (2.3\text{-}2)$$

This performance criterion improves linearly with wheelbase. The product

$$FPROP_{nose} \cdot (1\text{-}FPROP_{nose})$$

has a maximum of 0.25 at $FPROP_{nose} = 0.5$, i.e. at equal distribution of static load, which is certainly not achievable with conventional LG arrangement. However, within the usual range of $FPROP_{nose}$ (0.08 to 0.15) there is an almost linear increase of the product with $FPROP_{nose}$, i.e. with increasing l_{main}/WB.

2.3.2 Main Wheel Braking Efficiency

Braking relieves main LG vertical load. The magnitude of this relief depends on LG geometry and on the braking drag force.

It appears that the degree to which max. available braking drag coefficient can be converted into A/C deceleration is an appropriate performance criterion:

Brake Efficiency $BE = n_x/\mu_{Brake}$

$$n_x = F_{xBrake}/W$$

$$F_{xBrake} = F_{Vmain} \cdot \mu_{Brake}$$

hence

$$BE = (F_{Vmain}/W)_{braked}.$$

Since

$$F_{Vmain\ braked} = W \cdot l_{nose}/(WB + \mu_{Brake} \cdot h_{CG}),$$

braking efficiency becomes a function of LG geometry and max. available braking drag coefficient:

$$BE = l_{nose}/(WB + \mu_{Brake} \cdot h_{CG}) \qquad (2.3\text{-}3)$$

$$BE = 1-(l_{main} + \mu_{Brake} \cdot h_{CG})/(WB + \mu_{Brake} \cdot h_{CG}). \qquad (2.3\text{-}4)$$

Since the partial derivative of BE w.r.t l_{main},

$$\partial BE/dl_{main} = -1/(WB + \mu_{Brake} \cdot h_{CG}),$$

is comparatively small at a reasonably sized WB the brake efficiency criterion should not exert much influence on the definition of the optimum l_{main}.

2.3.3 Steady and Dynamic Nose Load Increment Due to Braking

With about 10% of aircraft weight, nose LG is relatively lightly loaded statically. However, load shift during steady braking may produce a nose wheel load which is more than twice the static load. If brakes are applied rapidly there is an additional dynamic load increment which in a first approximation may be equal to or even larger than the steady load increment. It can be larger because the progressive characteristic of the usual airsprings effect nonlinear dynamics.

If performance and design criteria of an aircraft comprise operations from bomb damaged and repaired runways this requirement could yield the critical vertical load case on nose LG because the load from the obstacle must eventually be accommodated on top of the dynamic load, but in any case on top of the steady braked load.

Fig.8 shows computer simulation results for a rapid (0.2 s Brake rise time) and a slow (1.0 s) brake application. However, unless automatically controlled, slow brake application cannot be enforced in an operational environment and can hence not be assumed in calculating design loads.

To consistently reduce nose LG load requires reduction of the nose LG load increment due to steady braking, δF_{Braked}.

$$\delta F_{Braked} = W \cdot l_{nose} \cdot \mu_{Brake} \cdot h_{CG}/(WB^2 + WB \cdot \mu_{Brake} \cdot h_{CG}) \qquad (2.3\text{-}5)$$

Eq. 2.3-5 deserves discussion because it offers $\delta F_{Braked} = 0$ for $l_{nose} = 0$ or $h_{CG} = 0$. However, $h_{CG} = 0$ is a physically meaningful solution (i.e. low C.G. position) whilst $l_{nose} = 0$ indicates that A/C weight is supported by nose LG alone and that, regardless of μ_{Brake}, the brake drag force on main LG is zero.

It is therefore necessary to apply performance criteria for nose load increment (Eq. 2.3-5) and for brake efficiency (Eq. 2.3-4) concurrently to obviate an "optimal" solution at $l_{nose} = 0$!

Deriving dynamic nose load increment as a function of LG geometry is a difficult task. However, $h_{CG} = 0$ is a physically meaningful solution (i.e. low C.G. porition) whilst $l_{nose} = 0$ indicates that A/C weight is supported by nose LG alone and that, regardless of μ_{Brake}, the brake drag force on main LG is zero.

It is therefore necessary to apply performance criteria for nose load increment (Eq. 2.3-5) and for brake efficiency (Eq. 2.3-4) concurrently to obviate an "optimal" solution at $l_{nose} = 0$!.

Deriving dynamic nose load increment as a function of LG geometry is a difficult task. However, two points can be deduced from linear dynamics:

- Dynamic load increment will be related to steady load increment.
- Dynamic load increment will reduce with an increase of the ratio of brake rise time to A/C pitch oscillation period.

Provided that brake rise time must not be extended, the latter criterion yields the better a performance the higher the A/C pitch natural frequency on its landing gear. Assuming linear spring stiffnesses c_{nose}, c_{main} pitch natural frequency becomes

$$f = \sqrt{(c_{nose} \cdot l_{nose} + c_{main} \cdot l_{main})/I_y}$$

Since in general c_{nose} and c_{main} are being determined by other considerations, l_{nose} and l_{main} are the design variables. If we further assume that l_{main}/WB , l_{nose}/WB are constants, we get

$$f = \sqrt{C1 \cdot WB/(I_{yo} + C2 \cdot WB^2)} \quad , \tag{2.3-6}$$

where,

$$C1 = c_{nose} \cdot l_{nose}/WB + c_{main} \cdot l_{main}/WB$$

and

$$C2 = m_{nose} \cdot \left(\frac{l_{nose}}{WB}\right)^2 + m_{main} \cdot \left(\frac{l_{main}}{WB}\right)^2 .$$

For conventional LG arrangements the contribution of landing gears to pitch moment of inertia (term $C2 \cdot WB^2$ in Eq. 2.3-6) will be in the order of 5% to 10%. Hence under normal circumstances an increase of wheel base will yield an improvement of pitch natural frequency. Eq.2.3-6 yields f=0 both at WB=0 and WB=∞.

f_{max} is reached at $WB = \sqrt{I_{yo}/C2}$:

$$f_{max} = \sqrt{C1}/(4 \cdot I_{yo} \cdot C2)^{0.25}$$

The term C1 vanishes when the performance criterion is defined as

$$\bar{f} = f/f_{max} = \sqrt{WB} \cdot (4 \cdot C2 \cdot I_{yo})^{0.25}/(I_{yo} + C2 \cdot WB^2)^{0.5} \tag{2.3-7}$$

2.3.4 Pitch Damping

LG damping also is apt to reduce dynamic nose LG load increment due to brake initiation.

There is a great many of possibilities to provide LG damping, ranging from simple constant orifice oil flow restriction over metering pin through semiactive to fully active damping force generation. For sake of simplicity we shall consider constant orifice damping only.

Brake application disturbs static equilibrium of the aircraft on its LG and initiates pitch down motion of the aircraft and diving of the nose LG. Assuming constant LG spring stiffness and A/C mass properties, kinetic energy of the pitching moment will be roughly proportional to the square of the nose LG load increment due to steady braking, and peak pitch rate will accordingly be roughly proportional to δF_{braked} from Eq. 2.3-5. Peak stroking velocity of the nose LG then is proportional to pitch rate times l_{nose}.

Hydraulic damping force is dependent on stroking velocity squared. The size of the damping orifices is in most cases chosen on landing sinkrate and/or on repaired runway considerations. Therefore it may be assumed that the hydraulic damping coefficient is not dependent on l_{nose}. Hence in our case the peak damping force can be assumed proportional to peak stroking velocity squared.

As a convenient performance measure one may use the ratio of peak damping force to the nose LG load increment from Eq. 2.3-5:

$$\bar{F} = F_{D_{peak}} / \delta F_{Braked} \sim \delta F_{Braked} \cdot l_{nose}^2 \quad ;$$

$$\bar{F} \sim \frac{W \cdot \mu_{Brake} \cdot h_{CG}}{1 + \mu_{Brake} \cdot h_{CG}/WB} \cdot \frac{l_{nose}^3}{WB^2} \quad . \qquad (2.3\text{-}8)$$

The result of this coarse assessment is that pitch damping performance of a hydraulically damped passive nose LG improves roughly proportional to l_{nose}.

3. CONCLUSIONS

There are some more landing gear functional performance criteria left to be treated in the future, especially w.r.t. ground roll stability and control with integrated consideration of ground forces and aerodynamic forces and moments.

As a summary from the various criteria discussed above it is concluded that functional performance of a landing gear improves with wheel base for almost any of the criteria treated except Nose Wheel Lift-off.

It is therefore deemed necessary in case of design conflicts to perform detailed dynamic simulations of nose wheel lift-off behaviour as early as possible in the course of a project; if the conflict cannot be resolved thereby serious effort should be applied to solve the problem by total aircraft design and not just by impairing landing gear functional performance.

REFERENCES

[1] Currey, Norman S.
Aircraft Landing Gear Design: Principles and Practices
AIAA, Washington D.C., 1988

[2] Franke, H. (Ed.)
LUEGER Lexikon der Technik, Band (Vol.) 12,
Stichwort "Bugradabheben" (Nose Wheel Lift-off)
Deutsche Verlags-Anstalt, Stuttgart 1967

List of Symbols

A	Nominal Wing Area
BE	Brake Efficiency
C_L	Lift Coefficient
C_M	Pitching Moment Coefficient
c	Spring Stiffness
$\bar{c}$	Mean Aerodynamic Chord
h_{CG}	Height of CG above Ground
I	Moment of Inertia
l_{main}	Horizontal Distance from Main Wheel to CG
l_{nose}	Horizontal Distance from Nose Wheel to CG
LIFTP	Powered Lift
MOMENTP	Powered Pitching Moment
m	Mass
V	Aircraft Speed
Subscript V	Vertical
W	Aircraft Weight
WB	Wheel Base, Distance from Nose Wheel to Main Wheel
κ	Angle between Vertical and a Straight Line from Main Wheel Ground Contact through C.G.
μ	Coefficient of Friction
ρ	Air Density
ω	Angular Rate

Superimposed dot means differentiation w.r.t. time

Abbreviations

CG	Center of Gravity
HTOL	Horizontal Take-off and Landing
LG	Landing Gear
MLG	Main Landing Gear
MWLO	Main Wheel Lift-off
NLG	Nose Landing Gear
NWLO	Nose Wheel Lift-off

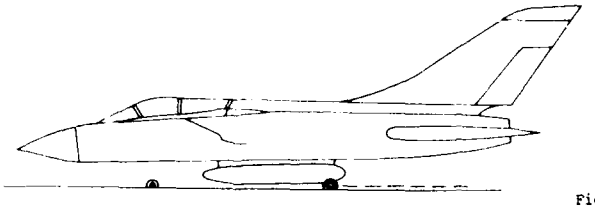

Fig. 1a "All Flat" Ground Roll Attitude

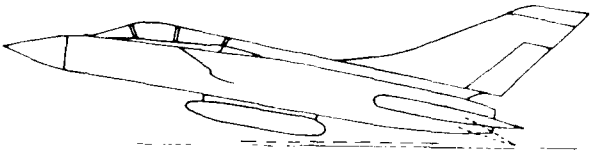

Fig. 1b "All Flat" Landing Attitude

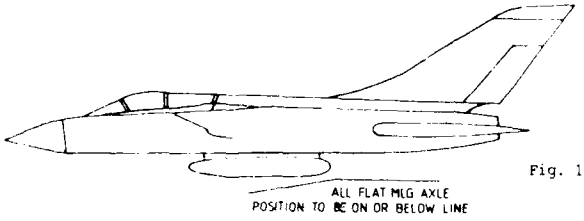

Fig. 1c Combined MLG Axle Positioning Boundary

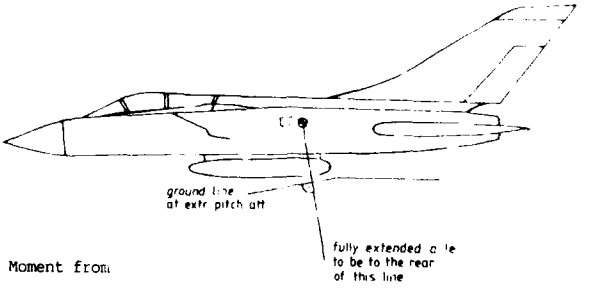

Fig. 2 MLG Axle Position w.r.t. Pitching Moment from Landing Impact

A/C PITCH ATTITUDE VERSUS LANDING SPEED

AT DESIGN SINKRATES

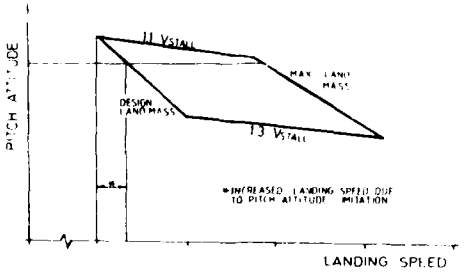

Fig. 3 Loss of A/C Performance due to Pitch Attitude Limitation

Fig. 4 Result of Dynamic Analysis of Reverse Braking

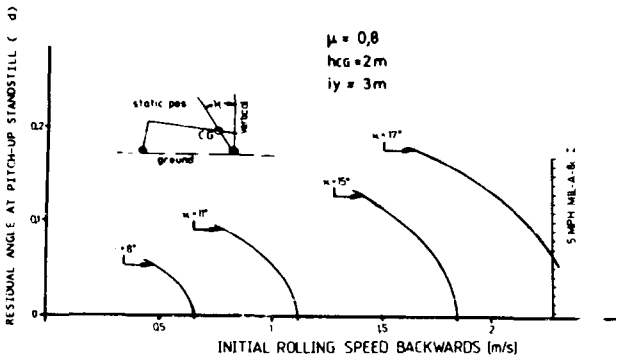

Fig. 5 MLG Position Reqt. due to Reverse Braking

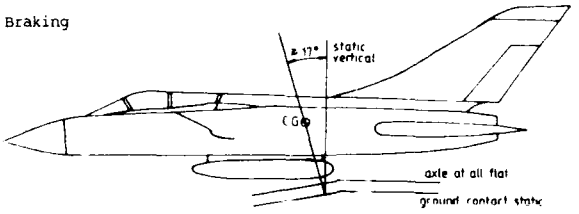

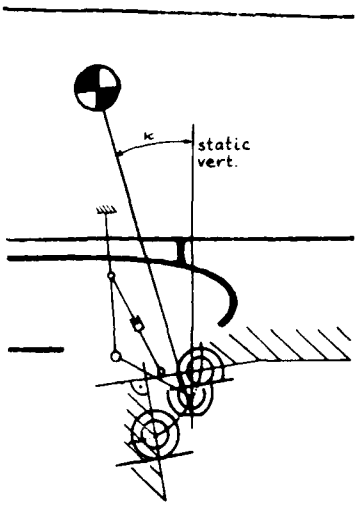

Fig. 6 Fitting of a Levered MLG Design

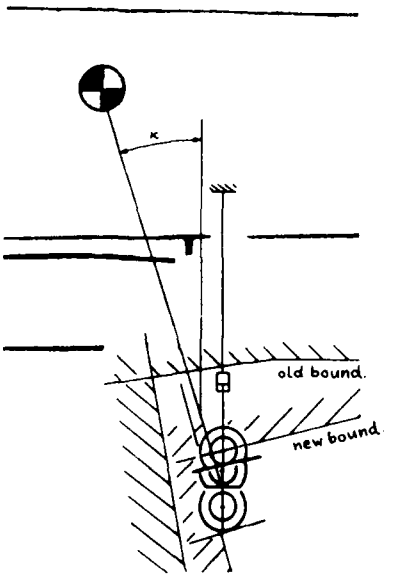

Fig. 7 Fitting of a Telescopic MLG Design at Increased Landing Pitch Angle

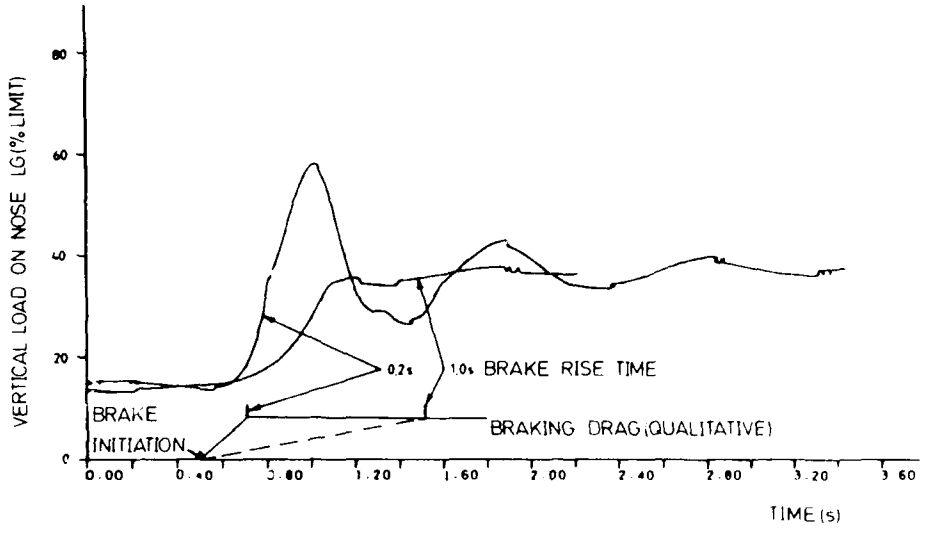

Fig. 8 Nose LG Histograms from Dynamic Braking Analyses

LONG TIME MEASUREMENTS OF LANDING GEAR LOADS ON SAAB SF-340 COMMUTER AIRCRAFT

by
A.L. Gustavsson, A.F. Blom
Structures Department
The Aeronautical Research Institute of Sweden (FFA)
P.O. Box 11021, S-161 11 BROMMA
Sweden

and
L. Helmersson
Aircraft Division
SAAB-SCANIA AB
S-581 88 LINKÖPING
Sweden

SUMMARY

This paper deals with strain gauge measurements of forces acting on the nose gear and main gears of the commuter aircraft SAAB SF-340. During initial flight tests forces in the longitudinal, transversal and vertical directions were measured for various manoeuvres such as take-off, landing, taxiing and towing. The investigation revealed high transversal loads at the main gears at touch-down. The nose gear is most severely strained when steering during taxiing run and when the aircraft is towed connected to a tractor with a tow-bar. The results from such initial measurements formed the basis for a subsequent investigation with on line data acquisition of landing gear loads on a commuter aircraft in service at Swedair AB. The data acquisition system and the data analysis methods are described in some detail. The data acquisition was continuously carried out during nearly six months including various parameters such as different aircraft weight and static landing gear loads. Results from these measurements are presented as cumulative exceedances of longitudinal, transversal and vertical loads obtained from the rain-flow count analyses performed on-line during the measurements.

1. INTRODUCTION

Historically, landing gear loads have been treated scarcely in the literature [1] and not until 1957 was a first attempt made to establish a main landing gear load spectrum [2]. Still 25 years later, the landing gear is one of the fixed wing aircraft's structural components that is most liable to collapse due to fatigue failure [3].

In modern airliners, the landing gear weight constitutes about 2-3 percent of the take-off weight and the landing gears often have to travel total distances in the same order of magnitude as buses and trucks do during a life time. In addition, high running speeds are reached at take off and landing [4]. Furthermore, the landing gear environment features temperature cycling, moisture, de-icing fluids, oil and shots from sand which has to be considered in the fatigue design besides the multi axial loads. In Fig. 1, three load components have been defined for the nose gear and the main gear. A vertical torque may also be included.

When deriving the ground load spectrum for the SAAB SF-340 commuter airliner little statistics were available in the literature for this category of aircraft. Statistics had to be taken from larger aircraft, e.g. the Airbus A300 measurements [5] or smaller aircraft, e.g. of FAR23 category [6]. Consequently, this research project was started which aims at producing landing gear load statistics for commuter airliners.

This paper firstly summarizes the flight test measurements of various manoeuvres, performed in order to obtain time histories of the loads acting on the nose and main landing gears. Secondly, load statistics from in-service measurements obtained during six months of actual usage are presented.

2. INSTRUMENTATION AND CALIBRATION

Strain gauges were applied to the aircraft nose and left main gears in order to measure forces acting on the gears during ground operation as seen in Figs. 2 and 3.

2.1 Initial Flight Test Measurements

Ten strain gauges formed, on each gear, four half bridges and one full bridge. The half bridges were mounted on the wheel hubs in order to measure strains due to bending of the hub caused by vertical and longitudinal forces. The bridges are denoted X_L, X_R, Z_L and Z_R in Fig. 2 and correspond, mainly, to the forces X and Z acting on left and right wheel, respectively. The full bridge, Y, was mounted on the shock strut forming a shear bridge which was believed to give signals proportional to Y-loads.

All gauges were applied below the shock strut to avoid the influence of the variable length of the strut on the forces calculated from the measured strains. Hence, the strain signal would be almost proportional to the force between tyres and ground.

The strain gauge signals were amplified and recorded on a tape recorder using PCM technique. The strain gauge signals were sampled at a frequency of 64 Hz.

The aim of this flight test was to record the forces acting on the landing gear during take-off, landing and ground operations. Consequently, a careful calibration had to be performed to evaluate the relation between measured strains and applied forces. Thus, the loads applied during the calibration must be introduced in a way that corresponds to the loads applied in the test on the runway as closely as possible.

During the calibration, the applied load was recorded together with the simultaneously occuring strains in all bridges. Thus, in the general case, a non-linear system of equations were obtained which relates five force components to five bridge signals. The calibration loads were applied stepwise and the obtained non-linear calibration curves were assumed to be stepwise linear between each calibration point. This can be justified due to the very smooth, almost linear, relationship between strains and loads. The system of non-linear equations was solved for each time-step of recorded strains during the flight test to yield the desired force components. However, the cross influences from one force to another strain gauge bridge were negligible as long as the loads are symmetrically distributed between the wheels of each gear and, hence, the bridge signals were proportional to respective force.

Seven calibration cases were carried out for each gear comprising symmetrical and unsymmetrical forces in both positive and negative x and y directions and in the positive z direction. It is to be noted that force components (F_x and F_z) for each wheel were evaluated but in this paper only the resultants F_x and F_z are presented together with F_y.

2.2 In-Service Measurements

The strain gauge instrumentation for the initial flight test described in the preceeding section was slightly changed for the in-service measurements. In these latter measurements, the half-bridges for measuring the vertical and longitudinal forces on each separate wheel hub in the flight test measurements were rearranged into two full bridges recording the total vertical and longitudinal forces, respectively. The gauges applied for the transversal load, were connected exactly as for the flight test measurements.

The Y gauge on the nose gear was covered with an ebonite protection ring. This ring was applied because it was feared that the nose gear shock strut would be fully compressed, during for instance hard brakings, and, hence, demolish the strain gauges. Generally, the strain gauges were carefully protected against environmental influences such as temperature and moisture, following the outlines in Ref. [4].

The strain gauge signals were amplified and processed on-line with three SWIFT MAS-boxes (a computer based data acquisition system) installed in the aircraft avionic rack. The system with capacity of six channels constitutes 7.5 kg and measure 300 mm × 250 mm × 150 mm, which fullfils the maximum size requirements due to limited installation volume.

The on-line analysis scheme is the so-called rain-flow count algorithm [7]. The size of the Markov-matrices are 64 × 64 in this case. Class number one is the lower limit and 64 the upper limit of the measuring ranges. The measuring ranges are displayed in Table 1 together with class-widths (i.e. accuracy) expressed in terms of forces, for each of the six channels. These measuring ranges and also filter frequencies were established using the flight test measurements as a basis.

When data were retrieved, bridge balances were checked and found stable. The strain gauge bridges were also calibrated electrically at these instances. The Markov-matrices stored in the data acquisition system hardware (RAM) were transferred to a "briefcase computer" and stored on microassettes. Lastly, the data were transferred to a VAX computer for final analysis and plotting.

The loads during the calibration were introduced in a way that was expected to correspond to the loads applied in reality as closely as possible. The vertical loads were applied by the aircraft's own weight measured by a scale positioned under each landing gear. The load was then increased by releasing the jacks carrying the aircraft.

The longitudinal and transversal loads were applied with hydraulic jacks and the landing gear being calibrated posed on a roller bed. Concerning the nose gear, a special device was mounted to the wheels to prevent the gear from rolling and turning around its steering axis during calibration. It should be noted that this load application, where the load is applied over the wheels, is not representative of towing which is performed with a tow-bar attached to the ends of the nose gear wheel hub.

During the calibration, the applied load was recorded together with the simultaneously occuring strains in all bridges. The linearity and one-to-one relation between loads and strains, obtained during the flight test, was confirmed. Thus, the use of bridge signals without corrections for cross-relations between bridges is justified as long as the load application is symmetrical over the wheels. The calibration curves and the linear relationship used to convert bridge signals to forces are given in Ref. [8].

3. LOAD CASES AND FLIGHT CONDITIONS

3.1 Initial Flight Test Load Cases

Four main load cases were considered in the flight test:

- towing
- taxiing
- take-off
- landing

These cases were performed as follows. During towing a tractor connected to the aircraft nose gear wheel hub with an ordinary tow-bar towed and pushed the aircraft over a hangar threshold. The threshold was passed at different angles between the towing path and the threshold: approximately 90°, 70° and 50°, respectively. During the towing and pushing recordings both the nose gear and left main gear passed the threshold. In this case, the treshold consisted of two parallel 40 mm high steel bars separated 165 mm.

The taxiing case consisted of several events as pivoting, symmetrical and unsymmetrical braking, engine run-up and turns. The events took place on the runway. The brakings and the steering manoeuvres were carried out at two different taxi speeds, one referred to as normal taxi-speed and one slower. During the steering manoeuvres the aircraft followed a zigzag path.

Four take-offs and landings were performed. The aircraft status at touch-down are presented in Table 2. The landings, performed in relatively high crosswinds, can be classified as rather hard landings which would occur seldom in service (every hundred to every ten thousand landing according to sink speed statistics [6]).

3.2 In-Service Flight Conditions

The in-service measurements presented in this paper were carried out during the time August 8, 1986, to January 16, 1987, which was divided into five periods. These periods are summarized in Table 3. At the end of each period, data were read out from the shipboard data acquisition system and stored. Also, the number of landings and the number of load sheets collected and processed are displayed in Table 3, together with static loads derived from the load sheets. The total number of landings were obtained from the aircraft's flight log. In Ref. 8, the weight, the number of passengers and the static vertical landing gear load distribution are given for the five periods, as derived from the load sheets. The mean values for each period of the static vertical loads, computed from the load sheets data were used in order to obtain the ground reaction factors described later on in this paper.

The data acquisition system was connected to a switch which was intended to be manually turned off during towing. This means that all ground loading cases except towing were meant to be included in the measurements, i.e. landing, take-off, braking and miscellaneous cases such as ground air-ground transition and others, as listed in Ref. [9].

Finally, Table 4 shows which recordings that have been included in this study (marked with X). Some data were lost due to different reasons. Regarding transversal loads, the strain gauges were applied to the shock strut which appeared to be unwise. Firstly, the surface is very hard and smooth which complicates the application of the strain gauges; the gauge bonding is very uncertain. Secondly, the sealing used firstly seemed to dissolve in the hydraulic oil. This problem was overcome later. Thirdly, concerning the nose gear, the shock strut almost closed during the operation as expected. However, despite the ebonite protection ring, the strain gauges were destroyed since the ring was twisted around the shock strut. These three circumstances caused all transversal load data at the nose gear to be discarded and, also, the two first ones of the main gear.

Regarding the amount of lost vertical load data of the main gear, it is explained by trouble with a pin plug. Also contact problem during data extraction caused the loss of F_x^m and F_y^m during period four.

4. RESULTS AND DISCUSSION

4.1 Initial Flight Tests

The results were originally presented in Ref. [10] as time-history plots and rain-flow count data in tables and graphs. Far from all that data will be presented here but the interest will be focussed upon some of the most revealing results.

The severity of nose gear longitudinal loads during towing and pushing has been pointed out earlier [9]. The high load intensities emanate from the connection of the tow-bar to the nose gear. However, the results have to be interpreted carefully since the load application during calibration was different from that when using the tow-bar. F_x measured during towing was therefore found to be too high, by a factor of about two, as is further discussed in the subsequent section.

For obvious reasons the nose gear will be strained at starting and stopping during towing as seen in Fig. 3. Furthermore, when the main gear passes an obstacle, in this case the hangar threshold, a high peak load on the nose gear occurs as seen at the arrow in

Fig. 3. From a fatigue point of view load ranges rather than individual load peaks are of relevance. Therefore, data may be presented as in Fig. 4. This figure displays half cycles of ground reaction factors from rain-flow count analyses of the individual towing records. The ground reaction factor is defined as the ratio between the studied load component and the static vertical load of that gear, e.g. $e_x = F_x/F_{z,stat}$.

Figure 5 shows a record of the main gear loads from the zigzag taxiing case at normal taxi speed. The variation in loads due to steering is clearly seen. By combining the peak values of each individual steering manoeuvre and evaluating the ratio $(F_z - F_{z,stat})/F_y$ a good correlation was found between F_z and F_y for the main gear when separating left and right turns as seen in Table 5. The difference between right and left turn results diminished when the taxi speed was lowered. Rain-flow count ranges of the lateral loads at zigzag taxiing are presented in Figs. 6 and 7, together with lateral loads at touch down, for the nose and left main gear. The large values shown in Fig. 6 are believed to be related to cross-relation of loads acting in different directions, as one of the wheels is lifted off the ground during manoeuvres at large angles.

Finally, a typical landing record is shown in Fig. 8. The three events, maximum vertical load at landing impact (T.D.), spin-up (S.U.) and spring-back (S.B.) can be seen first for the main gear and, slightly afterwards, for the nose gear. In Table 6, several ratios introduced in Ref. [9] are presented. It should be noted that the load F_y does not necessarily occur simultaneously as $F_{z,T.D.}$ but at the same landing. Also, worth noticing is the difference in the recorded dynamic $F_{x,S.B.}$ in this investigation and that of Ref. [9]. In the latter, the dynamics of almost the entire landing gear is included since the strain gauges are applied high up on the shock strut whereas the present study only includes the inertia of the wheels; the strain gauges are positioned on the wheel hubs. The ratios for the nose gear seem to be more unanimous than for the main gear. This may be a consequence of more uniform conditions when the nose gear reaches the ground, i.e. both main gears in contact with ground. As mentioned above, the lateral load factors at touch down are presented in Figs. 6 and 7 as rain-flow count ranges. It is clear that the load factor ranges are smaller at the main gear in general and that steering load ranges at the nose gear is much more pronounced compared to the landing loads than for the main gear. On the other hand, one shall bear in mind that the static vertical load at the main gear is about 5 times higher than at the nose gear. This obviously influences the magnitude of the ground reaction factors for the gears under consideration. The main gear maximum transversal ground reaction factors at landing was -0.53, 0.35, -0.33 and 0.39, respectively.

The results presented in Figs. 3-8 were obtained primarily to gain experience for the planning of the in-service measurements discussed below.

4.2 In-Service Measurements

Although the runway conditions ranged from dry or wet summer conditions to winter conditions with snow and ice no significant differences between the spectra for the different periods could be discerned.

For this reason the mean spectra, after removal of unrealistic cycles due to identified problems with the measurements as described below are presented herein. The number of cycles are normalized to 90 000 flights, which is the aircraft design life, and the range cycles refer to full cycles. The load levels in the spectra represent the middle of the classes in the rain-flow count registration. As the used instrumentation did not realistically monitor the towing loads these have been excluded in all the presented results.

Spectra for ground reaction factors obtained by dividing the measured forces with the mean vertical static load during each measuring period are presented in Figs. 9-13 for nose gear x- and z-directions and main gear x-, y- and z-directions, respectively. It should be noted that the actual vertical static load for an individual flight may differ roughly ±10 % from the used mean value. Due to the correlation between high loads and high vertical static loads this will result in the ground reaction factor spectra being conservative at the high load end and unconservative at the low load end (with the total effect on cumulative damage being conservative).

The remaining effects of the interference from Y-loads in the Z-loads measurements, described below, will have an additional conservative effect on the Z-loads spectra.

Figure 9 shows the x-ground reaction factor spectrum for the nose gear after removal of some recorded unrealistic load cycles. These unrealistic loads are due to towing and nose gear shimmy. As already noticed in the flight tests summarized above the equipment used for calibration of X-loads on the nose gear was not representative for actual towing during service. Therefore, it was decided to manually switch off the data acquisition system during towing. Unfortunately, however, this was forgotten in a number of cases. For periods 3 to 5 the relatively few unrealistically high nose gear x-loads due to towing are easily recognized against the rest of the loads in the spectra (spin-up, spring back and runway roughness) and are excluded from the spectra.

For periods 1 and 2 the numbers of unrealistically high nose gear x-loads are so high that they cannot be explained as towing loads only. During these periods nose gear shimmy was, however, reported. It is reasonable to assume that the measurements will give exaggerated X-loads for this condition, analogously to the exaggerated towing loads measured when the nose gear passes a threshold at an angle other than 90°. The frequency 15-20 Hz during nose wheel shimmy would also produce the registered number of cycles.

As the instrumentation is judged to give unrealistic loads for this condition, and as nose gear shimmy should normally never occur in-service, the nose gear X-load data from periods 1 and 2 are discarded.

Figure 10 shows the Z-ground reaction factor spectrum for the nose gear, also after removal of some unrealistic load cycles. The presence of towing and nose wheel shimmy during the measurements does not appear to significantly affect the nose gear Z-loads.

The nose gear Z-loads spectra for periods 2 and 3 look very different from those from the other periods with an unrealistically high number of cycles (roughly 1000 per flight) between the static ground load and zero. This is caused by a large number of trough values being registered as zero rather than as some positive value. This must evidently come from an intermittent lack of electrical contact during ground runs and the cycles are thus removed from the spectra. The relatively large number of cycles to zero for periods 1, 4 and 5, which are not cycles to the static ground loads are believed to be due to bouncing of the nose wheel due to the combination of a relatively hard shock absorber and runway roughness. This effect has been reported for other aircraft also, see Ref. [5].

The Z-load spectrum for the nose gear (and to a lesser extent for the main gear) contains some unrealistically high negative loads. The only negative Z-loads that occur in service are the massloads when the shock strut reaches its stop in extension. FAR/JAR 25.487 "Rebound landing condition" specifies a limit load factor of 20 g acting on the unsprung weights of the landing gear for this case. Assuming that these requirements represent the maximum realistic condition, and considering that only massloads from weights outboard of the strain gages will be measured by the FFA-instrumentation, results in a limit for realistic negative values in the measurements of -3.6 kN for the nose gear (-11.3 kN for the main gear). Cycles with larger negative values are thus removed from the spectra.

A discussion of the origin of the unrealistically high measured negative values is needed, however. Unrealistically high negative loads were present in the spectra from all the periods and the numbers were roughly the same as the number of X-loads from towing. It would thus be tempting to explain the loads as vertical loads introduced by towing but the time histories from the initial flight tests for towing and pushing across a hangar threshold gives no support for this.

A factor that may sometimes strongly affect the accuracy of the Z-loads measurements is that the strain gages on the wheel hubs, calibrated for Z-loads, will measure bending due to Y-loads also. In fact the leverage from the Y-load at the wheel-ground contact point to the strain gages is roughly 3 times that for the Z-load. As long as the Y-load is equally distributed between the left and right wheels of the gear this will not affect the measured Z-loads. For cases with an unequal distribution of the loads, such as a banked drift landing, significant errors will result, however. The difference in loads between the wheels is likely to be greater for small Z-loads than for large Z-loads and can explain the unrealistic negative loads which were measured.

The surprisingly high positive Z-loads which have sometimes been registered are believed to be mainly due to the nose gear touchdown after landing. This is supported by the fact that the nose gear shock strut was sometimes almost fully compressed during the measurements.

Figures 11-13 show the ground reaction factor spectra, for the main gear, in the x-, y- and z-directions, respectively. The only editing performed on the measured data is that cycles with z-loads outside of the limit for realistic negative values (-11.3 kN), see discussion for nose gear above, are removed from the spectrum shown in Fig. 13.

Finally, a comparison between the ground reaction factor spectra, normalized to the aircraft design life of 90 000 flights, for the nose gear and the main gear is shown in Fig. 14 for X-loads and in Fig. 15 for Z-loads. The ground reaction factor in these spectra are significantly higher for the nose gear which agrees with the results from other aircraft, see Ref. [5].

5. ACKNOWLEDGEMENTS

Financial support from the Swedish Board for Technical Development, the Swedish Civil Aviation Administration and SAAB-SCANIA AB is gratefully acknowledged. The authors are indebted to Bengt Johansson and Rickard Vinthagen at SAAB-SCANIA AB, to Karl-Erik Viklund and Hans Karlsson at SWEDAIR AB, and to Bo Norrbom, Ivar Ahlström and Inez Engström at the Aeronautical Research Institute of Sweden, for helpful co-operation during the course of this work.

6. REFERENCES

[1] Gustavsson, A.I.: "A Literature Survey of Ground Load Statistics for Landing Gear Fatigue Design Purposes". FFA TN 1984-39. The Aeronautical Research Institute of Sweden, Stockholm, 1984.

[2] McBrearty, J.F.: "A Review of Landing Gear and Ground Loads Problems". North Atlantic Treaty Organization Report 118, 1957.

[3] Campbell, G.S.: "A Survey of Serious Aircraft Accidents Involving Fatigue Fracture, Vol. 1, Fixed-Wing Aircraft", Aeronautical Note NAE-AN-7, NRC No. 21276, National Research Council Canada, April 1983.

[4] Ladda, V., and Zaschel, J.M.: "Long Time Measurements with Strain Gauges to Investigate the Landing Gear Loads on Airbus A300". (In German: "Langzeituntersuchungen mit Dehnungsmesstreifen zur Ermittlung der Fahrwerkskräfte am Airbus A300", Messtechnische Briefe 15, Heft 3, 1979.

[5] Buxbaum, O., Ladda, V., and Zaschel, J.M.: "Operational Loads at Nose- and Main Landing Gear of an Airplane of Type Airbus A300 B2 during Normal Service of the Deutsche Lufthansa". (In German: "Betriebslasten am Bug- und Hauptfahrwerk eines Flugzeuges von Typ Airbus A300 B2 während des Einsatzes bei der Deutschen Lufthansa"), Fraunhofer-Institut für Betriebsfestigkeit (LBF) Darmstadt, Final Report No. 3691, March 1981.

[6] Christian, R.D.: "FAR23 Fatigue Substantiation Procedures", GAMA Committee Report SAE 710403, March 1971.

[7] de Jonge, J.B.: "The Analysis of Load-Time Histories by Means of Counting Methods", NLR MP 820 39U, Report, National Aerospace Laboratory NLR, the Netherlands, August 1982.

[8] Gustavsson, A.I.: "In-Service Measurements of Saab SF-340 Landing Gear Loads". FFA TN 1987-48. The Aeronautical Research Institute of Sweden, Stockholm, 1987.

[9] Buxbaum, O.: "Landing Gear Loads of Civil Transport Airplanes". Proceedings of the 11th ICAF-Symposium held in Noordwijkerhout, The Netherlands, ICAF Doc. No. 1216, May 1981.

[10] Gustavsson, A.I. and Johansson, B.: "SF-340, Development Ground and Flight Test Report - Study of Landing Gear Loads". SAAB Report No. 72GTS4322, SAAB SCANIA AB, Linköping, Sweden, 1985.

Table 1 Summary of measuring ranges and accuracy during in-service measurements

Channel	Loading component	Lower limit [kN]	Upper limit [kN]	Class width [kN]
1	F_x^m	58.9	-59.2	1.85
2	F_y^m	-65.8	66.6	2.07
3	F_z^m	81.7	-81.3	2.55
4	F_x^n	48.3	-48.4	1.51
5	F_y^n	-23.4	23.4	0.71
6	F_z^n	46.0	-45.8	1.43

Table 2 Landing conditions during flight test measurements

Loading	Weight 10^3 kg	Angle of climb degree	Sinking speed m/s	Bank angle degree
1	11.0	5.79	0.76	-1.87
2	11.0	6.07	1.46	-8.14
3	10.9	5.16	0.76	0.14
4	10.9	3.50	2.13	0.01

Table 3 Summary of the measurement periods with corresponding static loading conditions

Period No.	Date From	Date To	No. of flights	No. of load sheets	$\bar{W}$ [kg]	s_W [kg]	$\bar{F}^m_{z,stat}$ [kN]	s_F [kN]	$\bar{F}^n_{z,stat}$ [kN]	s_F [kN]
1	860808	860829	250	205	10718	762	47.8	3.68	9.68	0.61
2	860930	861109	654	523	10667	784	47.5	3.80	9.71	0.67
3	861110	861204	326	215	10862	781	48.5	3.72	9.68	0.65
4	861205	861227	266	215	10558	836	47.2	4.64	9.32	0.62
5	861228	870116	183	159	10623	758	47.4	3.76	9.54	0.60

Table 4 Showing which recordings that were successful (X) and which ones that failed for different reasons (-)

Period	F^m_x	F^m_y	F^m_z	F^n_x	F^n_y	F^n_z
1	X	-	X	X	-	X
2	X	-	-	X	-	X
3	X	X	-	X	-	X
4	-	-	-	X	-	X
5	X	X	-	X	-	X

Table 5 Relation $(F_z - F_{z,stat})/F_y$ of left main gear during zigzag taxiing

Turning direction	Normal speed Mean	Normal speed Standard deviation	Low speed Mean	Low speed Standard deviation
Right	-0.86	0.12	-1.06	0.15
Left	-1.28	0.13	-0.94	0.13

Table 6 Certain load ratios obtained at landing with SAAB SF-340

	Nose Gear		Left Main Gear		
Landing No.	$\frac{F_{x,S.B.}}{F_{x,S.U.}}$	$\frac{F_{x,S.U.}}{F_{z,L.I.}}$	$\frac{F_{x,S.B.}}{F_{x,S.U.}}$	$\frac{F_{x,S.U.}}{F_{z,L.I.}}$	$\frac{\lvert F_y \rvert}{F_{z,L.I}}$
1	-0.26	-0.62	-0.12	-0.79	0.92
2	-0.26	-0.66	-0.52	-0.55	0.33
3	-0.22	-0.69	-0.53	-0.49	0.42
4	-0.30	-0.65	-0.23	-0.70	0.48
Mean	-0.24	-0.66	-0.35	-0.63	0.54
Standard deviation	0.06	0.03	0.21	0.14	0.26

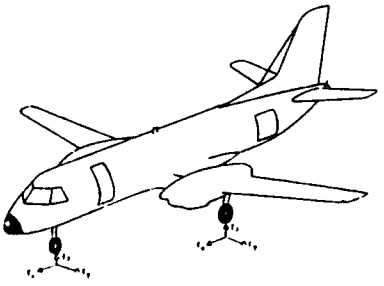

Figure 1. Definition of load components

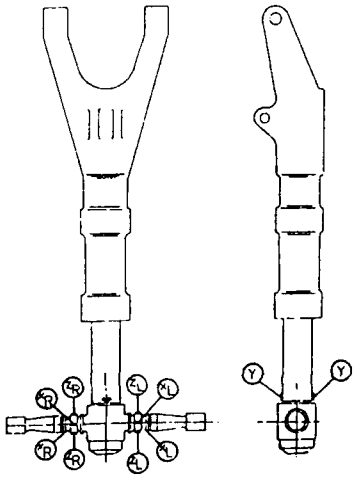

Figure 2. Strain gauge installation at the main gear of SF-340. The nose gear is instrumented in the same way

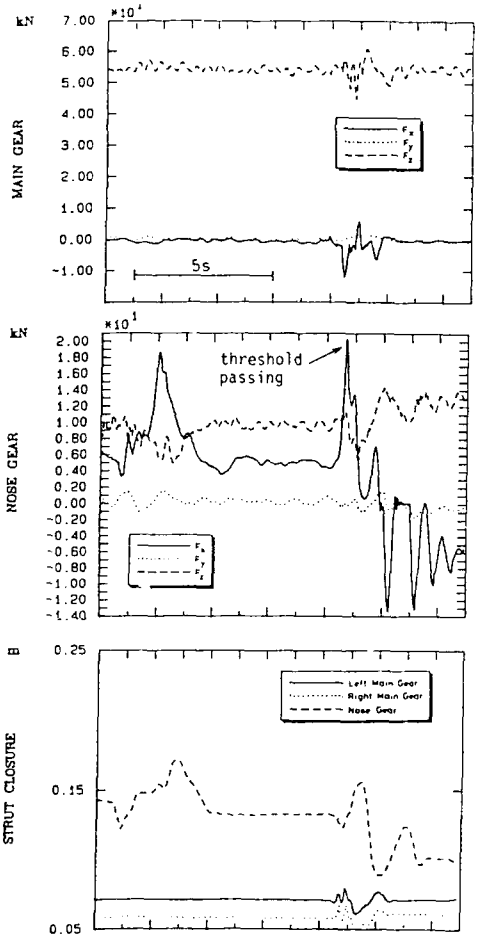

Figure 3 Time-histories of towing over a hangar threshold at 90° angle between towing path and threshold

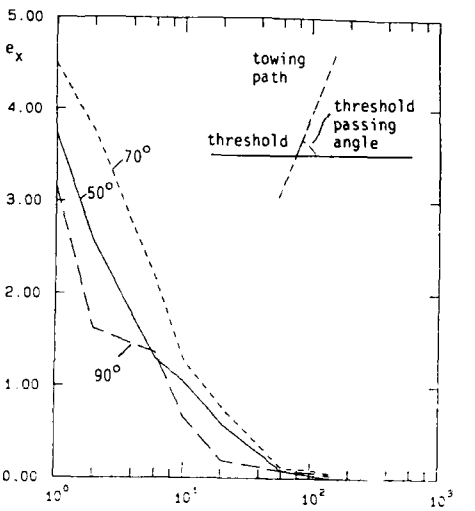

Figure 4 Cumulative frequency distribution of range-pair ranges of longitudinal ground reaction factor, e_x, at nose gear at towing. Ranges are presented as half cycles

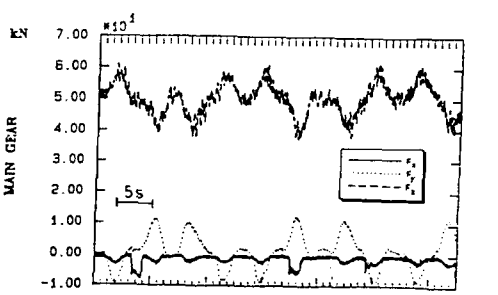

Figure 5 Main landing gear loads at normal speed during zigzag taxiing

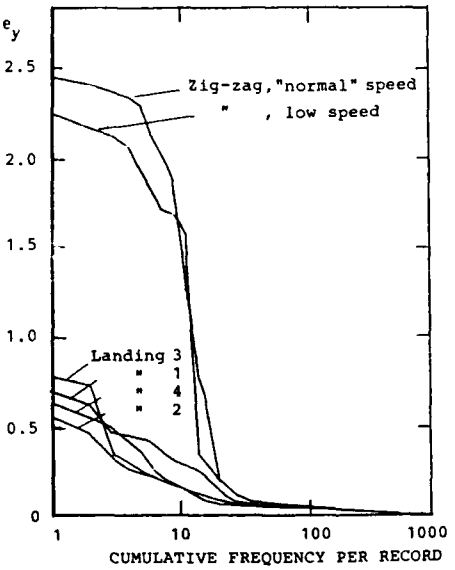

Figure 6 Cumulative frequency distribution of range-pair ranges of transversal ground reaction factors, e_y, at nose gear at zigzag taxiing and landing. Ranges are presented as half cycles

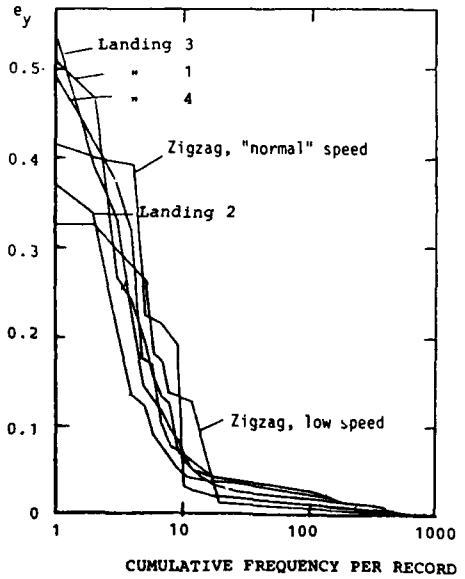

Figure 7 Cumulative frequency distribution of range-pair ranges of transversal ground reaction factors, e_y, at left main gear at zigzag taxiing and landing. Ranges are presented as half cycles

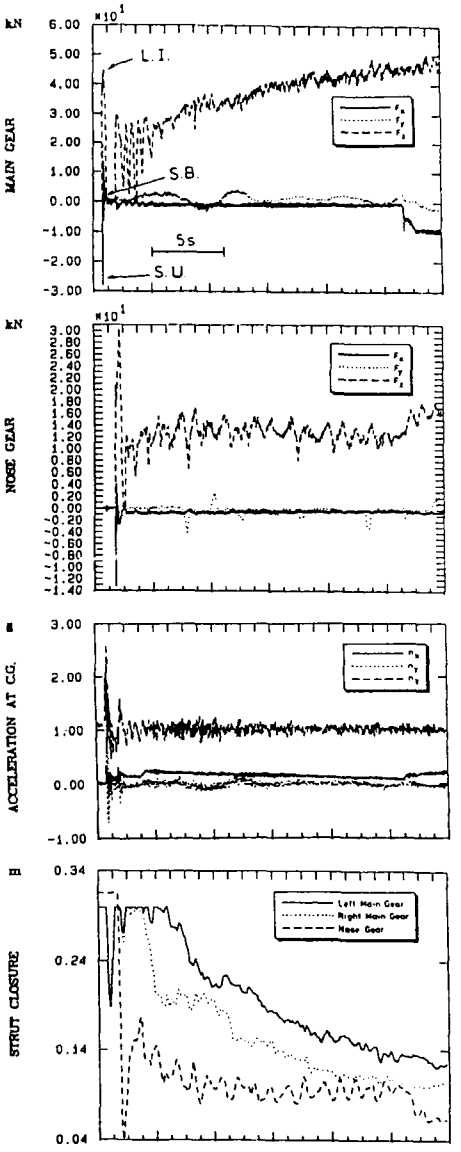

Figure 8 *Time-histories of a landing*

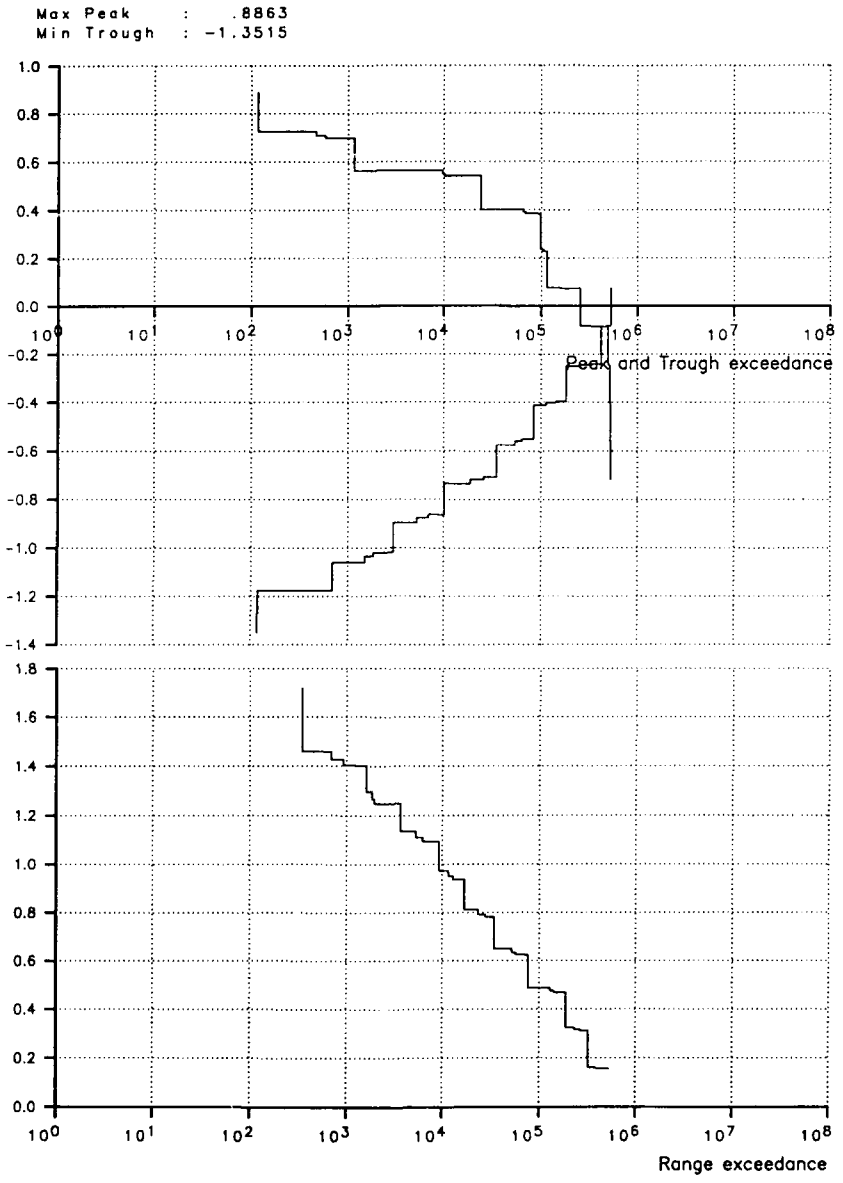

Figure 9 Nose gear spectrum. 90000 flights. Towing excluded.
X-ground reaction factor. FFA in-service measurements

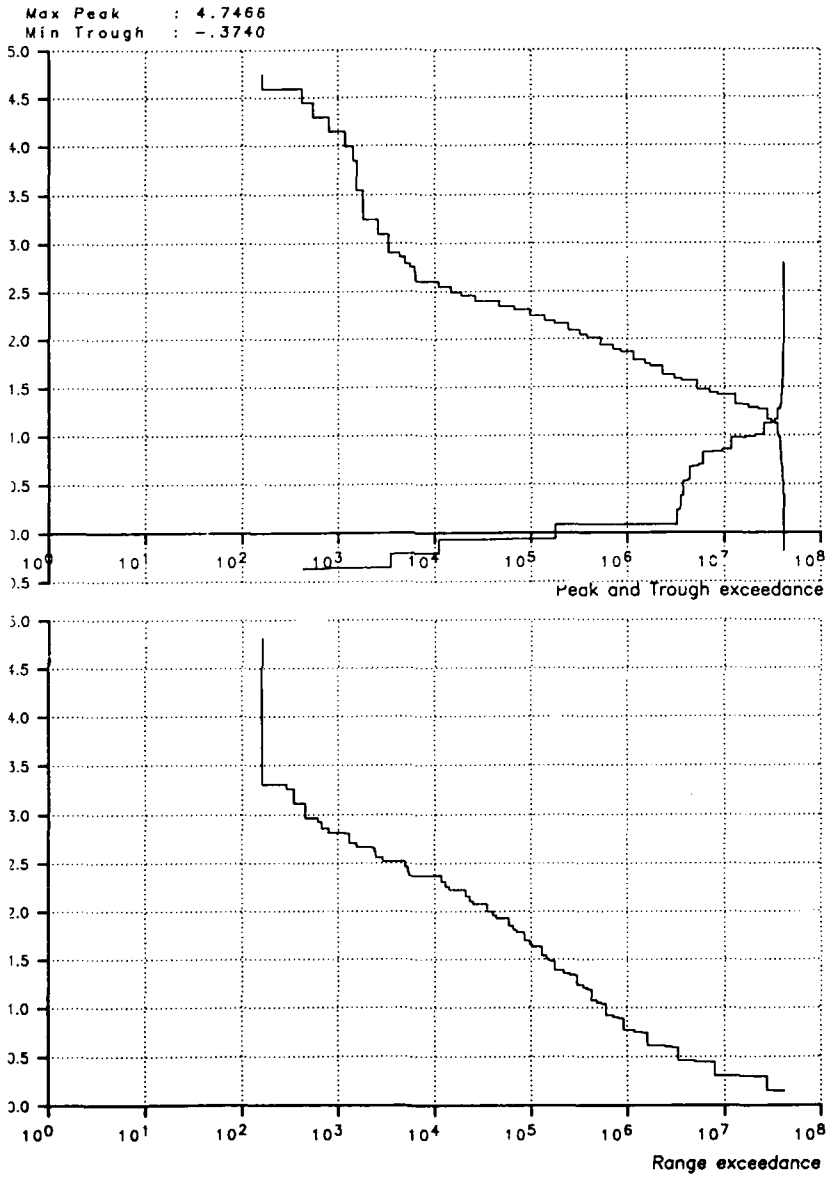

Figure 10 Nose gear spectrum. 90000 flights. Towing excluded.
Z-ground reaction factor. FFA in-service measurements

Max Peak : .5106
Min Trough : -.7219

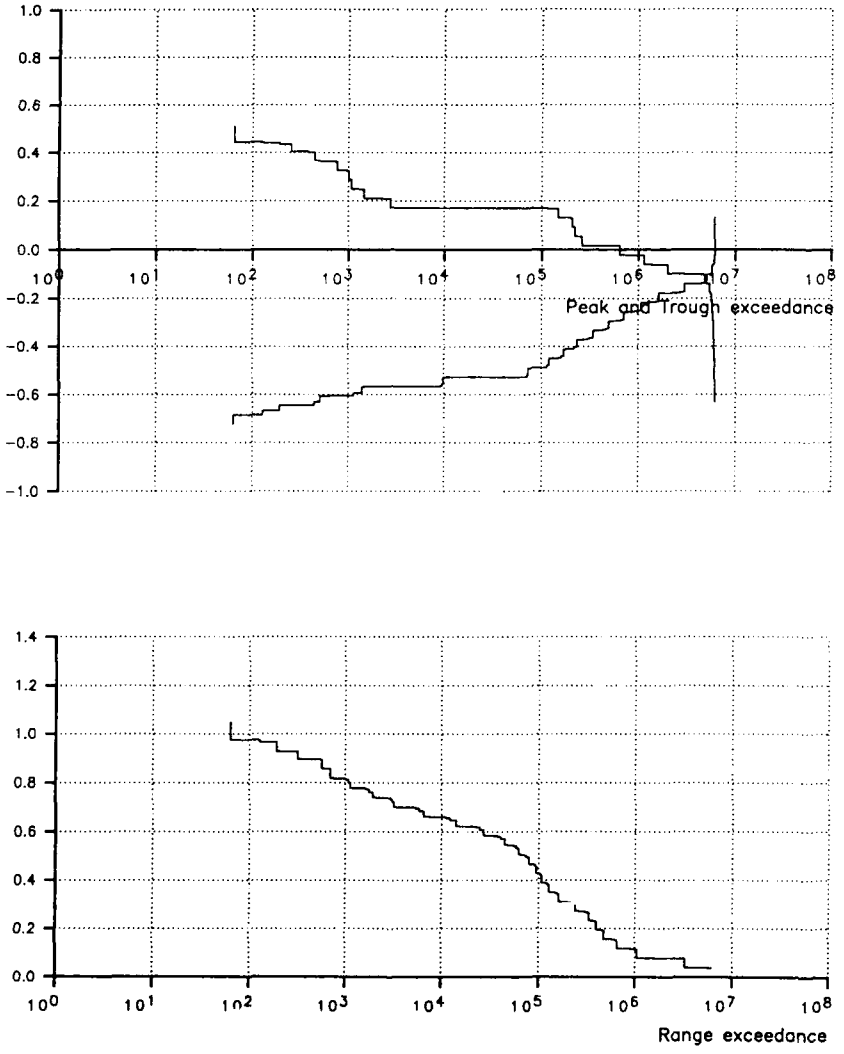

Figure 11 Main gear spectrum. 90000 flights. Towing excluded.
X-ground reaction factor FFA in-service measurements

Max Peak : .4988
Min Trough : -.4498

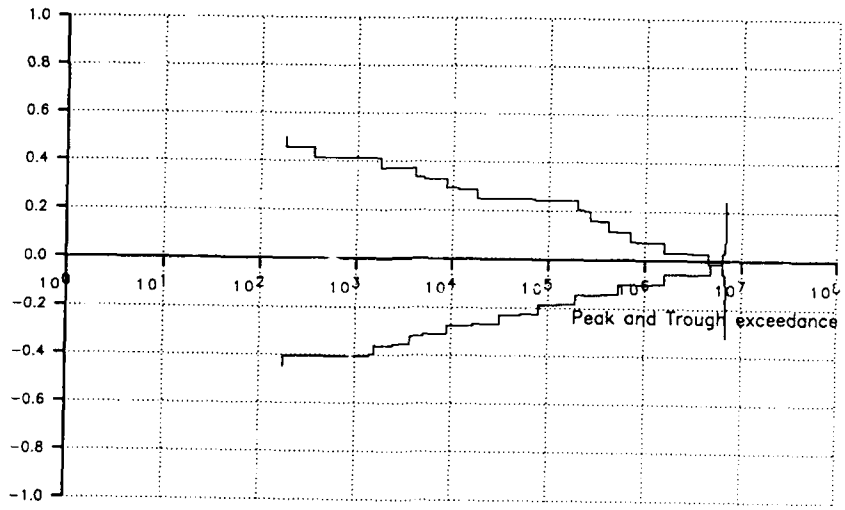

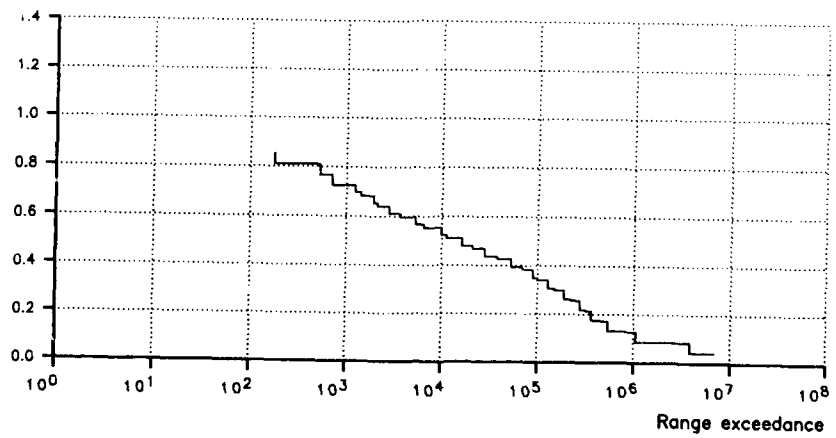

Figure 12 Main gear spectrum. 90000 flights. Towing excluded.
Y-ground reaction factor. FFA in-service measurements

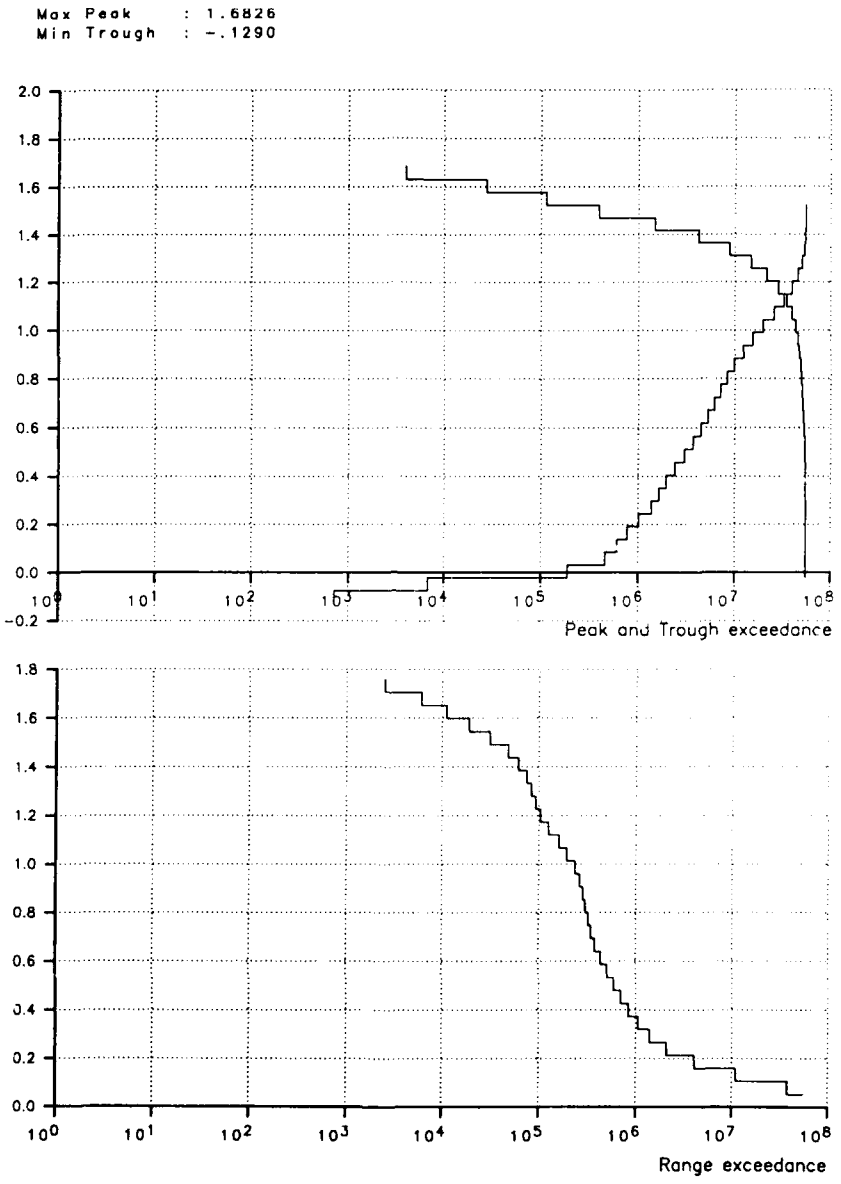

Figure 13 Main gear spectrum. 90000 flights. Towing excluded.
Z-ground reaction factor. FFA in-service measurements

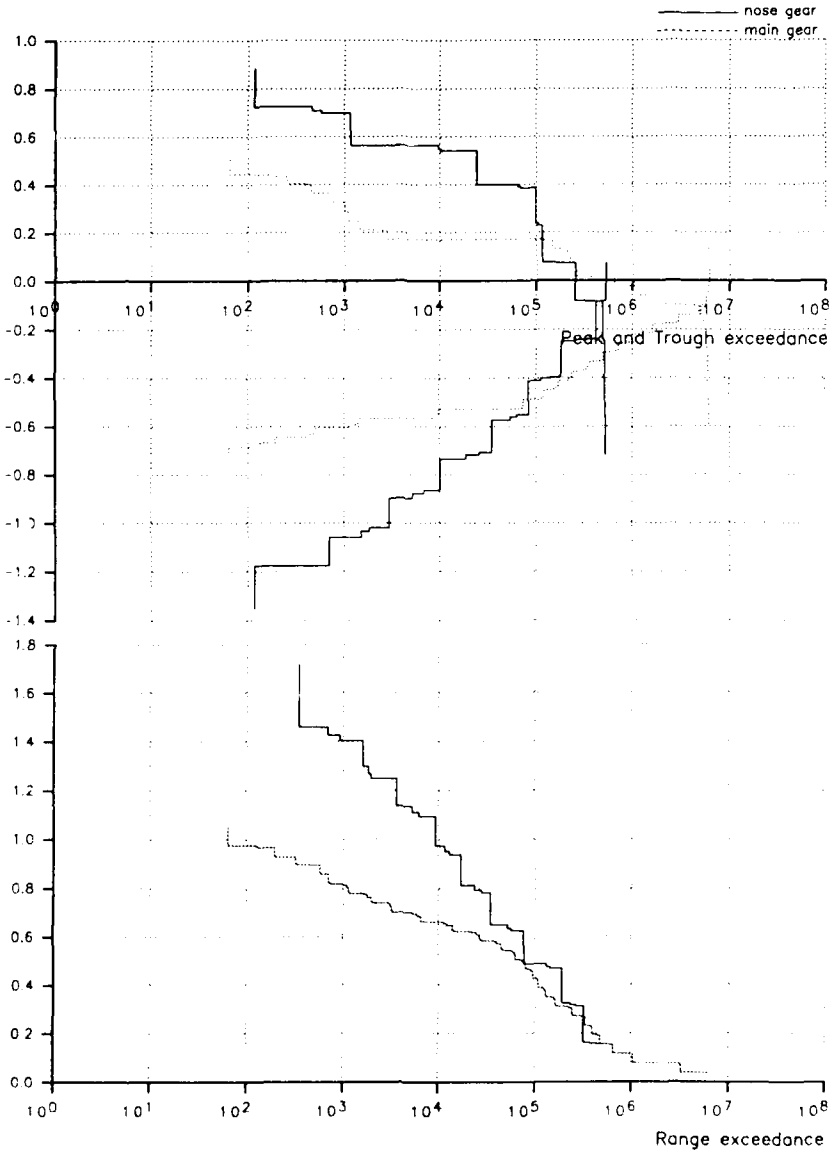

Figure 14 Comparison between spectra for nose gear and main gear for 90 000 flights.
Towing excluded. X-ground reaction factor. FFA in-service measurements

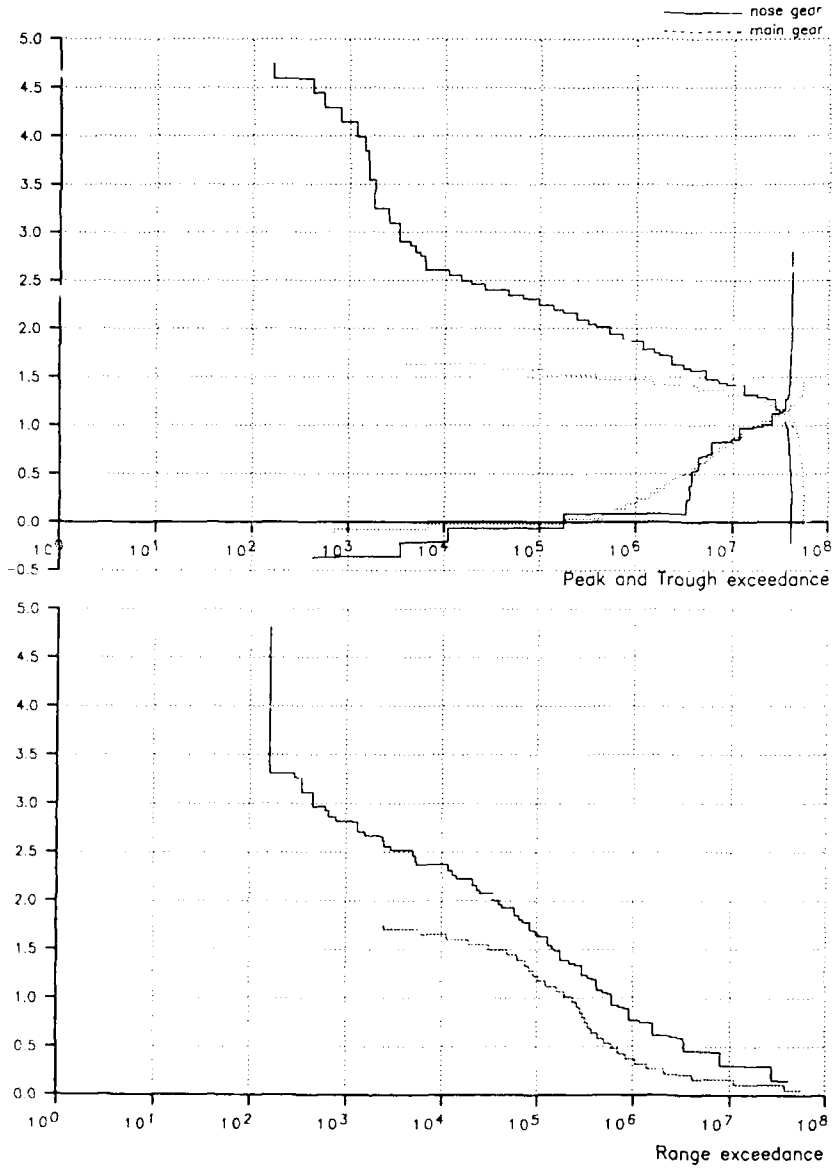

Figure 15 Comparison between spectra for nose gear and main gear for 90 000 flights.
Towing excluded. Z-ground reaction factor. FFA in-service measurements

OPERATIONAL LOADS ON LANDING GEAR

by

V.Ladda and **H.Struck**
Deutsche Airbus GmbH
Hunefeldstrasse 1—5
2800 Bremen 1
Germany

SUMMARY

Prior statistics of airworthiness authorities indicate that landing gear (safe life design) often fail during scheduled aircraft service. Therefore investigations have been carried out during the last two decades in Germany with the aims to determine the operational loads acting on the landing gear during service and to define the load cases which have to be taken into consideration for fatigue investigations related to landing gear and airframe.

Statistics about failures on landing gear for civil and military aircraft, relevant load cases as well as information about essential fatigue requirements are presented thoroughly in the first part. In the second part some results of different landing gear load measurements are compared and discussed. These results presented in form of cumulative frequency distributions for the load cases taxiing and landing impact originate from the following measurements:

Airbus A320; Airbus A310; Airbus A300; VFW 614; F-104 G

In the third part it is reported about the impact of towing and push back operations on the nose landing gear using conventional and advanced towing methods. In the conclusion the primary results of the landing gear loads measurements are accentuated, examples for the disposition of landing gear fatigue tests are considered and essential future actions concerning load monitoring activities including hard- and overweight landing detection are reviewed.

1. INTRODUCTION

The only components of the aircraft that are categorized as safe-life are parts of the landing gear [1], since a completely fail safe designed landing gear structure (no multiple load path design possible) as well as a damage tolerant designed landing gear structure (sufficient damage tolerance qualities can not be achieved because the detection of cracks is more complicated than it is for other aircraft components) are inapplicable up to now. Therefore the landing gear in its entirety is safe-life designed and represents a life limited structure. In opposite to the damage tolerance design cracks in the landing gear structure are not admissable. During fatigue tests the safe-life requirements under consideration of proper scatter factors (for landing gear nearly a factor of 5) have to be demonstrated.

Normally the landing gear have to be replaced before the aircraft reaches the Economical Repair Life (ERL). Due to runway roughness and maneuvers, (ground operations, take off and landings) repeated loads in x, y, and z-direction and torsion moments are acting on the landing gear simultaneously.

As a result of large leverarms great bending moments will be induced in the airframe. Additional severe environmental conditions (skydrol, salt, water, large gradients of the temperature etc.) lead to corrosion problems in some cases.
The landing gear therefore represents a highly loaded structural component. This is the reason why it is necessary to use ultra high tensile steels for the axles and legs. But this is combined with the disadvantages that these materials are sensitive concerning fatigue behaviour. Partly this could be avoided by introducing residual compressive stresses in critical areas [2, 3].

In [4] has been summarized that up to 82 percent of all fatigue failures on landing gear are caused by taxiing. Even changes in aircraft weight within typical service conditions have practically no effect on the fatigue life of landing gear but an increase in taxi speed from 25 to 50 km/h on the same runway roughness leads to a 35 percent increase in fatigue damage to the landing gear.

In a contribution about air transport landing gear maintenance from an airline point of view it was noted that the general design of landing gear usually is very good but the details of the gear create all sort of problems [5].

The distances covered by landing gear on taxiways and runways are enormous (assuming that the landing gear is not replaced before reaching the ERL). Taken into consideration that during 1 flight 8 km will be covered on ground, a total distance of nearly 400.000 km for an short haul aircraft will be accumulated. A distance which normally will be reached by commercial vehicles.

As mentioned above the reasons why landing gear could fail have been confirmed by prior statistics. They come to the conclusion that landing gear often fail during scheduled aircraft service. Therefore during the last two decades in Germany investigations have been performed to determine the operational loads acting on the landing gear and to define the load cases which have to be taken into account for fatigue investigations. In this contribution results of operational landing gear load measurements performed on aircraft A300B2, A310, A320, VFW 614 and F-104G will be presented and discussed.

1.1 Statistics of landing gear failures during service

In the MIL Specification a failure statistic from the period 1968 to 1978 has been published. In total 328 structural failure accidents have been analyzed. 65 percent of accidents have occured during ground operation and 44 percent of them during landing touch down and landing roll. A breakdown of accidents shows that 50 accidents were attributed to the landing gear structure, see Fig. 1. Six of them were attributed to fatigue problems, that means 8 percent, see Fig. 2 [6].

PERIOD	1968 to 1978
STRUCTURAL FAILURE	328
MAJOR	41%
MINOR	59%
DURING GROUND OPERATION	65%
(LANDING T.D. AND LANDING ROLL	44%)
BREAKDOWN OF ACCIDENTS LANDING GEAR STRUCTURE :	50 ACCIDENTS primary cause of accidents 163 ACCIDENTS secondary or induced failure

FIG.1 STATISTIC OF AIRFRAME AND LANDING GEAR STRUCTURAL FAILURE ACCIDENTS [6]

	TOTAL	ATTACK	FIGHTER	TRAINER	BOMBER	CARGO	UTILITY
MATERIAL	44	5	19	3	4	10	3
INADEQUATE DESIGN	1	0	0	0	0	1	0
NOT IN ACCORDANCE WITH TECHNICAL ORDERS	2	0	0	0	0	2	0
UNKNOWN	3	1	2	0	0	0	0
	BREAKDOWN OF TYPE OF FAILURE						
CORROSION	13	0	4	2	2	5	0
UNDERSTRENGTH	7	0	7	0	0	0	0
CRACKED	6	0	1	0	1	3	1
FATIGUE	6	0	3	1	0	2	0
OVERLOAD	5	2	0	0	1	2	0
UNKNOWN	12	4	6	0	0	0	2
OTHER	1	0	0	0	0	1	0
	BREAKDOWN BY MISSION PHASE						
TAXI	5	0	0	0	1	4	0
TURNING	4	0	1	0	2	1	0
TAKEOFF	7	2	3	1	1	0	0
LANDING T.D.	16	3	8	1	0	4	0
LANDING ROLL	18	1	9	1	0	4	3

FIG.2 ACCIDENTS ATTRIBUTED TO LANDING GEAR [6]

A similar result shows an investigation of 529 fatigue cracks that have occured during service of military and civil aircraft in the same period. 5 percent of them were detected on landing gears [7].

An analysis of serious age related airliner failures in the period of 1977 to 1987 shows that 18 airline accidents of civil aircraft were caused by landing gear failures possibly as a result of fatigue and corrosion problems [8].

A statistic of 95 aircraft accidents during scheduled passenger flight in 1988 implies that 6 accidents were attributed to structural landing gear failures [9].

1.2 Essential fatigue requirements

Essential guidelines how to fullfil the fatigue requirements have been choosen from the FAR-AC 25.571-1B for civil transport aircraft.

Fig. 3 shows the definition how to handle safe life structures and how to establish the typical loading spectra. Fig. 4 gives information how to perform the fatigue evaluation, to establish the scatter factor for *safe life* designed structures as well as their replacement times. The specification MIL A-87221 describes in similar terms the fatigue evaluations [6, 10, 11].

DEFINITIONS

SAFE LIFE MEANS THAT THE STRUCTURE HAS BEEN EVALUATED TO BE ABLE TO WITHSTAND THE REPEATED LOADS OF VARIABLE MAGNITUDE EXPECTED DURING ITS SERVICE LIFE WITHOUT DETECTABLE CRACKS.

THEREFORE THE TYPICAL LOADING SPECTRUM EXPECTED IN SERVICE HAS TO BE DERIVED:

THE LOADING SPECTRUM SHOULD BE BASED ON MEASURED STATISTICAL DATA .....

THE PRINCIPAL LOADS THAT SHOULD BE CONSIDERED ARE ....,

GROUND LOADS (TAXING, LANDING IMPACT, TURNING, ENGINE RUN UP, BRAKING, THRUST REVERSING AND TOWING....

FIG.3 ESSENTIAL FATIGUE REQUIREMENTS [10, 11]

FATIGUE EVALUATION

a. GENERAL. The evaluation of structure under the following fatigue (safe-life) strength evaluation methods is intended to ensure that catastrophic fatigue failure, as a result of the repeated loads of variable magnitude expected in service, is extremely improbable throughout the structure's operational life. Under these methods, loading spectra should be established, the fatigue life of the structure for the spectra should be determinded, and a scatter factor should be applied to the fatigue life to establish the safe-life for the structure. The evaluation . . .

b. SCATTER FACTOR FOR SAFE-LIFE DETERMINATION. In the interpretation of fatigue analyses and test data, the effect of variability should, under § 25.571(e), be accounted for by an appropriate scatter factor. Relating test results to the recommended safe-life is extremely difficult since there are a number of considerations peculiar to each design and test that necessitate evaluation by the applicant. These considerations will depend on the number of representative test specimens, the material, the type of specimen employed, the type of repeated load test, the load levels, and environmental conditions.

c. REPLACEMENT TIMES. Replacement times should be established for parts with established safe-lives and should, under § 25.571(a) (3), be included in the information prepared under § 25.1529. These replacement times can be extended if additional data indicates an extension is warranted. Important factors

FIG.4 ESSENTIAL FATIGUE REQUIREMENTS [10]

1.3 Relevant loading conditions

For fatigue evaluations more than 16 different loading conditions have to be taken into account [1, 20, 21, 22, 23]. Fig. 5 shows the loading conditions. As a result of the landing gear load measurement on A300B2 [12] the different loading conditions have been confirmed but the push back load case has been observed during the measurment for the first time.

- LANDING IMPACT
- SPIN UP
- SPRING BACK
- TAXIING
- TAKE OFF RUN
- LANDING RUN
- ENGINE RUN UP
- SYMMETRICAL AND UNSYMMETRICAL BRAKING
- TRANSIENT DRAG OSCILLATION
- TURNING
- BRAKED TURN
- PIVOTING
- TOWING
- PUSH BACK
- TIRE IMBALANCE
- SHIMMY

FIG.5 IMPORTANT LANDING GEAR LOADING CONDITIONS TAKING INTO ACCOUNT FOR FATIGUE EVALUATIONS [1,12]

2. LANDING GEAR LOADS

2.1 Sources of measured data

Fig. 6 and 7 indicate the sources of the data that will be the main part of this contribution. The most important data concerning statistical reliability is represented by the A300B2 landing gear load measurement, with the investigation of about 2200 flights as well as the A300, A310 towing and push back measurement. An important part in this contribution results from the landing investigation of A320. The contribution will be completed by the VFW 614 landing gear load measurement as well as by results of a fighter aircraft landing gear load investigation [12, 13, 14, 15, 16, 17, 18].

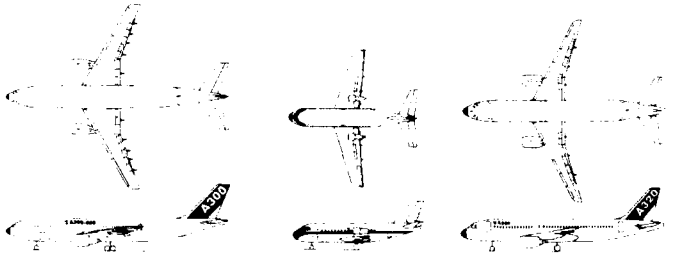

A300 B2
MAX TOW 137t
MAX LW 127,5t

VFW 614
MAX TOW 20 t
MAX LW 19 t

A320-100
MAX TOW t
MAX LW 63 t

FIG.6 TEST AIRCRAFT

1. A300 B2 LANDING GEAR LOAD MEASUREMENT [12,13,14,15]
   OPERATION SCHEDULED SERVICE AT LH
   NO. OF FLIGHTS: 2200
   ANALYZED TAXIING 300, LANDING 2200

2. VFW614 LANDING GEAR LOAD MEASUREMENT [16]
   OPERATION NEARLY COMPARABLE TO NORMAL SERVICE
   NO. OF FLIGHTS: 104
   ANALYZED 104

3. A320 LANDING GEAR LOAD MEASUREMENT [31]
   OPERATION DURING FLIGHT TEST (FERRY FLIGHTS, ROUTE PROOFING)

4. A300, A310 TOWING AND PUSH BACK MEASUREMENT [33]
   OPERATION SCHEDULED SERVICE OF LH AND AF
   NO. OF TOWINGS: 30 } TOWBAR 6 } HIGH SPEED TRACTOR
   NO. OF PUSH BACKS: 162 } 11 }

FIG.7 SOURCE OF MEASURED DATA

2.2 *Sign convention*

The sign convention of the loads is given on Fig. 8. In the direction of the arrows the loads are defined as positv.

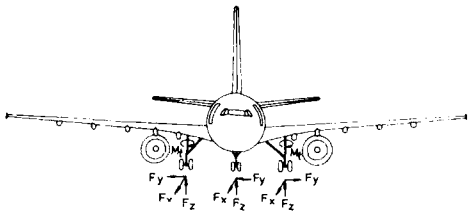

FIG.8 SIGN CONVENTION (POSITIV DIRECTIONS)

2.3 Presentation of the results on main and nose landing gear

2.3.1 General

The landing gear loads have been measured by strain gages calibrated and combined to produce pure vertical, lateral and longitudinal loads using Skopinski's method [13, 14, 19] on nose and L/H main gear.

A typical example of the measured load time histories during landing and taxiing is shown on Fig. 9. The maximum values during landing have been marked. These maximum loads have been analyzed by means of the extreme value distribution [24], the loads during taxiing by means of the statistical counting method level crossings [25].

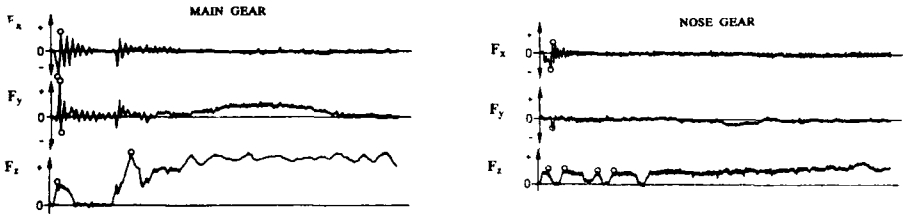

FIG.9 LOAD TIME HISTORIES OF THE LOADS ON THE MAIN AND NOSE LANDING GEAR [12]

2.3.2 Landing

The acceleration of the landing gear wheels to a circumferential speed which corresponds to the aircraft horizontal landing speed causes a longitudinal drag load, the so-called spin-up load. Caused by the energy built up in the main gear this leads to a so-called spring back load in form of an attenuated oscillation. In reason of the elasticity of the landing gears side loads occures during landing. Due to the vertical sinking speed of the A/C at the moment of touch down a landing impact in vertical direction comes off. Distributions of the sinking speed for different types of A/C are shown on Fig. 10, from which the vertical load can be derived.

The hatched scatter band represents operational data for transport aircraft [26] and is in agreement with [27]. The distribution marked by 1 depicts the spectra predicted for A320 as well as DC10 [26, 28]. Curve 2 results from an A320 landing gear investigation performed during flight tests, it lies in the upper region of the scatter band but under the predicted one. Curves 3 to 5 show landing sinking speed spectra for different military aircraft [6].

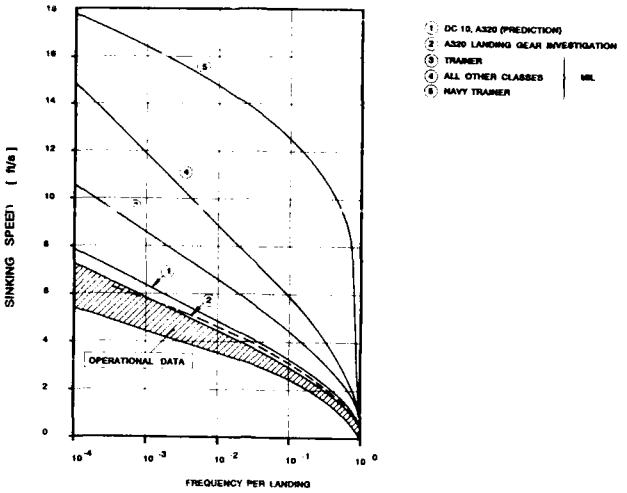

FIG.10 LANDING SINKING SPEED SPECTRA
[6, 26, 28]

On main landing gear equipped with tandem wheels (bogie gear) torsion moments directed to the vertical axis of the plane become evident because the spin up loads will never act on the four wheels simultaneously.

The description of the loads acting on main landing gear as mentiond above is valid in principle also for nose gear. The distinction is that the nose gear loads will be mainly influenced by the counter rotation of the A/C during landing due to the elevator deflection initiated by the pilot.

In total 2200 landings of A300B2 and 80 landings of A320 have been analyzed. During 76 landings of A300B2 a second characteristic landing impact in vertical direction was discovered on the main landing gear. On the nose landing gear additional vertical landing impacts were found during 972 landings. During one landing a sequence of 10 nose gear impacts have been observed [12].

The statistical results presented in form of frequency distributions for both the main and nose landing gear of A300B2 compared with those of A320 (for A320 were available only drag - and vertical loads on main gear and vertical loads on nose gear) are shown on Fig. 11.

The main gear results indicate that the spin up loads as well as the vertical loads for A320 are appreciably higher than for A300B2 while the spring back loads are comparable in magnitude. Possible reasons for the differences could be that the A320 has a "hard landing" characteristic based on the oleo spring of the main gear combined with a relatively high breakout force and that the results have been taken from flight tests that means severe service conditions. The vertical nose gear loads of A320 are in accordance with those of A300B2.

Comparing main- and nose landing gear loads together it is obviously that the spin up loads as well as the side loads on nose gear are relative higher. This knowledge is important since, in the past, in the absence of nose landing gear load measurement data, the main landing gear data has been assumed to be valid also for the nose landing gear. Another important fact for the nose gear is that 1.5 landing impacts have occured per landing as mean value.

2.3.3 Taxiing

The frequency distributions determined for the load case taxiing contain loads caused by runway roughness as well as by ground maneuvers (turning, braking). The sample size of the basic data for the analysis were 300 flights of A300B2 and 104 flights of VFW 614. The results of A300B2 have been compared with those of VFW614. From the VFW 614 measurement were available only drag- and vertical main landing gear loads and side- and vertical nose landing gear loads, see Fig. 12 [12, 16].

The comparison indicates that the main gear drag loads of the VFW 614 are much lower than those of A300B2. The reason could be that the braking loads of A300B2 are clearly higher during service. It has been observed that the A300B2 pilots in general prefer to take the first exit after landing if possible. The vertical loads however are comparable in magnitude and frequency.

The comparison of nose gear results show that the side loads of the VFW 614 are slightly higher while the vertical loads are lower than those of A300B2. The lower vertical loads of the VFW 614 could be explained by the higher main gear braking loads of A300B2 because braking loads on the main gears create an increase of the incremental vertical nose gear loads. In addition Fig. 13 shows a separation of the A300B2 taxi spectra for all different load cases.

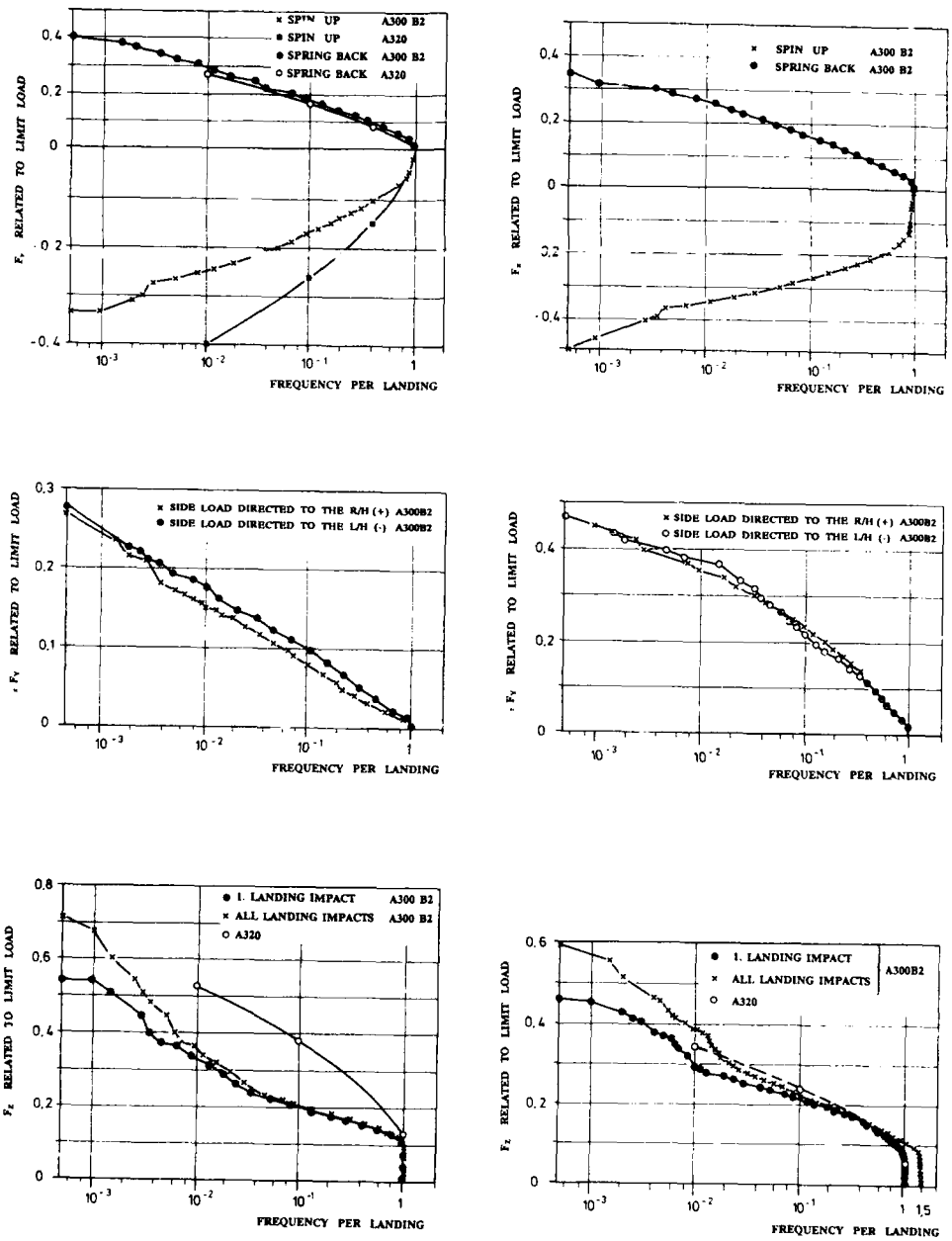

MAIN LANDING GEAR **NOSE LANDING GEAR**

FIG.11 FREQUENCY DISTRIBUTIONS OF THE LOADS ON THE LANDING GEAR DURING LANDING IMPACT [12]

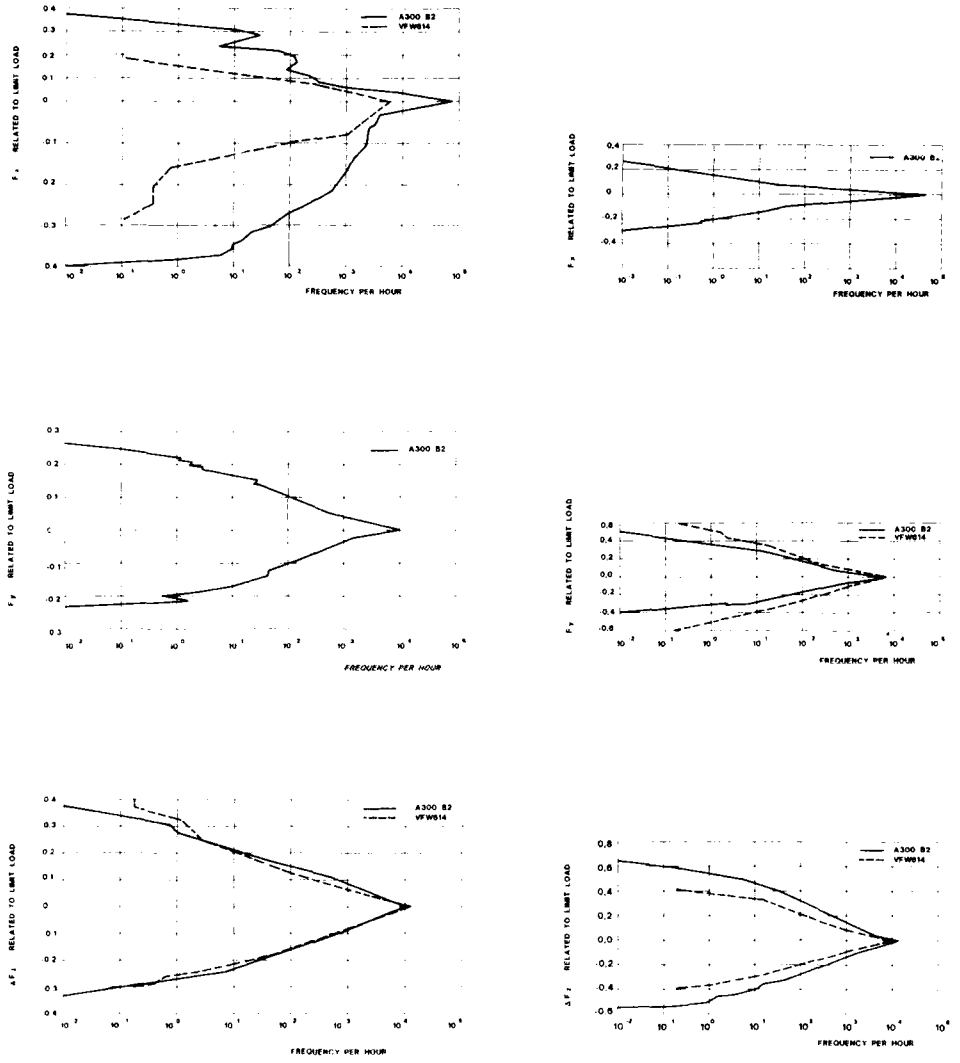

MAIN LANDING GEAR

NOSE LANDING GEAR

FIG.12 FREQUENCY DISTRIBUTIONS OF THE LOADS ON THE LANDING GEAR DURING TAXIING (INCLUDING MANEUVERS) [12, 16]

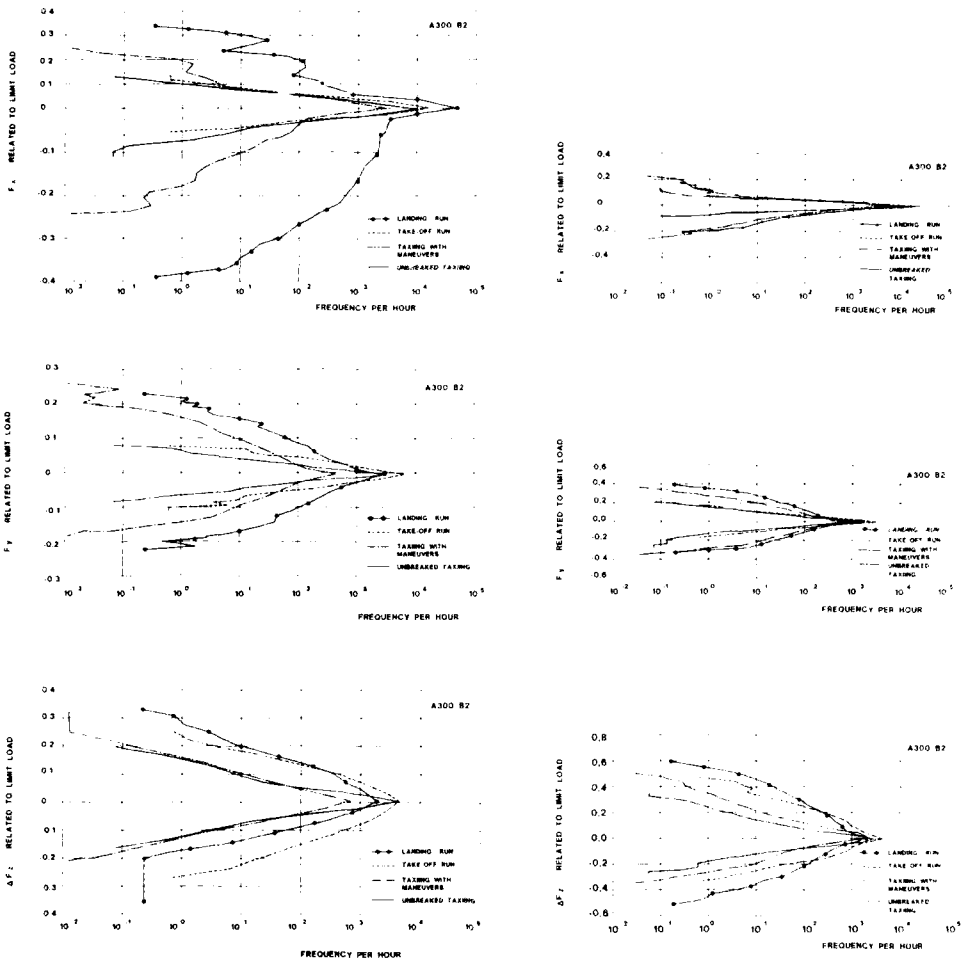

FIG.13 FREQUENCY DISTRIBUTIONS OF THE LOADS ON THE LANDING GEAR DURING TAXIING [12]

From the landing gear load measurement on a fighter aircraft the load spectra on Fig. 14, for unbraked taxiing were derived. The load factors represent ground reaction factors that means the loads are related to the vertical static landing gear load [17, 18].

Fig. 15 represents frequency distributions of the load factor at the center of gravity (Δnz) of A300B2 and VFW 614 compared with results taken from [6, 12, 16, 29].

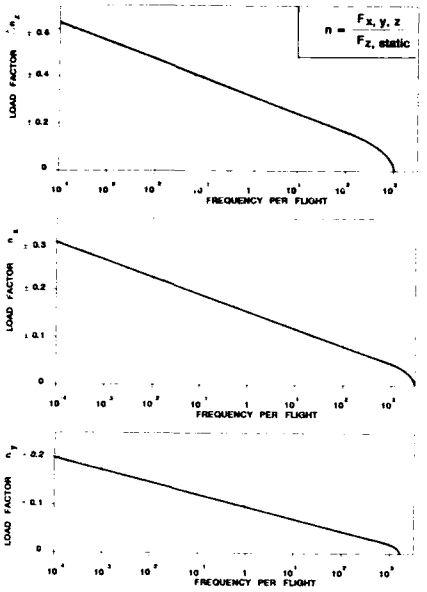

FIG.14 FREQUENCY DISTRIBUTIONS OF THE LOAD FACTORS ON THE MAIN LANDING GEAR DERIVED FROM A FIGHTER AIRCRAFT DURING UNBRAKED TAXIING [17, 18]

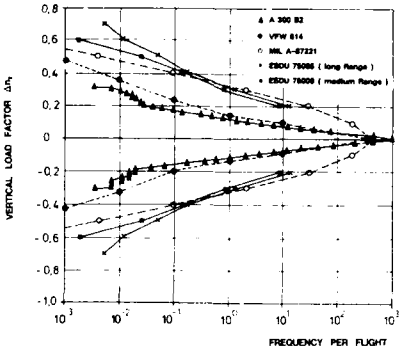

FIG.15 FREQUENCY DISTRIBUTIONS OF THE VERTICAL LOAD FACTOR DURING TAXIING OF TRANSPORT AIRCRAFT [6, 12, 16, 29]

2.3.4 Turning

To establish the turning spectra (pivoting is included) for the main and nose landing gear the measured side loads have been low pass filtered (Fy main gear = 0,25 Hz, Fy nose gear = 0,35 Hz). The turning spectra separated for pre flight and post flight turning are shown on Fig. 16 and 17. The number of turnings can be taken from the spectra with 4 during pre flight and 6 during post flight taxiing, see Fig. 17 [12].

Fig. 18 gives the turning spectrum derived from a measurement on a fighter aircraft. The load factor n_y represents a ground reaction factor that means that the load is related to the static vertical landing gear load [18].

2.3.5 Braking

For establishing the A300B2 braking spectra the load time history of the drag loads has been low pass filtered by 0.25 Hz. That means all load variation over 0.25 Hz were cut so that only the braking loads remains. The spectra are presented on Fig. 19. The numbers of brakings were determined with 3 pre flight brakings and 3 post flight brakings [12, 30].

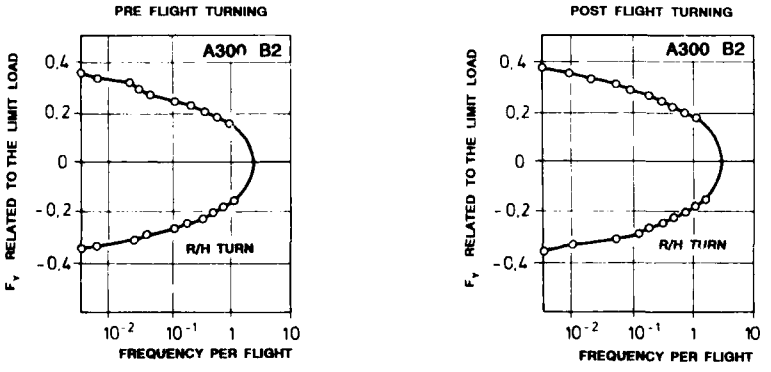

FIG.16 FREQUENCY DISTRIBUTIONS OF THE SIDE LOADS ON THE NOSE LANDING GEAR DURING TURNING [12]

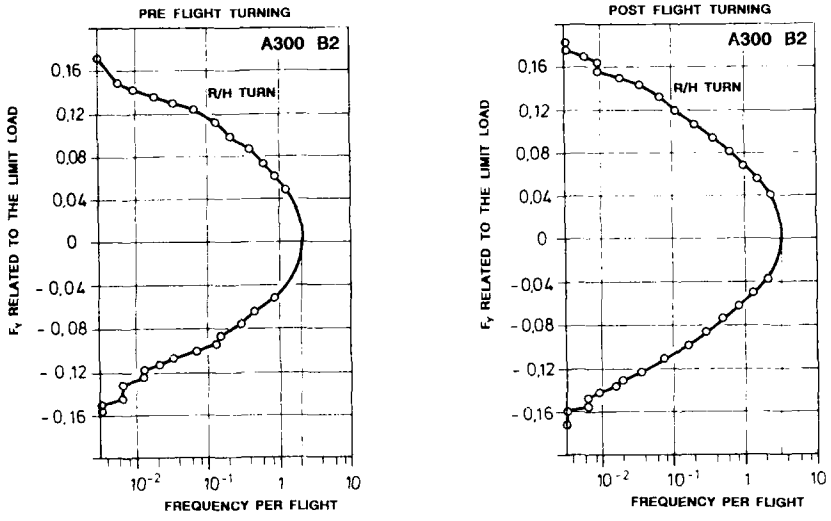

FIG.17 FREQUENCY DISTRIBUTIONS OF THE LOADS ON THE MAIN LANDING GEAR DURING TURNING [12]

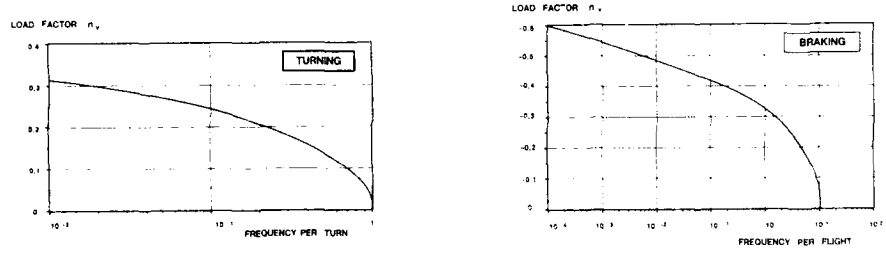

FIG.18 FREQUENCY DISTRIBUTIONS OF THE LOAD FACTOR ON THE MAIN LANDING GEAR OF A FIGHTER AIRCRAFT DURING TURNING AND BRAKING [17, 18]

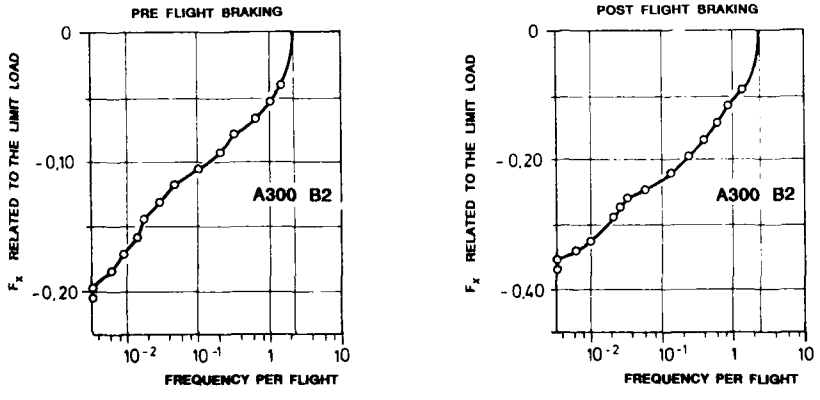

FIG.19 FREQUENCY DISTRIBUTIONS OF THE BRAKING LOADS ON THE MAIN LANDING GEAR [12]

A braking spectrum derived from measurements on a fighter aircraft is presented on Fig. 18. It shows that per flight 10 brakings have been observed. The load factor n_x is a ground reaction factor that means the load is related to the static landing gear load in vertical direction [18].

Fig. 20 shows a correlation between A300B2 braking loads occured simultaneously on left and right main landing gear. The relation indicates that exact symmetrical braking occures seldom because brakings during taxiing mostly are combined with turnings by supporting the nose gear steering [12].

Fig. 21 represents the correlation between braking loads on the left main landing gear and the load increase in vertical direction on the nose landing gear. It implies that the braking loads on the main gear cause an increase of the vertical incremental load by a factor of 1.8, that means $Fz_{NLG} = -1.8\ Fx_{MLG}$ [12].

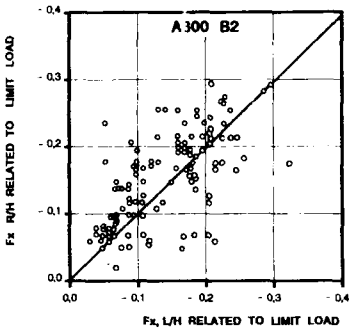

FIG.20 RELATION BETWEEN BRAKING LOADS ON THE L/H AND R/H MAIN LANDING GEAR [12]

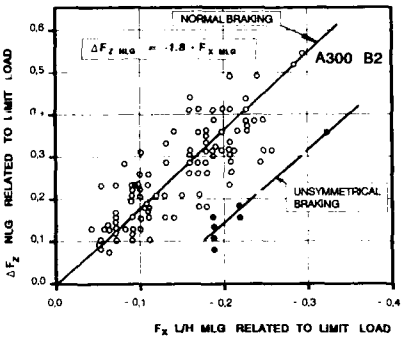

FIG.21 IMPACT OF THE BRAKING LOADS ON THE MAIN LANDING GEAR TO THE VERTICAL LOADS ON THE NOSE LANDING GEAR [12]

2.4 Statistics of ground operations

As shown at points 2.3.4 and 2.3.5 the number of turnings were in total 10 per flight and the number of brakings 6 per flight. These figures have been determined directly from the turning and braking spectra, respectively.

In addition the taxi times have been derived for A300B2 and VFW 614 in form of frequency distributions see Fig. 22. The results are comparable for A300B2 and VFW 614. The mean values for pre flight taxiing are 6.7 min for A300B2 and 8.0 min for VFW 614. The post flight taxiing times are 4.0 min for A300B2 and 6.0 min for VFW 614 [12,16].

Further more some statistics of A300B2 landings have been established. Fig. 23 shows the distribution of time differences between touch down of the right and left main landing gear. The distribution indicates that during every fourth landing (25 percent) a two point landing has been observed. The time differences vary between 0 and 2.5 seconds (L/H gear first) and 0 and 2.0 seconds (R/H gear first).

Fig. 24 represents a distribution of time differences between touch down of the main landing gear (which ever comes first) and the nose landing gear. During 70 percent of landings the time differences vary between 6 and 10 sec. The max. time difference detected during the measurement was 20 seconds [12].

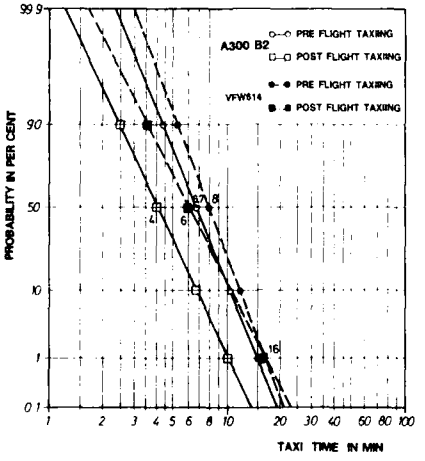

FIG.22 FREQUENCY DISTRIBUTIONS OF TAXI TIMES [12,16]

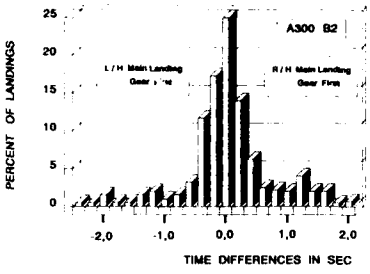

FIG.23 DISTRIBUTIONS OF THE TIME DIFFERENCES BETWEEN TOUCH DOWN OF L/H AND R/H MAIN LANDING GEAR [12]

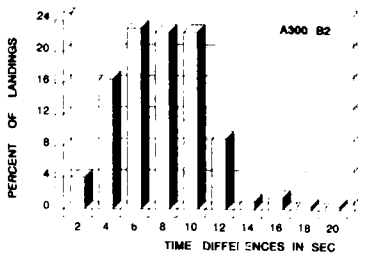

FIG.24 DISTRIBUTIONS OF THE TIME DIFFERENCES BETWEEN TOUCH DOWN OF MAIN AND NOSE LANDING GEAR [12]

2.5 Push back and towing operations

Modern civil airports are equipped with boarding piers.This requires a parking of the aircraft at or near the pier, so that passengers can leave the aircraft directly to the terminal. After boarding a special maneuver is necessary, a so-called push back. That means moving the aircraft backwards to a position from which the aircraft can taxi to the runway under it's own power [32, 33, 34].

2.5.1 Different towing methods

The towing procedure of aircraft from the terminal to the hangar and vice versa normally will be per med by towbar and tractor. To save fuel, reduce noise and shorten the towing times (compared to towbar towing) in the last years the so called high speed tractors were designed. The maximum towing speed will be about 50km/h. It is planed for the future that the tractors will also be used to move the aircraft from the terminal directly to the runway and back after landing. Examples of the different towing methods are presented on Fig. 25 [32].

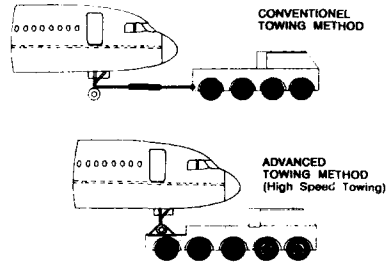

FIG.25 TOWING METHODS

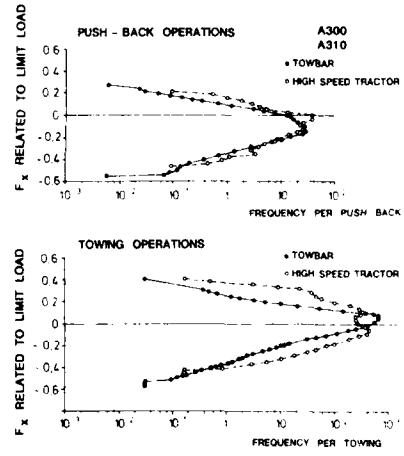

FIG.26 FREQUENCY DISTRIBUTIONS OF THE DRAG LOADS ON NOSE LANDING GEAR [32]

2.5.2 *Impact of the loading conditions* towing and push back on the nose landing gear

The importance of these load cases for the nose landing gear first were presented by the results of the measurement on Airbus A300B2 [12]. Normally the nose landing gear of the aircraft is unbraked but during towing and push back - the nose gear is coupled to the tractor - the nose landing gear acts as though it were braked, caused by braking and acceleration of the tractor driver. This leads to further towing and push back investigations during normal aircraft service of Deutsche Lufthansa at Frankfurt and Air France at Paris, CDG.

2.5.3 Drag loads during push back and towing operations

Fig. 26 show the frequency distributions of the drag loads on the nose landing gear using towbar and high speed tractor. During push back the measured drag loads are comparable in magnitude and frequency. The measured negative loads are in proportion to the nose gear spin up loads. During towing the loads are higher using high speed tractor. The loads are influenced insignificantly by the aircraft mass but severely by the acceleration and braking characteristics of the tractor.
Recently during a push back maneuver of an ATP aircraft at Bremen airport the nose gear and the fuselage attachment were havy damaged [32].

3. CONCLUSION

3.1 Summary of essential results

In this contribution a lot of results taken from long time measurements of different aircraft have been presented. It is to be hoped that the contribution clarly indicates that the landing gear as one of the most important components should not be neglected and that more attention should be paid to the landing gear design including fatigue evaluations. The different loading conditions of the landing gear as well as the real loads acting on the landing gear during service could be shown.

These facts have been elucidated not only by the failure statistics, but also by accidents and problems caused by landing gear of modern aircraft in the present. A surprising result was that the magnitudes of push back loads on the nose gear are in proportion to that of the spin up. This is important because the loading condition spin up is a design case for the nose gear up to now.

To make it easy to use the results for further treatments or transference for new design of landing gear and airframe structures the operational data have been presented in relation to the limit loads.

Correlations of the landing gear loads (simultaneously occured) have not been presented in this contribution. In [12] results of correlations were investigated thoroughly. From that it can only be noted, that a definite correlation between the loads does not exist. But depending on different frequency bands a better correlation becomes evident.

The comparison of A300B2 results with those of VFW 614 shows in general a good accordance although the A300B2 measurement only represents a scheduled in-service investigation.

The results of A300B2 for the loading condition landing impact show, that the nose gear is relativ more highly loaded than the main gear.

The push back and towing measurement was the first investigation to establish load spectra based on actual airline service.

All spectra as presented are transferable to military transport aircraft and the spectra derived from a fighter aircraft to combat aircraft, respectively.

3.2 Example for the disposition of landing gear fatigue tests.

Based on the results of the A300B2 landing gear load measureme. t the fatigue test set up has been revised and completed at that time.

How a typical fatigue test set up for the main gear of a transport aircraft could be disposed is shown on Fig. 27. It represents a typical, concerning the frequency simplified (compared to the real loadings) flight by flight test spectrum for the main landing gear. It is separated into the take of and landing spectrum. The different load cycles are dependent on the loading conditions. Landing gear actuator loads (simulation of retraction and extention) also will be applied.

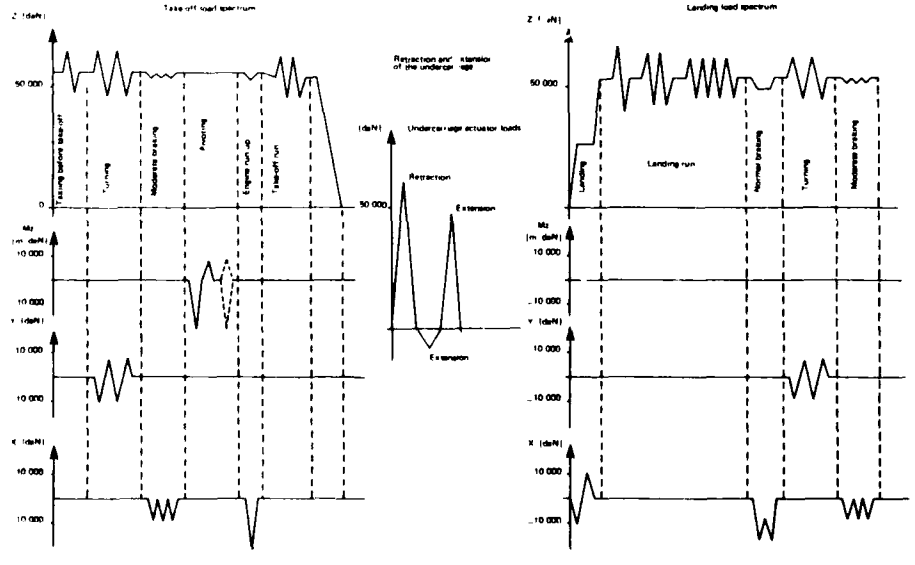

FIG.27 A300 B2 MAIN LANDING GEAR FATIGUE TEST SPECTRA

3.3 Load monitoring activities

In the last years some activities concerning load monitoring of the airframe during aircraft service have been developed.

A DA-proposal represents the Operational Loads Monitoring System, OLMS for A/C A320 which is under development. The working principle of OLMS is shown on Fig. 28. It indicates that OLMS only is the monitoring device integrated in the whole Airframe Condition Monitoring Procedure (ACMP). The aims of OLMS are the determination of load spectra of all aircraft components and correlations between loads occured simultaneously [35, 36]. In addition a special function, the event identification during landing and flight will be performed. That means detection of hard landings and limit load exeedances.

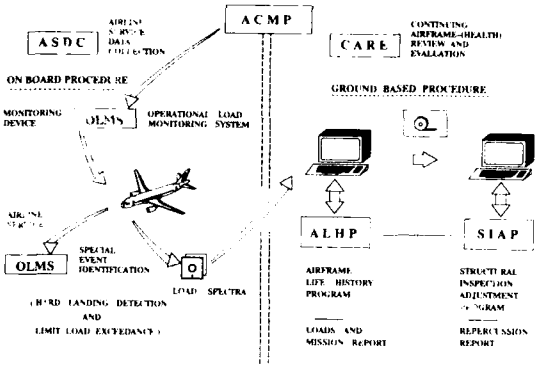

FIG.28 AIRFRAME CONDITION MONITORING PROCEDURE, ACMP

A first step was made for A320 using the Data Management Unit (DMU) offered to the customer as an option. The DMU served for monitoring hard landings and recording of extreme maneuver- and gust loadings.

It is intended to incorporate the landing gear completely into the monitoring activities in the near future. These will be solved when in connection with the development of the A320 Weight and Balance-System (WBS) proper landing gear sensors will be available.

4. REFERENCES

[1] J.E. Wignot
Structural Design of Transport Airplanes for Transient Environments
Lockhead-California Company
Burbank, California
ASME-Paper-AMD36, 1979

[2] Young, D.W.
Aircraft Landing Gear
The Fast, Present and Future
Proc. Inst. Mechanical Engineers
Vol. 200 No. D2, 1986, Pages 75-92

[3] Jenkins, S.F.N.
Landing Gear Design and Development
Institution of Mechanical Engineers, Proceedings, Part G1- Journal of Aerospace Engineering
Vol. 203, No. G1, Page 67-73, 1989

[4] A.M. Penkov, M.P. Zhdanowich and A.I. Radchenko
Statistical Investigation of the Operational Loading of the Landing Gear of a Mainline Aircraft
NASA-TT-F-11900 00, 1967, P.52-60

[5] Witt, W.W.
Air Transport Landing Gear Maintenance United Airline, Inc.
National Aeronautic and Space Engineers and Manufactoring Meeting
Los Angeles, Calif., 1965
SAE-Paper 650842

[6] Military Specification, Aircraft Structures
MIL-A-87221 (USAF)
28.02.1985

[7] H. Huth, D. Schütz
The Collection and Analysis of Fatigue Damage Occuring in Aircraft Service
RAE Paper Library Translation 1934, 1977

[8] Flight International, Sept. 1988

[9] Flight International, Jan. 1989

[10] FAA Advisory Circular 25.571-1B
Damage Tolerance and Fatigue Evaluations of Structure, March 1986

[11] JAR Part 25, Section2, Paragraph ACJ 25.571
Damage Tolerance and Fatigue Evaluations of Structure (Acceptable Means of Compliance)
Amendment 7, Nov. 1980

[12] O. Buxbaum, V. Ladda, J.M. Zachel
Betriebslasten am Bug- und Hauptfahrwerk eine Flugzeuges vom Typ Airbus A300B2 während des Einsatzes bei der Deutschen Lufthansa
Operational Loads on Nose- and Main Landing Gear of an Airplane of Type Airbus A300B2 during Normal Service of the Deutsche Lufthansa
Fraunhofer Institut für Betriebsfestigkeit (LBF), Darmstadt
BMFT Report FB-W 82-010, 1982

[13] Ladda, V.; Zaschel, J.M.:
Landing Gear Load Measurement A300B2, A/C 026
Calibration of the L/H Main Landing Gear
2. Interim Report
Fraunhofer Institut für Betriebsfestigkeit (LBF) Darmstadt
LBF-Report No.: 3107/3380/2, 20.3.1977
in German, unpublished

[14] Ladda, V.; Zaschel, J.M.:
Landing Gear Load Measurement A300B2, A/C026
Calibration of the Nose Landing Gear
1. Interim Report
Fraunhofer Institut für Betriebsfestigkeit (LBF) Darmstadt
LBF-Report No. 3107/3380/1, 01.10.1976, in German, unpublished

[15] Ladda, V.; Zaschel, J.M.:
Long-Term Measurements of Service
Loads on the Landing Gear of a Commercial Airliner
Reports in Applied Measurements
RAM Vol.1 (1985) No. 2
Published by Hottinger Baldwin Messtechnik GmbH
D-6100 Darmstadt

[16] Rauscher, E.; Pries, M.:
Auswertung und Darstellung von Langzeitmessungen an Flugzeugbauteilen am Beispiel der VFW 614
(Analysis and Presentation of Long Time Measurements on Aircraft Components of VFW 614)
Vereinigte Flugtechnische Werke GmbH, Bremen
BMV-Report 5-78, 31.10.80, in German

[17] Buxbaum, O.:
Betriebskräfte am Hauptfahrwerk von Flugzeugen des Types F-104G
(Operational Loads on Main Landing Gear of Aircraft of Type F-104G)
Fraunhofer Institut für Betriebsfestigkeit (LBF), Darmstadt
LBF-Report No. FB 82 (1969), in German

[18] Luftfahrttechnisches Handbuch
Band Belastungmechanik
BM 64000-02, BM 64000-03 (1970)
Herausgeber: Arbeitskreis Belastungsmechanik (ABM)

[19] Skopinsky, TH.; Aiken, W.S.; Huston, W.B.:
Calibration of Strain Gage Installation in Aircraft Structures for the Measurement of Flight Loads
NACA T.R. No. 1179

[20] Moreland, W.J.:
The Story of Shimmy
Journal of Aeronautical Sciences, Vol. 21, No. 12, December 1954,
pp. 793-808.

[21] Pacejka, H.L
The Wheel Shimmy Phenomenon
V.R.B. Kleine, Groningen, 1966

[22] Gamon, M.A., T. Mahone:
Active Shimmy Control System
AFDL-TR-75-136, December 1975

[23] Wignot, J.E. and F.M. Hobilt:
Landing Gear Oscillations Due to Unstable Skidding Friction
Journal of the Aeronautical Sciences, Vol. 16, No. 8, august 1949, p. 491

[24] Buxbaum, O.:
Verfahren zur Ermittlung von Bemessungslasten schwingbruchgefährdeter Bauteile aus Extremwerten von Häufigkeitsverteilungen
(Procedures for the Determination of Design Loads of Fatigue Critical Components by Extreme Values of Cumulative Frequency Distributions)
Fraunhofer Institut für Betriebsfestigkeit (LBF), Darmstadt
LBF-Report No. FB75 (1967), in German

[25] Buxbaum, O.:
Statistische Zählverfahren als Bindeglied zwischen Beanspruchungsmessung u. Betriebsfestigkeitsversuch (Statistical Couting Methods as Connecting link between Load Measurement and Fatigue Test)
Fraunhofer Institut für Betriebsfestigkeit (LBF) Darmstadt
LBF-Report No. FB75 (1967), in German

[26] M. Stone
Airworthiness Phisloeophy Developed From Full-Scale Testing
Biannual Meeting of the ICAF
London, UK, 1973
Douglas Paper 6099

[27] Taylor, James
Manual on Aircraft Loads
AGARDO graph 83, 1965

[28] MBB - A320 Loads Manual
Basic Data: Statistics and Initial Spectra
Report No.: MBB 00D010 K72002 22, 1988
Deutsche Airbus GmbH, Bremen

[29] Frequencies of Vertical and Lateral Load Factors
Resulting from Ground Manoeuvres of Aircraft
Engineering Sciences Data Unit - London
ESDU No. 75008, Sept. 1979

[30] Allen, R.H. and R.C. O'Massey:
Longitudinal Instability in Braked Landing Gear
ASME Publication 80-WA, DSC-12, November 1980

[31] John R. McGehee and Robert C. Dreher
Experimental Investigation of Active Loads Control for Aircraft Landing Gear
NASA Technical Paper 2042, 1982
Longley Research Center
Hampton, Virginia

[32] V. Ladda
Drag Loads at Nose Landing Gear During High-Speed Towing Operations
in: Review of Investigations on Aeronautical Fatigue in the Federal Republic of Germany
Published by O. Buxbaum and H. Huth, LBF, Darmstadt
ICAF Conference 1985 - LBF Report S-173

[33] Hoover, E.A.:
Evaluation of the Impact of Towing DC-9 Transport Airplanes at Boston Logan Airport.
Douglas Aircraft Co., Long Beach, Final Report prepared for U.S. Department of Transportation , FAA,
Contr. No. DOT-FA 87 WA-4198, October 1979

[34] Gamon, M.A.:
Evaluation of the Impact of Towing the L-1011 Airplane at Boston Logan Airport.
FAA-NA-80-24, May 1980

[35] H.-J. Meyer, V. Ladda
The Operational Loads Monitoring System, OLMS
Deutsche Airbus GmbH
Paper presented to 15th Symposium of the International Committee on Aeronautical Fatigue
Jerusalem, Israel, June, 1989

[36] Ladda, V.; Meyer, H.-J.:
Technical Description of the Operational Loads Monitoring System, OLMS
Technical Note, No. TN-TE243/101/88
Deutsche Airbus GmbH, Bremen, 1988

Landing Gear Improvements for Transport Aircraft

by
J. Greer McClain
Senior Mechanical Engineer
Wright Research and Development Center
Wright-Patterson AFB, Ohio 45433 USA
and
B. M. Crenshaw
Staff Engineer
Lockheed Aeronautical Systems Company
86 S. Cobb Drive, Marietta, Georgia 30063 USA

SUMMARY

This paper discusses development, testing, and analysis of retrofit nose and main landing gears designed for improvement in C-130 transport aircraft rough field capabilities, concentrating primarily upon analytical model prediction aspects which might be applicable to other gear designs. Two levels of improvement were examined, with the second level resulting in a new longer stroke strut designed to retract into existing stowage volume. All improved gears were qualified by laboratory drop tests and also evaluated for rough field performance by laboratory shaker testing. Extensive analytical model studies were compared with test results. Model improvements were developed where necessary, with particular attention to representing strut friction, predicting strut rebound damping, and modeling transition from isothermal toward adiabatic conditions in the strut inflation gas. Rough field capability estimates for the C-130 equipped with these gears have been made. Recommendations for further analytical model improvements are included.

1. INTRODUCTION

Concepts of future warfare envision combat operations from and air delivery of cargo to austere airfields, repaired bomb damaged runways, or in some cases onto hastily prepared unpaved surfaces, all expected to be quite rough and very short. If additional runway roughness tolerance can be achieved through landing gear improvements, bomb damage repair times could be reduced, or alternatively taxiways or grass strips might be utilized, thus greatly diminishing the potential effectiveness of an airfield attack. One tactical transport, the C-130, could potentially reap enormous benefits in this scenario through improvements in landing gear design.

One way to accommodate short runways is to reduce forward speed and the kinetic energy to be dissipated during rollout by using higher approach glide slopes. Higher glide slopes generally mean higher landing impact sink speeds. Design sink rate for Short Takeoff and Landing (STOL) aircraft is usually assumed to be 15 FPS (Reference 1.) Rates higher than 15 FPS would likely provide diminishing benefits because of higher landing gear weight to achieve necessary gear stroke. Current land based aircraft are designed for 10 FPS sink rate, or on some older models, 9 FPS.

The C-130 transport is a 9 FPS aircraft and considerable attention has been directed to methods for improving its sink rate and ground roughness capability. The desirability of landing gear modifications became increasingly apparent during the joint US/UK HAVE BOUNCE program (Reference 2.) Frequent bottoming of the nose gear and the lack of ability to maintain strut positions set during service first directed attention to the strut behavior. Fortunately, the availability of good instrumentation made it possible to compare operational pressures with theoretical predictions. Under high compressive loads, significant pressure loss frequently occurred. Occasionally under decreasing loads, as during takeoff, pressure recovered.

Subsequently, the instrumented nose and main (one strut) gears were installed by the UK on another C-130 for unpaved surface testing (Reference 3.) During short flights, dramatic pressure variations were found in the main gear from liftoff to the next touchdown. Figure 1 shows results from a series of three takeoff and landing runs from a paved surface where extended strut pressure recovery varied between 140 psi and 60 psi while in the air.

Upon completion of aircraft testing, the instrumented gears were shipped to the U. S. Air Force Wright Aeronautical Laboratories for further study. Tests of the nose gear showed that duplication of aircraft measured dynamic strut position resulted in pressure variations similar to the previously collected aircraft data.

There have been sporadic reports of gear servicing problems (i. e. flat struts although following recommended procedures.) It is believed that these incidents are a manifestation of the same pressure loss/recovery phenomenon observed during the test programs.

Figure 2 illustrates the dilemma faced in servicing struts with variable pressure behavior. If servicing is done with the aircraft on jacks, any subsequent gas loss under load will lower the airspring curve and may even allow the strut to bottom, forcing the aircraft to taxi with only the tire spring. Of course bottoming is undesirable as there is no damping by the strut. If servicing is done under load with some gas already in solution, over charging could result. Pressure recovery could cause excess gas pressure adding proportionately to the orifice load at landing impact, and increasing peak load at all rates of sink.

If the orifice peak load happens to set the design limit load at design rate of sink, overload could occur should this sink rate be reached. Even though the landing gears might be strong enough to withstand the added loads, restrictions on allowable wing fuel might be required to offset the additional aircraft load.

2. LANDING GEAR MODIFICATIONS

Shortly after the HAVE BOUNCE program, the Lockheed preliminary design organization began a program to investigate ways to improve C-130 gear performance. The study covered a number of concepts and two of these resulted in experimental hardware.

To increase surface roughness and sink rate capability, both improved and STOL landing gears have been built and tested. This report focuses primarily upon the surface roughness capabilities with these gears as predicted by analysis. The extended stroke gears are now being flown on Lockheed's High Technology Test Bed aircraft which is shown in Figure 3; however, testing at high sink rates and over test runway profiles has not yet been accomplished.

a. Retrofit Kits for Improving Existing Gears

Retrofit modifications were designed which would, hopefully, prevent gear bottoming and severe deviations in gas pressure from expected values. These modifications are referred to as improved gears.

Figure 4 shows the changes made to the standard nose gear. The inverted cone orifice and bulkhead are removed. A new inner cylinder is placed inside the existing piston. The new cylinder contains a floating piston which serves as a separator between gas and oil. A new main damping orifice is placed in the top of this cylinder. The existing gas inflation port is sealed and gas inflation is moved to the bottom of the inner cylinder, resulting in an "inverted strut" having fluid above the inflation gas. Production versions will have a gas purging device installed in the existing inflation port at the top of the strut to facilitate purging of any gas which may leak past the separator piston.

A new upper bearing assembly contains orifices and a flap valve to control extension rate by restricting flow from the chamber between the piston and outer cylinder. The rebound orifices were sized experimentally to achieve the recommended maximum extension rate of approximately one third the landing impact closure rate (Reference 4.) Originally, a flap valve was installed on the main orifice, but tests showed cavitation in the main oil chamber, consequently this flap valve was removed. A replacement lower bearing with a chamfered lower edge is used to minimize friction during wheel spin-up.

These modifications are designed for retrofit. Maximum use is made of existing landing gear parts including all existing forgings. The changeover can be accomplished on later series one piece forging struts by mechanical disassembly and parts replacement. On earlier 2-piece forging/welded struts, machining of the orifice plate is necessary to allow clearance around the new inner cylinder.

Figure 5 compares existing and improved main gear struts. Again, the goal was to provide a kit that could be installed by parts substitution without machine shop re-work of existing gears. As shown, the existing oil chamber bulkhead and the orifice plate are removed and replaced with a bulkhead supporting a metering pin having an oil spray deflector counter piston mounted on its top end. The counter piston minimizes oil spray during strut rebound. A new upper bearing assembly has orifices and a control flap valve. By shortening the bearing length, stroke is increased from 10.5 in. to 11 in.

One each nose and main gear modification kits were constructed for laboratory testing and installed in the instrumented nose and main struts previously used in the HAVE BOUNCE program. No installations have yet been made on an aircraft.

b. Extended Stroke Landing Gears

During the time improved gears were being developed, a test aircraft was obtained for evaluating aerodynamic devices, flight controls, and electronic equipment related to STOL operation. New landing gears developed for this test aircraft, in addition to providing longer stroke, incorporated features built into the improved gears. STOL operation gears are referred to as extended stroke gears.

Figure 6 shows sketches of extended stroke gears. One each nose and main gear struts for laboratory testing and one aircraft ship set for flight testing were built by Menasco to Lockheed drawings. These struts are similar to the improved nose and main gears. They incorporate gas/oil separation, rebound damping, and for the main gear, a metering pin. In addition, the nose gear stroke is increased from 10.5 in. to 18 in. and the main gear stroke is increased from 10.5 in. to 24 in.

Since these struts will not fit into the existing wheel well when fully extended, a compression feature has been built into both nose and main gears, wherein ship's hydraulic pressure is used to compress the struts prior to retraction. Insufficient door clearances on the test aircraft required the use of smaller tires on a temporary basis. Should these gears be installed on production aircraft, modifications to the compression system will be made to accommodate current tire sizes.

Figure 7 shows a comparison of the standard and extended stroke main landing gears. The additional energy absorption potential of the longer stroke gear is readily apparent in this figure.

Both types of new gears may be retrofitted to existing aircraft or incorporated into new production C-130's.

3. LANDING GEAR LABORATORY AND FLIGHT TESTING

Guidance for development of these landing gear modifications and replacements have been and continue to be dependent upon extensive testing.

a. Aircraft Testing

There have been three recent opportunities to collect flight test results to evaluate C-130 landing gears. These were the programs described in References 2 and 3, and current testing on Lockheed's High Technology Test Bed aircraft. Prior to the HAVE BOUNCE test program, most C-130 testing utilized either oscillographic recording or FM analog techniques that were not readily usable to the level of detail required to determine gear performance. Main concerns during earlier tests were the magnitudes of peak loads and only a limited amount of strut performance data was available for analysis in time history or cross plot format. Internal pressures were not usually measured, and string potentiometers used for stroke measurements were not very accurate.

Figure 8 shows an example of the high quality time history data collected in the HAVE BOUNCE program. For the first time, it became practical via computer to cross plot measured pressures vs. stroke and to superimpose theoretical pressure/strokes with test results as shown in Figure 9. Having this capability, particular attention could be directed toward gear response as was the case during the grass surface trials program.

Flight tests have also emphasized the significance of main gear telescoping friction. Figure 10 shows main gear strut friction during a landing rollout. It is seen that strut motion occurs in a series of steps as load changes, indicating only limited shock absorption. All four main struts on the High Technology Test Bed aircraft have been instrumented. The data from four main struts has also revealed interesting main gear friction behavior as shown in Figure 11. The differences in the amount of telescoping friction between the left and right landing gears is believed to illustrate a lateral drift (left) landing where friction is increased due to outboard loading of the right pair of struts and decreased due to inboard loading of the left pair of struts.

Only limited landing gear data has been obtained from the test aircraft. STOL evaluation testing is now underway.

b. Laboratory Testing

Both the improved and extended stroke landing gears have gone through extensive laboratory testing as individual struts. All tests were performed by the Air Force Wright Aeronautical Laboratories at Wright-Patterson Air Force Base, Ohio, using Numbers 3 and 4 drop towers, as sketched in Figure 12.

For drop testing, the gears were suspended beneath a ballast container and allowed to free fall onto an instrumented platform. Backward pre-rotation of the tires simulated spin-up. At the position where the tire just touched the platform, further downward motion of the ballast container was resisted by air cylinders at a pressure calculated to equal the ballast weight, thus simulating aircraft lift.

Instrumentation consisted of strain gage measurement of vertical load, main hydraulic chamber oil pressure, gas inflation pressure, rebound chamber pressure, and in some cases inflation gas temperature. Vertical displacement and acceleration of the ballast container were recorded. For shaker testing, hydraulic shaker ram pressure and displacement were added. For drop tests, drop platform vertical and drag loads were included.

Figure 13 illustrates a fitting used to gain access for rebound chamber pressure measurement directly through the strut sidewall. This technique was for laboratory use only and was not considered for any gear installed on an aircraft.

Since no increase in sink rate or aircraft landing weights were planned for the improved gears, they were drop tested to the same conditions as originally specified for the standard struts. Any gains for landing impact are thus realized by lower landing loads.

References 5 and 6 report drop test results for the improved landing gears and References 7 and 8 report drop test results for the extended stroke gears. For both improved and extended stroke gear sets, preliminary drops were made for sizing rebound damper orifices and main gear metering pins. The extended stroke gears, being essentially a new design were drop tested to the specifications of MIL-T-6053. They are fully qualified for flight.

Figure 14 compares drop tests for 3, 5, 6, 9, and 10 FPS sink rates of the improved nose gear with the drop tests of the standard C-130 nose gear. These comparisons show that initial load build up is more rapid in the improved gear as a result of deletion of the inverted cone orifice, that significantly less stroke is used at each sink speed, that no bottoming occurs, and that rebound is slower. Lower loads and higher strut efficiencies could be achieved with a larger main orifice; however, it was felt that the increased damping of the orifice size chosen would be beneficial in reducing aircraft porpoising over runway roughness.

For shaker testing, the instrumented drop platform was replaced by a platform attached to a large hydraulic shaker capable of producing programmed vertical displacements equivalent to the excitation seen by the tire when passing over an actual obstacle at various speeds. All operations except rolling tire effects and tire wraparound of obstacle sharp corners are accounted for. Of course, since individual nose and main struts were tested separately, aircraft pitching, pilot response, engine thrust and aerodynamic effects are not included.

During specific rough surface simulation the ballast container was unrestrained in vertical motion. In order to study response to a particular motion such as step closure or extension, and to run slow rate load/stroke curves, the ballast container was restrained to prevent vertical movement.

Figure 15 illustrates typical shaker tests of the extended stroke main gear. Gear vertical load is shown for 50, 75, 100, and 125 ft./sec. simulated aircraft speeds over a 7.2 in. (1-cosine) shaped dip, also shown in Figure 15. Because of ballast container and support structure weight, these tests were run at 50,000 lb. strut load, corresponding to an aircraft weight of over 200,000 lb. substantially greater than current aircraft weight limits. This capability illustrates the robust design of these struts.

4. COMPUTER SIMULATION FOR LOAD PREDICTIONS

Prior to the development of powerful desktop computers in the early to mid 1980's, the cost of computer time limited to a large degree the number and complexity of simulation studies that could be carried out. Computational cost for non-linear landing gear studies can no longer be considered to be a limiting factor within even very modest size organizations, as the newer 32-bit cpu micro computers have the capacity and speed to run extensive landing gear simulations in combination with a flexible aircraft model. Prospects are good for achieving even greater computational capability over the next several years.

While not as spectacular as computer hardware improvements, software techniques have also progressed. Reference 9 presents a variable step size integration technique that is several times faster than the popular Runge-Kutta fixed step size methods. Data presentation methods have also evolved, as cheap and easy to use graphics devices have proliferated.

In order to more accurately simulate performance of improved and extended stroke gears, several changes to the usual C-130 modeling techniques were made. These included polytropic gas compression, revised strut friction, and representation of rebound damping. These changes have resulted in an acceptable level of correlation. Simulation and test results comparisons, based on individual struts, increases confidence in the predictions of loads in the whole aircraft simulation.

The modeling techniques developed for these gears are expected to be beneficial for other landing gears since they resulted in increased understanding of several previously troubling areas in gear simulation.

a. Isothermal/Adiabatic Transition for Gas Separated Struts

A first task in validating a landing gear simulation model is to establish a correct pressure vs. stroke relationship, as this determines the gear spring characteristics and primarily the response frequency. Accurately measured pressures and strokes are vital to establish this relation. Once the correct pressure/stroke is defined, other model features such as strut friction can be more easily established.

Usually, analyses are made on the basis of an assumed constant polytropic gas compression/expansion coefficient (Reference 1), perhaps 1.0 for struts without gas/oil separation and 1.3 - 1.4 for struts with gas/oil separation. In the case of taxi with the strut starting from isothermal equilibrium, there have been few ways to transition to the higher coefficients without encountering a fictitious pressure step.

Reference 10 indicated that transition might be accounted for during compression by making the compression/expansion exponent an exponential function of stroking velocity. This approach was tried in an experimental simulation and found to work satisfactorily during compression; however, at maximum stroke when strut velocity goes to zero the exponent drops back to the isothermal value of 1.0 resulting in a sudden drop in computed pressure.

Reference 11 points out that the polytropic exponent is a variable and is dependent upon the ratio of heat transfer to work done. It was decided to experimentally model the compression/expansion coefficient as a function of the work done on the gas. This method was found to work quite satisfactorily and accounts for both heating and cooling of the strut. Figure 16 shows the exponential functions which were fitted for the nose and main landing gears. Additionally provision is made for an initial exponent which may differ from 1.0 due to prior heating or cooling of the strut.

Also, tests at slow rates of loading produced pressures less than those calculated by a simple isothermal process, even when the gas and oil were separated. Approximation of the effects of material expansion and hydraulic oil compressibility as a function of pressure were required. For the extended stroke gears these quantities were determined to be .001587 $in.^3/psi$ for the nose gear and .0070588 $in.^3/psi$ for the main gear. With this modification the pressure becomes an implicit function which must be solved by iteration at each time step.

Figure 17 illustrates that the variable thermodynamic coefficient and the compression/expansion modeling functions result in a close match of the pressure vs. stroke relations for both gears. There is a substantial improvement over methods which do not allow for these effects.

b. Modeling Strut Telescoping Friction

The level of strut friction in a gear can usually be readily seen from test results in a cross plot of strut load and stroke. Changes in load while the strut position stays fixed is an indication of friction.

Figure 18 shows examples of slow and rapid rates of loading for the high sink rate main gear. The stairstep characteristic at the slow rate is indicative of a stick/slip situation. As stroking velocity increases, the load/stroke curve becomes smooth; however, when the strut reverses direction a large change in load occurs before the strut moves. Since damping is zero and air pressure remains constant while the strut is stationary, friction is the remaining unknown force.

A calculation of normal force in the strut shows that usually assumed friction coefficients for teflon on steel are much too low to generate the levels of friction observed. It is theorized that bending of the strut causes the piston/cylinder/bearing combination to become oval in shape as illustrated in Figure 19. Binding between the bearing and cylinder at the upper bearing and between the bearing and piston at the lower bearing are believed to cause the large friction forces observed.

Figures 20 and 21 illustrate the importance of representing strut friction in the simulation model. Test results illustrate the standard C-130 main landing gear loaded in the laboratory by a simulated 5 in. amplitude (1-cosine) bump at a simulated speed of 50 ft./sec. Since there were significant differences in measured pressure/stroke vs. theoretical values, an isothermal curve fit was made to minimize errors from the airspring. Figure 20 shows results of the simulation and test comparisons with the fitted airspring plus friction, with good correlation indicated. Figure 21 shows similar results with the friction model removed, and comparisons are poor. It is assumed that discrepancies resulting from poor friction modeling have not previously been so apparent because airspring errors have partially compensated for friction errors.

c. **Rebound Damper Simulation**

Pressure measurements from shaker tests were used to determine effective flow coefficients from the rebound chambers. Figure 22 shows rebound chamber and main oil chamber pressures for the extended stroke main gear. It is seen that each time the gear extends the flap valve closes, producing a pressure drop across the rebound orifices in the upper bearing, limiting the extension rate of the strut. Two E-bump profiles were used for the gear simulation.

As indicated in Figure 23, the extended stroke nose gear flap valve does not close promptly as the strut starts to extend. The same 2 E-bump profile is used so the difference in behavior of the main and nose struts in attributable to mechanical causes. Figure 24 shows a plot of the mathematically calculated derivative of strut displacement along with the rebound chamber pressure. Flap valve closure occurs in the neighborhood of 30 in./sec. extension velocity. For simulation purposes, it was necessary to set flap valve closure criteria as a function of both rebound chamber pressure and strut extension rate. The values selected were; rebound chamber pressure dropping below 600 psi and strut extension rate exceeding 27 in./sec. Using this criteria, fairly good rebound chamber pressure calculations were obtained as illustrated in Figure 25. For a range of other speeds, simulated flap valve closure was reasonably consistent with test results.

Successful correlation for the extended stroke nose gear would have been unlikely without benefit of the rebound chamber pressure test measurements, as flap valve sticking is not directly detectable from load and stroke measurements.

d. **Simulation vs. Test Load Comparisons**

With the previously discussed modifications to the polytropic gas exponent, derived rebound chamber orifice coefficients, flap valve closure criteria, and a modified friction model for the main gear, overall model accuracy can be evaluated by comparing strut load with test results. Figures 26 and 27 show comparisons for the extended stroke nose and main gears. Overall agreement between simulation and test is seen to be good. These models are now considered suitable for analytical studies of aircraft capability.

e. **Gas Solubility in Current Struts**

Since no analytical model is yet available to adequately represent gas solubility and subsequent dissolution, it is necessary to resort to approximations to generate adequate comparisons between analysis and test results. For a particular strut, the best approximation can be generated by plotting test generated pressure vs. stroke and then fitting an analytical curve to the resulting data. For portions of the time history where the fitted curve is close to actual values, overall agreement between test and simulation is usually good. For the other portions of the time history, results are usually poor.

For the HAVE BOUNCE program, fitted data from a number of tests were averaged to produce a composite curve fit. Comparisons with test data using the averaged fit data were less accurate than the comparisons using fits for individual runs; however, the averaged values were considered more suitable for parametric studies, and have been used on an interim basis until a better model is developed.

A good analytical model of gas solubility would be useful for a number of current gear designs, and also for future gears in which gas/fluid separation might not be feasible.

5. ESTABLISHMENT OF AIRCRAFT ROUGHNESS TOLERANCE

An aircraft's response to runway roughness is a non-linear resonant system having highest loads at certain excitation frequencies. From an operational standpoint, this translates into a question of how fast the aircraft is going over a particular rough spot on the runway, and does that speed represent a resonant situation.

It is not possible to pre-define the distribution of roughness wavelengths along a runway. Although many attempts have been made to develop generalized prediction methods, none have proven to be totally acceptable. Reference 12 is probably the latest examination of the roughness problem. It is concerned with loading from runway bomb damage repairs and was directed primarily toward occurrences of multiple bumps.

In addition to considering candidate levels of roughness for landing gear design, Reference 12 went into considerable detail about methods of analysis and presentation of results. One approach was to select

worst case combinations of speed, wavelength, and bump amplitude, and use this recognizing the resulting severe restrictions on allowable runway bump amplitudes. Another approach was to recognize that some additional capability could be obtained if certain speed and roughness wavelength combinations could be avoided. Here the term wavelength could be used with reference to a single bump or to the periodic excitation for multiple bumps.

To illustrate critical combinations of speed and wavelength from this second approach, a data presentation method, called the load contouring approach, was developed in Reference 12. To generate gear load information, a matrix of simulations are made with speed and wavelength varying in a prescribed manner. By using interpolation, contours of load amplitude can be extracted from a matrix of peak loads from these computer simulations. For most purposes, limit load would be used. Unless some part of the aircraft is known to always be the first to reach its limit, loads for a number of locations must be monitored. These load contours can be generated for different conditions, i.e. taxi, takeoff, rollout, etc. and for specified roughness.

The loads contouring methods from Reference 12 are general and can also be applied to roughness specifications other than bomb damage repairs. In this report they are used to study roughness capability with respect to the specification roughness of MIL-A-8862 as shown in Figure 28. These curves were derived from measurements of potential runway sites and are thus at least semi-realistic. Three levels of roughness classifications are contained in this specification.

For evaluating this aircraft, the semi-prepared surface was chosen since there is little question of the C-130's ability to operate from paved surfaces, and the unprepared surface roughness is so severe few aircraft could operate at that level, except at very restricted taxi speeds.

Figure 29 shows estimated capability with respect to a semi-prepared surface for a C-130 at design landing weight for encountering a single dip having the amplitude and wavelengths relationships specified. It is assumed that the aircraft is operating during rollout with full reverse thrust, with full up elevator to minimize nose gear loads, and with no wheel braking. Figure 29(a) shows estimated capability of the aircraft as equipped with a standard landing gear. Figure 29(b) shows estimated capability of the aircraft equipped with the improved nose landing gear along with standard mains. Since the improved main gears do not have full gas/oil separation and only a minor increase in stroke, aircraft capability would not be significantly changed with their inclusion. Figure 29(c) shows estimated capability of the aircraft when equipped with the extended stroke nose and main landing gears.

These results show an unrestricted capability of approximately 70 percent of the semi-prepared roughness level with the standard gears, approximately 80 percent capability with the improved nose gear, and approximately 100 percent capability with the extended stroke gears. In all cases nose gear vertical load limits established these capabilities.

6. LESSONS LEARNED

Experience with several configurations of gears for a single type of aircraft, along with extensive laboratory and flight testing, has provided guidance for better application of the load regulating techniques incorporated into these gears as well as providing data for improved landing gear modeling. Some of the lessons learned were:

a. Landing Gear Design

- There should be generous allowance for flap valve clearance in order to prevent erratic damping behavior and provide for prompt valve closure at the start of gear extension.
- Although there may be cases where separation of hydraulic oil and inflation gas may not be practical or desirable, laboratory results from these gears would indicate that this is a useful means of achieving better control over strut internal pressures and aids servicing reliability. Further flight measurements should reveal any operational problems that might not be seen from laboratory tests.
- Although simple floating separator pistons should not have significant pressure drops, there is a possibility for leakage. Evidence of gas or fluid transfer past separators in these gears was not seen in laboratory tests of C-130 gears; however, conversations with individuals experienced with other gears indicate that chamber purging capability needs to be provided, as well as attention to good sealing.
- Possible binding of internal floating pistons from cylinder deformation under load should be considered.
- The effects of strut deformation in contributing to high friction are believed to be significant. Possible contributions of high binding loads to strut fatigue damage should be considered.
- For struts which must be partially compressed for retraction, adequate hydraulic supply pressure and pressure area should be provided to ensure closure during specified gear retraction time and to ensure that sufficient pressure is available to overcome adiabatic compression pressure inside the strut.

b. Landing Gear Testing and Computer Modeling

Among the lessons learned from testing and simulation correlation efforts are:

- o Airspring Definition

  One of the most important contributions to success of a gear analytical simulation, and a definite first step, is to ensure that the correct strut airspring is modeled. This should be based on measurements of stroke and air chamber pressure. If the strut model (i. e. isothermal, polytropic, or whatever) do not agree with test results, it is advisable to empirically fit an approximate pressure/stroke relationship through the test results before proceeding with determination of other model parameters, otherwise important gear behavior for which there are no direct measurements may be overlooked.

- o Strut Friction Modeling

  Strut friction should be included in simulation models for load calculations. Without adequate test measurements, the magnitude and importance of friction may not always be recognized. Friction is more significant for gears with wheel load paths offset from the strut centerline, but high friction may also occur in symmetric strut configurations during wheel spin-up and during braking or turning.

- o Stroke Measurement

  Stroke measurements should utilize instrumentation with positive physical connections to the strut axle and cylinder. Experience on other aircraft have shown that string potentiometers which rely on a stiff spring to assure positive tension are not adequate for this application.

- o Rebound Chamber Pressure Measurement

  The complicated flow patterns through multiple small orifices that may be used with rebound chambers make measurements of rebound chamber pressure advisable during laboratory testing. These measurements help to establish flow efficiency factors for analytical predictions and also help to identify binding or sticking of rebound valves.

- o Benefits of Simulated Roughness Testing with Shakers

  Little information about gear performance in taxi, landing rollout, or takeoff is provided by traditional landing gear drop testing. For example, high strut friction could be beneficial in dissipating landing impact energy, yet be high enough to make the strut essentially rigid for low to medium runway surface roughness. Strut velocities during taxi are normally much lower than those occurring at the design sink rates, therefore hydraulic damping may be far from optimum for taxi loading. Roughness testing of C-130 landing gears using hydraulic shakers has proven to be useful. Roughness testing is recommended in addition to the currently required drop tests, particularly if an aircraft is expected to operate from other than high quality smooth paved runways.

7. ITEMS FOR FUTURE DEVELOPMENT

Although much progress has been made over the past several years in improving transport landing gear design and analysis, there is opportunity for further improvement. The major items which have become apparent during the development and testing of C-130 transport landing gears are:

a. Strut Thermodynamics

Despite the success achieved in modeling isothermal to adiabatic transition, the technique remains empirical in that it must be fitted to each strut. A more satisfactory and accurate model should result from a thorough investigation of heat transfer between the inflation gas and strut walls under dynamic conditions. Initial efforts have been made as illustrated in Figure 30; however, the accuracy level obtained in simulation does not yet equal that of the empirical method. With additional work a good thermodynamic model can probably be developed.

b. Structural Deformation and Strut Binding

The significance of strut binding upon the response of struts has been illustrated in this report. Reference 13 indicates that high friction may be serious enough to induce strut cracking. It is therefore advantageous to understand the strut binding problem as thoroughly as possible.

Research into strut deformation could include analytical (perhaps finite element) modeling of deformed struts to calculate localized pressure loading at the bearing/cylinder interface. Design efforts should be directed toward minimizing deformations consistent with reasonable weight and manufacturing costs. Statistics on the severity of friction induced cracking would be useful. If some struts are found to be more immune to cracking than others, then the reasons for the differences should be investigated.

c. Rebound Chamber Design and Optimization

Adequate experimental or theoretical data are not available for optimizing the size and number of rebound orifices to be built into a gear. Current models assume the same flow characteristics as conventional damper orifices, though intuitively one would conclude that there are differences which should be recognized and accounted for. Experimental determination of effective flow coefficients needs to be made, since flap valve action and subsequent fluid flow cannot be relied upon to always behave as anticipated.

A series of general flow experiments varying orifice flow paths and flap valve tolerance in a consistent and orderly manner would be valuable for developing reliable flow coefficients. The savings realized through reduced re-work, more accurate initial sizing, and reduced test times should repay research costs.

d. Gas Solubility and Fluid Mixing

There is no general method yet available to predict the degree and timing of inflation gas solubility and the occasional sudden release from solution. Solubility might be modeled on the basis of work (and rate) input to the gas; but detailed internal gear design may result in variations from gear to gear. Careful laboratory experimenting will be required to develop a generally applicable model. Perhaps experiments could be carried out with a simplified strut made from hydraulic cylinders where orifices, fluid to gas ratios and inflation pressures could be easily varied. Results might be more useful than those aimed toward a particular landing gear.

8. CONCLUSIONS AND RECOMMENDATIONS

Development of improved retrofit landing gears for the C-130 has demonstrated the practicality of modifying existing hardware to improve rough airfield performance. The unique opportunity to evaluate both minor internal modifications as well as substantial stroke length changes provides valuable guidance for making tradeoffs in cost vs. level of improvement. The roughness tolerance increase for each strut modification has been quantified for comparison and technique demonstration purposes, utilizing one selected surface roughness criteria.

Of equal importance, especially for future landing gear design, was the experience gained from the several cycles of testing, analysis, and performance comparisons of these gears. Efforts to refine the analytical models for better representation of gear response has produced lower cost techniques with higher accuracy than previously available. Significant improvements included dynamic variations in polytropic gas exponent, a fairly realistic representation of strut binding, and rebound chamber hydraulic damping with allowances for flap valve sticking. Analytical models of the C-130 gears are considered to be adequately validated for parametric studies over other roughness criteria.

Although these studies have produced quite satisfactory results for the C-130, it is recognized that more effort is needed to achieve a sound theoretical basis for application to new gears. It is recommended that work continue in the areas of gas exponent modeling, thermodynamic equations, binding friction from structural deformation, and rebound chamber fluid flow characteristics with a goal of calculating these quantities from strut geometry and volume without relying exclusively on experimental data to provide the necessary relationships. This work should encompass continued analysis of existing data for these landing gears as well as plans for future general purpose landing gear testing.

9. REFERENCES

1. Currie, Norman S., "Aircraft Landing Gear Design: Principles and Practices," AIAA Education Series, American Institute of Aeronautics and Astronautics, Inc., Washington, D. C., 1988.

2. Crenshaw, B. M., and Owen, M. M., "C-130 Response to Bomb Damage Repaired Runways," Volumes 1 and 2, ESL-TR-82-23, Engineering and Services Laboratory, Air Force Engineering Services Center, Tyndall Air Force Base, Florida 32403, December 1983.

3. Crenshaw, B. M., "C-130 MK3 Hercules Grass Trials," LG82ER0082, Published Under University of Dayton P. O. RI-17781, August, 1981.

4. Conway, H. G., "Landing Gear Design," Chapman and Hall Ltd., London, 1958.

5. Crenshaw, B. M., "Summary of Standard and Improved C-130 Nose Landing Gear Performance Testing," AFWAL-TR-3093, Air Force Wright Aeronautical Laboratories, Wright-Patterson Air Force Base, Ohio, March, 1988.

6. Crenshaw, B. M. "Summary of Standard and Improved C-130 Main Landing Gear Performance Testing," AFWAL-TR-87-3094, Air Force Wright Aeronautical Laboratories, Wright-Patterson Air Force Base, Ohio, March 1988.

7. Vennel, W. W., "C-130 Extended Stroke Nose Landing Gear Drop Test Results, "LG86ER0085, Lockheed Georgia Company, Marietta, Georgia, July 1986.

8. Vennel, W. W., "C-130 Extended Stroke Main Landing Gear Drop Test Results, "LG86ER0086, Lockheed Georgia Company, Marietta, Georgia, July 1986.

9. Shampine, Lawrence F., and Gordon, Marylin K., "Computer Solution of Ordinary Differential Equations," W. H. Freeman and Company, 1975.

10. Anon, "Service Experience of Shock Absorbers with Gas Separator Pistons," Dowty Presentation to SAE-A5.

11. Wahi, M. K., "Oil Compressibility and Polytropic Air Compression Analysis for Oleopneumatic Shock Struts,", Journal of Aircraft, Vol 13, No. 7, July 1976.

12. Anon," Aircraft Operation on Repaired Runways," Report of Working Group 22 of the Structures and Materials Panel, NATO/AGARD, Paris France, (In Publication).

13. Fewtrell, H. E., "Consideration of Mechanical, Physical, and Chemical Properties in Bearing Selection for Landing Gears of Large Transport Aircraft," Journal of the American Society of Lubrication Engineers, March 1983 pp 153-157.

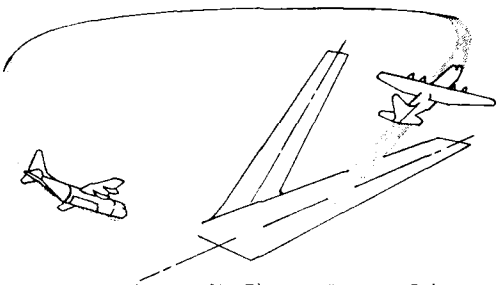

Pressure at Takeoff - psi.	Delta Time in Air - sec.	Pressure Prior to Landing - psi.
310	171	450
360	190	450
390	235	450

Figure 1. Example of Main Gear Pressure Variations during Frequent Landing and Takeoff Operations.

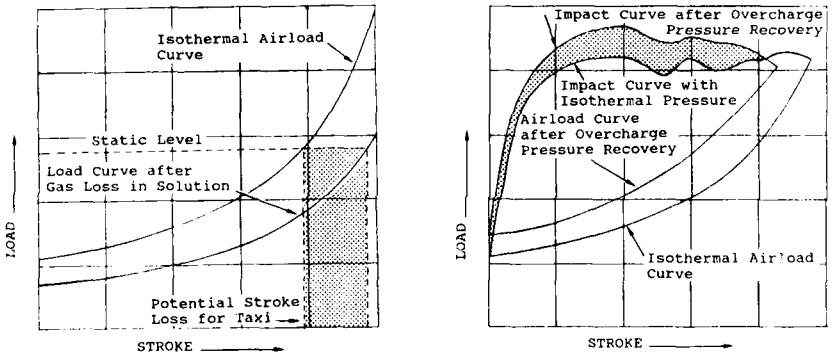

(a) Servicing on Jacks (b) Servicing Under Load

Figure 2. Difficulties in Servicing a Landing Gear with Gas Solubility.

Figure 3. C-130 Transport Aircraft with High Sink Rate Landing Gears Installed.

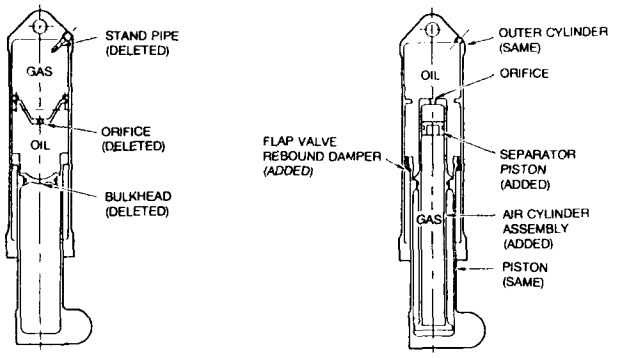

(a) Basic Strut (b) Improved Strut

Figure 4. Schematics of Standard and Improved C-130 Nose Gear Struts.

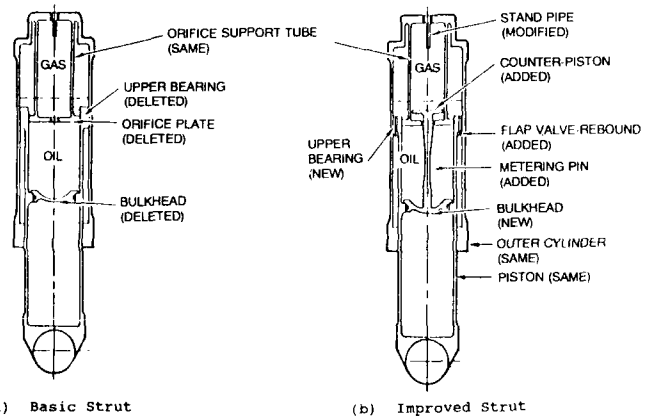

(a) Basic Strut (b) Improved Strut

Figure 5. Schematics of Standard and Improved C-130 Main Gear Struts.

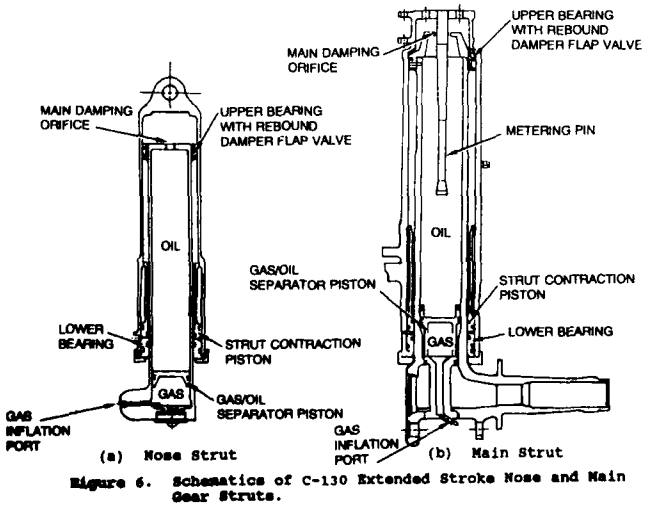

(a) Nose Strut (b) Main Strut

Figure 6. Schematics of C-130 Extended Stroke Nose and Main Gear Struts.

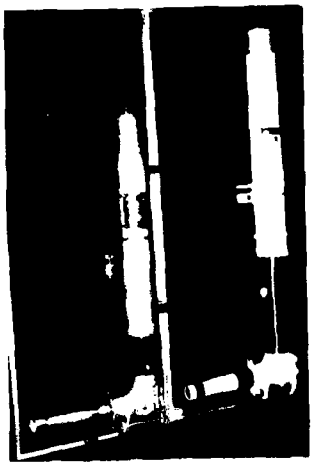

Figure 7. Comparison of the Standard and Extended Stroke Main Landing Gear .

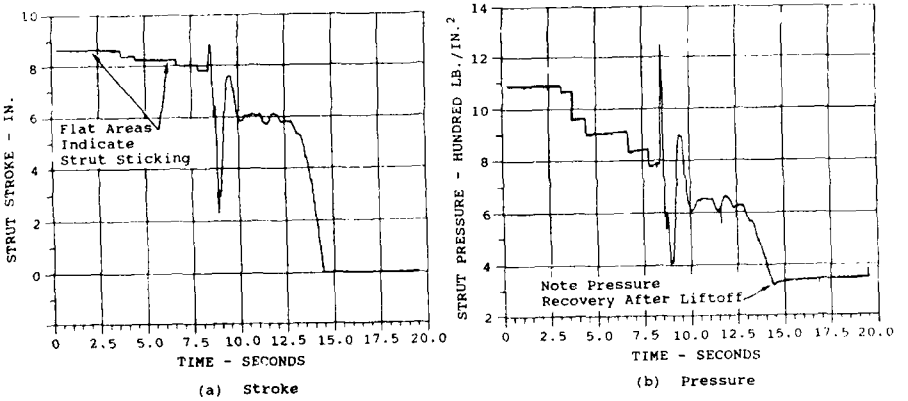

(a) Stroke (b) Pressure

Figure 8. Example Results of Stroke and Pressure Measurements *from the HAVE BOUNCE Program.*

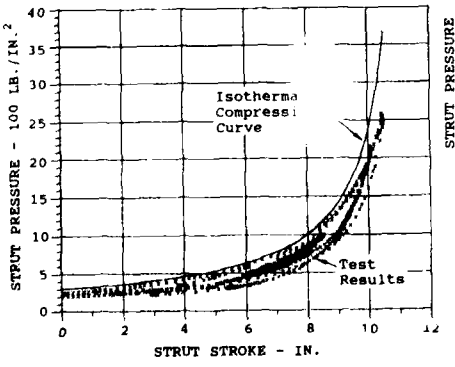

Figure 9. **Superimposed Theoretical and Test Pressure/Stroke Relations *for the Standard C-130 Main Gear.***

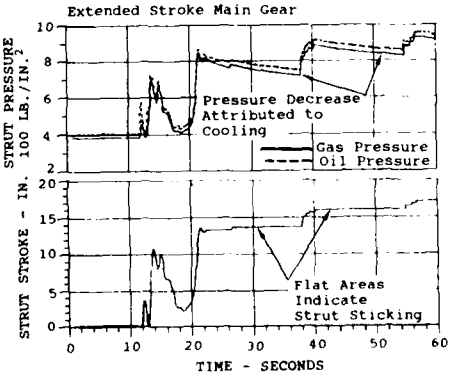

Figure 10. Example of Main Landing Gear Strut Friction during Landing Rollout.

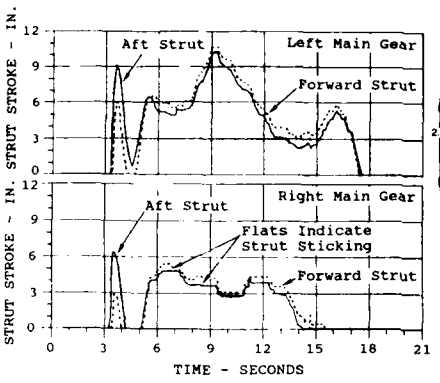

Figure 11. Example of Strut Friction during a Lateral Drift Landing.

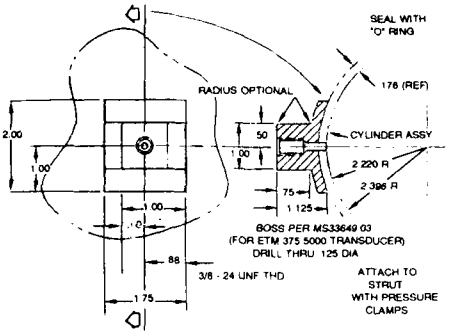

Figure 13. Example of a Rebound Chamber Pressure Tap Fitting.

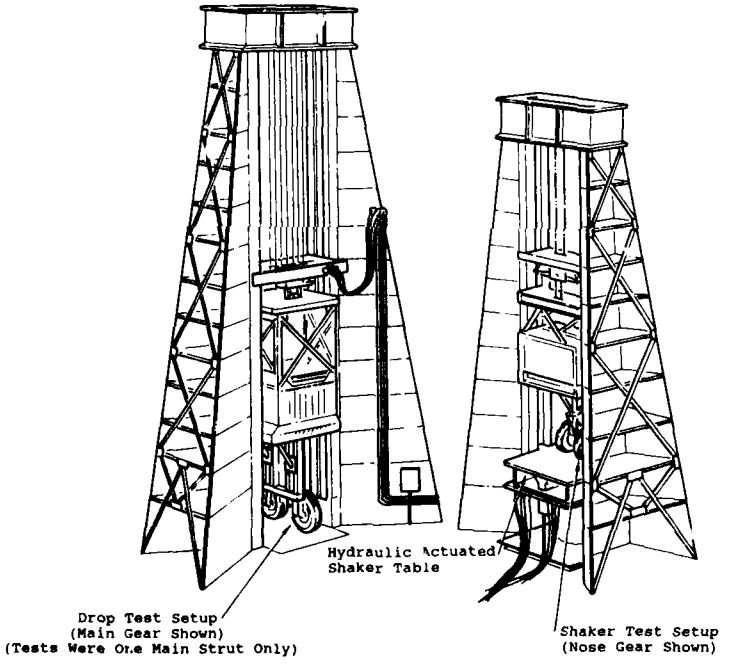

Figure 12. Drop Test and Shaker Test Setups at WPAFB Ohio.

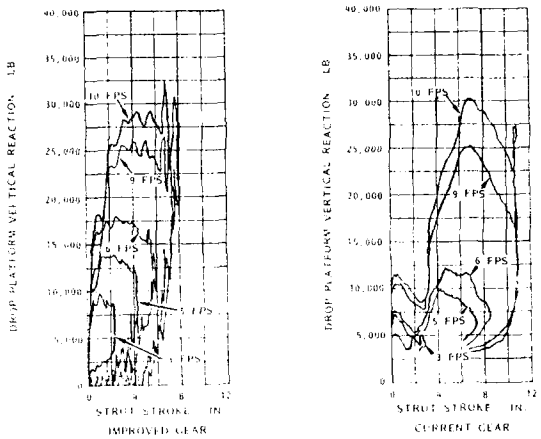

Figure 14. Comparisons of Drop Test Results for Standard and *Improved Nose Gears.*

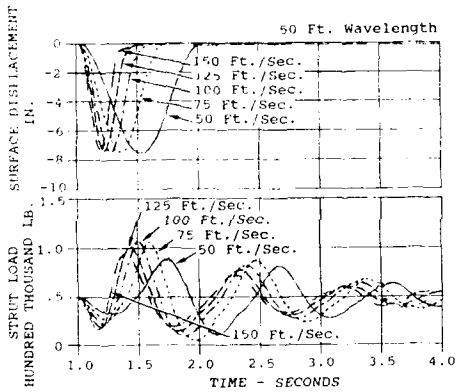

Figure 15. Example Results of Laboratory Shaker Testing of High Sink Rate Main Gears.

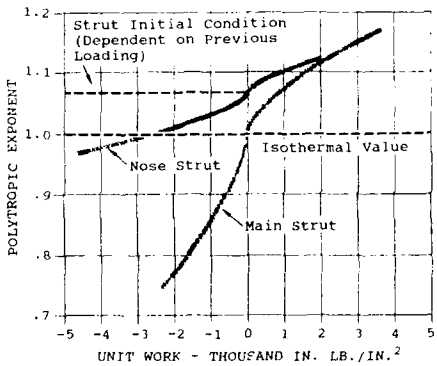

Figure 16. Dynamic Variations of Polytropic Gas Exponent in Simulation Model.

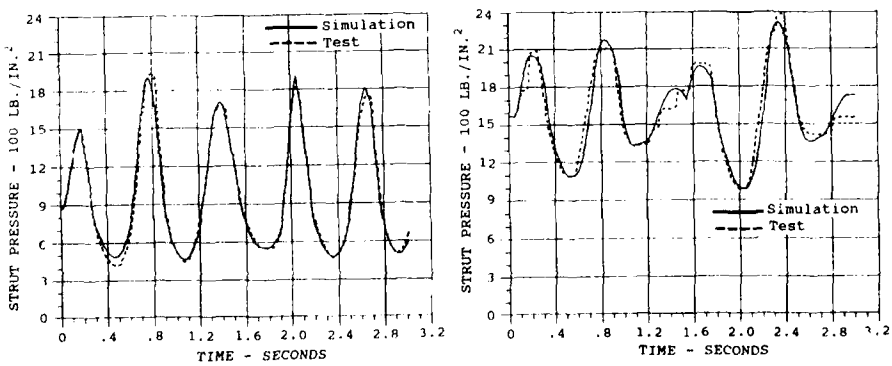

(a) Extended Stroke Nose Gear

(b) Extended Stroke Main Gear

Figure 17. Example Comparisons of Calculated Adiabatic Pressure Simulations with Laboratory Test Results.

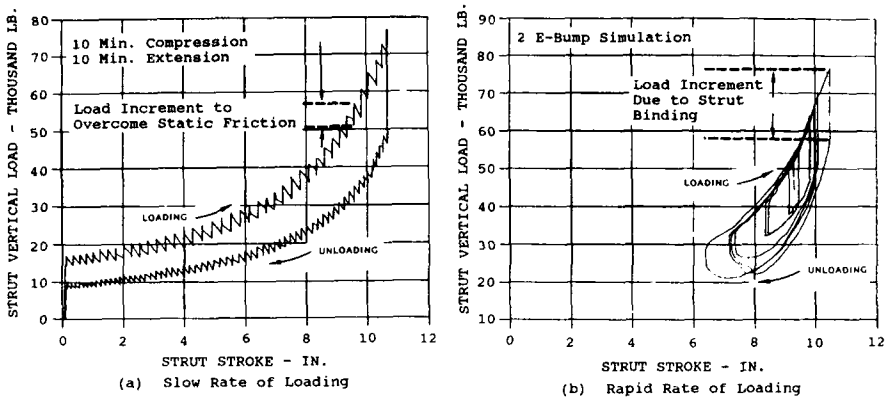

Figure 18. Illustration of Main Gear Strut Friction during Various Rates of Loading.

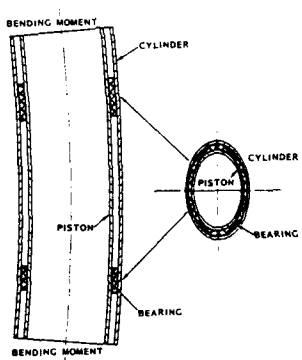

Figure 19. Distortion and Binding of a Strut Assembly by High Bending Moments.

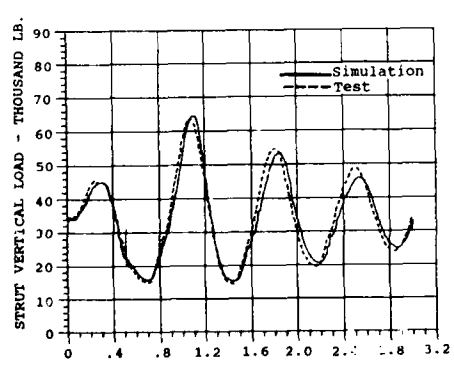

Figure 20. Strut Load Comparisons for a Standard Main Gear with Strut Friction Model Incorporated.

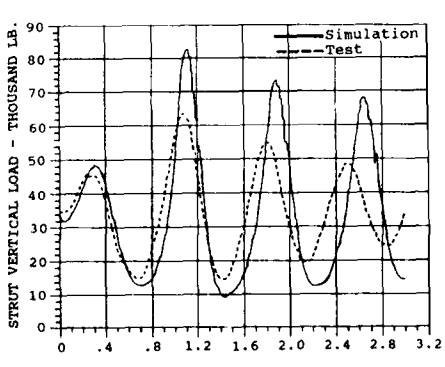

Figure 21. Strut Load Comparisons for a Standard Main Gear with Strut Friction Model Removed.

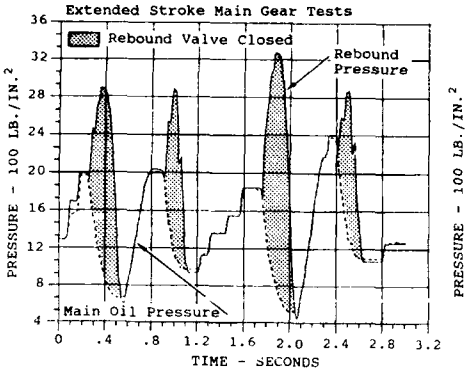

Figure 22. Rebound Chamber Damping without Valve Binding.

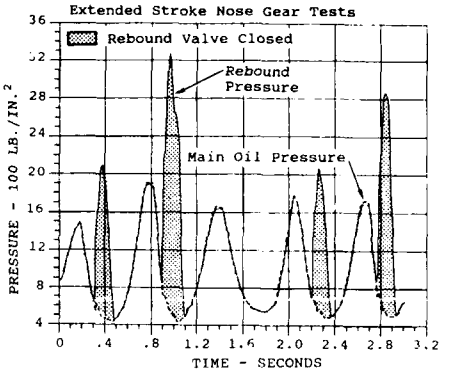

Figure 23. Rebound Chamber Damping with Valve Binding.

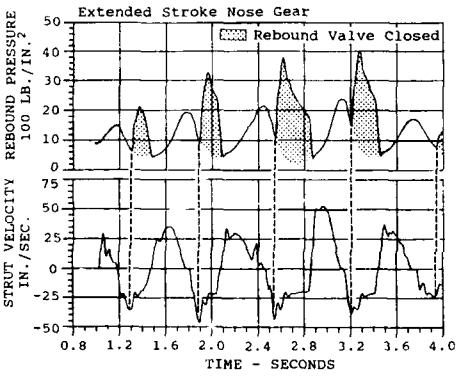

Figure 24. Correlation Between Strut Extension Velocity and Flap Valve Seating.

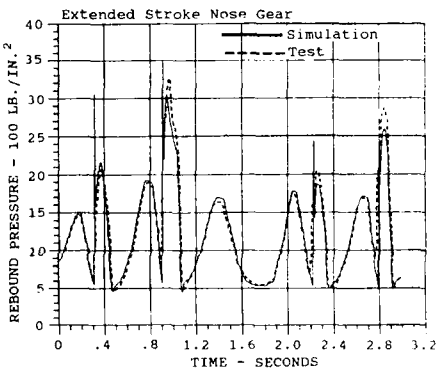

Figure 25. Comparisons of Measured Rebound Chamber Pressures with Pressures Calculated in Simulation Model.

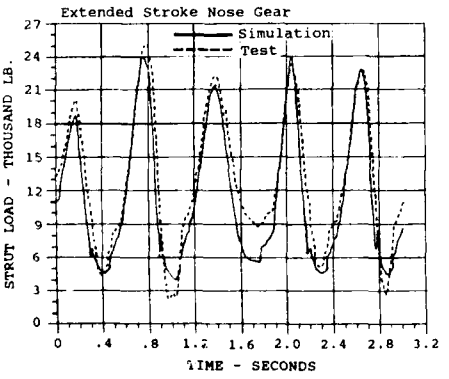

Figure 26. Individual Nose Strut Load Comparisons Between Simulation and Test Results.

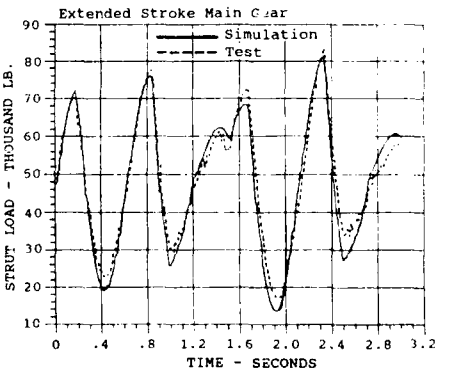

Figure 27. Individual Main Strut Load Comparisons Between Simulation and Test Results.

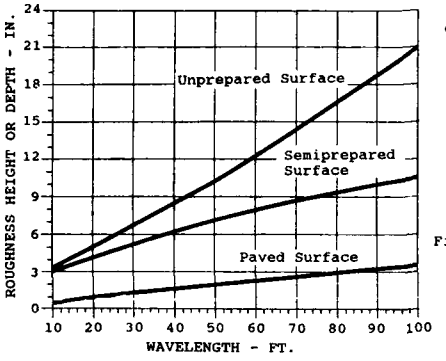

(Only Wavelengths for Capability Study Shown)

Figure 28. MIL-A-8862 Roughness Amplitude vs. Wavelength.

Simulation Conditions:

- o Design Landing Weight
- o Single Dip
- o No Braking
- o Rigid Surface

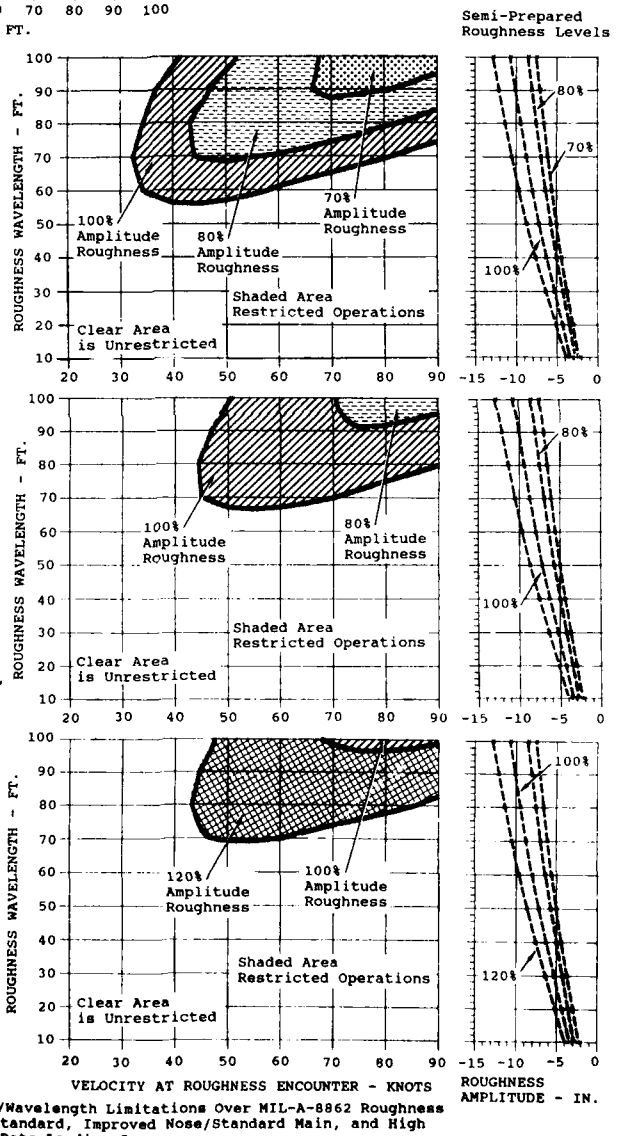

Figure 29. Speed/Wavelength Limitations Over MIL-A-8862 Roughness for Standard, Improved Nose/Standard Main, and High Sink Rate Landing Gears.

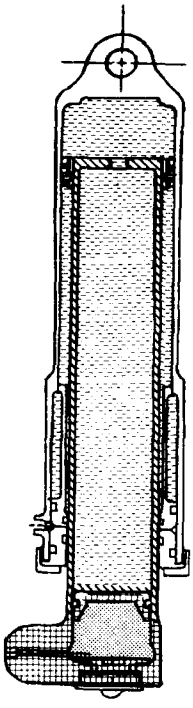

(a) Strut in compressed position

Cooling area = 0

Heating area = $1.78\left[12\pi_{in}(S_{tot} - S_{max}) + 2\pi_{in}\left(\frac{V_R}{A_p}\right)\right] + 2(2\pi_{in})^2$

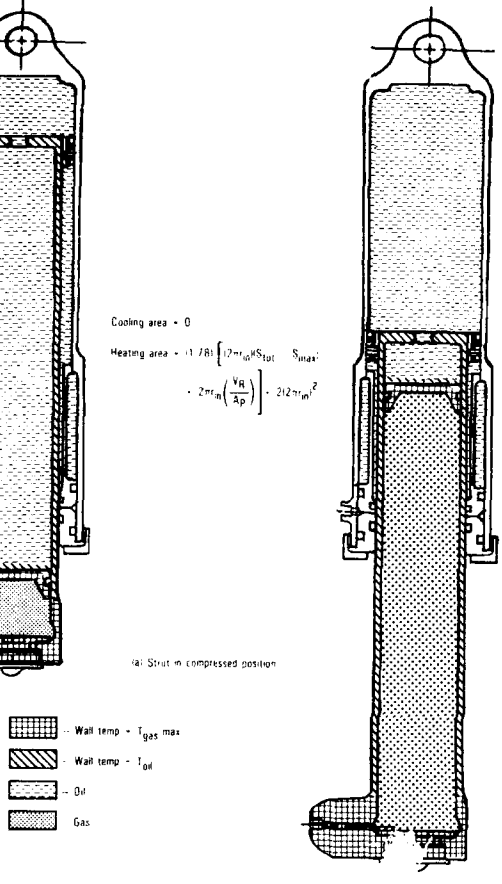

(b) Strut in extended position

Cooling area = $(2\pi_{in})(1.78)(S_{max} - S)$

Heating area = $1.78\left[(2\pi_{in})(S_{tot} - S_{max}) + 2\pi_{in}\left(\frac{V_R}{A_p}\right)\right] + 2(2\pi_{in})^2$

Stroke of gas piston = 1.78 × gear stroke

Wall temp = $T_{gas\ max}$

Wall temp = T_{oil}

Oil

Gas

$$\cdot\dot{T}_{gas} = \frac{2\pi K B}{P_0 V_0 C_v \ln\left(\frac{r_{out}}{r_{in}}\right)}\left[\left(T_{gas_{max}} - \left(1.78\left[S_{tot} - S_{max} + \frac{V_R}{A_p}\right] + 2R_{in}\right)\left(T_{gas} - T_{gas_{max}}\right)\right.\right.$$

$$\left.\left. + (T_{oil} - 1.78(S_{max} - S) - T_{gas} - T_{oil}\right]\right.$$

$$- \frac{A_p(K \quad 1.}{V_0}\left[\frac{T_{gas}}{\left(\frac{A_p S}{V_0}\right)}\right]\dot{S}$$

$$\cdot\cdot P_{gas} = \frac{P_0}{T_{0_{gas}}}\left[\frac{T_{gas}}{1 - \frac{A_p S}{V_0}}\right]$$

* Reference 11, equation 21 (modified)

** Reference 11, equation 22

Figure 30. Strut Heating and Cooling Model Approach for Future Thermodynamic Analysis.

SIMULATION NUMERIQUE DU COMPORTEMENT DYNAMIQUE DES ATTERRISSEURS

Jean Luc ENGERAND
MESSIER-BUGATTI
58 Rue Fénelon - 92542 MONTROUGE - FRANCE

ABSTRACT

During the design phase, at pre-project step, there is an increasing need for a comprehensive, integrated numerical simulation tool, capable of providing the design engineer with the complete answer to his analysis problems : kinematic, thermal, mechanical, linear or non-linear (static, dynamic, fatigue).

Numerical simulation of dynamic behaviour is a priority area for landing gear, as there are many problems to be solved (landing impact, taxiing, shimmy, retraction and extension, active control, crash landing, etc...) and they are far from simple (non-linearity, sometimes acute, due to large rotations, shock absorber friction, hydraulic damping laws,...)

The aim of the paper is to describe the Messier-Bugatti analysis and numerical simulation system used for solving landing gear dynamics problems, which is designed around a finite elements software package for the analysis of mechanisms and flexible bodies.

The following examples of applications are examined :

- Simulation of landing
- Simulation of taxiing on rough fields or repaired runways
- Simulation of extension and retraction
- Simulation of catapulting
- Analysis of shimmy stability.

RESUME

Dans une approche rationnelle de l'analyse des charges dynamiques appliquées au train d'atterrissage, Messier-Bugatti a mis en oeuvre un outil de simulation numérique construit autour d'un logiciel éléments finis d'analyse de systèmes articulés flexibles. Cet outil permet de résoudre les problèmes nombreux concernant les atterrisseurs (simulations de l'impact à l'atterrissage, appontage et catapultage, roulage sur pistes saines ou sommairement aménagées, manoeuvres de rentrée/sortie, shimmy, etc...) et délicats (non-linéarités parfois aiguë).

Après une rapide description des performances de ce logiciel, différents exemples d'application sont examinés, et l'accent est mis sur les corrélations calculs/essais.

1 - INTRODUCTION

Au stade de la conception, et dès la phase d'avant-projet, il est nécessaire de disposer d'un système complet et intégré de simulation numérique capable d'apporter à l'ingénieur la solution complète à ses besoins d'analyse : cinématique, mécanique linéaire ou non linéaire pour le dimensionnement en dynamique, statique, fatigue des structures d'atterrisseurs, voire thermique (environnement roue possédant un puits de chaleur).

Messier-Bugatti, concevant et réalisant la chaîne complète d'équipements nécessaires aux fonctions atterrissage et freinage (à savoir : trains

d atterrissage, roues et freins, systèmes de commande et régulation de freinage, systèmes d'orientation des roues, organes hydrauliques) a donc mis en oeuvre un tel système performant d'aide à la conception. En ce qui concerne plus particulièrement la simulation numérique du comportement dynamique des atterrisseurs, simulation complexe car présentant des non-linéarités accentuées, le calcul repose sur une méthode aux éléments finis d'analyse cinématique et dynamique de systèmes articulés flexibles.

Les développements successifs effectués, notamment pour la création d'une bibliothèque d'éléments spécifiques, permettent la simulation des efforts appliqués à la structure de l'atterrisseur lors des phases d'impact à l'atterrissage, catapultage ou appontage sur porte-avions, roulage sur pistes sommairement aménagées ou réparées, manoeuvres de relevage et descente, freinage dynamique, etc...

De tels exemples d'application sont présentés ci-après. Ils démontrent que, pour un coût de calcul raisonnable, on peut accéder de façon rationnelle aux efforts au sol et aux attaches très tôt dans la phase de conception, puis conduire des analyses complémentaires plus spécifiques. Parmi ces dernières, nous retiendrons l'analyse de la stabilité au shimmy, ainsi que l'étude de suspensions "intelligentes", qu'il s'agisse d'amortisseurs à contrôle actif ou bien encore d'amortisseurs du type "Jump-strut".

2 - L'OUTIL DE SIMULATION

Il repose sur le concept de modélisation par éléments finis appliqué aux systèmes complexes flexibles et polyarticulés, partant de la méthodologie employée dans les codes de calcul dynamique des structures par voie implicite. En l'occurrence, le solveur est celui du logiciel MECANO, module intégré dans le code de calcul SAMCEF développé par la société SAMTECH avec le concours du LTAS de l'Université de LIEGE (BELGIQUE).

Il permet de modéliser le comportement dynamique, en présence de grandes rotations, de structures constituées de poutres déformables avec leur densité, de ressorts sans masse, de masses ou inerties concentrées en un point, avec toute une bibliothèque d'éléments de liaisons mécaniques (rotule, butée en translation, butée en rotation, glissière, charnière, joint prismatique ou cylindrique, jeux, etc...).

Par ailleurs, pour les besoins spécifiques du train d'atterrissage, ont été développés des éléments spéciaux tels que le vérin hydraulique ainsi qu'un élément de liaison entre un pneumatique flexible et le sol avec les propriétés de mise en rotation, de ripé et de freinage.

Messier-Bugatti a développé pour ses propres besoins un élément utilisateur décrivant l'amortisseur oléo-pneumatique monochambre ou bichambre, prenant en compte les lois de laminage de l'huile en Kv^2, les lois polytropiques de compression de l'azote, les frottements de paliers et garnitures de l'amortisseur, la compressibilité de l'huile, etc... La programmation de cet élément ayant été faite au sein de notre société, elle inclut de ce fait tout notre savoir-faire en matière d'amortisseurs ; de plus, cet élément peut aisément être développé pour prendre en compte de nouvelles technologies d'amortisseurs.

Ce logiciel offre, comme fonctionnalité supplémentaire, l'utilisation de super-éléments à modes composants générés dans le module d'analyse dynamique linéaire, ce qui permet de réduire considérablement le nombre de degrés de liberté du modèle tout en conservant une très bonne précision pour le comportement dynamique des sous-structures correspondantes.

On peut traiter des systèmes pouvant comporter plusieurs centaines de degrés de liberté.

Enfin, le schéma d'intégration temporelle est une méthode implicite du type NEWMARK, modifié par HILBERT, HUGHES et TAYLOR pour améliorer la stabilité de la procédure itérative par l'intermédiaire d'un coefficient d'amortissement numérique des composantes hautes fréquences (réf. 1). Sa résolution est menée à bien grâce à la méthode itérative de NEWTON-RAPHSON.

3 - APPLICATIONS AU CALCUL DE PERFORMANCES DYNAMIQUES D'UN ATTERRISSEUR

Comme indiqué précédemment, la détermination des efforts appliqués au train d'atterrissage lors des cas d'atterrissage ou d'évolution au sol passe par des calculs rationnels, menés le plus souvent sur un modèle avion complet équipé de ses 3 atterrisseurs.

En cela, la tendance est donc d'aller bien au-delà des exigences réglementaires lorsque ces dernières n'imposent que des cas de charges forfaitaires.

Les exemples d'applications qui suivent, s'inscrivent dans cette tendance.

3.1 Simulation d'impact à l'atterrissage

L'exemple retenu est celui de l'atterrisseur avant d'un avion de transport, type AIRBUS.

Cet exemple a été choisi du fait de l'existence de courbes d'essais dynamiques de certification effectués sur cet atterrisseur, permettant une vérification calculs-essais. Pour cette raison, le modèle numérique doit prendre en compte tous les ensembles constituant l'atterrisseur, avec leurs masses et leurs souplesses, à savoir :

- le caisson
- le tube tournant
- l'amortisseur et la tige coulissante
- le système de contreventement
- les roues et les pneumatiques

La figure *1.a* montre une vue du modèle en position tout détendu.

Le calcul présenté correspond à un essai de chute avec les paramètres suivants :

- vitesse verticale V_z = 3,04 m/s
- vitesse horizontale Vx = 51,14 m/s, obtenue par une prérotation équivalente des roues
- assiette avion piqué 0°40
- masse réduite Mr = 12790 kg
- force travaillante nulle : la portance équilibre le poids de l'atterrisseur

Pour ce calcul, le pas de temps retenu est de 1 ms.

Les deux courbes de la figure *1.b* permettent de constater un recalage satisfaisant des efforts verticaux entre l'enregistrement de l'essai et la simulation de calcul équivalente, compte-tenu des nombreux paramètres difficiles à quantifier avec précision pour le calcul (coefficients pneumatiques et coefficients de frottements amortisseur, comportement global du pneumatique, principalement l'incertitude sur le coefficient de frottement pneu-sol dûe au dépôt de gomme sur la table dynamométrique).

En complément du calcul classique des efforts verticaux, l'avantage d'un tel modèle en atterrisseur souple est d'obtenir une approche rationnelle des efforts longitudinaux du phénomène de mise en rotation et de retour élastique, ainsi que des déformations des éléments structuraux, en particulier ceux constituant le contreventement.

3.2 Simulation d'appontage avec accrochage dans les brins

Le cas retenu est celui d'un avion embarqué se présentant à l'appontage dans un mouvement rectiligne uniforme, la crosse interceptant un brin du porte-avions au temps t = 0 de la simulation .

Les conditions initiales sont principalement :
la masse avion, la vitesse verticale par rapport au pont Vz, la vitesse horizontale par rapport à l'air Vx, la vitesse d'entrée dans les brins Veb, l'incidence α et l'assiette de présentation θ. La loi de freinage dans les brins est celle préconisée par la norme MIL-STD-2066, avec une distance d'arrêt de 98 m (loi pseudo-sinusoïdale prenant en compte les oscillations du câble après accrochage).

Le modèle est constitué (voir figure *2.a*) :

- de l'avion complet rigide
- des 3 atterrisseurs finement modélisés, incluant la loi de mise en rotation des pneumatiques
- de la crosse d'appontage et son amortisseur propre
- du câble d'accrochage

Le calcul tient compte de lois aérodynamiques fournies par l'avionneur.

Il permet, entre autres, la détermination des efforts au sol et dans les amortisseurs des 3 atterrisseurs, mais aussi les efforts dans l'amortisseur de crosse et les mouvements de celle-ci.

Pour cette application, le pas de temps a été adapté à chacune des phases étudiées, variant entre 0,5 milliseconde et 5 millisecondes.

Nous présentons figures *2.b*, *2.c* et *2.d* quelques résultats de cette simulation.

On constate que :

. Les atterrisseurs principaux impactent au temps t = 0,27 s.

. L'atterrisseur auxiliaire impacte au temps t = 0,45 s. D'autre part, il est à noter que la vitesse d'impact est supérieure à la vitesse verticale initiale de l'avion du fait du phénomène d'abatée induite par la vitesse angulaire de l'avion.

. L'amortisseur de crosse est soumis à de fortes oscillations juste après l'accrochage dans les brins.

L'illustration de cette simulation d'appontage avec accrochage dans les brins est fournie figure *2.e*, présentant une visualisation du modèle à 4 instants différents :

- t = 0 : accrochage dans les brins
- t = 0,1 s : allongement du brin avant impact
- t = 0,3 s : impact sur les atterrisseurs principaux ; la rotation des roues est schématisée par la rotation de la croix placée au centre roue.
- t = 0,5 s : impact sur l'atterrisseur auxiliaire, avec mise en rotation de la roue.

Ce calcul a permis l'optimisation des paramètres des trois amortisseurs, ainsi que celui du vérin/amortisseur de crosse, répondant ainsi aux spécifications émises par l'avionneur.

3.3 Simulation de fin de catapultage

On considère cette fois le catapultage par l'atterrisseur avant d'un avion embarqué. La loi d'effort de catapultage est fixée forfaitairement et le calcul tient compte de l'application de la poussée moteur correspondant au plein gaz sec, ainsi qu'une loi de portance propre à l'avion.

Comme précédemment, le modèle comporte l'avion complet muni de ses 3 atterrisseurs. De plus, l'atterrisseur auxillaire est équipé de la barre de catapultage et du mécanisme qui en permet l'articulation (ensemble de biellettes, ressorts de rappel, vérin de manoeuvre).

A noter également que pour cette application, le réglage de l'amortisseur avant correspond à une configuration "train sauteur" par un dispositif contrôlant la détente de celui-ci lors de la restitution d'énergie en fin de catapultage.

Pour ce calcul, le pas de temps a été choisi constant, égal à 2 ms.

Au temps t = 0 de la simulation, la barre se désolidarise du sabot de catapultage, et l'amortisseur commence à se détendre.

Une vue générale de l'atterrisseur est donnée figure *3.a*. Le modèle en filaire correspondant est donné figure *3.b*.

Les figures *3.c* et *3.d* décrivent le mouvement de la barre de catapultage et de son mécanisme associé, lors de la détente de l'amortisseur.

On constate que la barre commence par s'incliner vers le bas relativement à l'atterrisseur sous l'effet des charges d'inertie, puis va rechercher sa position d'équilibre sous l'action de ressorts de rappel. Au temps t = 0,42 secondes, la barre est en butée, dans une position sensiblement perpendiculaire à l'axe atterrisseur.

Par ailleurs, dans la même approche et à partir d'une modélisation sensiblement identique, cet outil nous a permis de simuler numériquement la phase entière de catapultage, depuis la mise en pression de la catapulte et la rupture du "hold-back", jusqu'au décollage en sortie de pont. Cette simulation a permis la mise au point et l'optimisation des paramètres internes d'un atterrisseur de type "train sauteur" (jump-strut).

3.4 Simulation du relevage d'un atterrisseur

L'exemple retenu est celui de l'atterrisseur avant de type direct étudié au paragraphe 3.1 dont on étudie ici le relevage dynamique complet, depuis la position verrouillée basse jusqu'à la position verrouillée haute.

La modélisation prend en compte :

- La description complète des différents constituants de l'atterrisseur : caisson, tige coulissante, tube tournant, contrefiches principale et secondaire avec leurs ressorts de rappel.
- Les efforts non linéaires engendrés par les vérins de manoeuvre et de déverrouillage, calculés par intégration des équations régissent les pressions des 2 chambres de chaque vérin. Un élément spécifique "vérin hydraulique" a été construit et pour lequel on a modélisé une loi de "dash-pot".
- Les butées en translation et en rotation.

La figure *4.a* présente une vue du modèle en position verrouillée train bas.

La pression du circuit hydraulique est initialisée à la pression de bâche de 10 bars.

Au temps t = 0 de la simulation, les deux vérins sont alimentés simultanément par une pression de 206 bars agissant sur leur chambre 2 (rétraction).

Les figures *4.b* et *4.c* présentent différentes positions intermédiaires lors de la manoeuvre de relevage, la position train bas étant représentée en traits pointillés.

A noter que le pas de temps choisi pour la simulation est évolutif : il passe de 5 millisecondes en début de manoeuvre pour atteindre 250 millisecondes dans une phase où les gradients sont moins prononcés.

La figure *4.d* présente l'évolution des pressions dans les chambres 1 et 2 du vérin de manoeuvre.

Les gradients importants observés au temps t = 4,2 secondes proviennent de l'activation d'un dash-pot en fin de course du vérin, lorsque la distance entre les points d'attache est réduite à 602 mm.

Au temps t = 6,3 secondes, la contrefiche brisoise est alignée et verrouillée par une butée en rotation. Les pressions se stabilisent à 206 bars pour la chambre alimentée et à 10 bars (pression de bâche) pour l'autre chambre.

La figure *4.d* présente également la loi d'effort développé par le vérin de manoeuvre.

La figure *4.e* présente la variation de longueur du vérin de déverrouillage. Le déverrouillage est initialisé par la rétraction de ce vérin, puis subit une loi cinématique non linéaire.

Enfin la figure *4.e* révèle également la loi d'effort développé par le vérin de déverrouillage. La courbe présente plusieurs paliers s'amorçant à t = 0,9 seconde, t = 2,4 secondes et t = 4 secondes. Ils correspondent au fait que le vérin est tantôt moteur, tantôt résistant et de manière à tenir compte des effets de frottement, la force résultante est pondérée d'un coefficient λ, valant 0,9 dans le cas moteur et 1,1 dans le cas résistant.

Ces résultats ont corrélé de façon très satisfaisante les mesures effectuées sur bâti de relevage, puis lors des essais en vol.

3.5 Simulation du roulage d'un avion sur piste réparée ou sommairement aménagée

Comme indiqué précédemment, un tel outil de simulation s'avère indispensable pour l'étude et l'optimisation de suspensions améliorées, qu'elles soient à contrôle actif ou adaptatives ou bien encore du type "jump-strut".

Nous présentons à titre indicatif, figures *5.a* et *5.b*, les efforts au sol issus de simulation de roulage d'un avion de combat sur une piste comportant 3 bosses successives (réparations sommaires type AM2-MAT) de 114 mm de hauteur, puis sur une piste sommairement aménagée, dont le profil est en (1-cos) conformément à la norme américaine MIL-A-8863B.

La figure *5.c* précise ces profils de piste. Le modèle est constitué de l'avion complet avec ses 3 atterrisseurs dotés d'amortisseurs adaptés à cette configuration "roulage sur mauvais terrain".

3.6 Simulation du comportement au shimmy d'un atterrisseur avant d'un avion de type AIRBUS

Modélisation par éléments finis

Chacune des parties articulées constituant le train est modélisée dans un superélément dont le nombre d'éléments internes varie entre 5 et 65 dans le modèle décrit en figure 6.a.

Le modèle présenté comporte 770 ddl et inclut des vérins amortisseurs non linéaires ($F = kV^2$) ainsi que de multiples liaisons rotules ou charnières. Le pas de temps adopté pour les simulations présentées est de 5 ms.

- *Simulation d'un balourd*

  Les figures 6.b, 6.c et 6.d montrent la réponse angulaire de l'atterrisseur soumis à l'effet d'un balourd.

  La figure 6.b décrit le comportement de l'atterrisseur soumis à une fréquence d'excitation correspondant à sa fréquence propre en torsion. Dans ce cas, on considère le cas extrême où l'avion a perdu la totalité du fluide hydraulique assurant l'amortissement anti-shimmy (K = 0).

  La figure 6.c reprend le cas précédent pour un amortissement donné, non nul (K = 100 000 SI). On constate l'établissement rapide d'une solution stationnaire (en 0,5 seconde, la solution se stabilise à 0,8°).

  Enfin, la figure 6.d illustre l'effet d'une variation de vitesse. Dans le cas d'une augmentation de 25 % de la vitesse et bien que l'effort de balourd augmente de 50 %, l'amplitude de la réponse diminue de 50 %.

- *Simulation d'un choc*

  La sollicitation appliquée dans la figure 6.e est la représentation d'un choc appliqué sur l'essieu. On peut noter le très faible niveau de la réponse, dû à l'action quasi instantanée des vérins amortisseurs dans le cas d'une action brève.

4 - CONCLUSION

Les exemples d'application cités précédemment ont présenté l'outil de simulation numérique et la méthodologie employée chez Messier-Bugatti pour la détermination rationnelle des performances dynamiques d'un train d'atterrissage.

Malgré la complexité des problèmes à résoudre provenant de la non-linéarité du système d'équations (laminage d'huile, frottements internes amortisseurs,...) ce logiciel permet de procéder à un très grand nombre de simulations dynamiques et cinématiques, à un coût de calcul raisonnable et dans des délais compatibles avec la phase de projet de tout nouvel atterrisseur.

Par ailleurs, cet outil s'avère indispensable pour l'étude de suspensions à technologie avancée, telles que suspensions semi-actives, compte-tenu du très grand nombre de paramètres à balayer afin d'évaluer efficacement le système.

INDEX BIBLIOGRAPHIQUE

réf [1] : "Time integration of the equations of motion in mechanism analysis"
A. CARDONA et M. GERADIN
LTAS - Dynamique des constructions mécaniques - Université de LIEGE - rue Ernest Solvay, 21 - B4000 LIEGE - BELGIUM

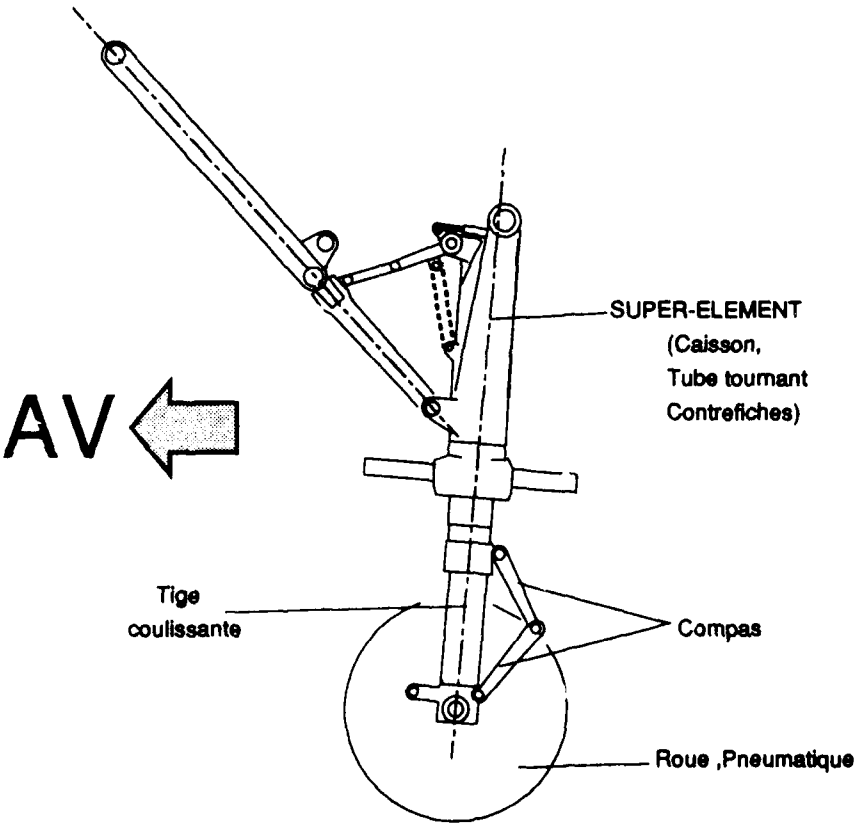

Figure 1a — Simulation d'impact à l'atterrissage vue du modèle en position tout détendu

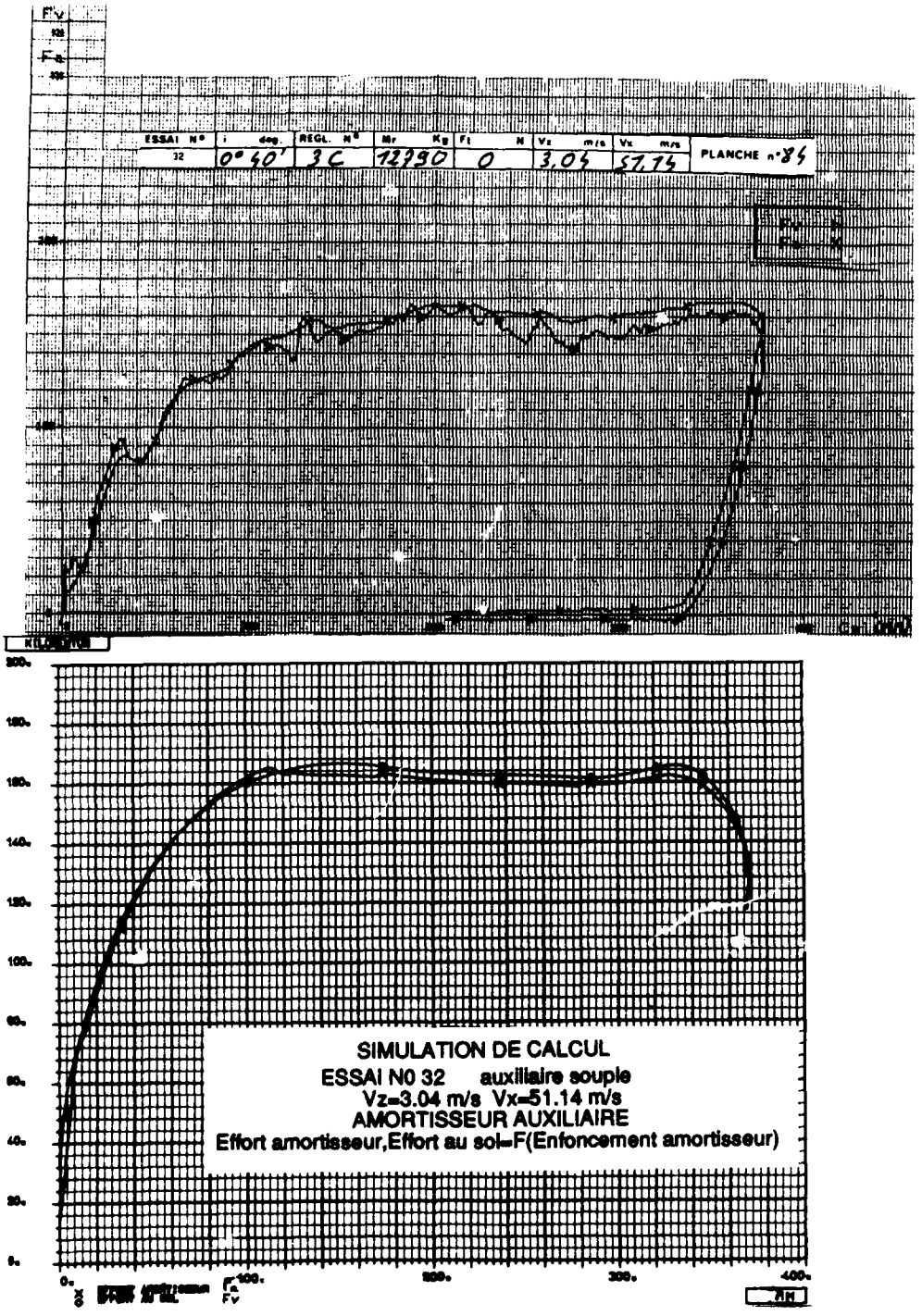

Figure 1b — Simulation d'impact à l'atterrissage comparaison essai — calcul

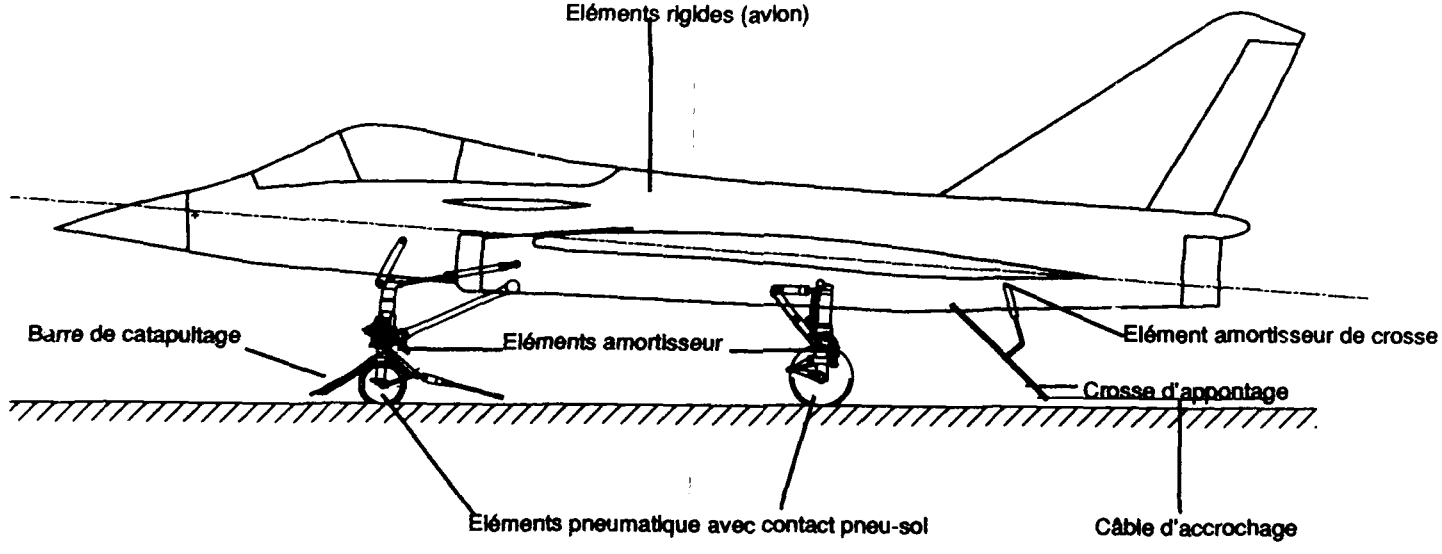

Figure 2a — Simulation d'appontage schéma du modèle

ACCROCHAGE EN VOL AVION EMBARQUE
ASSIETTE TETAO _ VITESSE DE CHUTE VZO _ VITESSE HORIZONTALE VXO

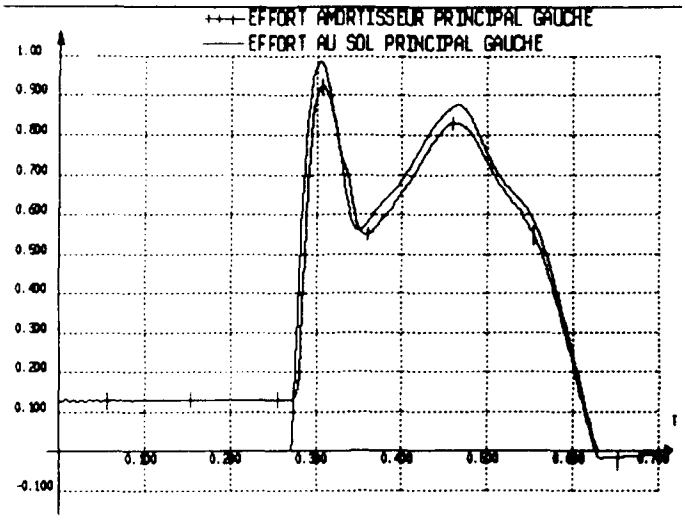

Figure 2b — Simulation d'appontage résultats atterrisseur principal

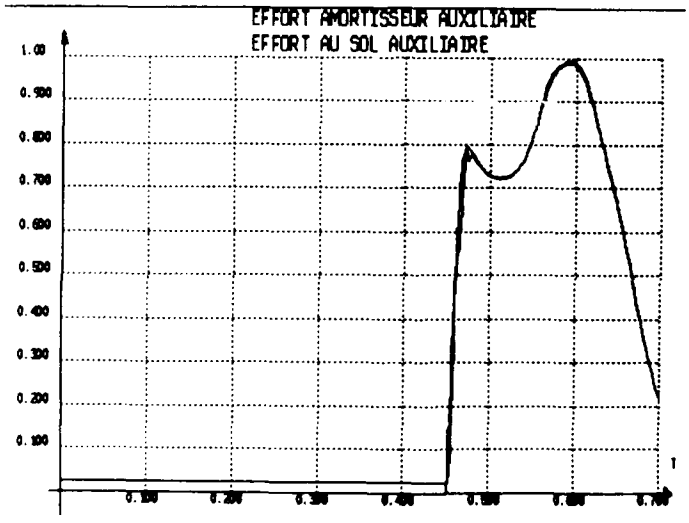

Figure 2c — Résultats atterrisseur auxiliaire

ACCROCHAGE EN VOL AVION EMBARQUE
ASSIETTE TETA0 _ VITESSE DE CHUTE VZ0 _ VITESSE HORIZONTALE VX0

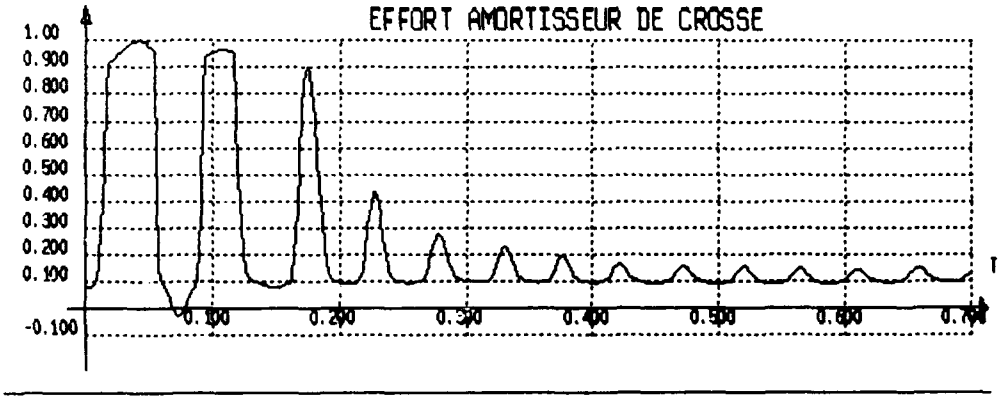

ACCROCHAGE EN VOL AVION EMBARQUE
ASSIETTE TETA0 _ VITESSE DE CHUTE VZ0 _ VITESSE HORIZONTALE VX0

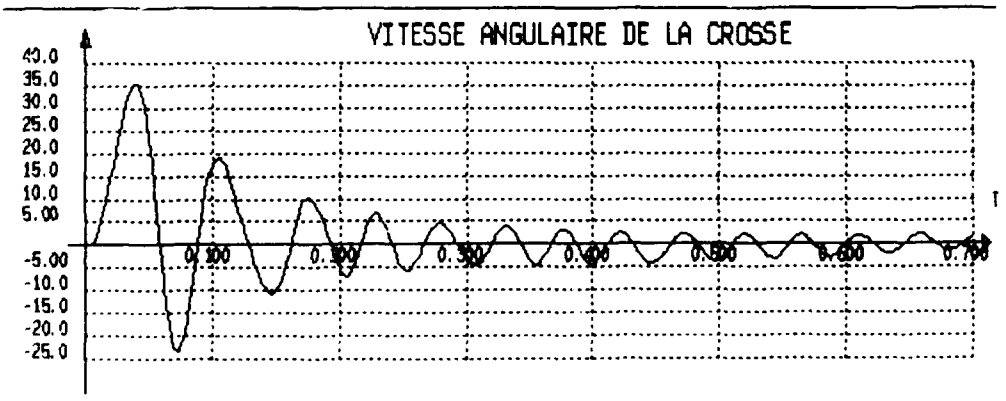

Figure 24 — Simulation d'appontage résultats amortisseur de crosse

ACCROCHAGE EN VOL AVION EMBARQUE

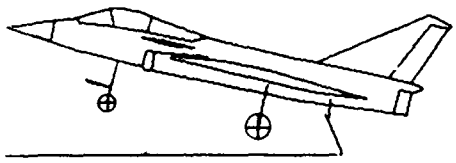

T = 0 s : Accrochage dans les brins

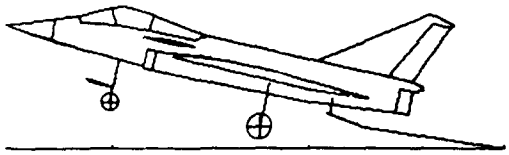

T = 0.1 s : Allongement du brin avant impact

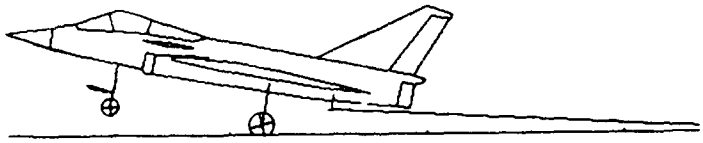

T = 0.3 s : Impact sur les trains principaux : rotation des roues

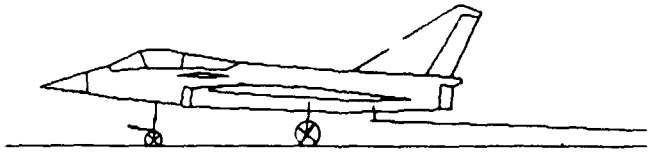

T = 0.5 s : Impact sur le train auxiliaire : rotation des roues

Figure 2e — Simulation d'appontage visualisation du modèle

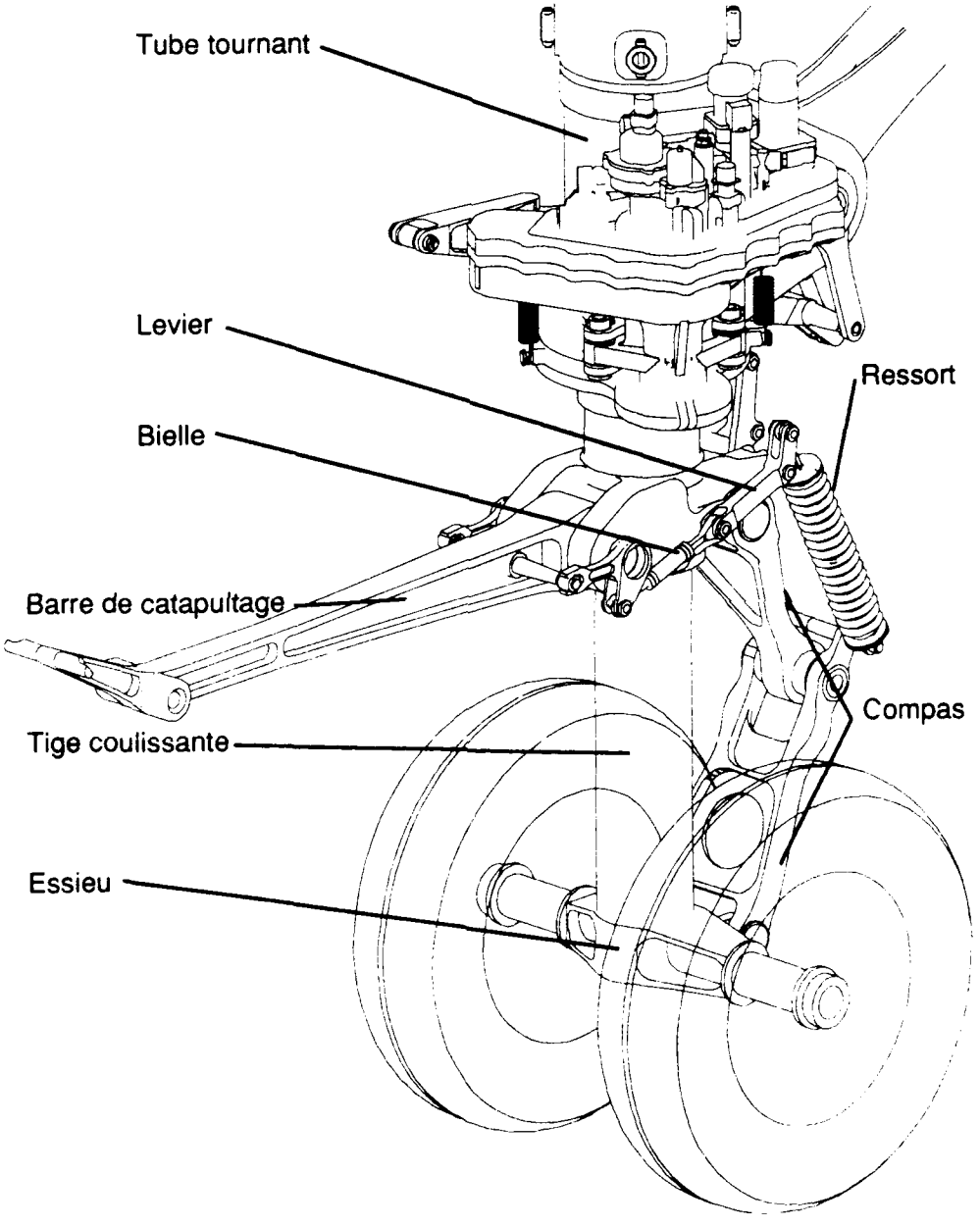

Figure 3a — Simulation de catapultage vue générale de l'atterrisseur

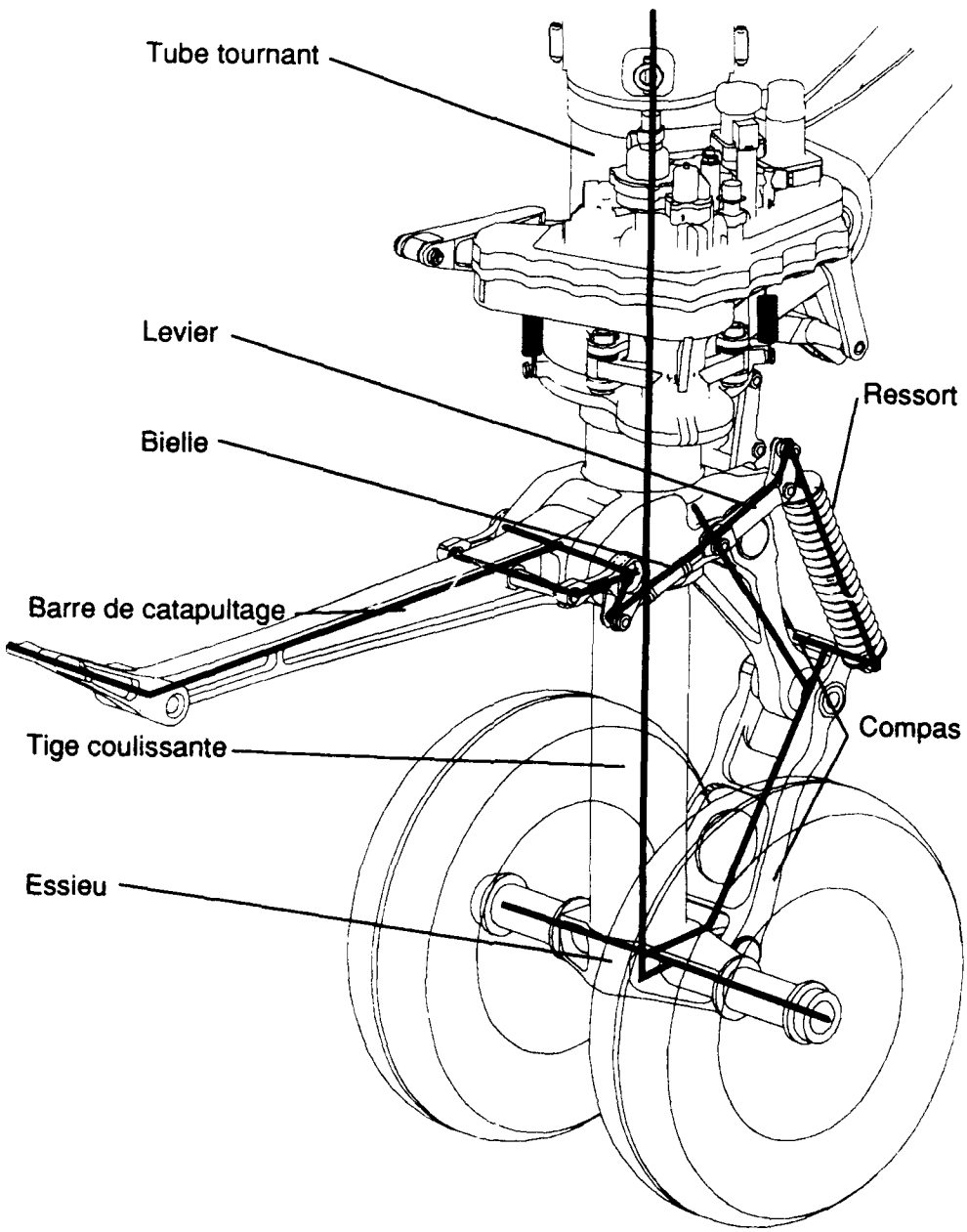

Figure 3b — Simulation de catapultage vue générale de l'atterrisseur

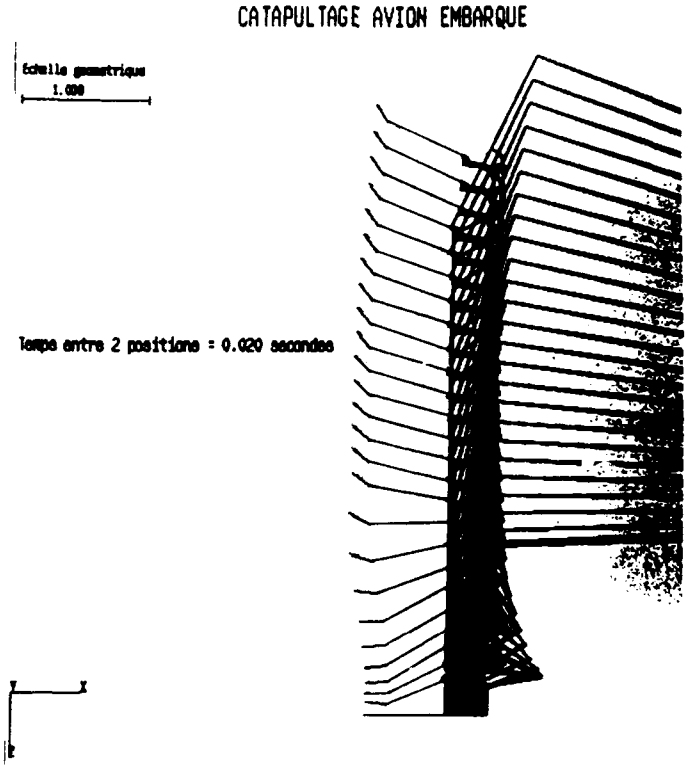

Figure 3c — Simulation de catapultage
Mouvement de la barre de catapultage lors de la détente de l'atterrisseur

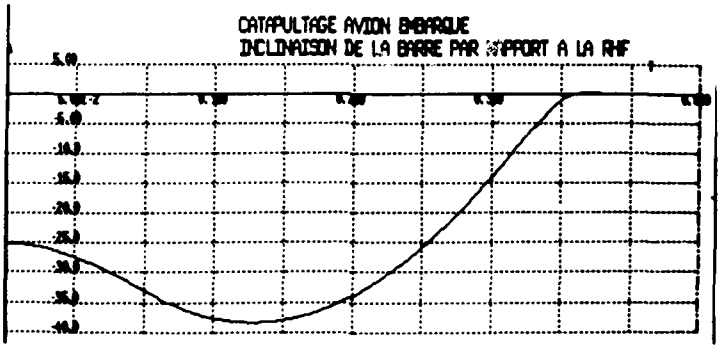

Figure 3d — Catapultage avion embarqué inclinaison de la barre par rapport à la RHF

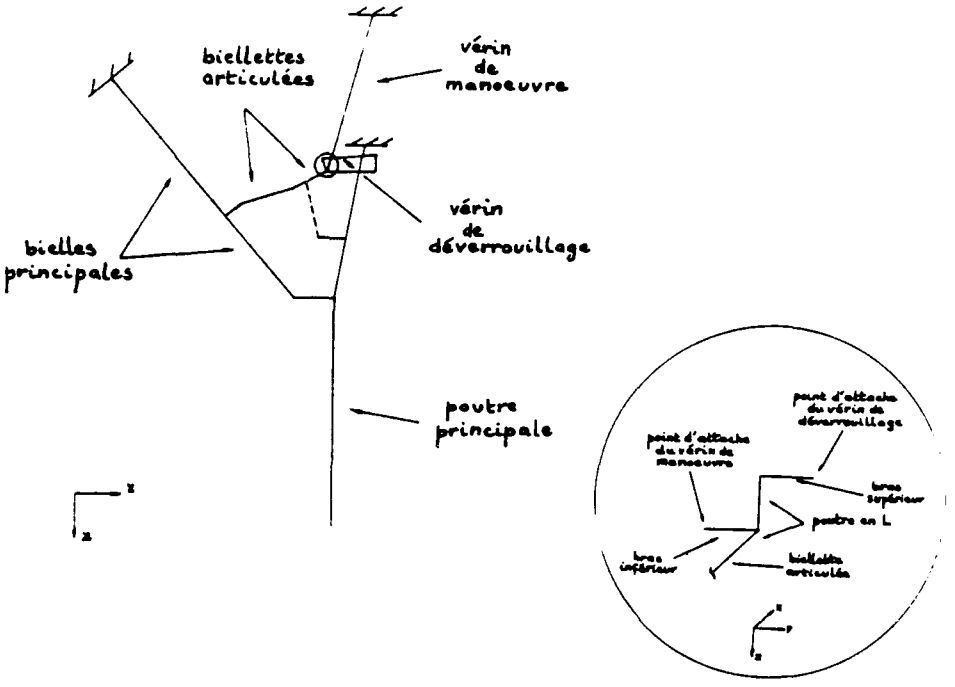

Figure 4a — Simulation de relevage d'un atterrisseur vue du modèle en position train bas

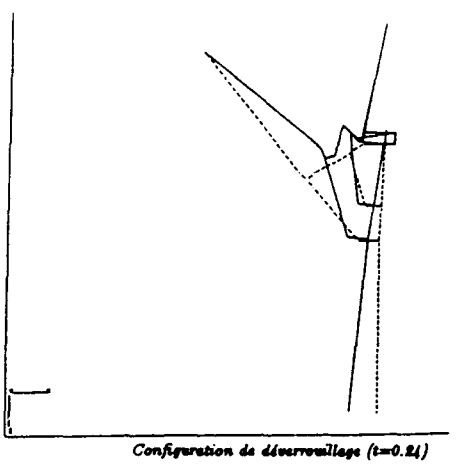

Configuration de déverrouillage (t=0.24)

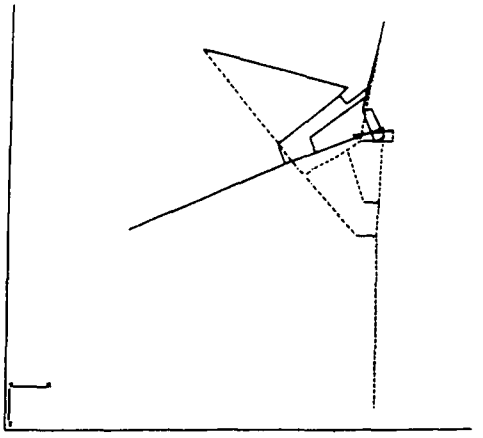

Configuration intermédiaire (t=3.66)

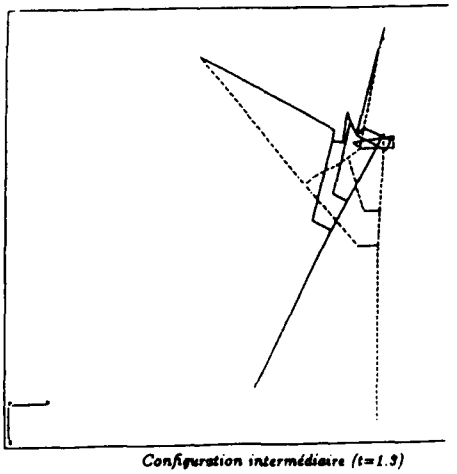

Configuration intermédiaire (t=1.9)

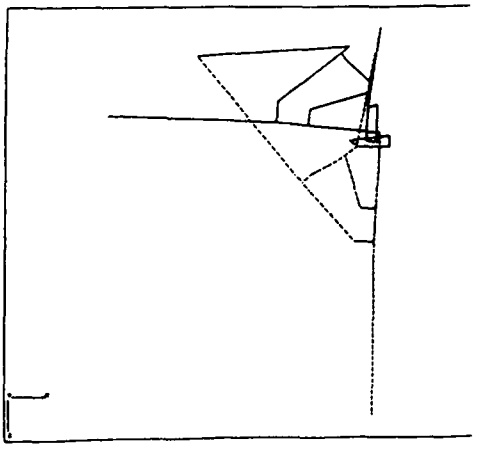

Configuration finale(t=7.)

Figure 4b

Figure 4c

Simulation du relevage d'un atterrisseur

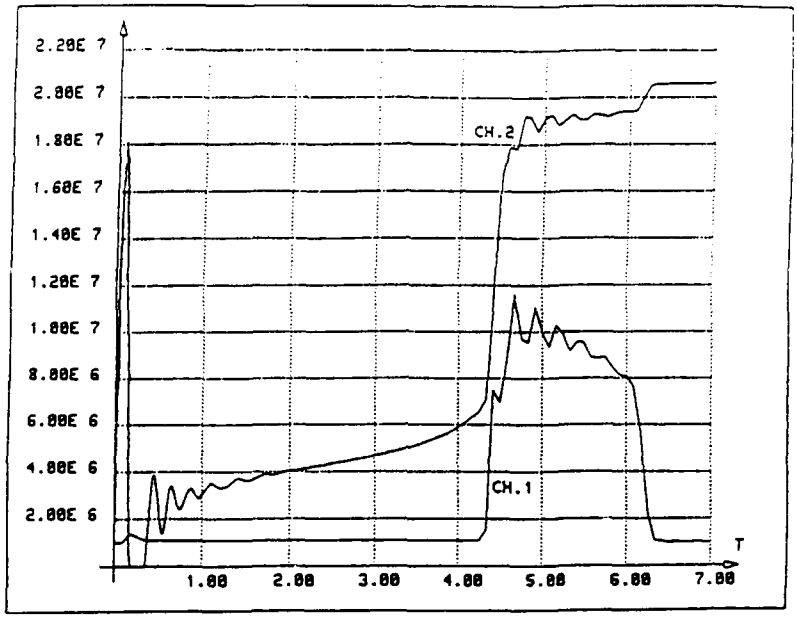

Evolution des pressions dans le vérin principal

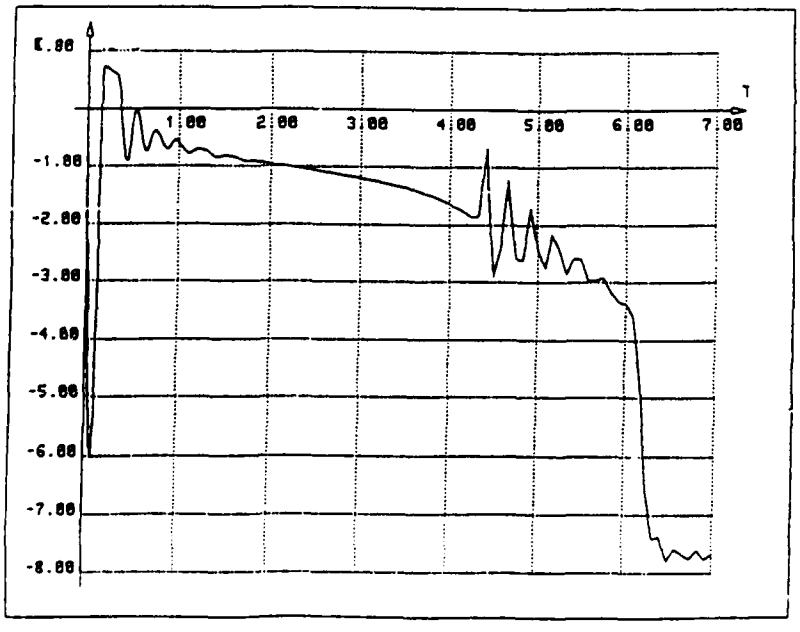

effort développé par le vérin principal

Figure 4d — Simulation du relevage d'un atterrisseur

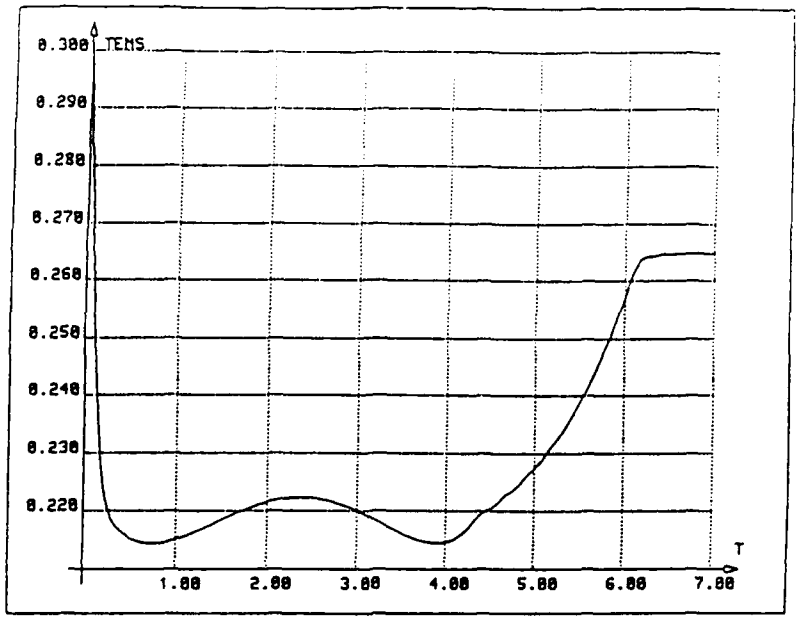

Variation de longueur du vérin secondaire

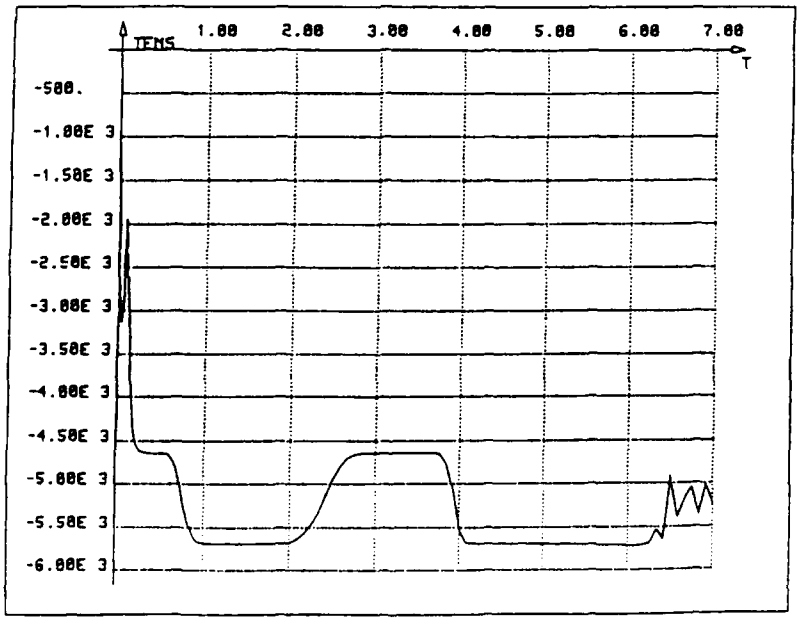

Force produite par le vérin secondaire

Figure 4e — Simulation du relevage d'un atterrisseur

COMPARAISON AMORTISSEUR SERIE ET ADAPTATIF - AVION MILITAIRE

TAXIAGE MISSION STRATEGIQUE

PISTE REPAREE 3% H=114 mm L=12.50 m S= 10 m

TRAIN AUXILIAIRE

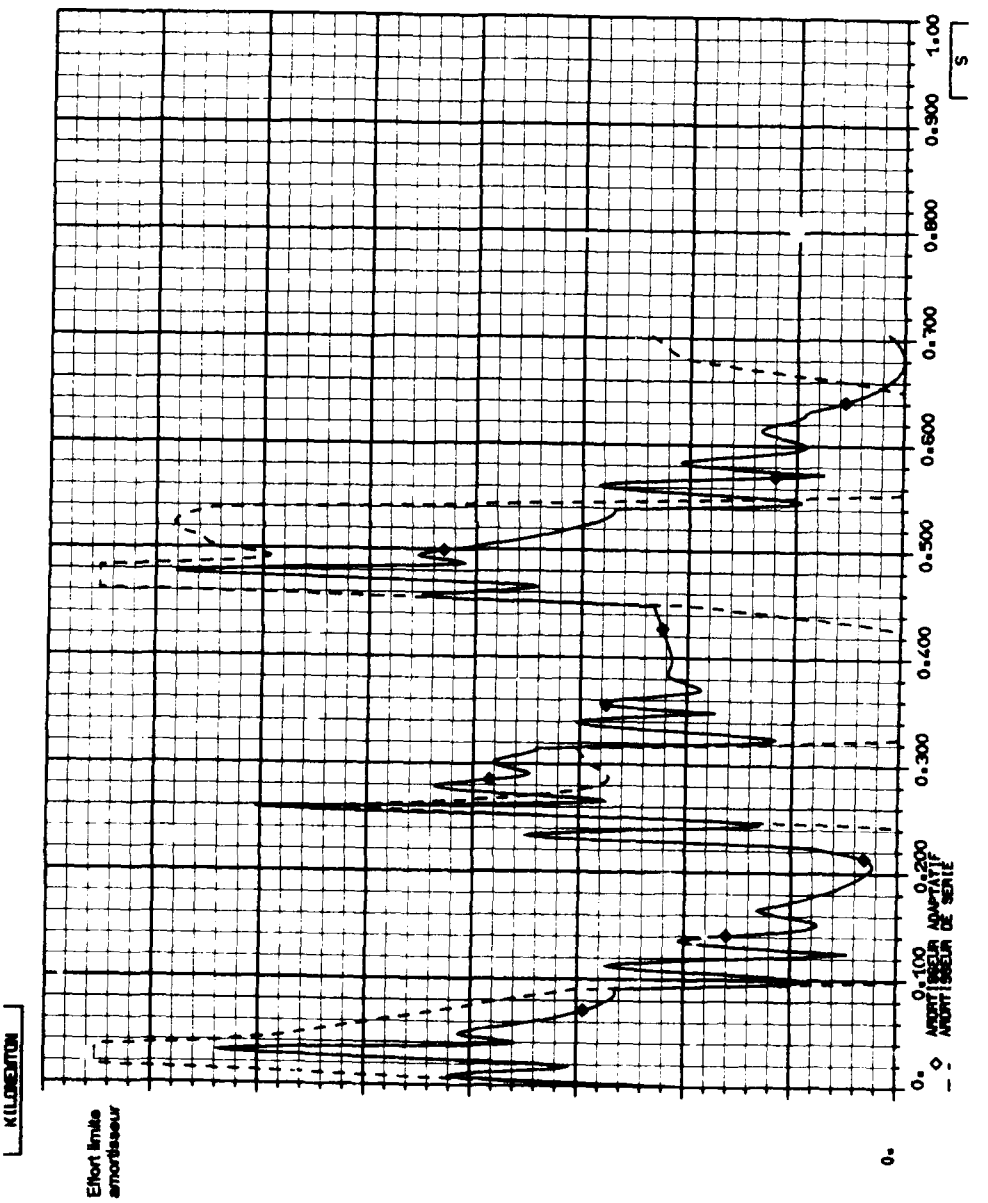

Figure 5a — Simulation de roulage sur piste sommairement réparée

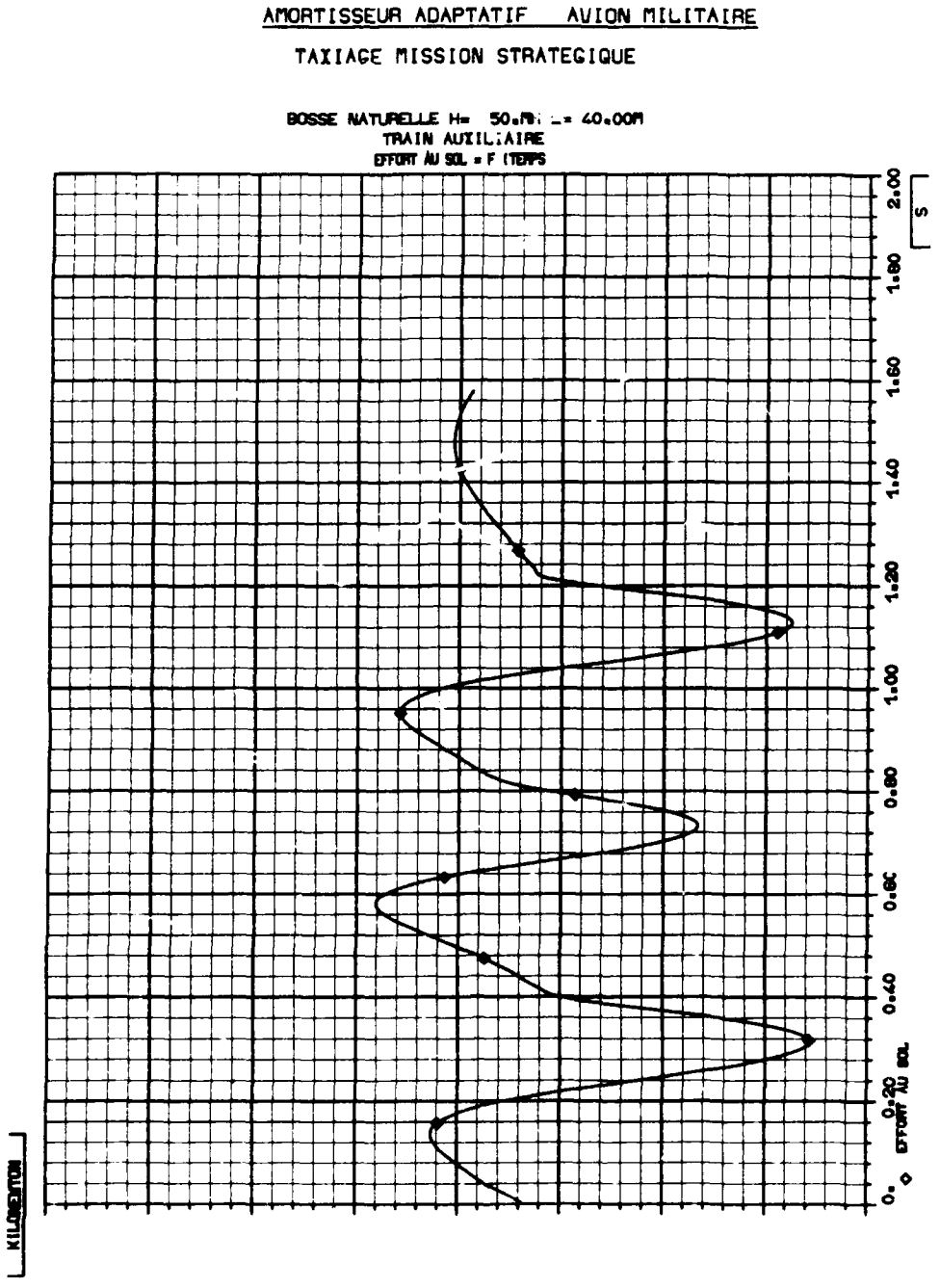

Figure 5b — Simulation de roulage sur piste sommairement aménagée

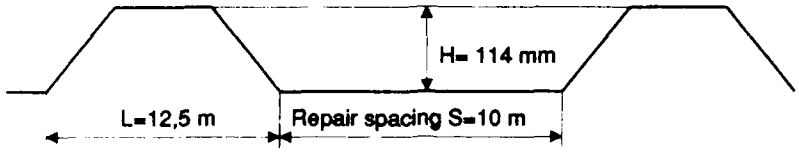

PISTE SOMMAIREMENT REPAREE (3 BOSSES CONSECUTIVES)

$$Z=\frac{H}{2}(1-\cos\frac{2\pi x}{L})$$

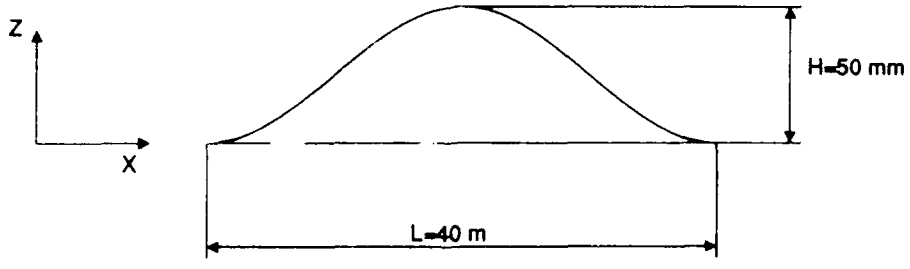

PISTE SOMMAIREMENT AMENAGEE (3 BOSSES CONSECUTIVES)

Figure 5c – Simulation de roulage profils de pistes considérés

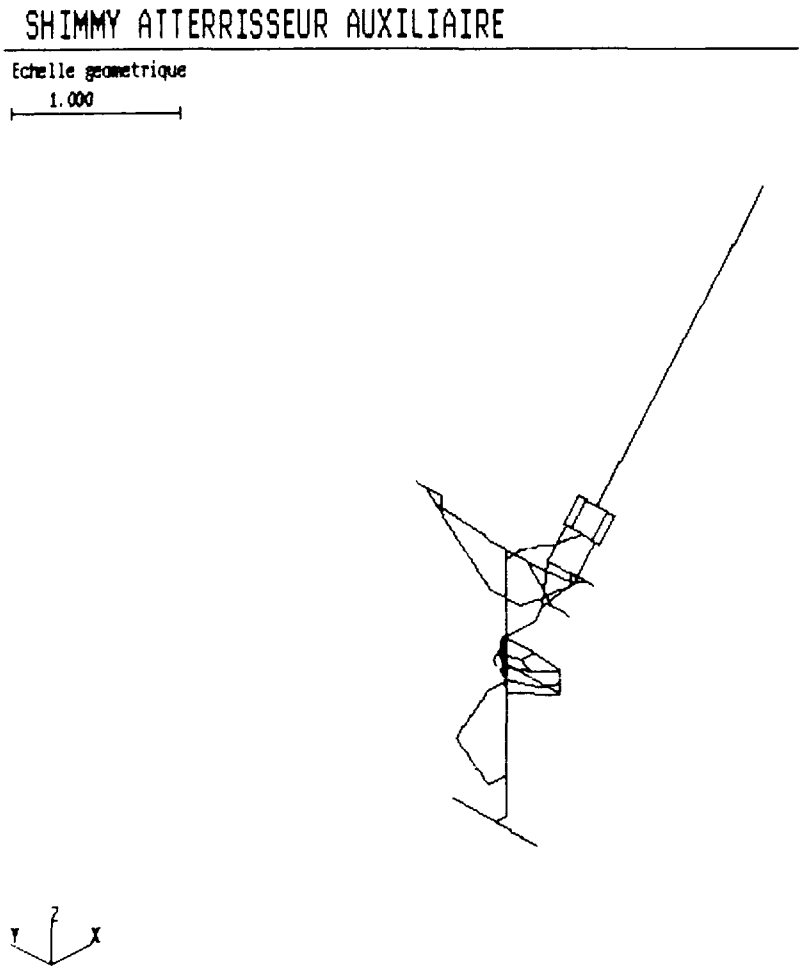
SHIMMY ATTERRISSEUR AUXILIAIRE
Echelle geometrique
1.000
Z
Y
X

Figure 6a

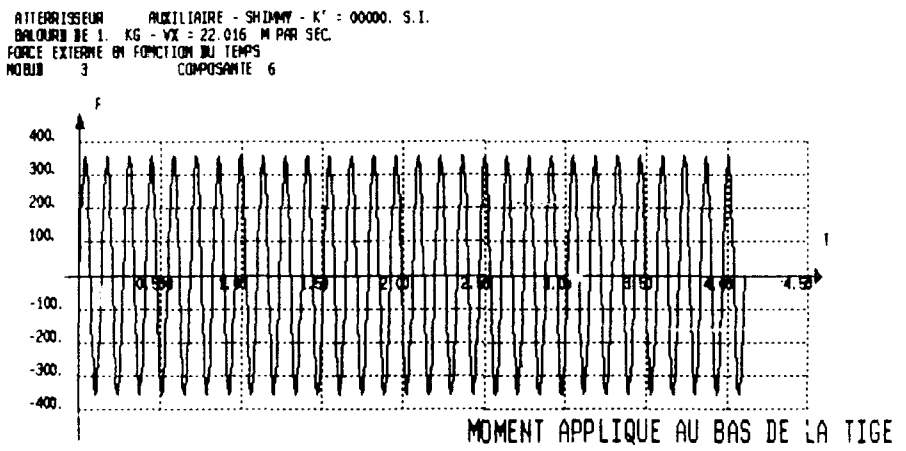
ATTERRISSEUR AUXILIAIRE - SHIMMY - K' = 00000. S.I.
BALOURD DE 1. KG - VX = 22.016 M PAR SEC.
FORCE EXTERNE EN FONCTION DU TEMPS
NOEUD 3 COMPOSANTE 6
F
400.
300.
200.
100.
-100.
-200.
-300.
-400.
T
0.500
1.00
1.50
2.00
2.50
3.00
3.50
4.00
4.50
MOMENT APPLIQUE AU BAS DE LA TIGE

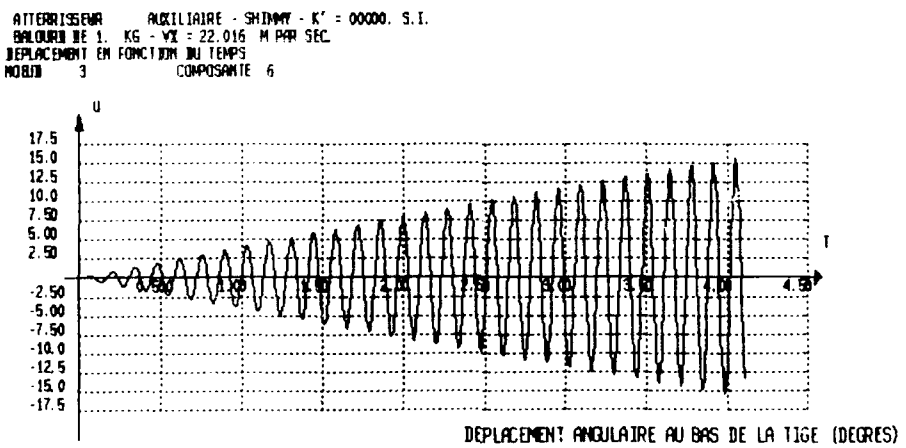
ATTERRISSEUR AUXILIAIRE - SHIMMY - K' = 00000. S.I.
BALOURD DE 1. KG - VX = 22.016 M PAR SEC.
DEPLACEMENT EN FONCTION DU TEMPS
NOEUD 3 COMPOSANTE 6
U
17.5
15.0
12.5
10.0
7.50
5.00
2.50
-2.50
-5.00
-7.50
-10.0
-12.5
-15.0
-17.5
T
0.500
1.00
1.50
2.00
2.50
3.00
3.50
4.00
4.50
DEPLACEMENT ANGULAIRE AU BAS DE LA TIGE (DEGRES)

Figure 6b

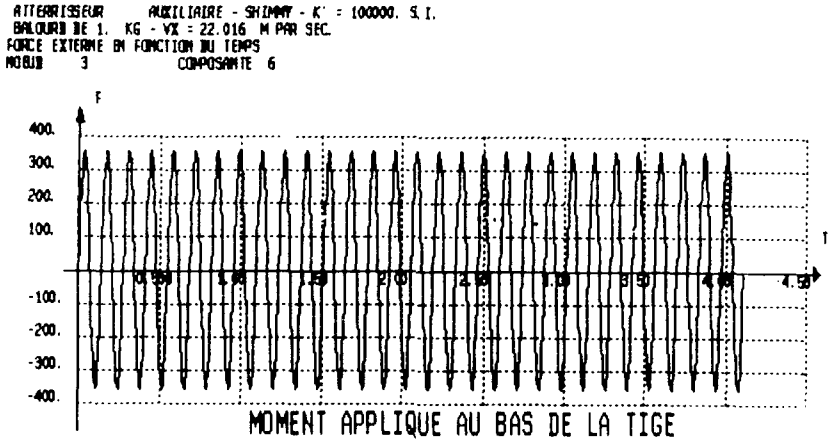
ATTERRISSEUR AUXILIAIRE - SHIMMY - K' = 100000. S.I.
BALOURD DE 1. KG - VX = 22.016 M PAR SEC.
FORCE EXTERNE EN FONCTION DU TEMPS
NOEUD 3 COMPOSANTE 6
F
400.
300.
200.
100.
-100.
-200.
-300.
-400.
T
MOMENT APPLIQUE AU BAS DE LA TIGE

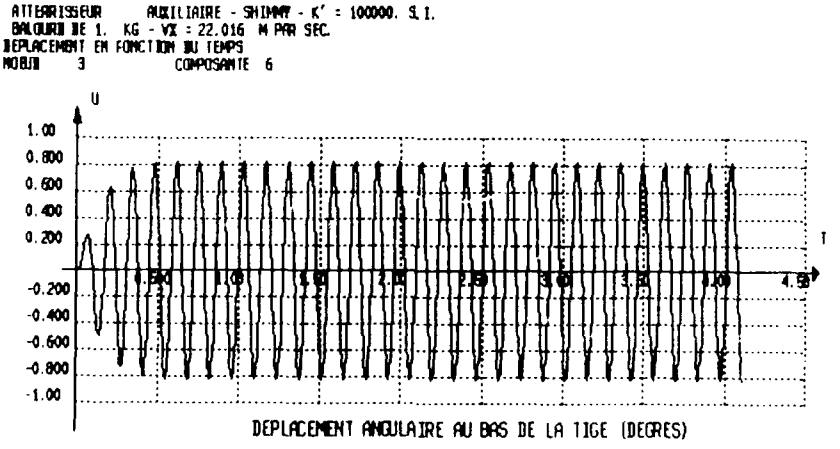
ATTERRISSEUR AUXILIAIRE - SHIMMY - K' = 100000. S.I.
BALOURD DE 1. KG - VX = 22.016 M PAR SEC.
DEPLACEMENT EN FONCTION DU TEMPS
NOEUD 3 COMPOSANTE 6
U
1.00
0.800
0.600
0.400
0.200
-0.200
-0.400
-0.600
-0.800
-1.00
T
DEPLACEMENT ANGULAIRE AU BAS DE LA TIGE (DEGRES)

Figure 6c

ATTERRISSEUR AUXILIAIRE - SHIMMY - K' = 100000. S.I.
BALOURD DE 1. KG - VX = 27.143 M PAR SEC.
FORCE EXTERNE EN FONCTION DU TEMPS
NOEUD 3 COMPOSANTE 6

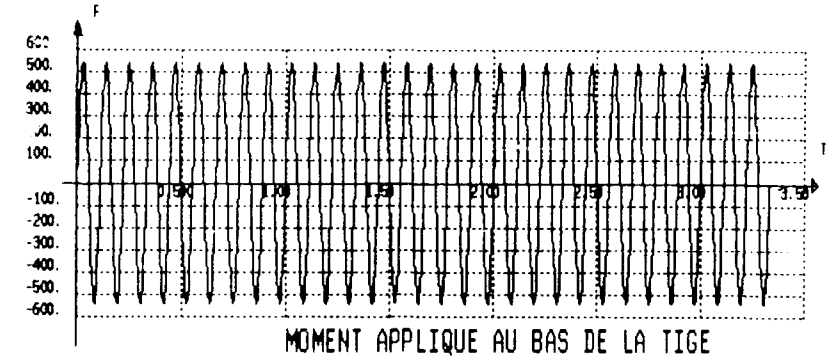

ATTERRISSEUR AUXILIAIRE - SHIMMY - K' = 100000. S.I.
BALOURD DE 1. KG - VX = 27.143 M PAR SEC.
DEPLACEMENT EN FONCTION DU TEMPS
NOEUD 3 COMPOSANTE 6

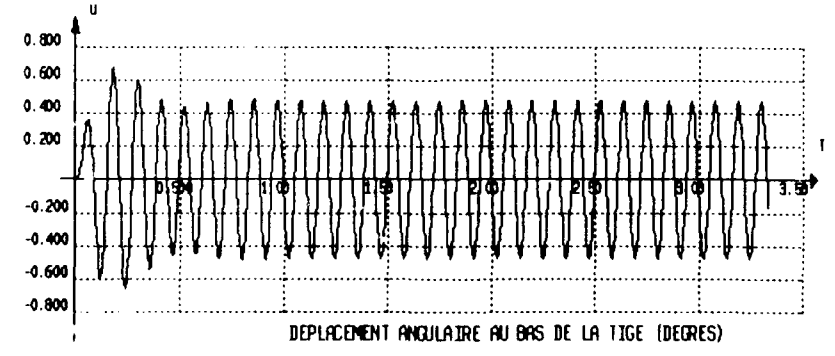

Figure 6d

ATTERRISSEUR AUXILIAIRE - CHOC - K' = 250000. S.I.
COUPLE IMPOSE DE 1.00978803 M.M EN BAS DE TIGE
FORCE EXTERNE EN FONCTION DU TEMPS
NOEUD 16 COMPOSANTE 6

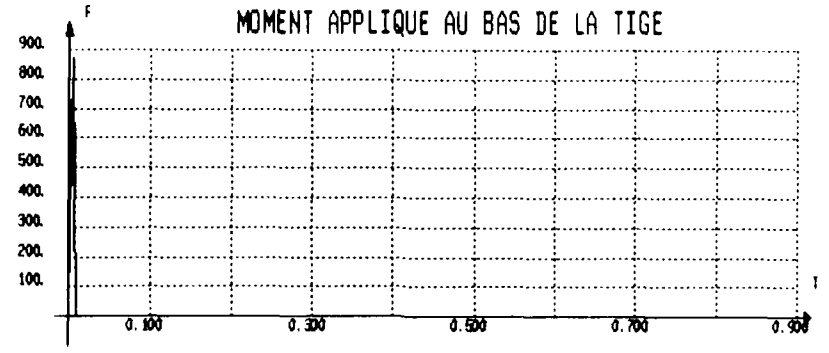

ATTERRISSEUR AUXILIAIRE - CHOC - K' = 250000. S.I.
COUPLE IMPOSE DE 1.00978803 M.M EN BAS DE TIGE
DEPLACEMENT EN FONCTION DU TEMPS
NOEUD 16 COMPOSANTE 6

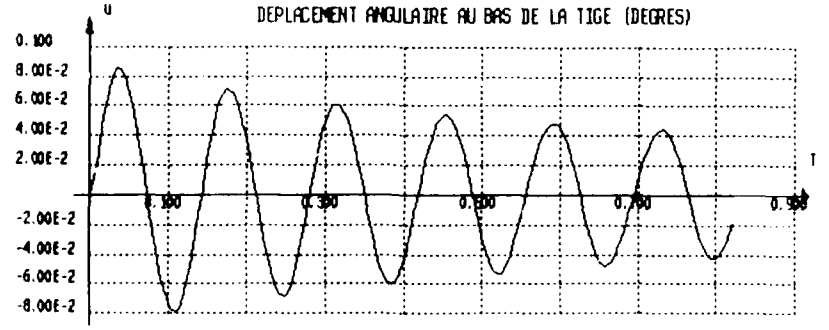

Figure 6e

Calcul des interactions entre avion et trains d'atterrissage

par

Yves MARTIN-SIEGFRIED

DASSAULT AVIATION

78, quai MARCEL DASSAULT - 92214 SAINT-CLOUD - FRANCE

ABSTRACT:

We present the present state-of-the-art for the calculation of the ground dynamic response of the aircraft.

The analyse tool described below forms a special branch of the CATIA-ELFINI system, the general purpose programme for CAD and structural analysis of DASSAULT.

The system handles a large set of problems for ground dynamic response, as: landing impact, rough runway rolling and take off, catapulting and landing on carrier etc....

In these calculations, the structure is represented by a finite element model of the whole aircraft coupled with models of landing gears, aerodynamics, F.C.S., and other special systems (e.g. catapult).

The time integration is performed via implicite finite differences scheme.

The method handles non linearities with three levels of condensation:

- one time before integration, condensation of linear parts of the frontier of non linear systems. It concerns mainly structure (dynamic condensation), aerodynamic coupling and FCS.

- At each time step linearisation of "smooth non linearities" (e.g. large rotations) and condensation of the problem for only "non linearzable" D.O.F. (as lamination).

- Resolution at each time step of this few number of "hard" non linear equations by a special B.F.G.S. method.

With these organization computer time gives the possibilities to sweep wide number of configurations (e.g. for statistical approach of landing load).

We present some significant types of simulation stemmed from analyses of Mirage III, Super-Etendard, Mirage 2000 and Rafale.

1- INTRODUCTION:

La réponse dynamique de l'avion sur ses trains d'atterrissage est un phénomène complexe à simuler du fait du caractère aléatoire de nombreux paramètres comme, par exemple, les conditions initiales, les lois de frottement, le profil de piste etc...

Une autre complexité résulte de la présence de nombreuses non-linéarités issues des grandes rotations, du contact avec le sol et des comportements notamment des amortisseurs.

Les performances d'un outil de calcul doivent donc résider dans un traitement très efficace de ces non-linéarités pour ne pas pénaliser les temps de calcul à cause des nombreuses configurations de paramètres qu'il faut simuler.

Nous présentons les moyens spécifiques de calcul, le programme FELAND, développés par DASSAULT AVIATION dans le cadre de son logiciel de CAO et d'analyse des structures CATIA/ELFINI. Ce programme est développé depuis une vingtaine d'années [1].

L'accent est porté sur les algorithmes qui contribuent de façon majeure aux performances de FELAND et sur la façon efficace d'intégrer dans le programme le modèle de calcul des efforts généraux de l'avion grâce aux fonctionnalités de ELFINI notamment au niveau de la condensation dynamique.

Nous donnons quelques exemples d'application de FELAND au MIRAGE III, au SUPER-ETENDARD, au MIRAGE 2000 et au RAFALE.

2- DESCRIPTION GENERALE DE FELAND:

FELAND est le module de ELFINI qui calcule la réponse dynamique tridimensionnelle de l'avion au sol selon l'organigramme présenté planche 1.

Il permet de répondre à tous les problèmes de roulage, de virage, de décollage, d'atterrissage et de freinage ainsi que les problèmes d'appontage et de catapultage des avions marins.

La description du mouvement de l'avion est constamment réactualisée dans le repère Galiléen confondu aux axes de l'avion.

L'avion est modélisé par éléments finis. Il s'agit en pratique du modèle de calcul des efforts généraux à plusieurs dizaines de milliers de degrés de liberté (D.D.L.). Le modèle du RAFALE est montré planche 2.

L'emploi des techniques de condensation permet de réduire le nombre de D.D.L. à quelques centaines ou quelques dizaines.

Les trains d'atterrissage et d'autres systèmes éventuels (crosse d'arrêt, catapulte, holdback etc..) sont discrétisés par méthode de Lagrange et couplés à l'avion. Le modèle couplé de la version marine du RAFALE au catapultage sur porte-avions est représenté planche 3.

La position initiale de l'avion au sol est réalisée automatiquement par calcul non-linéaire utilisant la boucle d'intégration dynamique sans les termes d'inertie.

L'intégration dynamique est menée par un schéma inconditionnellement stable. Les non-linéarités douces (les grandes rotations par exemple) sont linéarisées à chaque pas de temps autour de la position courante. Les non-linéarités aiguës (les amortisseurs) sont traitées exactement après condensation dans l'espace de ces seuls degrés de liberté non-linéaires.

Le programme prend en compte les ordres du pilote éventuellement filtrés par des commandes de vol électriques.

La mémorisation de la solution en base réduite à un instant sélectionné permet ultérieurement la reconstruction dans la base éléments finis de l'état de sollicitations de l'ensemble de la structure. Le choix des instants de sélections est fait à partir de l'analyse du suivi dans le temps de jauges témoin.

3- PRINCIPES THEORIQUES:

3-1- MODELISATION DE L'AVION:

3-1-1- Formulation dans la base éléments finis:

De façon classique les équations relatives à l'avion seul s'écrivent après discrétisation par éléments finis:

$$[M_a] \frac{d^2X_a}{dt^2} + [C_a] \frac{dX_a}{dt} + [K_a] X_a = F_a + F_{sys/avion}$$

relation dans laquelle:

$[M_a]$: est la matrice de masse
$[C_a]$: est la matrice d'amortissement
$[K_a]$: est la matrice de raideur
$F_{sys/avion}$: est l'action des systèmes sur l'avion
(trains d'atterrissage, crosse etc ...)
F_a : sont les autres forces extérieures
(poids, forces aérodynamiques, poussée moteurs etc...)

3-1-2- Technique de condensation:

On procède à une approximation des déplacements sur un nombre réduit de déformées fondamentales.

$$X_a = [\varphi_a] x$$

$[\varphi_a]$ sont des déformées modales ou sous charges statiques.

La base réduite est constituée en général à partir:

- des modes rigides et de quelques dizaines de modes souples de l'avion dans une configuration de base,

- de chargements unitaires aux points de couplage avec les systèmes,

- de chargements d'inertie en des points de masse de carburant et d'emports.

En pratique deux bases réduites sont constituées, l'une en configuration de base au décollage et l'autre à l'atterrissage.

Pour chacune de ces configurations sont construits le cas de masse de base et les cas de masse de carburant et d'emports qui par combinaison permettent des variations de masse et de centrage.

Le système d'équations s'écrit en base réduite:

$$[\ m_a\ ]\ \frac{d^2x}{dt^2} + [\ c_a\ ]\ \frac{dx}{dt} + [\ k_a\ ]\ x = f_a + f_{sys/avion}$$

avec :

$[\ m_a\ ] = [\ \varphi_a\ ]^T\ [\ M_a\ ]\ [\ \varphi_a\ ]$

$[\ k_a\ ] = [\ \varphi_a\ ]^T\ [\ K_a\ ]\ [\ \varphi_a\ ]$

$f_a = [\ \varphi_a\ ]^T\ F_a\ ;\ f_{sys/avion} = [\ \varphi_a\ ]_d^T\ F_{sys/avion}$

$[\ \varphi_a\ ]_d$ est la restriction de $[\ \varphi_a\ ]$ aux points de couplage de l'avion avec les systèmes

3-2- MODELISATION DES SYSTEMES:

Les systèmes sont discrétisés par la méthode de Lagrange selon la description détaillée dans la référence [1].

$$[\ M_s\ ]\frac{d^2q}{dt^2} + [\ C_s\ ]\frac{dq}{dt} + [\ K_s\ ]q = f_s + f_{am} + f_{avion/sys}$$

avec:

f_{am} : non-linéarités aiguës(forces de laminage des amortisseurs)

3-3- COUPLAGE:

Les degrés q sont décomposés selon qu'ils dépendent ou non des degrés avion x:

$$q = \begin{vmatrix} q_i \\ q_d \end{vmatrix}$$

q_d : D.D.L. dépendants de x ; $q_d = [\frac{\partial q_d}{\partial x}]\ x$

q_i : D.D.L. indépendants de x

Par ailleurs:

$$f_{sys/avion} = - [\ \frac{\partial q_d}{\partial x}\ ]^T\ f_{avion/sys}$$

Deux variantes de couplage sont possibles:

- <u>Couplage en raideur:</u>

En éliminant q_d, les équations de l'avion et des systèmes sont combinées:

$$[\ M_k\ ]\frac{d^2Y}{dt^2} + [\ C_k\ ]\frac{dY}{dt} + [\ K_k]Y = f_a + [\frac{\partial q_d}{\partial x}]^T\ (f_s + f_{am})$$

avec $Y = \left|\begin{matrix} x \\ q_i \end{matrix}\right|$

- <u>Couplage en flexibilité:</u>

Les équations résultant de l'application du schéma d'intégration sont de la forme:

$$[\ K_{adyn}\ ]x = f_{adyn} + f_a + f_{sys/avion}$$

On les condense sur les degrés de couplage q_d :

$$q_d = [\ G\ ]([\frac{\partial q_d}{\partial x}]\ (f_{adyn} + f_a) - f_{avion/sys})$$

avec $[\ G\ ] = [\frac{\partial q_d}{\partial x}]\ [\ K_{adyn}\ ]^{-1}\ [\frac{\partial q_d}{\partial x}]^T$

On élimine $f_{avion/sys}$:

$$[\ M_f\ ]\frac{d^2q}{dt^2} + [\ C_f\ ]\frac{dq}{dt} + [\ K_f\ ]q = f_s + f_{am} + [\ G\ ]\ [\frac{\partial q_d}{\partial x}]\ (f_{adyn} + f_a)$$

3-4- INTEGRATION:

Le système d'équations à intégrer est du second degré:

$$[M_k] \frac{d^2Y}{dt^2} + [C_k] \frac{dY}{dt} + [K_k] Y = F$$

L'interpolation dans le temps de Y est faite en 3 ou 4 points au moyen de fonctions N_i du second ordre:

$$Y = N_i \; Y_i$$

L'intégration sur la période de temps d'interpolation est faite par méthode des résidus pondérés [2]:

$$\int W([M_k] Y_i \frac{d^2N_i}{dt^2} + [C_k] Y_i \frac{dN_i}{dt} + [K_k] Y_i N_i)dt = 0$$

En pratique nous utilisons la méthode de Newmark en limite de stabilité.

3-5- RESOLUTION EXACTE DES NON-LINEARITE AIGUES:

Les équations qui résultent de l'application du schéma d'intégration dans le temps sont de la forme:

$$[K_{dyn}] \Delta Y = F - [V_{am}] F_{am}$$

avec:

$[K_{dyn}]$: matrice dynamique tangente

ΔY : déplacement incrémental entre t-Δt and t

$F = F_0 + F_{dyn}$

F_0 : forces extérieures autres que les forces amortisseurs

F_{dyn} : termes d'inertie résultant du schéma d'intégration dans le temps

$[V_{am}]$: $\Delta ENF_{am} = [V_{am}]^T \Delta Y$

F_{am}, ENF_{am} : force et course amortisseur

Pseudo-potentiel des forces amortisseurs:

La force de laminage de l'amortisseur j s'écrit:

$$F_{amj} = \text{sign}(Venf_{amj})\ Clam_j\ (Venf_{amj})^2$$

avec:

$Clam_j$: le coefficient de laminage de l'amortisseur

$Venf_{amj}$: la vitesse d'enfoncement

En appliquant le schéma d'intégration dans le temps pour exprimer la vitesse d'enfoncement on obtient un polynôme du premier degré par rapport à l'incrément de déplacement:

$$Venf_{amj} = a_j\ \Delta ENF_{amj} + b_j$$

F_{amj} est donc un polynome du second degré en ΔY.

On peut construire le pseudo-potentiel W_{amj} tel que $F_{amj} = \frac{\partial W_{amj}}{\partial \Delta ENF_{amj}}$

qui est un polynome du troisième degré en ΔY.

Formulation variationnelle:

La solution ΔY rend minimal le potentiel $P(\Delta X)$:

$$P(\Delta X) = \frac{1}{2}\ \Delta X^T\ [K_{dyn}]\ \Delta X - \Delta X^T\ F + W_{am}$$

Condensation sur les seuls degrés non-linéaires:

Une condensation de Gauss est effectuée::

$$\Delta Y = [\ K_{dyn}\ ]^{-1} F - [\ K_{dyn}\ ]^{-1}\ [\ V_{am}\ ]\ F_{am}$$

Introduisant: $[B] = [V_{am}]^T [K_{dyn}]^{-1} [V_{am}]$

et $\Delta ENF_{am0} = [V_{am}]^T [K_{dyn}]^{-1} F$

on obtient le potentiel à minimiser dans la base des degrés non-linéaires:

$$P(\Delta ENF_{am}) = \frac{1}{2} \Delta ENF_{am}^T [B]^{-1} \Delta ENF_{am} - \Delta ENF_{am}^T [B]^{-1} \Delta ENF_{am0} + \frac{1}{2} \Delta ENF_{am0} [B]^{-1} \Delta ENF_{am0} - \frac{1}{2} F^T [K_{dyn}]^{-1} F + W_{am}$$

Méthode de résolution:

On utilise une méthode itérative avec technique de line-search très performante qui comprend à chaque itération:

- la recherche d'une direction de descente V_i

  (Raphson-Newton, gradient conjugé etc...)

- la minimisation scalaire du potentiel dans la direction V_i:

$$\frac{\partial P(\Delta ENF_{am\ i-1} + \rho V_i)}{\partial \rho} = 0 \quad \Rightarrow \quad \rho_{opt}$$

$$\Delta ENF_{am\ i} = \Delta ENF_{am\ i-1} + \rho_{opt} V_i$$

3-6- MODELISATION DES CABLES:

La simulation de l'arrêt d'détresse sur piste d'un avion ou l'appontage d'un avion marin requiert la modélisation d'un câble.

Le fait que le câble se déroule a motivé le choix d'une représentation partiellement eulérienne du câble plutôt qu'une représentation lagrangienne.

L'état du câble en un point est représenté par le vecteur V défini par:

$$V = (x, z, u, v, w, \gamma, \mu)^T$$

avec:

y: la coordonnée d'Euler selon l'axe transversal à la piste

x(y,t), z(y,t): les coordonnées de Lagrange longitudinale et verticale

u(y,t), v(y,t), w(y,t) : les vitesses selon x, y, z

$\gamma(y,t)$: l'élongation

$\mu(y,t)$: la masse linéique

Equations d'équilibre:

$$\frac{\partial \vec{T}}{\partial y}\frac{\partial y}{\partial s} = \mu\vec{\Gamma} - \mu\vec{g}$$

avec:

$\vec{T}(y,t)$: la tension du cable

s : l'abscisse curviligne

$$\vec{\Gamma} = \begin{vmatrix} \Gamma_x = v\, u_{,y} + u_{,t} \\ \Gamma_y = v\, v_{,y} + v_{,t} \\ \Gamma_z = v\, w_{,y} + w_{,t} \end{vmatrix}$$

$$\mu \frac{\partial s}{\partial y} = \mu \sqrt{1 + x_{,y}^2 + z_{,y}^2}$$

Les trois équations d'équilibre s'écrivent:

$$\left(\mu\sqrt{1 + x_{,y}^2 + z_{,y}^2} \right)\left(v\, u_{,y} + u_{,t} \right) = \left[\frac{T\, x_{,y}}{\sqrt{1 + x_{,y}^2 + z_{,y}^2}} \right]_{,y} \qquad (1)$$

$$\left(\mu\sqrt{1 + x_{,y}^2 + z_{,y}^2} \right)\left(v\, v_{,y} + v_{,t} \right) = \left[\frac{T}{\sqrt{1 + x_{,y}^2 + z_{,y}^2}} \right]_{,y} \qquad (2)$$

$$\left(\mu\sqrt{1 + x_{,y}^2 + z_{,y}^2} \right)\left(v\, w_{,y} + w_{,t} + g \right) = \left[\frac{T\, z_{,y}}{\sqrt{1 + x_{,y}^2 + z_{,y}^2}} \right]_{,y} \qquad (3)$$

Conservation de la Masse:

$$\mu(s + vdt, t + dt)\ ds_{t+dt} = \mu(s,t)\ ds_t$$

$$d\mu = (\mu_{,t} + v\ \mu_{,y})dt = \mu \left[\frac{ds_t}{ds_{t+dt}} - 1 \right] \qquad (4)$$

avec

$$(ds_t)^2 = (1 + x_{,y}^2 + z_{,y}^2)\ (dy)^2$$

$$(ds_{t+dt})^2 = [(1 + v_{,y}dt)^2 + (x_{,y} + u_{,y}dt)^2 + (z_{,y} + w_{,y}dt)^2]\ (dy)^2$$

Elongation du câble:

Par définition:

$$\gamma = \frac{1}{2} \left(\frac{(ds_t)^2 - (dy)^2}{(dy)^2} \right)$$

En différenciant on obtient:

$$1 + 2(\gamma + \gamma_{,y}vdt + \gamma_{,t}dt) = \frac{(ds_{t+dt})^2}{(ds_t)^2}\ (1 + 2\gamma) \qquad (5)$$

Comportement élastique:

Le travail virtuel des forces intérieures a pour expression:

$$\delta W_e = \int_s T\ \delta s = \int_y T\ \frac{\delta s}{dy}\ dy = \int_y T\ \frac{dy}{ds}\ \delta\gamma\ dy = \int_y T / \sqrt{1 + 2\gamma}\ \delta\gamma\ dy$$

d'où la tension de Kirchhoff P du câble:

$$T = P \sqrt{1 + 2\gamma} \qquad (6)$$

avec pour loi de comportement: $P = E\ S\ \gamma + P_0$

P_0 est la tension de Kirchhoff initiale.

Système d'équations à résoudre:

On dispose des deux équations supplémentaires suivantes:

$$x_{,t} = u - v\, x_{,y} \qquad (7)$$

$$z_{,t} = w - v\, z_{,y} \qquad (8)$$

Les huit relations référencées précédentes sont les équations à résoudre:

$$V_{,t} = A\, V + B \quad ; \quad T = f(\gamma)$$

A, B sont des fonctions des dérivées partielles dans l'espace.

Méthode d'intégration:

Le schéma d'intégration utilisé est le schéma explicite de LAX centré dans l'espace et décentré dans le temps:

$$X_{,y} = \left(\frac{\partial X}{\partial y}\right)_j^n = \frac{X_{j+1}^n - X_{j-1}^n}{2\Delta y}$$

$$X_{,t} = \left(\frac{\partial X}{\partial t}\right)_j^n = \frac{X_j^{n+1} - \frac{1}{2}\,(X_{j+1}^n - X_{j-1}^n)}{\Delta t}$$

La condition de stabilité est: $\left(\frac{\Delta y}{\Delta t}\right)\frac{1}{C} \geq 1$

$c = \sqrt{\frac{ES}{\mu}}$ est la célérité de l'onde longitudinale

Le pas d'espace est déterminé de façon à restituer avec une précision suffisante la célérité des ondes longitudinale et transversale.

Le couplage du câble et de la crosse est explicite. A chaque pas de temps les équations du câble sont intégrées compte tenu de la position et de la vitesse de l'extrémité de la crosse. Il en résulte les efforts à appliquer à la crosse pour l'intégration du mouvement de l'avion.

4- EXEMPLES D'APPLICATION:

4-1- Roulement sur piste réparée:

Nous présentons planche 4 les performances calculées du roulement du Mirage III sur un type de piste réparée en fonction de la vitesse de l'avion et l'espacement des réparations.

Ce résultat est le fruit de 144 simulations chaînées automatiquement avec un temps de calcul total non prohibitif (quelques minutes sur ordinateur IBM 3090).

4-2- Impact:

La planche 5 illustre le très bon niveau de restitution par calcul de l'effort d'impact du train d'atterrissage principal bi-chambre du Mirage 2000 comparé au résultat d'essai de chute au C.E.A.T..

4-3- Appontage et catapultage:

La version marine du Rafale a fait l'objet d'études spécifiques à cause des sollicitations particulières que subit un avion embarqué sur porte-avions notamment au cours de l'appontage et du catapultage.

L'expérience acquise avec l'Etendard et le Super-Etendard a constitué un atout précieux pour la validation de notre outil de calcul comme le montrent les comparaisons de calculs aux essais en vol qui figurent sur les planches 5 et 6.

A propos de l'appontage planche 5, la roulette avant franchit un feu de pont simultanément à l'effort maximum d'impact.

Le câble d'arrêt est modélisé de façon à reproduire finement la cinématique et les efforts de la crosse. Le déroulement du câble aux poulies de bord de pont est calculé à chaque pas de temps de façon à suivre la courbe d'effort du système d'arrêt.

Un logiciel d'animations permet en post-processeur une visualisation sophistiquée des phénomènes simulés (planche 7).

En ce qui concerne le catapultage, le modèle de calcul simule les phases de prétention de la catapulte, de rupture de la barre de rétention (holdback), de traction et de sortie de pont.

Sur la planche 8 l'avion se présente désaxé sur la catapulte ce qui constitue un cas de dimensionnement du train avant aux efforts latéraux.

Ces études bénéficient des performances en temps de calcul de notre outil ce qui permet de simuler de nombreuses configurations.

5- CONCLUSION:

Nos calculs des interactions dynamiques entre l'avion et les trains d'atterrissage sont complètement intégrés au modèle de calcul des efforts généraux.

Grâce à plusieurs niveaux de condensation et un traitement efficace des non-linéarités, les performances de notre outil de calcul permettent d'étudier de nombreuses configurations pour une approche statistique des efforts.

Le développement d'une visualisation animée spohistiquée des résultats augmente la fiabilité d'utilisation du logiciel.

BIBLIOGRAPHIE:

[1] METHODE DE SIMULATION NUMERIQUE DU SYSTEME AVION ATTERRISSEUR - C. PETIAU et A. CELIER - CESME 1982 - AGARD CONFERENCE PROCEEDINGS N° 326.

[2] THE FINITE ELEMENT METHOD - O.C. ZIENKIEWICZ - 1977 - McGRAW-HILL.

FELAND

3D DYNAMIC AIRCRAFT TAKE OFF AND LANDING SIMULATIONS

ORGANIZATION CHART

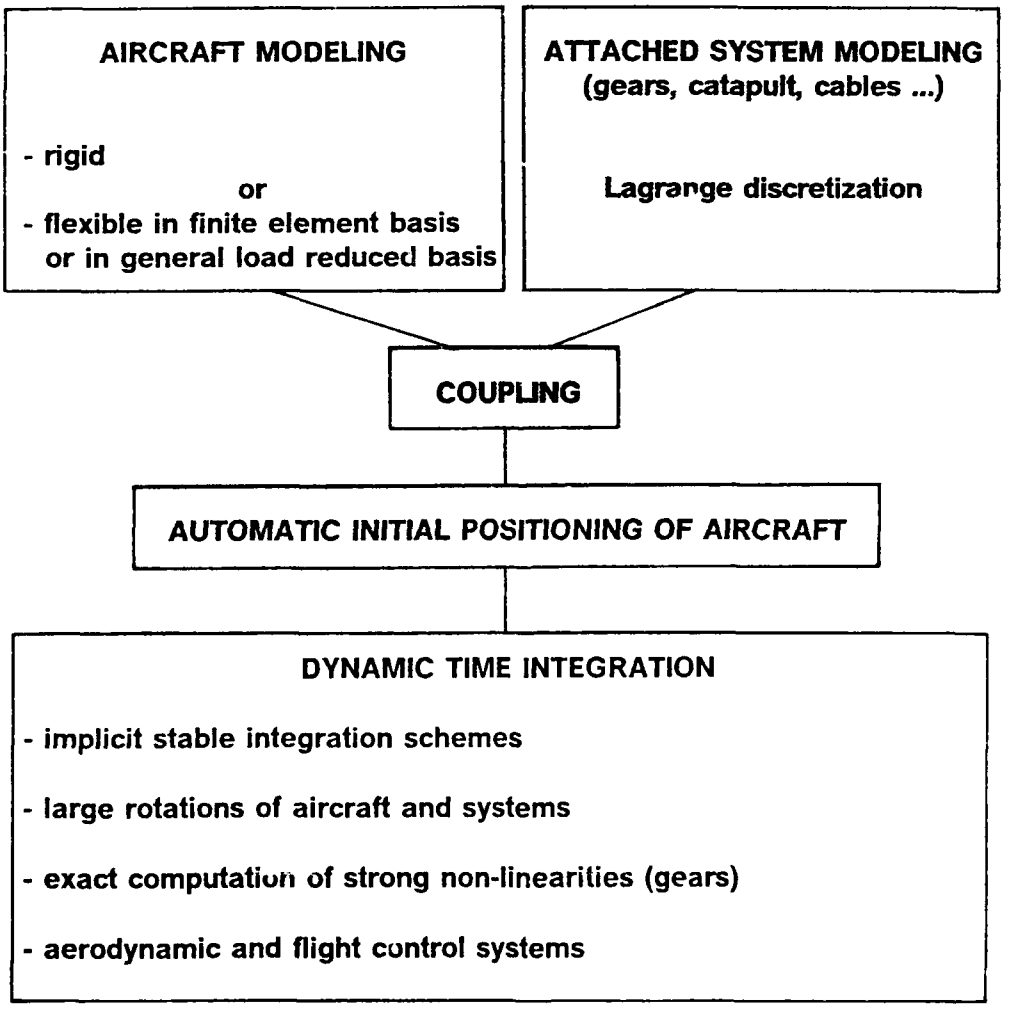

Planche 1

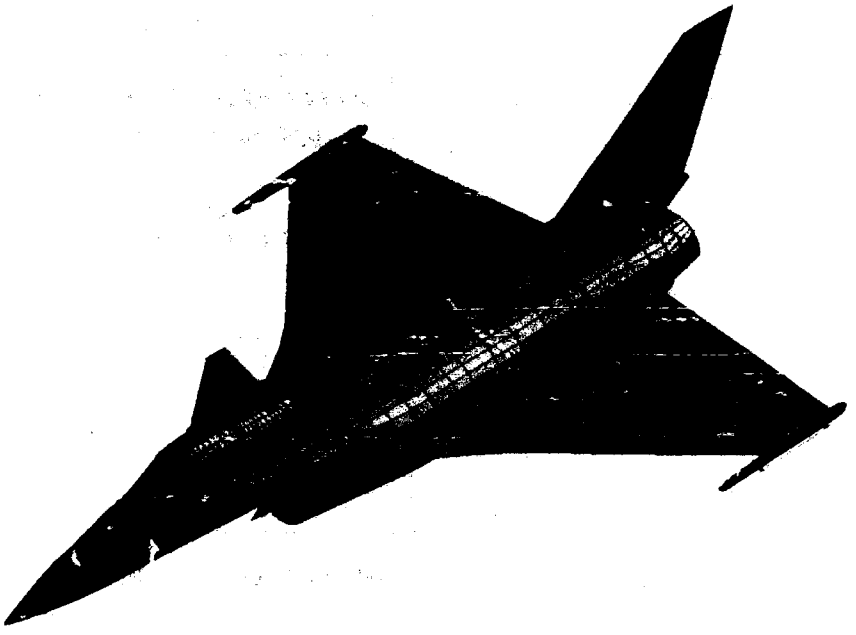

RAFALE

Planche 2

FELAND : 3 D DYNAMIC AIRCRAFT TAKE-OFF AND LANDING SIMULATIONS

RAFALE M - CATAPULTING

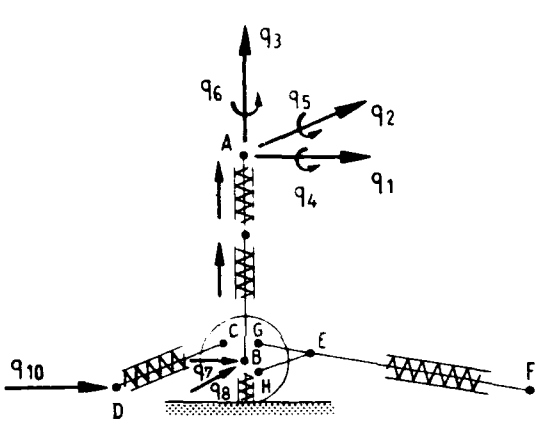

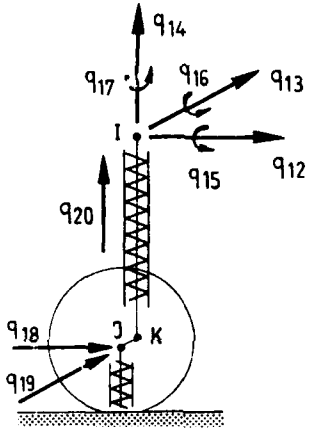

DEGREES OF FREEDOM

- AIRCRAFT SUBSTRUCTURE : 78
  (Reduced Load Basis)
- SYSTEMS : 29
  (Nose landing gears with catapult and Hold Back, 2 main landing gears)

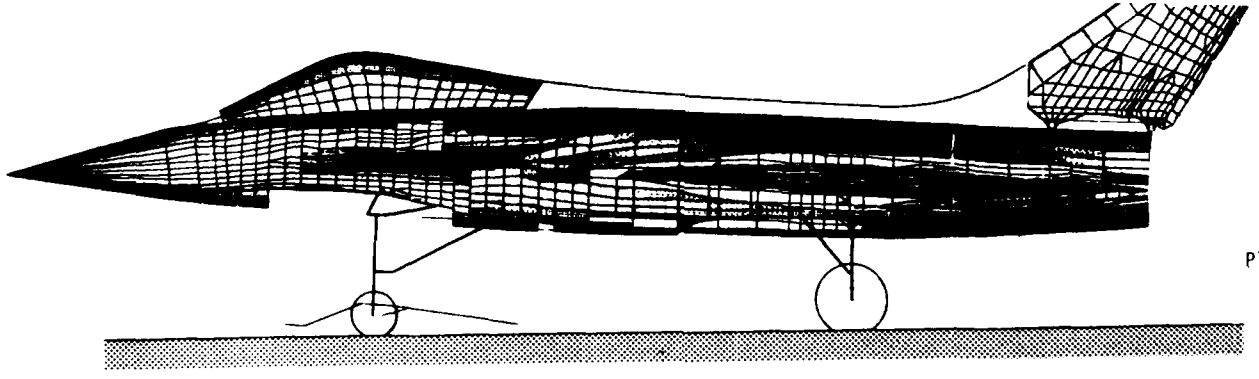

Planche 3

MIRAGE III

PERFORMANCE ON REPAIRED RUNWAYS

MAIN GEAR

SHOCK STRUT AXIAL LOAD (% OF STATIC LOAD) = F (VX, S)

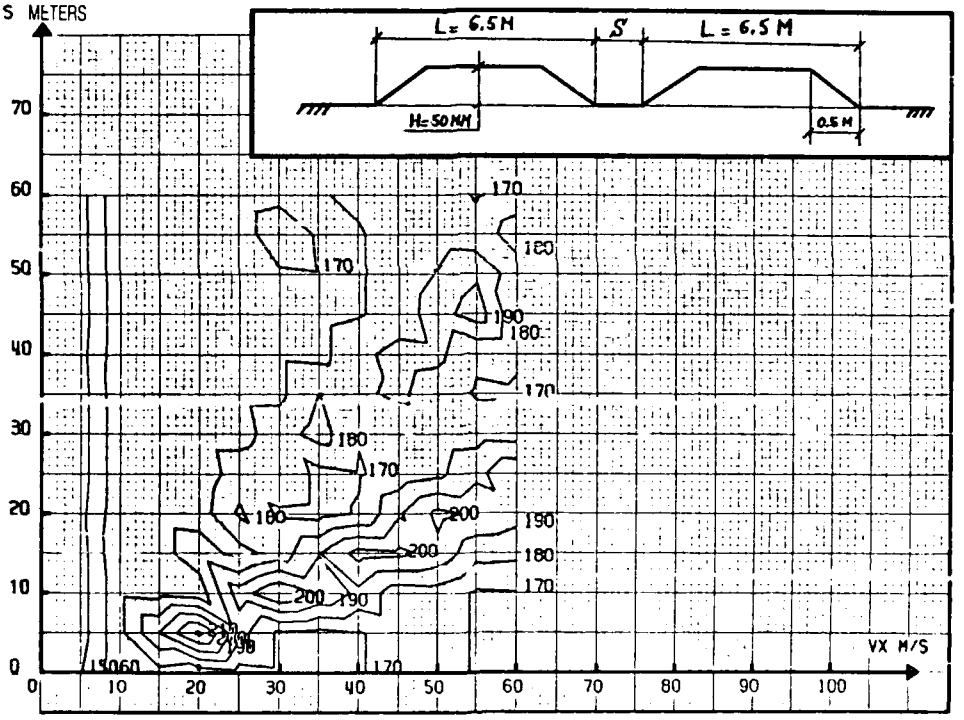

Planche 4

MIRAGE 2000

MAIN GEAR - DROP TEST

COMPARISON OF CALCULATION AND TEST RESULTS

DUAL CHAMBER, SHOCK STRUT AXIAL LOAD

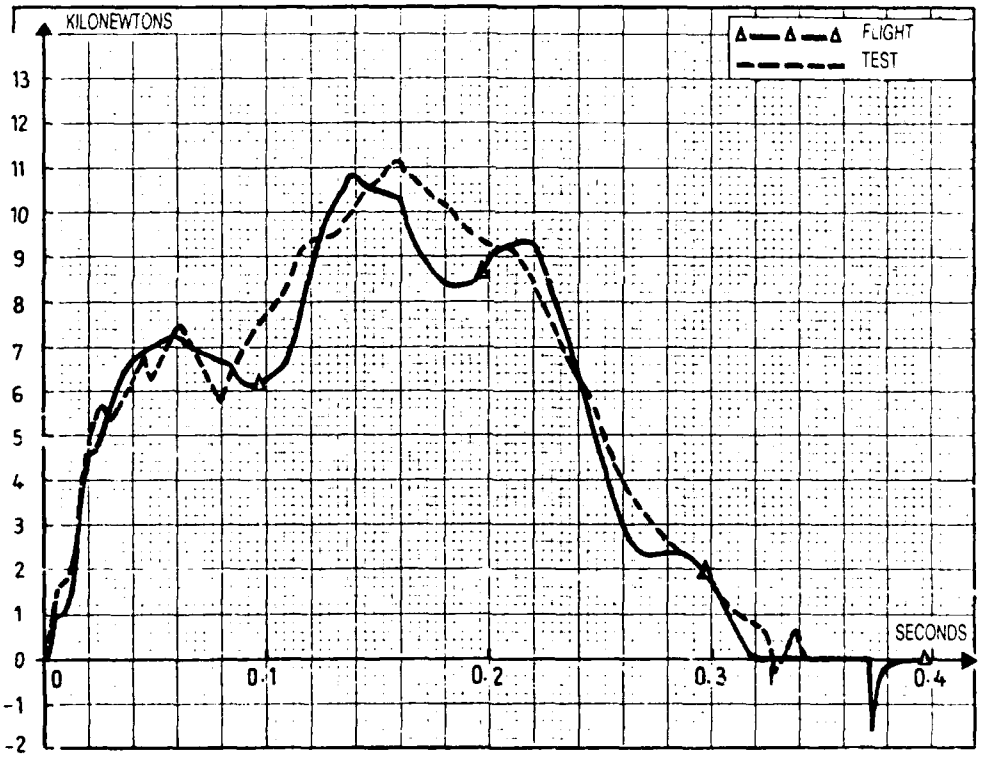

Planche 5

SUPER ETENDARD
DECK LANDING
NOSE GEAR

COMPARISON OF CALCULATION AND TEST RESULTS

SHOCK STRUT AXIAL LOAD

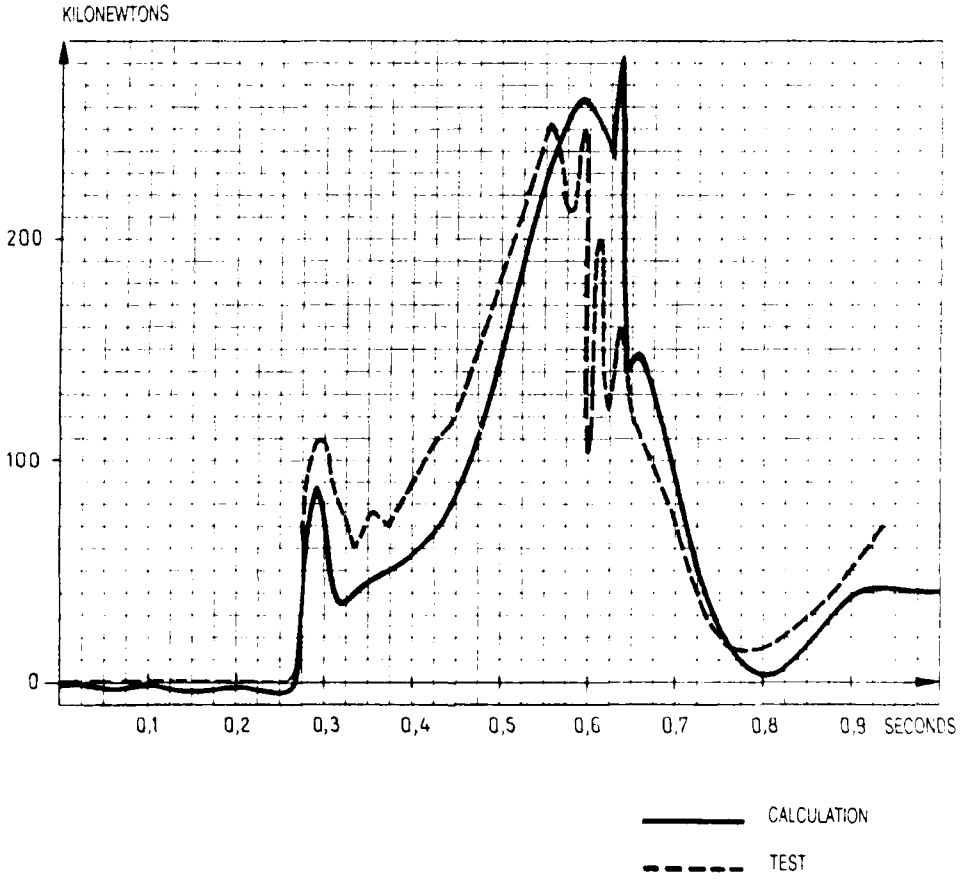

Planche 6

ETENDARD IV

CATAPULTING

MAIN GEAR

COMPARISON OF CALCULATION AND FLIGHT TEST RESULTS

VERTICAL AXLE LOAD

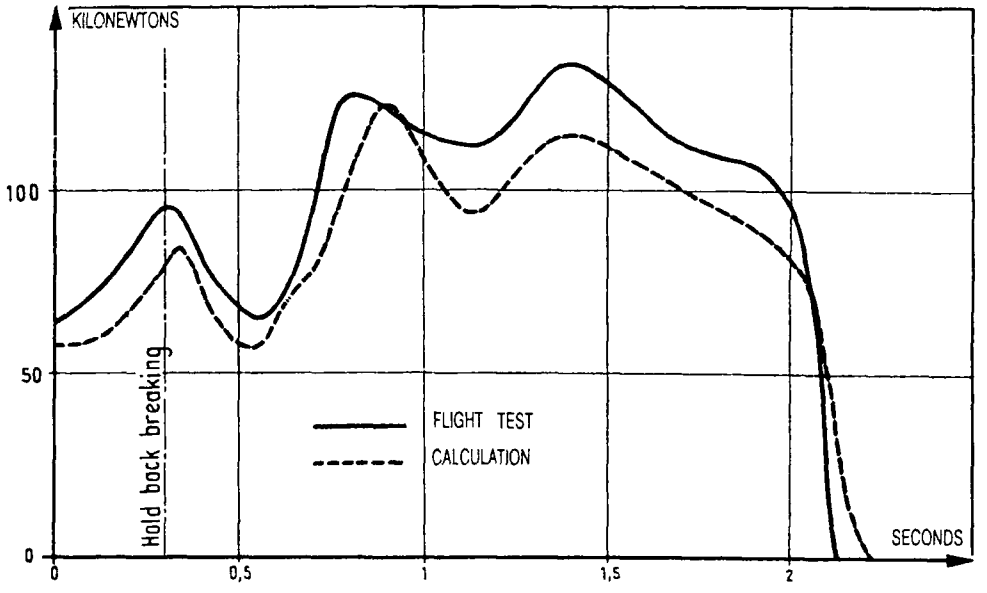

Planche 7

FELAND

RAFALE DECK LANDING SIMULATION

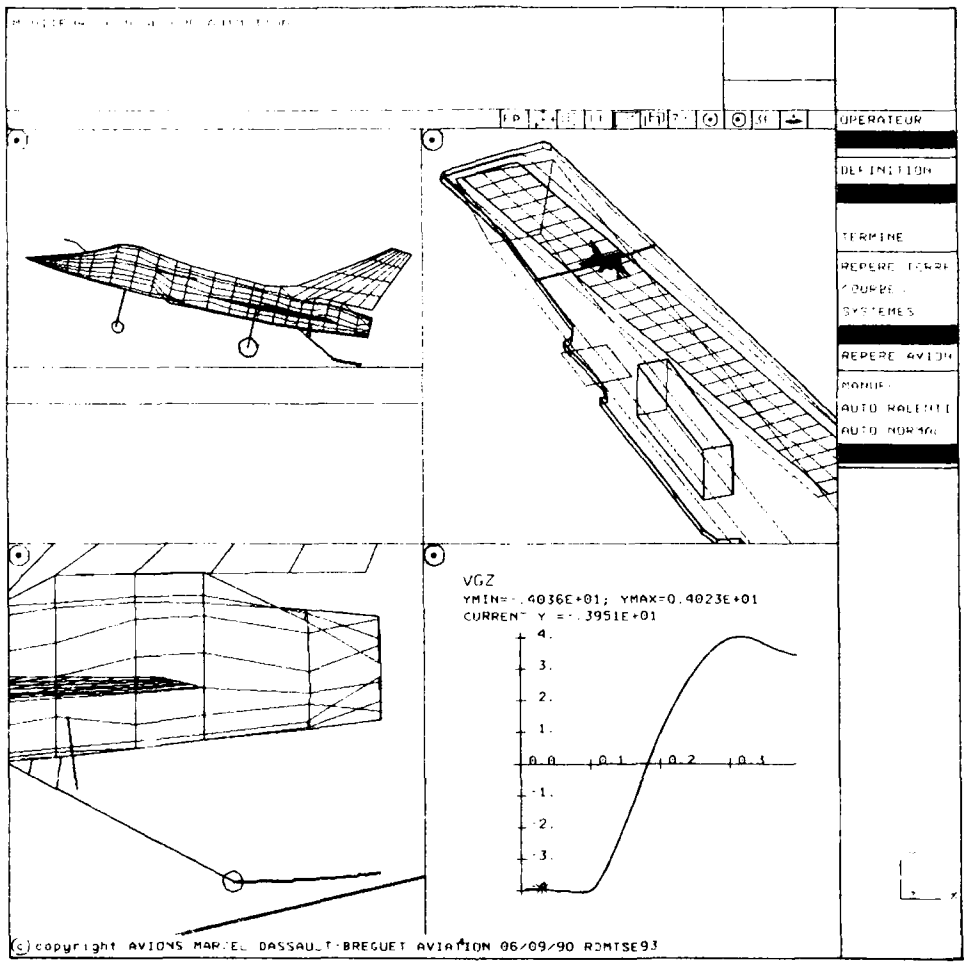

Planche 8

FELAND

RAFALE CATAPULTING SIMULATION

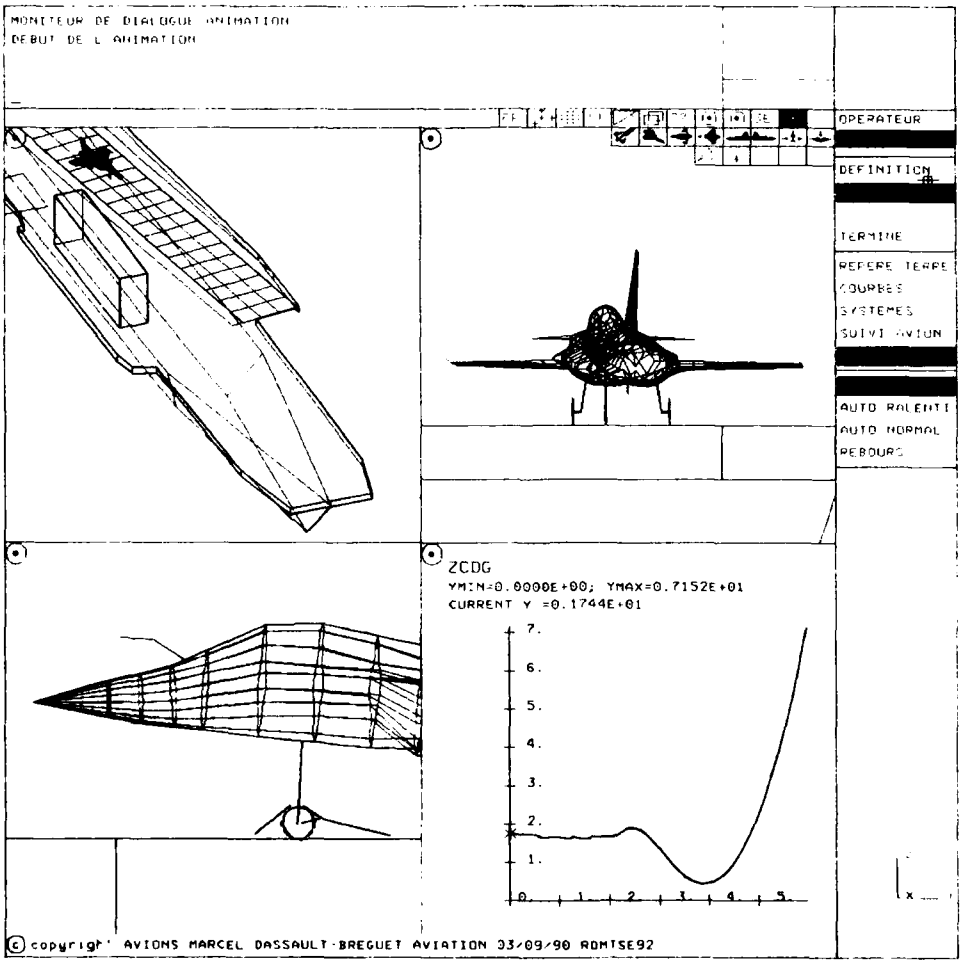

Planche 9

THE USE OF MONTE CARLO SIMULATION IN DETERMINING LANDING GEAR LOADS DURING LANDING

by

R.van der Valk
Fokker Aircraft B.V.
EDBS/B00 SO67-32
1117 ZJ Schiphol
The Netherlands

INTRODUCTION.

Landing gears, back-up structures and other major components of the Fokker 100 aircraft, are designed in agreement with the loading conditions as laid down in JAR and FAR requirements.[1,5]
The limit load conditions during landing are based on a vertical velocity of descent of 10 fps combined with a maximum landing weight, a critical centre of gravity position and a critical forward velocity, the ultimate load conditions are derived by applying a factor of 1.5 to the limit load conditions.
The introduction of automatic landing systems on aircraft has led to additional airworthiness requirements, which apply a statistical approach to the loads as developed during automatic landing.
The additional requirements are laid down in the JAR-AWO.[4]
The following results and requirements are set forth:

- The safety level in automatic landings may not be less than that achieved in normal landings.
- The probability of exceedance of the sink rate for which the aircraft has been certified for structural loads, must be:
  $\leq 10^{-4}$ in average conditions
  $\leq 10^{-5}$ in limiting conditions
- The probability of exceedance of the lateral velocity or slip-angle associated with limit structural loads, must be:
  $\leq 10^{-4}$ in average conditions
  $\leq 10^{-5}$ in limiting conditions

(A limiting condition means that from all input distributions one distribution is set at a maximum value. In this case the air turbulence distribution is set at a maximum value. ref. [4])

The JAR-AWO approach suggests that, for instance for vertical loading conditions, the descent velocity of the aircraft is the determining quantity.
That implies that if it can be shown that the probability of exceedance, in the sink rate distribution, of the 10 fps point is less then 10^{-4} (average), the limit loads in vertical direction are exceeded with a probability which is lower than once every 10^{4} landings. So on the base of the sinkrate distribution judgement is passed about the load cases.
This is also applicable for lateral load conditions with respect to the aircraft slip-angle (or lateral velocity) distribution.
From the physical and statistical points of view it is not true , however, that if the sink-rate distribution meets the requirements, also the "corresponding" load (case) distributions meet automatically these requirements. Therefore in this paper a more direct approach is given based on the loads themselves; in this context the additional requirements are reinterpreted as follows:

the probability of exceedance of
- a limit load must be $\leq 10^{-4}$ in average conditions.
- an ultimate load must be $\leq 10^{-5}$ in limiting conditions.

The static strength justification in this paper is based on three load cases, which are assumed to be representative for the landing gear and the aircraft:

a) the main and nose landing gear bending moments at the lower bearing.
b) shear force jump and bending moment jump between front and rear spar of the fuselage.
c) the side-stay load (main landing gear only).

In the future, however, the static strength justification could be based on more load cases.
From these three load cases only the bending moments at the lower bearing and the side-stay loads shall be dealt with extensively.
For the sake of completeness the distributions of loads of the regular FAR/JAR requirements, collected from the simulation runs, are also presented. (TABLES XV, XVI and XVII).

Statistical information about loads (and stresses) in any section of the landing gear or aircraft can be collected by means of Monte Carlo simulation of the landing process.
For this purpose the aircraft with full aerodynamics, undercarriages and tyres, is modelled with six degrees of freedom. Control laws are included, representing the behaviour of an automatic pilot.
Windshear is ignored during the landing process.
Throughout this paper flapsettings of respectively 42° and 25° are assumed.
For a detailed derivation of equations of motion reference is made to [8].

MONTE CARLO SIMULATION.

One of the most convenient methods for solving problems involving input data with known or assumed probability distributions is the Monte Carlo simulation.
This method involves a repeated simulation process using a randomly collected set of input data, from the probability distributions, in each simulation (run).
A sample from a Monte Carlo simulation is similar to a sample of experimental observations, therefore the results obtained by Monte Carlo simulation may be treated statistically.

The first question is, what number of runs is required for validity? Basically the number of runs depends on the risk level one wishes to cover. That means, if acceptable risk levels are in the order of $1:10^4$ a minimum of 10^4 runs is required.
But now a practical problem arises.
For this landing simulation one run requires about 5s CPU time, thus 10^4 runs require roughly 1400 CPU hours, which is impractically long.
So the high number of runs must be reduced to a practible number of runs.
A widely accepted method is to assume normally distributed output data. Then, by means of the X^2-distribution, it can be shown that a number of runs of 1500 is acceptable.[7]
Of course with 1500 runs , only a statement about a risk level of 1:1500 can be substantiated.
So if the desired risk level is in the order of $1:10^4$ one must try to find a possibility to extend the probability of exceedance curves down to this level.
A simple method is to plot the probability of exceedance, on for instance normal paper, and extend the curve by "fitting by eye" down to the desired risk level.
In applying this method one extrapolates beyond the validity range of the data set and (possibly serious) errors can occur.
A better method is to find out which probability distribution is followed by the output quantity.
A wide scala of statistical methods is available to test the hypothesis wether or not data sets are normally, log-normally or otherwise distributed.[2] If one is able to identify a statistical distribution which fits the data well, it is possible to read the probability of exceedance plot at the desired (low) risk level. If one is not able to find such a probability distribution, there are possibilities to transform the data to new data which hopefully will fit a known distribution.[3]
Another method which works reasonable well under certain circumstances is: try to fit only the upper part of the distribution by a known distribution.
If all the methods fail, only one possibility remains: "fit-by-eye".
If it is known that the load (or stress) under consideration possseses a physically upper boundary below the limit (ultimate) load, there is no need for extrapolation to the low risk level. The load can simply not exceed this value.
So a high number of runs has the advantage to make the estimation of variables at low risk levels more certain.
As allready mentioned a number of 1500 runs is used in this paper.

In order to reduce the amount of input data for the landing simulations, some realistic assumptions are made:

- the aircraft lateral velocity as well as the rotational velocity are zero at the moment of touch down (t=0).
- the runway friction coefficient, the airfield height and the ISA-deviation are not varied because no realistic distributions could be found. However, a μ_{max}=0.8, an airfield height zero and a ISA are probably conservative with respect to the output distributions.

Taking into account these assumptions, the landing impact simulations only require probability distributions of the following set of input data:

- mass of the aircraft (GRAPH I, TABLE I)
- moments of inertia I_{xx}, I_{yy} and I_{zz}. (TABLE I)
- centre of mass. (TABLE I)
- aircraft ground speed.
- aircraft airspeed.
- aircraft descent velocity.
- aircraft pitch, yaw and roll angles.

Detailed information about the input distributions is given in the next chapter.

INPUT DATA.

In GRAPH I a scatter plot of the aircraft mass versus the aircraft centre of mass is given. The boundaries of the official mass and centre of mass diagram for this aircraft configuration are indicated.
The graph shows that in 4.3% (65 out of 1500) of the landings an "overweight" landing is assumed.
In TABLE I relevant statistical parameters of mass data are summarized for different flapsettings and in average and limiting conditions.
In TABLES II, III, IV and V statistical parameters of airspeed, groundspeed, pitch, yaw and roll angles are presented.

VALIDATION OF THE MODEL.

The mathematical model of the aircraft landing process used to get the results given in this paper, is implemented in the computer program LANDAU.[8] This model is validated by examining the vertical and the lateral behaviour of the aircraft.
The vertical behaviour of the aircraft during the landing process is calculated by means of a set of equations which are in agreement with the equations used for the simulation of droptests and the determination of the deterministic landing loads.
The lateral behaviour can be checked by comparing measured loads and accelerations with calculated loads and accelerations.
Comparison of measured and calculated loads show good agreement.

STATIC STRENGTH JUSTIFICATION.

Bending moments at the main and nose landing gear lower bearings.

In GRAPH II a scatter plot of left versus right hand main landing gear bending moments is presented for $\delta_{r,i}$=42° in the limiting condition.
By this scatterplot it is suggested that the probability distributions of left and right hand landing gear bending moments are "similar".
A distribution-free statistical test confirms this hypothesis indeed.[2]
This is equally applicable to the $\delta_{r,i}$=25° (average, limiting) simulations.
For this reason the events of left and right hand main landing gear are taken together.
In TABLES VI and VII statistical parameters of the bending moment distributions are presented.
Probability of exceedance plots on normal (Gaussian) paper (see GRAPH III) show that in none of the four cases the fit against the normal distribution is acceptable. (Compare the Anderson-Darling statistic (AD) with the AD-90% value. If AD>AD-90% the hypothesis of normally distributed bending moments is rejected).
So "extrapolation" procedures (as mentioned already in the chapter Monte Carlo Simulation) are examined .
Once it is decided which "extrapolation" procedure is the most valid one, it is possible to read the bending moment values, at their desired risk levels,from the probability distribution plots. (see GRAPH IV as an example).
These bending moment values can then be compared with the limit and ultimate bending moments available from deterministic load calculations.
The results are summarized in TABLE VIII.

TABLE VIII Main landing gear bending moments at lower bearing.

$\delta_{r,i}$ (degr.)	condition	risk level	"extrapolation" method	bend.moment value at risk level (Nm)	limit/ultimate bending moment (deterministic) (Nm)
25	average	$1:10^{-4}$	upper-half/lnor	109000	130560
25	limiting	$1:10^{-3}$	by eye/lnor	<100000	195841
42	average	$1:10^{-4}$	upper-half/lnor	106600	130560
42	limiting	$1:10^{-3}$	bye eye/lnor	<150000	195841

A more satisfactory approach is to define an ultimate or limit load (or stress) by means of its value at the desired risk level. This approach meets far more real world experience of people.

For the nose landing gear bending moment the same methods and procedures are applicable. A summary of the results is presented in TABLE VIIIA. Statistical parameters of the distributions of the nose landing gear bending moments are presented in TABLE IX. (see also GRAPH V). (Although the teststatistic AD>AD-90%, these distributions are accepted because it is the best obtainable result).

TABLE VIIIA. Nose landing gear bending moments at lower bearing.

$\delta_{r,i}$ (degr.)	condition	risk level	"extrapolation" method	bend.moment value at risk level (Nm)	limit/ultimate bending moment (deterministic) (Nm)
25	average	$1:10^{-4}$	by eye/weib.	<15000	29078
25	limiting	$1:10^{-3}$	by eye/weib.	<15000	43616
42	average	$1:10^{-4}$	bye eye/weib.	<20000	29078
42	limiting	$1:10^{-3}$	upper-half/weib	17380	43616

The side-stay load (main landing gear only).

The side-stay loads are examined in the same way as was done before for the bending moments.
It appears that no known probability distribution fits well.
The results of the "extrapolation" procedures are given in TABLE X.
A summary of statistical parameters is presented in TABLES XI up to XIV inclusive.
Conventional load cases distinguish between push and pull loads. So for every set of simulations ($\delta_{r,i}$=25°,42° and average, limiting) two load distributions must be investigated.

TABLE X Main landing gear side-stay loads.

δ_{r1} (degr.)	condition	risk level	"extrapolation" method	side-stay load at risk level (N)	limit/ultimate side-stay load (deterministic) (N)
			PULL		
25	average	$1:10^{-4}$	upper-half/weib	350000	778455
25	limiting	$1:10^{-5}$	upper-half/weib	310000	1167683
42	average	$1:10^{-4}$	upper-half/weib	420000	778455
42	limiting	$1:10^{-5}$	by eye/weib.	830000	1167683
			PUSH		
25	average	$1:10^{-4}$	upper-half/weib	425000	468188
25	limiting	$1:10^{-5}$	upper-half/weib	380000	702282
42	average	$1:10^{-4}$	upper-half/weib	440000	468188
42	limiting	$1:10^{-5}$	by eye/weib.	700000	702282

CONVENTIONAL LOADCASES.

For the sake of completeness the parameters of the probability distributions of all landing loadcases for δ_{r1}=42° (average only) are presented in the TABLES XV up to XVII inclusive.
In TABLE XVIII the corresponding deterministic JAR/FAR loadcases are given for comparison.
If one tries to compare the simulated loadcases with the deterministic loadcases a problem arises.
A loadcase is not the load itself but a combination of loads (and shockabsorber deflection) which define a certain situation as asked for by JAR/FAR (the spin-up or maximum vertical reaction loadcase for instance).
To compare loadcases one wishes to have the multidimensional correlated probability distributions of the relevant parameters by which the loadcase is defined.
For instance the spin-up loadcase is defined by the spin-up (drag) load together with the corresponding vertical load and shockabsorber deflection. Each of these three parameters has its own probability distribution and in most cases these distributions are also correlated. So a three dimensional, correlated, probability distribution must be found which describes the probability distribution of the **loadcase.**
In most practical situations it is very difficult to find such kind of distributions and one is forced to use approximation procedures to be able to extrapolate the probability distribution to the desired risk level.
The whole proces is a very complicated one and in most cases no probability distribution can be found which fits the loadcase well. Also extrapolation by means of "fitting by eye" can not be performed due to the three dimensional character of the distribution.
On the other hand it is sufficient to determine loads or stresses directly for any particular section where stress calculations are made. This makes at least the probability distribution of the determining load for this section one dimensional.
A more direct approach is thus to calculate the loads directly which are needed to make a stress calculation for a certain section of the construction.
From this point of view the whole concept of loadcases is superflous (apart from preliminary design)..
Another point is that nowadays the FAR/JAR loadcases **define** the limit or ultimate loads against the structure is designed.
It is, however, more conform the daily reality to **define** an ultimate or limit load (stress) by means of its values at the desired and accepted risk level.

FATIGUE.

It is known that the fatigue-damage of a varying load depends primarily on the amplitude, the variation in load, rather than the absolute load.level reached. [6]
That means that maxima (or minima) of load time histories, as collected from Monte Carlo simulated runs, can not be used for fatigue purposes. From the fatigue point of view the whole time history of loads is of importance and must be collected and stored rather than only the maxima (minima) of the time history.
If the time history of a varying load in a section is known, this time history can be analyzed by means of, for instance, a rainflow counting method [6].
Due to the computer storage capacity it is, however, not possible to store the whole time history of every relevant load. An acceptable burdening of computer memory is obtained if only a few relevant Fourier components of each time history are stored.
Fourier analysis of the time history is then performed by means of a Fast Fourier Transform (FFT). By means of the inverse Fourier transform the time history can be reconstructed (approximately).
All kinds of (rainflow) counting methods can be applied afterwards to these reconstructed time histories.
Unfortunately at the moment this paper was written, no calculated data were available so no example can be presented.

CONCLUSIONS.

It is perceived by the airworthiness authorities that certification of automatic landing systems can only be done by applying statistical methods. [4]
However, if these particular statistical requirements are satisfied, there is no guarantee for the aircraft manufacturer that local limit and ultimate loads (stresses), developed during landing, occur at acceptable risk levels.
In this paper another approach is proposed, which is based on direct calculation of local loads by means of Monte Carlo simulation.
In this context the concept of load cases is superfluous (apart from preliminary design). Limit and ultimate loads are obtained by reading probability of exceedance distributions at desired risk levels.
Maxima and minima are used for calculation of limit and ultimate loads. The whole time histories are used for the calculation of fatigue loads.

REFERENCES.

1. Federal Aviations Regulations, PART 25, Airworthiness Standards, Transport Category Airplanes.

2. Fokker Handbook; Methods of probability and statistics, TH 47, issue 6, 7-7-1988.

3. Hahn G.J. and Shapiro S.S., Statistical models in engineering, John Wiley and Sons, Inc. 1967.

4. JAR-AWO, Section I, Automatic Landing Systems.

5. Joint Airworthiness Requirements, JAR-25, Large Airplanes.

6. de Jonge J.B.,The analysis of load-time histories by meens of counting methods. In AGARD report:Helicopter fatigue design guide. National Aerospace Laboratory NLR. 1976. The Netherlands.

7. Shakarian A., Applications of Monte Carlo techniques to the 757/767 autoland dispersion analysis by simulation, American Institute of Aeronautics and Astronautics, Inc., 83-2193,1983.

8. v.d.Valk R., Fokker 100 Autoland System: Structural Integrity Justification, Fokker B.V., L.G.-100-105, issue 2, 10-5-1988.

TABLE I: Inertia data

	MASS (kg)	CG (% MAC)	i_x (kgm²)	I_y (kgm²)	I_z (kgm²)
n	1500	1500	1500	1500	1500
mean	34115	20.84	403425	1738549	2018226
standard deviation	2602	6.148	157731	103872	73192
β_1	0.011	0.0046	0.0603	0.0125	0.0011
β_2	2.4449	2.3039	1.0883	1.3742	2.4450
sample minimum	28017	7.050	227435	1573866	1846739
sample maximum	40661	34.70	575000	1887521	2202337
H_o:randomness [2]	not	not	not	not	not
(significance level 10%)	rejected	rejected	rejected	rejected	rejected

TABLE II

AVERAGE δ_{T1}=42°	V_{CAS} (m/s)	V_{GROUND} (m/s)	$V_{DESCENT}$ (fps)	PITCH (degree)	ROLL (degree)	YAW (degree)
n	1500	1500	1500	1500	1500	1500
mean	62.186	59.839	1.927	2.759	-0.016	-0.064
standard deviation	2.694	4.135	0.781	0.722	0.743	1.127
β_1	0.0056	0.0002	2.0225	0.4683	0.222	0.0035
β_2	2.6844	3.1184	7.0279	3.5810	3.5795	7.5259
sample minimum	54.531	43.856	0.004	0.100	-2.700	-6.800
sample maximum	70.625	71.133	7.187	4.800	2.900	6.800
H_o:randomness [2]	not	not	not	not	not	not
(sign. level 10%)	rejected	rejected	rejected	rejected	rejected	rejected

TABLE III

LIMITING δ_{T1}=42°	V_{CAS} (m/s)	V_{GROUND} (m/s)	$V_{DESCENT}$ (fps)	PITCH (degree)	ROLL (degree)	YAW (degree)
n	1500	1500	1500	1500	1500	1500
mean	62.183	54.561	3.345	2.740	-0.015	-0.210
standard deviation	3.315	6.120	1.425	1.374	1.232	3.789
β_1	0.0201	0.5229	0.0689	0	0.0004	0.0030
β_2	2.9958	2.9371	2.7402	2.8025	2.2317	2.6074
sample minimum	52.611	41.862	0.158	-1.200	-3.800	-10.500
sample maximum	73.923	73.607	8.194	7.200	3.500	11.200
H_o:randomness [2]	not	not	not	not	not	not
(sign. level 10%)	rejected	rejected	rejected	rejected	rejected	rejected

TABLE IV

AVERAGE δ_{T1}=25°	V_{CAS} (m/s)	V_{GROUND} (m/s)	$V_{DESCENT}$ (fps)	PITCH (degree)	ROLL (degree)	YAW (degree)
n	1500	1500	1500	1500	1500	1500
mean	67.172	65.068	1.523	3.997	-0.025	0.050
standard deviation	2.887	4.333	0.772	0.607	0.964	1.164
β_1	0.0150	0.0077	2.4928	0.3811	0.0034	0.0677
β_2	2.7199	2.8881	7.3897	3.4892	3.5030	4.4523
sample minimum	59.518	49.580	0.061	1.875	-3.719	-5.471
sample maximum	76.639	79.272	6.424	5.932	3.082	4.556
H_o:randomness [2]	not	not	not	not	rejected	rejected
(sign. level 10%)	rejected	rejected	rejected	rejected		

TABLE V

LIMITING δ_{T1}=25°	V_{CAS} (m/s)	V_{GROUND} (m/s)	$V_{DESCENT}$ (fps)	PITCH (degree)	ROLL (degree)	YAW (degree)
n	1500	1500	1500	1500	1500	1500
mean	67.137	59.688	2.969	4.018	-0.031	0.154
standard deviation	3.417	6.295	1.295	1.066	1.499	3.829
β_1	0.0086	0.4849	0.0710	0.0173	0.0064	0
β_2	2.888	2.8212	2.5747	3.0400	2.1366	2.5067
sample minimum	57.474	45.866	0.109	0.948	-4.175	-10.897
sample maximum	77.739	80.166	7.789	8.304	3.568	9.563
H_o:randomness [2]	not	rejected	not	not	not	not
(sign. level 10%)	rejected		rejected	rejected	rejected	rejected

TABLE VI: Bending moment at landing gear lower bearing.

MAIN LANDING GEAR	AVERAGE		LIMITING	
δ_{y1} = 25°	M_{1max} (Nm)	M_{rmax} (Nm)	M_{1max} (Nm)	M_{rmax} (Nm)
n	1474	1474	1464	1464
mean	24171	24264	28565	28770
standard deviation	6461	6441	5841	5654
β_1	0.1788	0.1146	0.0034	0.0435
β_2	3.6215	3.2921	3.8331	3.7946
sample minimum	12465	12735	13108	13860
sample maximum	59789	59048	57249	50246
H_0:randomness [2]	not	not	not	not
(significance level 10%)	rejected	rejected	rejected	rejected

TABLE VII: Bending moment at landing gear lower bearing.

MAIN LANDING GEAR	AVERAGE		LIMITING	
δ_{y1} = 42°	M_{1max} (Nm)	M_{rmax} (Nm)	M_{1max} (Nm)	M_{rmax} (Nm)
n	1489	1489	1488	1488
mean	26367	26256	45845	45591
standard deviation	6548	6678	16106	15913
β_1	0.3903	0.7748	1.2309	1.3205
β_2	4.4767	5.8668	4.4392	4.7911
sample minimum	13314	13006	13319	14803
sample maximum	60447	75589	115267	124893
[illegible]:randomness [2]	not	not	not	not
(significance level 10%)	rejected	rejected	rejected	rejected

TABLE IX: Bending moment at landing gear lower bearing.

NOSE LANDING GEAR	AVERAGE		LIMITING	
	δ_{y1} = 25°	δ_{y1} = 42°	δ_{y1} = 25°	δ_{y1} = 42°
n	1474	1489	1464	1488
mean	10514	11033	10212	11460
standard deviation	1011	1234	1126	1222
β_1	0.7469	0.4840	0.1731	0.0965
β_2	2.9085	2.9785	2.0939	4.1586
sample minimum	7576	6877	7519	6584
sample maximum	12631	15421	12439	15170
H_0:randomness [2]	not	not	not	not
(significance level 10%)	rejected	rejected	rejected	rejected

TABLE XI: Side-stay loads.

MAIN LANDING GEAR	LEFT HAND		RIGHT HAND	
δ_{y1} = 25° AVERAGE	PULL (N)	PUSH (N)	PUSH (N)	PULL (N)
n	1448	1450	1448	1450
mean	-21687	28212	-24593	24611
standard deviation	32129	38198	36241	32668
β_1	4.7816	3.6426	4.5920	3.0479
β_2	9.9631	7.6123	9.1089	6.7280
sample minimum	-302203	18	-307664	18
sample maximum	-8	265940	-8	238853
H_0:randomness [2]	not	not	not	not
(significance level 10%)	rejected	rejected	rejected	rejected

TABLE XII: Side-stay loads.

MAIN LANDING GEAR	LEFT HAND		RIGHT HAND	
δ_{y1} = 25° LIMITING	PULL (N)	PUSH (N)	PUSH (N)	PULL (N)
n	1388	1386	1387	1386
mean	-29342	40127	-35459	32879
standard deviation	39801	50652	48231	41552
β_1	2.1616	1.7595	2.0663	1.8799
β_2	4.5361	4.0261	4.3006	4.2871
sample minimum	-213859	21	-244256	21
sample maximum	-7	247093	-7	219233
H_0:randomness [2]	rejected	not	rejected	not
(significance level 10%)		rejected		rejected

TABLE XIII: Side-stay loads.

MAIN LANDING GEAR	LEFT HAND		RIGHT HAND	
δ_{r1} = 42° AVERAGE	PULL (N)	PUSH (N)	PUSH (N)	PULL (N)
n	1419	1424	1422	1424
mean	-24594	30410	-26889	27490
standard deviation	36474	42922	40704	37868
β_1	4.7764	4.4224	5.4101	3.6271
β_2	9.8935	9.0407	10.7391	7.5401
sample minimum	-334588	9	-371147	9
sample maximum	-23	337500	-6	376144
H_0:randomness [2]	not	not	not	not
(significance level 10%)	rejected	rejected	rejected	rejected

TABLE XIV: Side-stay loads.

MAIN LANDING GEAR	LEFT HAND		RIGHT HAND	
δ_{r1} = 42° LIMITING	PULL (N)	PUSH (N)	PUSH (N)	PULL (N)
n	1420	1396	1420	1396
mean	-86903	106713	-98491	93740
standard deviation	111114	131116	126692	114924
β_1	1.5715	1.1545	1.4993	1.2779
β_2	3.5899	2.983	3.4239	3.2251
sample minimum	-542359	10	-592438	10
sample maximum	-33	577567	-34	511681
H_0:randomness [2]	not	not	not	not
(significance level 10%)	rejected	rejected	rejected	rejected

TABLE XVIII: Deterministic JAR/FAR loadcases.

CASE DESCRIPTION	Drag (N)	Vertical (N)	Side (N)	S/A deflection (m)
SPIN-UP (1) (M)	201576	232213	-	0.085
SPIN-UP (2) (M)	237697	250351	-	0.186
SPIN-UP (N)	67423	85612	-	0.065
SPRING-BACK (M)	-216791	219430	-	0.183
SPRING-BACK (N)	-55611	100477	-	0.133
MVR (M)	72932	291730	-	0.329
MVR (N)	28042	112619	-	0.281
LAT.DRIFT(1)(M)	-	145865	+11692 -87519	0.165
LAT.DRIFT(2)(M)	87519	218798	±54700	0.247

Legenda: M,N denotes that the loads are applicable to the main repectively nose landing gear.
MVR denotes Maximum Vertical Reaction.
Lateral drift for the nose landing gear is no regular loadcase.

$\delta_{f1} = 42^0$ AVERAGE TABLE XV

n=1482	Q_{SU} (N)	s_Q (N)	$\hat{\beta}_1$	$\hat{\beta}_2$	F_{SU} (N)	s_F (N)	$\hat{\beta}_1$	$\hat{\beta}_2$	Δl_{SU} (m)	$s_{\Delta l}$ (m)	$\hat{\beta}_1$	$\hat{\beta}_2$
L/H MUC	44051	11707	0.3090	5.7778	50086	16230	1.5532	[illegible].3377	0.044	0.026	0.2688	2.7820
R/H MUC	[illegible]	11994	0.6274	7.6557	51073	[illegible]	1.8256	[illegible]	[illegible]	0.026	0.2688	2.7820
NLC	22421	2000	0.1831	3.4075	25182	1842	0.0891	3.3264	0.059	0.007	0.0686	3.8801
	Q_{SB} (N)	s_Q (N)	$\hat{\beta}_1$	$\hat{\beta}_2$	F_{SB} (N)	s_F (N)	$\hat{\beta}_1$	$\hat{\beta}_2$	Δl_{SB} (m)	$s_{\Delta l}$ (m)	$\hat{\beta}_1$	$\hat{\beta}_2$
L/H MUC	[illegible]	10922	0.5330	6.2308	49925	17754	0.4971	[illegible].1346	0.050	0.035	2.5821	7.5990
R/H MUC	[illegible]	11326	1.3308	10.133	51098	18296	1.1830	[illegible].2424	0.051	0.036	2.7231	[illegible].0727
[illegible]	[illegible]	1766	0.1551	3.2176	25065	[illegible]	0.0085	[illegible]	0.083	0.007	0.2065	[illegible].1573

First four moments of S/A loads and S/A deflections at spin-up and spring-back time.

F_s : shock absorber force // S/A ℄.
Q_s : effective structural force ⊥ S/A ℄.
Δl : shock absorber deflection.

PIN-UP

SPRING-BACK

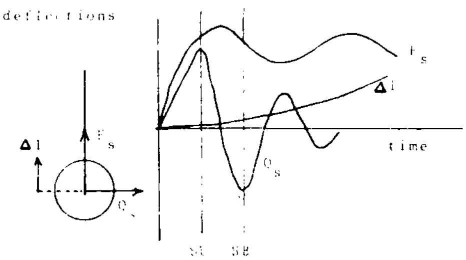

$\delta_{f1} = 42^0$ AVERAGE TABLE XVI

n=1482	Q_{MVR} (N)	s_{MVR} (N)	$\hat{\beta}_1$	$\hat{\beta}_2$	F_{MVR} (N)	s_{MVR} (N)	$\hat{\beta}_1$	$\hat{\beta}_2$	Δl_{MVR} (m)	s_{MVR} (m)	$\hat{\beta}_1$	$\hat{\beta}_2$
L/H MUC	-906	5262	[illegible]	194.9	146861	25372	0.7450	4.1095	0.251	0.026	2.8073	[illegible]
R/H MUC	-1030	5105	137.7	176.2	149447	25800	0.3823	3.1720	0.254	0.027	4.3380	[illegible]
NLC	[illegible]	[illegible]	[illegible]	127.8	[illegible]	3929	0.0062	[illegible].7269	[illegible]	[illegible]	[illegible]	[illegible]

First four moments of S/A loads and S/A deflection at maximum vertical reaction time.

F_s : shock absorber force // S/A ℄.
Q_s : effective structural force ⊥ S/A ℄.
Δl : shock absorber deflection.

MAXIMUM VERTICAL REACTION

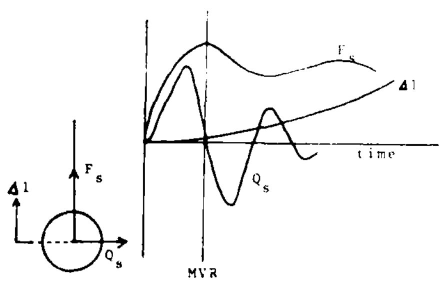

$\delta_{f1} = 42^{o}$ AVERAGE TABLE XVII

n=1482	F_y (N)	s_{F_y} (N)	$\hat{\beta}_1$	$\hat{\beta}_2$	F_s (N)	s_{F_s} (N)	$\hat{\beta}_1$	$\hat{\beta}_2$	Δl (m)	$s_{\Delta l}$ (m)	$\hat{\beta}_1$	$\hat{\beta}_2$
L/H MUC	-4553	6870	10,01	20,273	82820	31390	0,0124	1,5200	0,367	[illegible]	[illegible]	1,0843
	[illegible]	[illegible]	[illegible]	[illegible]	[illegible]	[illegible]	[illegible]	[illegible]	[illegible]	[illegible]	[illegible]	[illegible]
R/H MUC	[illegible]	[illegible]	[illegible]	[illegible]	[illegible]	[illegible]	[illegible]	[illegible]	[illegible]	[illegible]	[illegible]	[illegible]
	4036	6852	4,682	32,956	85420	31759	0,0095	1,4815	[illegible]	[illegible]	[illegible]	[illegible]
NPC	[illegible]	[illegible]	[illegible]	[illegible]	[illegible]	[illegible]	[illegible]	[illegible]	[illegible]	[illegible]	[illegible]	[illegible]
	[illegible]	[illegible]	[illegible]	[illegible]	[illegible]	[illegible]	[illegible]	[illegible]	[illegible]	[illegible]	[illegible]	[illegible]

First four moments of S/A loads and S/A deflection at instant of maximum or minimum side load.

F_y : side load between tyre and ground.
F_s : shock absorber force // S/A $\mathcal{C}$.
Δl : shock absorber deflection.

LATERAL DRIFT

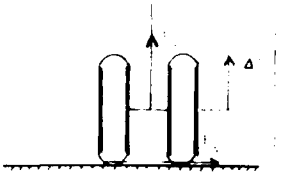

GRAPH 1

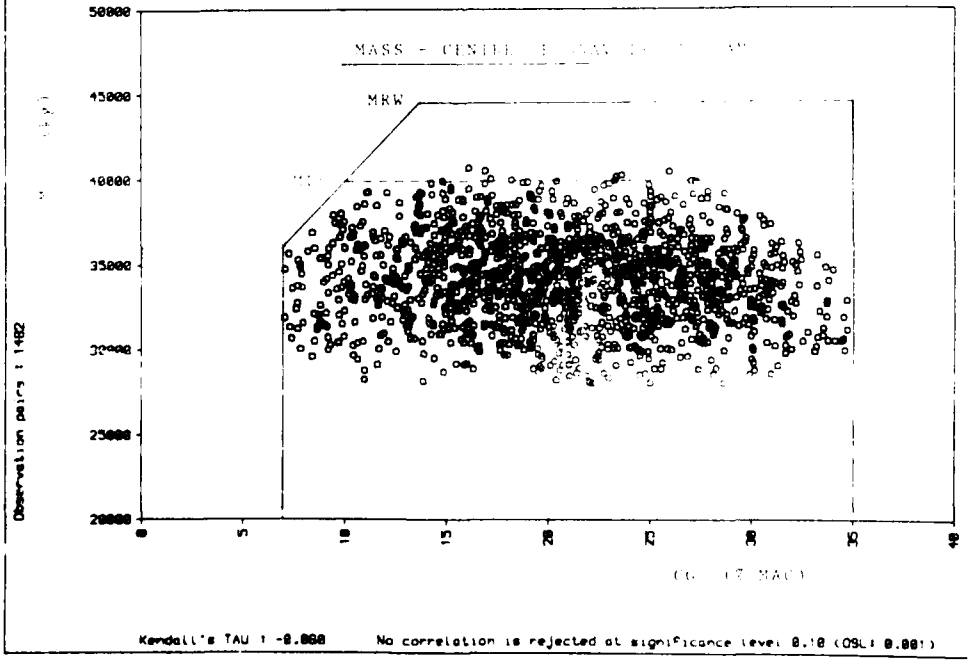

Kendall's TAU : -0.008 No correlation is rejected at significance level 0.10 (OSL: 0.881)

Bending moment at landing gear lower bearing.

δ_{f1} = 42 degr. SNAPH II

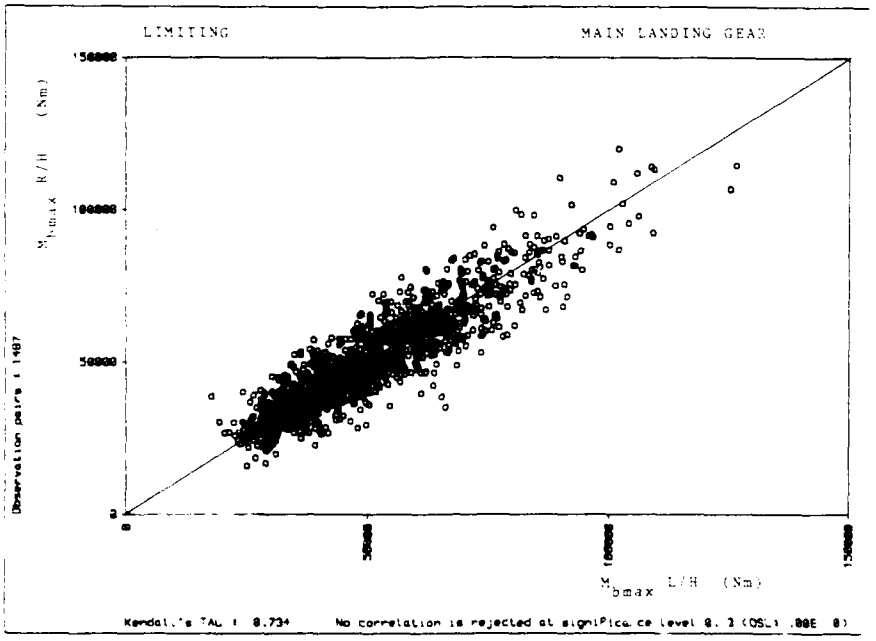

Bending moment at landing gear lower bearing.

δ_{f1} = 23° SNAPH II

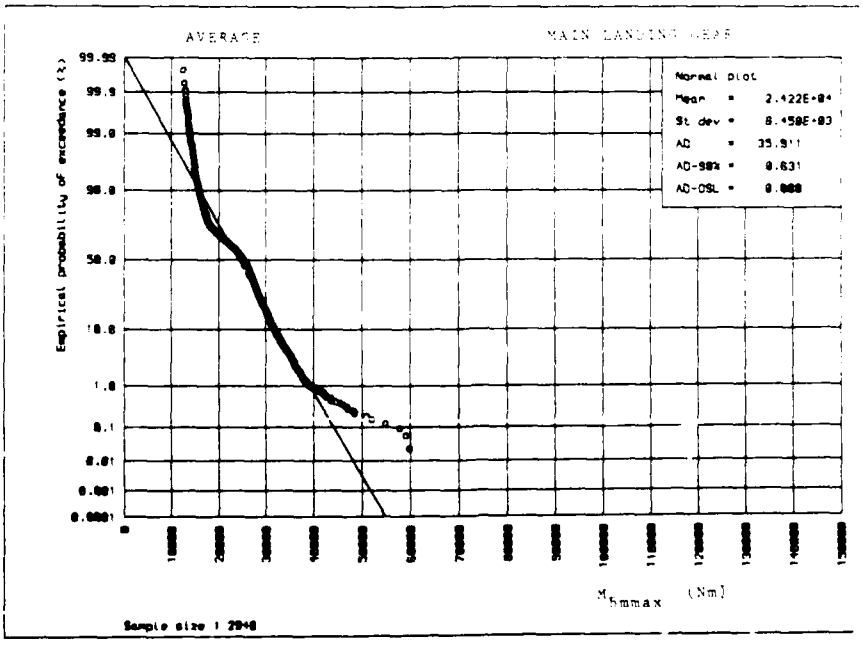

Bending moment at landing gear lower bearing.

$\delta_{r_1} = 25°$ GRAPH IV

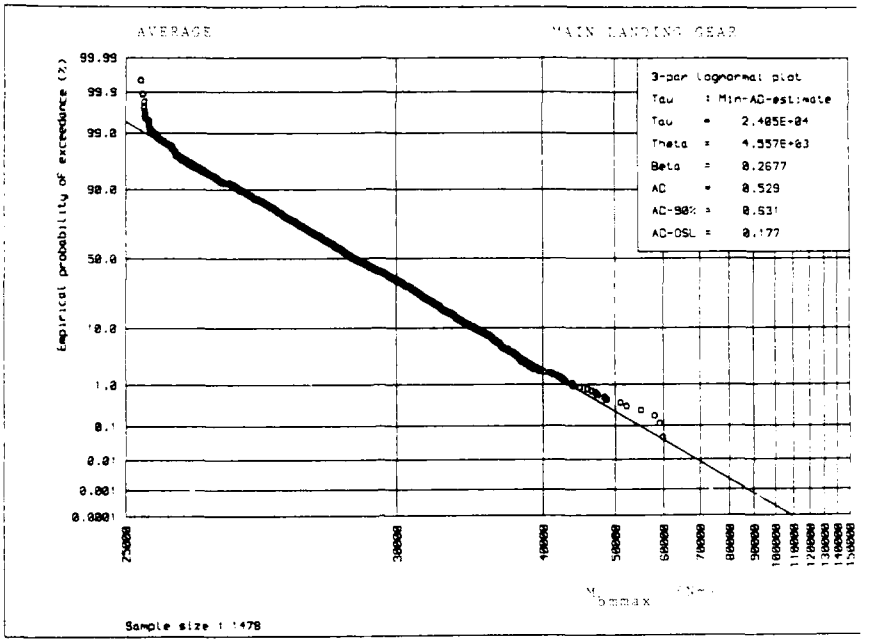

Only upper-half values taken into account

Bending moment at landing gear lower bearing.

$\delta_{r_1} = 5°$ GRAPH V

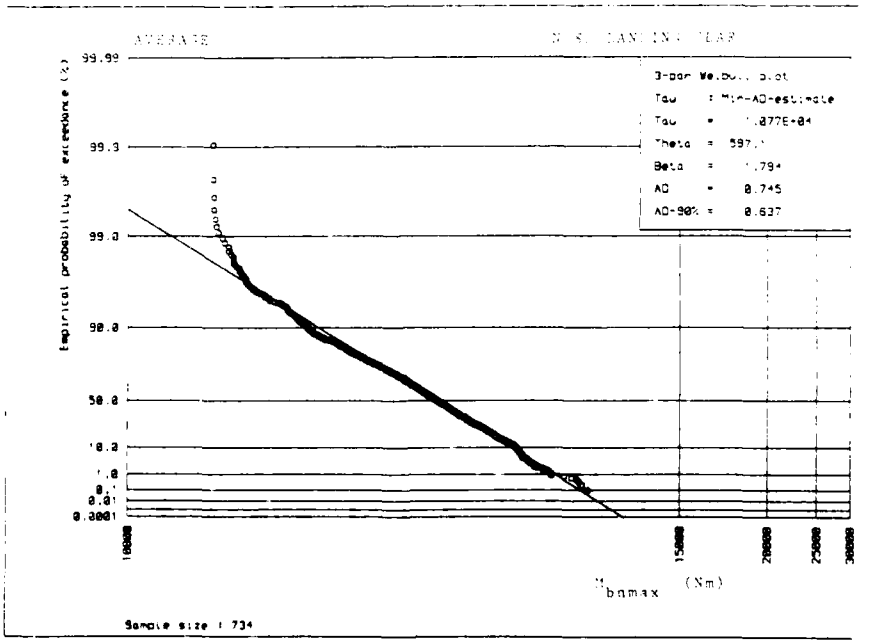

Only upper-half values taken into account

DESIGN LANDING LOADS EVALUATION

BY DYNAMIC SIMULATION OF FLEXIBLE AIRCRAF

by

G.L.GHIRINGHELLI

Dipartimento di Ingegneria Aerospaziale,
Politecnico di Milano, Milano, ITALY

and

M.BOSCHETTO

Air Vehicle Technology Department,
AERMACCHI S.p.A., Varese, ITALY

SUMMARY

This paper presents some significant applications of the integrated system GRAALL (Ground Roll Air And Landing Loads) to the analytical prediction of aircraft landing loads carried out at Aermacchi.
The capabilities of the system, able to treat both rigid and flexible models, make it a tool that can be profitably used during different phases of the design process.
The results reported herein describe the whole development of an actual design application; comparisons between analytical and experimental data are also provided.

LIST OF SYMBOLS

Mlan	design landing weight at gear
Wlan	design landing mass at gear
Vv	design vertical velocity
FVstatic	vertical static load
FVmax	*maximum* vertical load
Sshabs	shock absorber stroke
Stire	tire deflection
Nshabs	shock absorber efficiency
Ntire	tire energy absorption efficiency
Wnose	design mass at nose landing gear
Wmain	design mass at main landing gear
W	aircraft design landing mass
U	friction coefficient
Ki	touch-down load factor
K	design load factor
Ngear	landing gear efficiency
Sgear	wheel axle stroke

INTRODUCTION

The need to satisfy more and more demanding performance requirements in all operational conditions makes integration of all design phases a must for the designers of modern and, in particular, of innovative aircraft.
Landing gear design is no exception in this respect. While still giving due consideration to the general operating characteristics of the system, the landing gear, like any other aircraft system, should not be designed merely to match the airframe, but together with it, with the aim of achieving the optimal solution, while the tendency is often to neglect the landing systems in the early design process.
The assessment of the ground loads and gear structural design are interacting activities, each generating a mutual feed-back. The interactions between aircraft structure and landing gear are also very significant, and the loads applied by the gear are much influenced by aircraft elasticity and gear configuration. It is therefore essential to consider all the effects of structure elasticity and to keep updated the load computational model.
The solution found at Aermacchi, in cooperation with the Department of Aerospace Engineering of the Politecnico di Milano, consists of the system of integrated programs called GRAALL (Ground Roll Air And Landing Loads). This system permits an interdisciplinary exploitation of a single data base so that each engineering area (flight mechanics, flutter, landing gear, etc.) may profitably and timely use the most up-to-date and/or suited structural model.
The first results obtained and a detailed description of the analytical model are given in [1].
This paper provides a model outline limited to the simulation of landing and ground handling, and emphatises the central role of GRAALL as effective working tool for integrated landing gear design.

A set of comparisons between simulation and experimental data from drop tests and landing tests is also provided.

DESIGN PROBLEMS

A possible flow chart of the activities concurring to the full development of design is shown in figure 1. The flow lines are solid for operations and dashed for design loops. The preliminary phase of the study involves the integration of the data from the most important applicable standards and specifications (MIL, AVP, AIR), and the study of the energies involved at touch-down according to the well known relation [6]:

TIRE ENERGY + SHOCK ABSORBER ENERGY + STRUCTURE ENERGY = KINETIC ENERGY

Repeating this computation for different design assumptions permits the ground reaction behavior for changing shock absorber strokes and sink speeds to be assessed.
The obtained charts also enable a first evaluation of the parameters that concur in the definition of the design landing load. Figure 2 depicts a few examples of how the maximum vertical load changes with varying shock absorber strokes and sink speeds.
Two methods may be used to calculate the design load in this phase:

A) the energy balance method; in this case the energy absorbed by each landing gear is:

ENERGY ABSORBED = 1/2*Wlan*Vv**2+(Mlan-Lift)*(Sshabs+Stire)

and the maximum vertical reaction is given by the product of static reaction by the design load factor:

FVmax = FVstatic*K

at this point, if the tire and shock absorber absorption efficiency, drawn from literature or previous experience, is used, it is possible to write:

$$K = \frac{1/2*Vv**2+((Mlan-Lift)/Wlan)*(Sshabs+Stire)}{g*(Nshabs*Sshabs+Ntire*Stire)}$$

B) gear pertaining mass method; based on energy considerations and directions provided by MIL-A-8862, mass can be computed as follows (see fig.3 for geometric parameters):

```
Wnose = W*(Lm+U*H)/Lt                    B1) Wheel spin up
Wmain = (W-Wnose)/2

Wnose = W*Lm/Lt                          B2) Wheel spinning (steady rate)
Wmain = (W-WNose)/2
```

The maximum vertical reaction will, therefore, be given by the product of the above mass by the touch-down load factor:

FVmax = Ku*(Want or. Wpri)

where

Ki = Vv**2/(2*g*Ngear*Sgear)

After calculating the necessary terms, the design load factor can be defined:

K = FVmax/FVstatic

The experience acquired so far has demonstrated that method B is better suited to this phase of design, in which the type of the landing gear is still undefined.
At this stage, there starts an iterative cycle including in the loop draftsmen, system and stress engineers; this aims at producing the first hypothesis of a structural and kinematic solution.
After the system geometry and the order of magnitude of the loads the structure is required to absorb are known, the parameters needed to define the shock absorber model are available. Obviously, the type of shock absorber depends not only on the energy to be dissipated, but also on the landing gear configuration (conventional design, leveled suspension, triangulated), and the choice is very frequently dictated by the need to design a retraction system compatible with the aircraft structural configuration.
In this phase, however, the analysis should not be confined to touch-down, but should encompass also the aspects related to ground handling and bump traversal. This is why there is needed a tool allowing several hypotheses from the different engineering areas (system and stress engineers, etc.) to be analyzed, and able to help design the shock absorbers most suited to the intended configuration. Moreover, if it is considered that many of these parameters are interdependent, it becomes evident that the problem to handle features many variables and calls for a flexible computational procedure, i.e. a procedure that adapts to all interwoven problems and ensures the largest possible integration of the different engineering areas. Failure to integrate would in fact give rise to subsequent design problems able to be removed only through compromise solutions impairing aircraft optimization.

GRAALL SYSTEM (GROUND ROLL AIR AND LANDING LOADS)

GRAALL system enables the determination of the loads acting on an aircraft for many types of maneuvers, taking into due account the flexibility of the structure. It is comprised

of several computer programs and of the interfaces with some other programs used at Aermacchi [2, 3].
A few characteristics of this method are described hereafter and refer to touch-down, ground roll and taxiing only.
GRAALL system can be divided into three main portions (fig. 4):

-structural and aerodynamic modeling, accomplished by use of a finite element program (NASTRAN) (fig. 5) integrated with aerodynamic derivatives for overal motions from an existing data base;
-maneuver simulation, which is performed through an explicit integration procedure based on a fifth order Runge-Kutta Megson method possibly associated, in a hybrid formulation, to Newmark's Beta method for the structural part, both featuring automatic time step control. Symmetric and anti-symmetric landing and/or ground handling on both smooth and bumpy runways, and in-flight maneuvers can be simulated;
-analysis of the results; different types of printouts and plots can be generated, while the most significant parameters may also be analyzed, both versus time or other quantities, in graphic form. Graphic depictions of the aircraft motion can also be obtained, which can be used to produce animations of the complete maneuver.

The analytical model is the result of a hybrid formulation of the problem, which mixes static and vibration modal elements and physical quantities in the description of the aircraft motion that includes rigid motions, elastic modes, landing gear linkage motion and control surface motion.
The aircraft rigid motions consist, in general, of the six degrees of freedom associated to the mean principal inertia axes of the aircraft in the examined configuration.
The formulation permits large rotations to be correctly dealt with.
As far as the elastic modes are concerned, they are considered as small deflections adding up to the rigid motions; besides, they are composed of a set of natural vibration modes, orthogonal to one another and to the rigid motions of the mean axes system, and of a set of static deformation shapes which, conversely, are neither orthogonal to one another nor to the other rigid and elastic modes.
The choice of the deformation shapes is left with the user. They are introduced to speed up convergence in particular as far as the evaluation of stresses or internal forces in presence of large external loads [2], as, for example, the ground reactions on the tires, is concerned. The difficulty to achieve convergence to the exact solution in the modal approach, in particular when the distribution of the loads in the structure depends on high frequency modes (for instance, masses suspended under wing pylons), is, in fact, known.
On the other hand, the modal formulation is the only one to be effectively practicable because of the high number of simulations to be accomplished in the design phases in which the procedure is used; and this is even truer if it is included in an overall optimization process.
Both sets of modes are normalized in amplitude and are determined, together with the main aircraft characteristics, through a finite element model of the examined configuration (extended landing gear and shock absorber compressed at intermediate position).
The modal mass and stiffness matrices of the model are:

$$[M] = \begin{bmatrix} M_{TT} & & & & \\ & M_{RR} & & & \\ & & M_{VV} & M_{VS} & \\ & & & M_{SS} & \\ \text{SIM} & & & & \end{bmatrix} \quad [K] = \begin{bmatrix} 0 & & 0 & & \\ & 0 & & & \\ & & K_{VV} & K_{VS} & \\ & & & K_{SS} & \\ \text{SIM} & & & & \end{bmatrix} \tag{1}$$

where subscripts mean:

T: rigid translational degrees of freedom
R: rigid rotational degrees of freedom
V: natural vibration modes
S: non-natural vibration modes (static deformation shapes)

If the mass and stiffness matrices of the aircraft model are represented by $[M_G]$ and $[K]$, and $[\Phi_s]$ and $[\Phi_v]$ represent the eigenvector matrices including the vectors of rigid motions and static deformation shapes, the modal base described in (1) is determined through:

$$[\Phi] = [\Phi_V \mid \Phi_S]$$

$$[M] = [\Phi]^T [M_G] [\Phi] \tag{2}$$

$$[K] = [\Phi]^T [K_G] [\Phi]$$

The data base contains also the information related to the distribution of displacements and internal forces and/or stresses, corresponding to the modes in $[\Phi]$. These matrices

will be combined through participation coefficients to achieve the correct distribution of displacements and forces for the considered maneuver.
The data base is completed by the matrices necessary for the calculation of the incremental generalized aerodynamic forces in a quasi-steady formulation referred to a trimmed configuration. The coefficients of said matrices are obtained from processings performed on the aerodynamic model by using MSC/NASTRAN flutter procedure 4 , as far as the terms involving elastic modes are concerned, while for aircraft rigid body motions use was made of the aircraft aerodynamic data base. Forces related to elastic modes motion are normally utilized in the simulation of in-flight maneuvers, while their poor contribution to touch-down, ground roll and ground handling response has been verified.
The motion of the landing gear, outlined in figure 6, accommodates large rotations due to the particular type of linkage adopted, and is schematized through the following independent motions:

- motion due to shock-absorber stroke β ;
- steeering motion γ ;
- tire rotation θ .

Rotations β , γ , and θ , which describe these motions are dealt with as independent degrees of freedom of the mechanical system, and are integrated with respect to time. It is worth pointing out that as this description is made with rotation axes and arm dimensions, it can describe also very general landing gear configurations.
The shock-absorber is oleo-pneumatic, and details such as:

- displacement of the air/oil separator piston;
- independent variable flow orifice for extension and retraction strokes;
- variation of the viscous coefficient with cross-section ;

are considered [5, 6, 7].

The degree of freedom related to the rotation of the wheel may be integrated starting from different initial conditions so that drop tests with pre-spun wheel or wheel spin-up in flight, if required, can be simulated.
The computation model of the forces deriving from tire deflection includes the pressure variation effects and realistic models for the evaluation of longitudinal and side friction [8].
The possibility of moving the steering through an open-loop control is provided, and so is the simulation of the control linkage chain through data representative of its compliance and damping.

INTEGRATION IN THE DESIGN FLOW

Figure 3 depicts the flow of activities needed to design a landing gear system to be in turn integrated into the design of the complete aircraft, as obtained based on the experience acquired by AERMACCHI from specific applications and studies in recent years. The solid box indicates the operations of the flow that can be performed by use of GRAALL. A few application examples, and comparisons with experimental data, where available, will be described hereafter, following the flow chart.
The first application of the procedure concerns the definition and refinement of the shock absorber design starting from the results of the preliminary calculations. In this phase it is expedient to simulate a landing gear drop test simply defining the linkage kinematic properties. The effectiveness of the tool allows oleo-pneumatic shock absorbers, with both conventional orifice and variable diameter metering pin, to be studied, thus providing useful indications for improvement of their design.
When a sufficient shock-absorber optimization is achieved, the maximum vertical loads computed in the first analysis can be compared to those obtained with the designed shock absorber. Figure 7 shows the comparison chart.
After all landing gears (nose and main) have been defined, GRAALL can be further used to generate a rigid model of the complete aircraft. This model makes it possible to commence to study the behavior of the complete aircraft in different landing and ground handling conditions, and to start analyzing, in particular, the load increases occurring during operations from roughly repaired runways or traversal of bumpy terrain as defined in the applicable MIL specification.
Figure 8 depicts the results of the simulation and highlights the important role this loading condition may play in the definition of the nose landing gear dimensional characteristics. Note that, in this simulation, the loads acting on the gears are normalized with respect to the corresponding static loads.
Sufficient information for landing gear sizing has thus been collected, and it is possible to proceed to the examination of the single gear drop tests; in this case, the simulated gears are elastic.
A comparison between the maximum vertical load of a rigid model and that of an elastic model is shown in figure 9, related to two different aircraft. It is quite apparent that if, as very often happens, the loads obtained with the elastic model are lower, the designer has two additional options. That is, he can choose to design a structural modification aimed to reduce weight, or decide to expand the landing gear envelope.
The elastic model also allows the assessment of the sensitivity of the drop test results in regard to stiffness of the landing gear attachment to the drop test rig, which must be representative of that of the gear attachment to the aircraft (Fig. 10). This data is needed by the Experimental Department for test rig set-up. A comparison between the results yielded by a rigid attachment, and by an elastic one,is illustrated in figure 11. This figure plots the curve of the loads applied to a structural element, in this case

the drag brace. From the plot, it is possible to observe that the load on the drag brace is higher in the case of an elastic attachment.
Figure 12 shows some comparisons between the axial force on a structural element and vertical load, obtained from the calculations, and the experimental data from the drop tests of the nose landing gear. Figure 13 in turn plots the simulated actual behavior of vertical loads versus shock absorber stroke at two different sinking speeds, for the main landing gear.
An elastic model of the landing gear and an elastic model of the complete fuselage (supplied by the structural analysis engineers) are available at this point; this allows a flexible model of the complete aircraft to be prepared, which can be used to analyze the aircraft behavior during different maneuvers, and to evaluate the final loads.
Thence, not only the time history of the loads applied to the landing gear, but also the stresses acting on all the elements of the complete aircraft model can be obtained.
Figure 14 shows some of the stresses affecting elements of the complete aircraft (fuselage wings and empennages) at touch-down and during the first instants of ground roll.
At this stage, a comparison of the final loads obtained with the complete aircraft elastic model with those assumed in the preliminary phase, may highlight the margins available for possible structural optimizations or improvement of aircraft landing and ground handling performance (Fig. 15).
An experimental test carried out on an aircraft with nose landing gear fitted with strain gages, permitted the loads generated during and after landing with brake application to be acquired; then, through the computer simulation of this landing it was possible to perform a comparison between the theoretical and experimental data, and to evaluate the simulation reliability.
The results of the comparison are given in figures 16 through 18, that show a satisfactory agreement between the numerical and experimental data.

The availability of the aircraft elastic model allows the simulation of entire landing maneuvers, even of those which would be difficult to perform experimentally and a careful evaluation of the extreme operational possibilities without taking up on the burden to carry out experimental tests that can be very hard to set up;moreover the animation of the structural response can be very useful in the analysis of a large amount of data.
Figure 19 displays some frames of the animation developed by using GRAALL; the structural model has been paneled in such a way to pictorially reproduce the actual shape of the aircraft: the figure delineates the maximum stroke condition, the deformation is magnified to highlight its behavior.
At this point, the designer can verify whether there exist problems of taxiing/ground roll instability, and modify the stiffness of some components or study additional damping devices, still in the early design phase.
Fig. 20 shows the conditions for possible shimmy initiation on a conventional design landing gear due to brake application; presently this condition cannot be fully investigated with GRAALL because the available tire model is still unsuited to describe this phenomenon correctly.
Eventually, the flexibility of GRAALL allows collateral problems to be investigated, such as the presence of overswing at touch down or during ground roll/taxiing on bumpy or wavy runways in the case of aircraft with high aspect ratio wings and/or carrying underwing stores: figures 21÷22 shows the time histories of the displacement of the extremities of an underwing store at touch down and bump traversal and the animation of ground clearances during asymmetric landing.

DEVELOPMENTS

It is at present envisaged that the developments of this procedure will occur along three main guidelines:

- description of tire strain through independent parameters, to correctly simulate shimmy phenomena;
- integration in the structural optimization procedure already in use at Aermacchi (3);
- implementation of an active shock absorber and utilization of the integration procedure as an analysis tool in the design of the control system.

CONCLUSIONS

The experience gained with the use of GRAALL for the evaluation of the landing and ground handling loads proved that this system is easy to use, reliable, and is a flexible tool in the hands of the designer. The use of physical quantities in the model contributes to make this system particularly "user-friendly". The designer has in fact in this way an immediate perception of the actual values involved, and only minimal tuning is required to achieve satisfactory results.
The unified approach typical of this method permits the same model to be utilized for the simulation of all types of in-flight and ground maneuvers.
On the other hand, a few critical aspects have emerged:

- the estimate of structural damping to assign to modes: if it is underestimated, the internal forces show increases (decreases are noted if, conversely, it is overestimated), while the kinematic terms and ground forces in the response do not change significantly;

- the selection of the modes to keep in the analysis set: their evaluation as far as the participation coefficients are concerned, is very important for the results it is desired to achieve; these can, in fact, be required in terms of constant response (both kinematic or ground reaction forces), or in terms of internal forces.

Eventually, GRAALL proved to be not only a suitable tool for the determination of the ground loads, but also a simulation procedure fit for many other applications and providing a solution to many of the problems related to the study and development of an aircraft as far as landing, take-off and ground handling are concerned.

REFERENCES

[1] G.L.GHIRINGHELLI, V.GIAVOTTO, P.MANTEGAZZA, M.BOSCHETTO, A.CASAZZA, G.LA PERNA,: "Ground and Manoeuvre Load Prediction of a Flexible Aircraft", l'AEROTECNICA MISSILI E SPAZIO, June 1986

[2] V.GIAVOTTO, P.MANTEGAZZA, T.MERLINI, L.DE OTTO, M.LUCCHESINI, R.MANTELLI: "Fast Flutter Clearance by Parameter Variation", on AGARD-CP-354, 1983

[3] M.LANZ, P.MANTEGAZZA, T.MERLINI, W.BASSO, D.FACCETTI: "An Integrated Methodology for Aircraft Aeroelastic Design", AIDAA Torino, September, 1985

[4] D. BELLINGER: "MSC/NASTRAN Aeroelastic Supplement ", June 1980

[5] E.BAZZOCCHI: "Metodi di calcolo degli ammortizzatori oleopneumatici e confronti coi risultati ottenuti dalle prove", L'AEROTECNICA MISSILI E SPAZIO, 1955

[6] N.S. CURREY: "Landing Gear: Design Handbook", Lockheed, July 1984

[7] J. ROSKAM: "A_plane Design", Vol.4, The University of Kansas, 1989

[8] R.F.SMILEY, W.B.HORNE: "Mechanical Properties of Pneumatic Tyre with Special Reference to Modern Aircraft", NASA TR-R64, 1960

ACKNOWLEDGMENTS

The authors wish to thank prof. V.GIAVOTTO and prof. P.MANTEGAZZA of the Dipartimento di Ingegneria Aerospaziale, Politecnico di Milano, for their precious help, and Mrs. R. Fischer of the Aermacchi Translation Unit for preparing the English text.

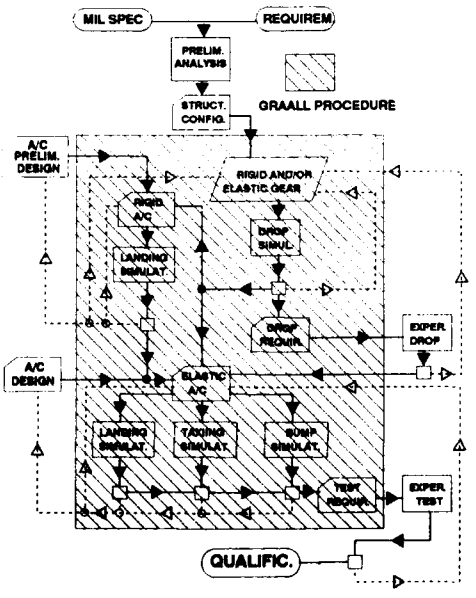

FIG. 1 - Landing system design flow

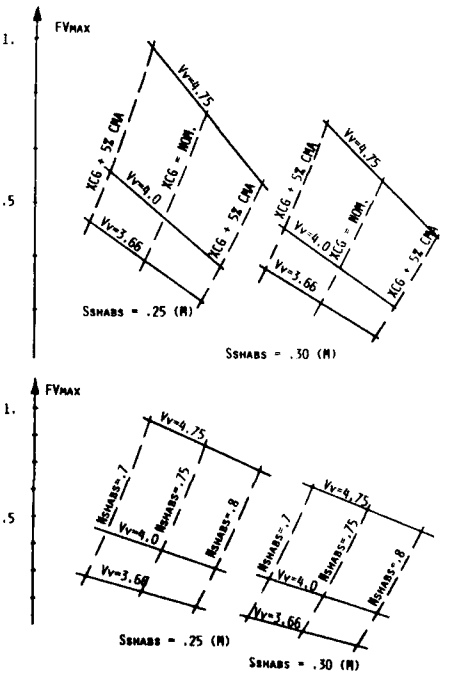

FIG. 2 - Parametric diagrams for gear vertical loads evaluation

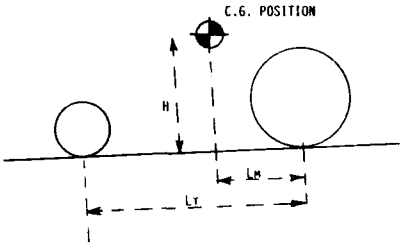

FIG. 3 - Pertaining mass method geometric parameters

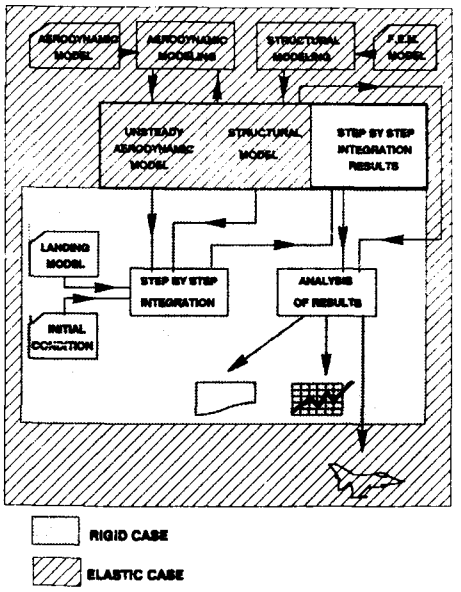

FIG. 4 - GRAALL functional scheme

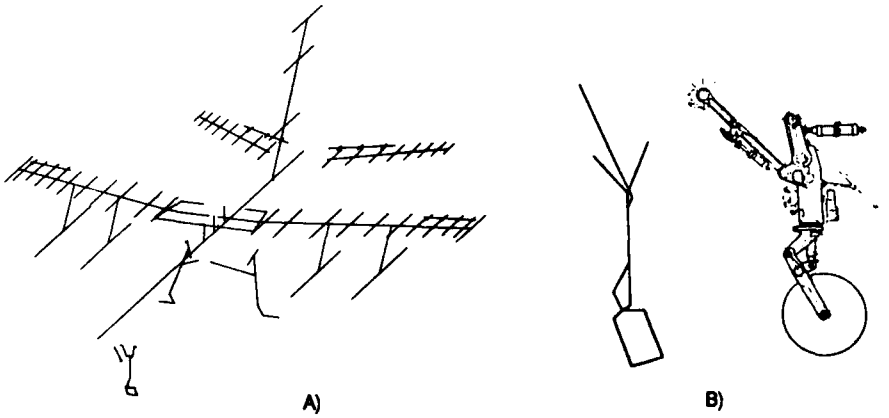

FIG. 5 - F.E. dynamic model: A) complete aircraft, B) gear model for drop test

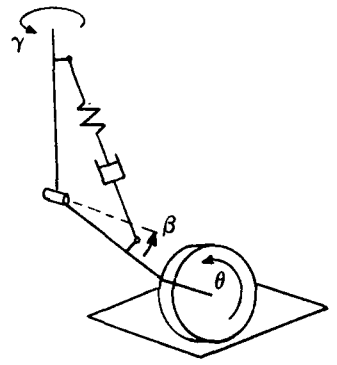

FIG. 6 - Landing gear kinematic scheme

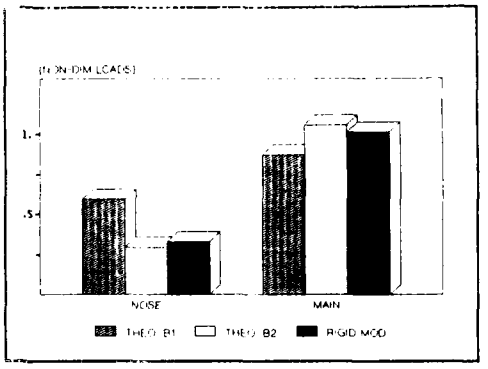

FIG. 7 - Comparison between non dimentional vertical loads in drop test simulation

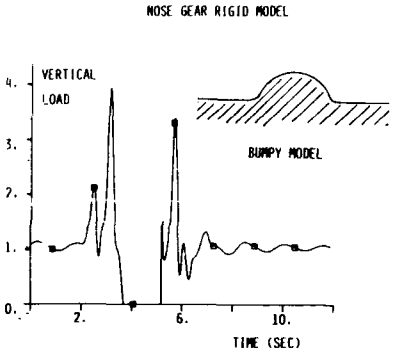

A)

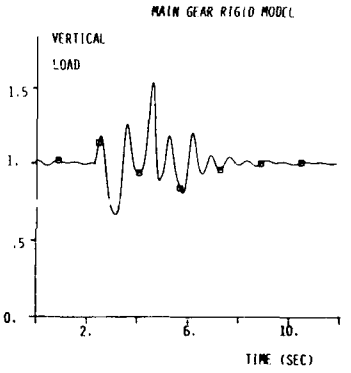

B)

FIG. 8 - Non dimentional vertical load with bump traversal simulation:
A) nose gear , B) main gear

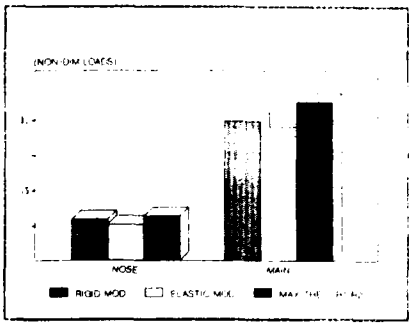

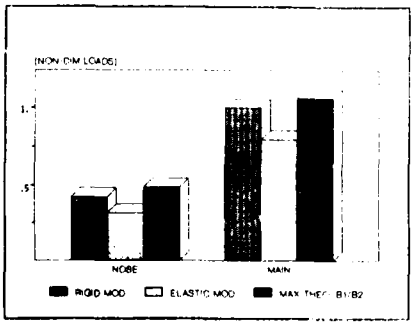

FIG. 9 - Comparison between rigid and elastic model for two different aircraft

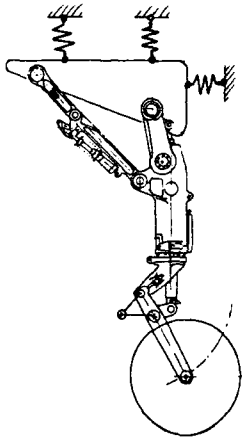

FIG. 10 - Elastic attachement of landing gear in a drop test

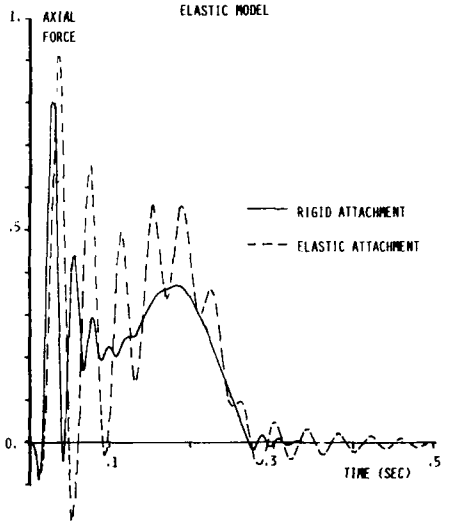

FIG. 11 - Comparison between influence of rigid and elastic attachment in drop test: non-dim drag brace axial force vs time

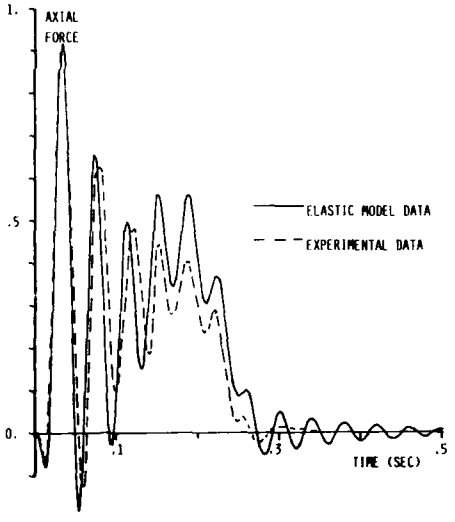

A)

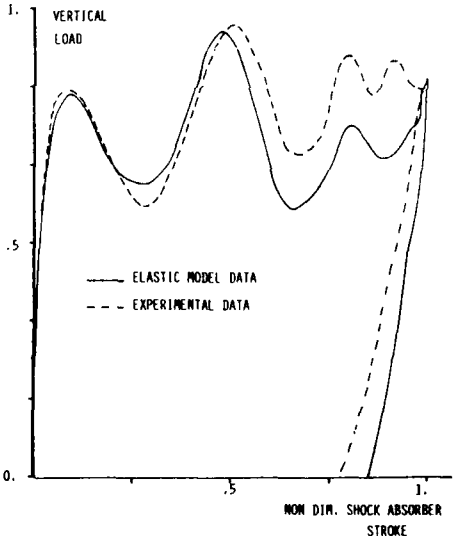

B)

FIG. 12 - Comparison between experimental data and numerical results for a drop test:
A) non-dim drag brace axial force vs time
B) non-dim vertical load vs shock absorber stroke

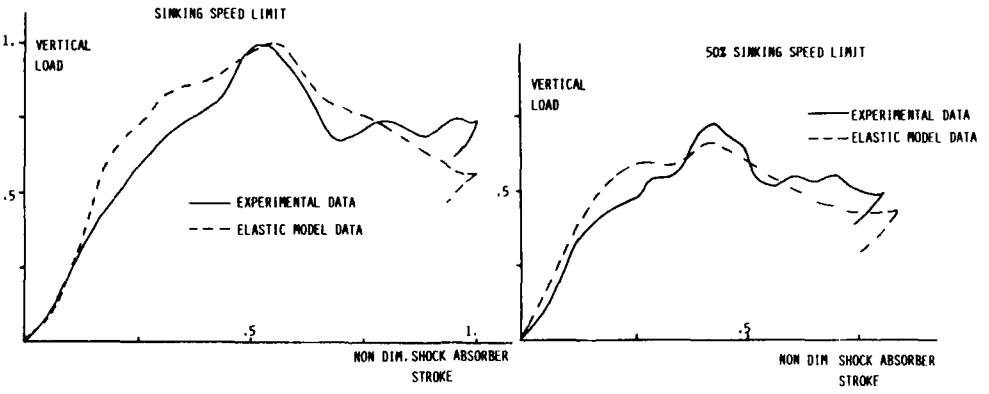

FIG. 13 - Shock absorber functional diagrams for two different sinking speeds, for the main gear

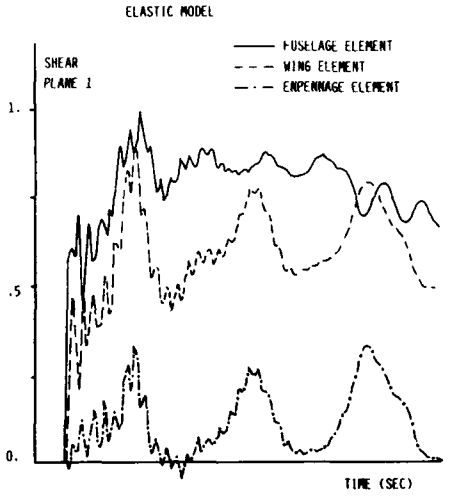

FIG. 14 - Non-dimensional loads in aircraft structural elements

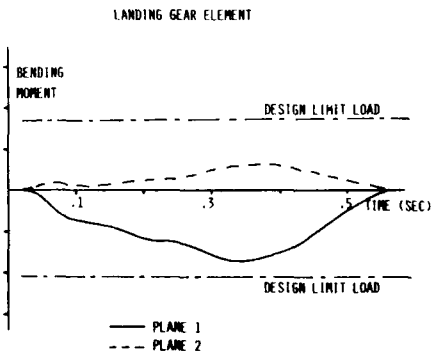

FIG. 15 - Design limit loads verification with simulation results

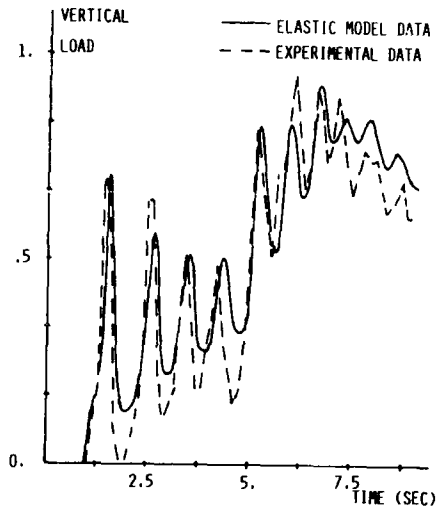

NOSE GEAR

FIG. 16 Comparison between numerical and experimental non-dimensional loads

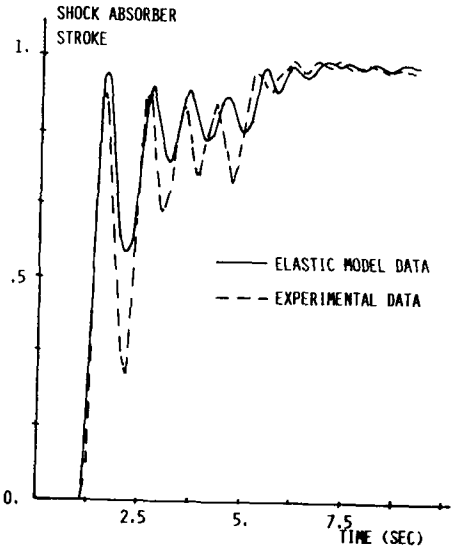

NOSE GEAR

FIG. 17 - Comparison between numerical and experimental non-dimensional nose shock absorber stroke

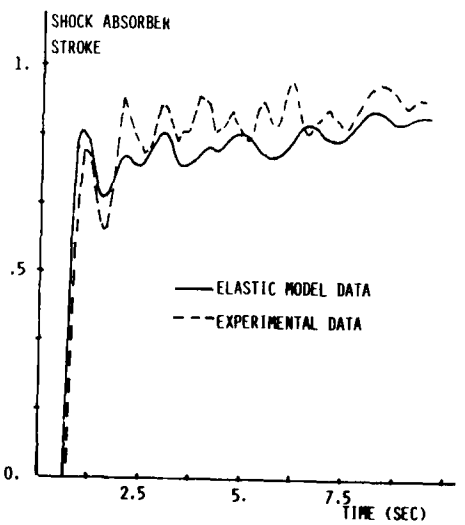

MAIN GEAR

FIG. 18 - Comparison between numerical and experimental non-dimensional main shock absorber stroke

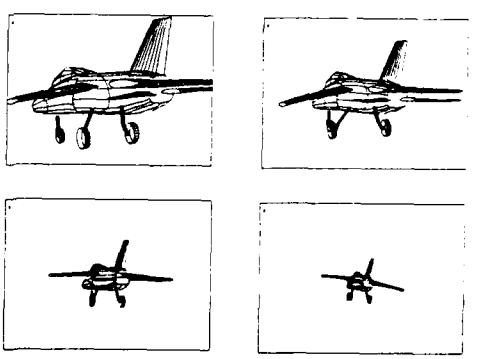

FIG. 19 - Sample frames of an asymmetric landing animation

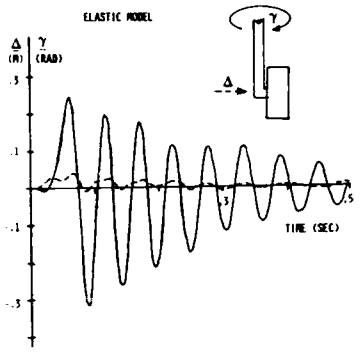

FIG. 20 - Taxiing testing

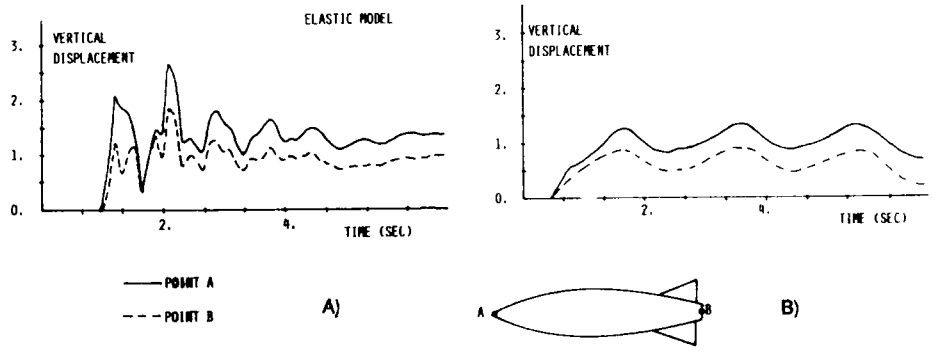

FIG. 21 - Ground clearance of the underwing store:
A) landing simulation B) bump traversal simulation

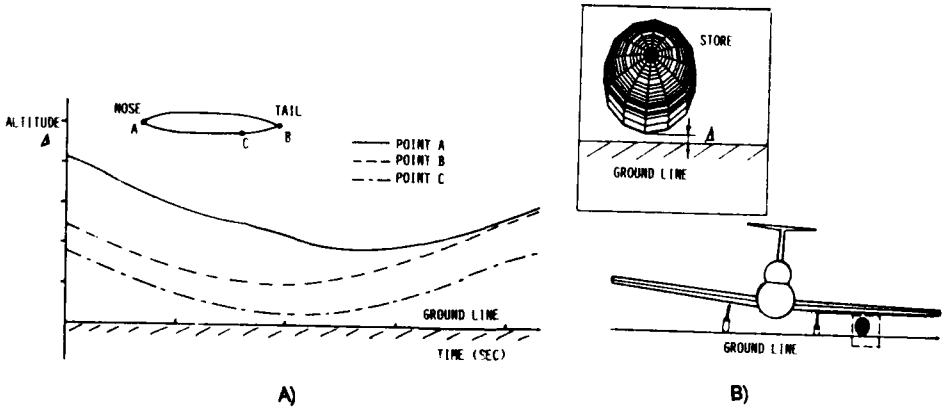

FIG. 22 - Ground clearance of the underwing store:
A) time history
B) worst condition animation representation

F-106B AIRPLANE ACTIVE CONTROL LANDING GEAR DROP TEST PERFORMANCE

William E. Howell, John R. McGehee, and Robert H. Daugherty
NASA-Langley Research Center, Mail Stop 497
Hampton, VA 23665

and

William A. Vogler, Staff Engineer
Lockheed Engineering and Sciences Company
NASA-Langley Research Center, Mail Stop 497
Hampton, VA 23665

SUMMARY

Aircraft dynamic loads and vibrations resulting from landing impact and from runway and taxiway unevenness are recognized as significant factors in causing fatigue damage, dynamic stress on the airframe, crew and passenger discomfort, and reduction of the pilot's ability to control the aircraft during ground operations. One potential method for improving operational characteristics of aircraft on the ground is the application of active-control technology to the landing gears to reduce ground loads applied to the airframe.

An experimental investigation was conducted on series-hydraulic active control nose gear. The experiments involved testing the gear in both passive and active control modes. Results of this investigation show that a series-hydraulic active-control gear is feasible and that such a gear is effective in reducing the loads transmitted by the gear to the airframe during ground operations.

INTRODUCTION

Aircraft dynamic loads and vibrations resulting from landing impact and from runway and taxiway unevenness are recognized as significant factors in causing fatigue damage, dynamic stress on the airframe, crew and passenger discomfort, and reduction of the pilot's ability to control the aircraft during ground operations. The ground-induced structural vibrations on large, flexible airplanes can reduce the pilot's capability to control the airplane during high-speed ground operations. These ground-induced dynamic loads and vibrations are magnified for supersonic-cruise aircraft because of the increased structural flexibility inherent in these slender-body, thin-wing designs. Such operational problems with supersonic-cruise airplanes have occurred at high take-off and landing speeds on some runways which are only marginally acceptable for most subsonic commercial airplanes. One potential method for improving operational characteristics of such airplanes on the ground is the application of active-control technology to the landing gears to reduce the ground loads applied to the airframe.

Previous analytical studies (references 1 and 2) have been conducted to determine the feasibility and potential benefits of applying active load control to the airplane main landing gear to limit the ground loads applied to the airframe. The results reported in reference 2 indicate that a shock strut incorporating a hydraulically controlled actuator in series with the passive elements of a conventional shock strut have acceptable properties and would be quite feasible to implement. Based on the results of reference 2, a modified version of the series-hydraulic active gear which eliminated the actuator and effected control by using a servovalve to remove or add hydraulic fluid to the shock-strut piston (lower cylinder) was analytically and experimentally investigated in references 3 through 6. Based on the results described in these references, the gear from a F-106B was modified for drop tests. The purpose of this paper is to present the results of passive and active drop tests of the F-106B nose gear.

SERIES-HYDRAULIC ACTIVE-CONTROL GEAR

Control Concept

The series-hydraulic control concept limits the gear force applied to the airframe by regulating the damping force (hydraulic pressure) in the piston of the oleo-pneumatic shock strut. To incorporate this active control concept into a conventional gear requires a modification to the gear to control the flow of fluid in or out of the shock-strut with a servovalve. A schematic drawing of a series-hydraulic landing gear that has been fabricated to permit experimental verification of the concept is shown in figure 1. The gear represented is a simple generic oleo-pneumatic shock strut without a metering pin. The control concept is designated series-hydraulic because the control servovalve is in series with the shock-strut piston and hydraulic fluid is removed from or added to the piston to provide force regulation.

The actual gear selected for inclusion of the active control concept was the nose gear of the F-106B with no metering pin. The gear was modified to accommodate the control by adding a three-tube arrangement to the orifice as shown in figure 2. A collection chamber at the top of the 3 tubes connects the fluid in the shock-strut piston to one side of the secondary piston. The other side of the secondary piston is connected to the servovalve. The purpose of the secondary piston is to mechanically limit the amount of fluid that can be taken out or added to the shock strut for flight safety.

The control hardware required for the active gear test program included a 200 GPM (0.76 m^3/min) servovalve, a low-pressure (atmospheric) reservoir, a 9 GPM (0.04 m^3/min) hydraulic pump, a high-pressure (3000 psi (20.7 MPa)) accumulator, an electronic controller, and feedback transducers. The isolation valve allowed isolation of the gear from the control hardware to permit passive gear testing.

System Operation

System operation is briefly described as follows. The electronic controller determines the operational mode (take-off or landing), and implements the control laws. The control laws programmed into the controller are based on the following logic. At touchdown, the controller receives a signal from a transducer to measure the instantaneous sink rate. Assuming a constant mass, the present energy is then calculated. An integration of the acceleration is also begun at this time so that the gear upper mass velocity is known at all subsequent times. As the gear compresses, the remaining work capability of the shock strut is calculated using the instantaneous values of acceleration (or force) and stroke remaining. This remaining work capability is then compared with the present energy of the upper mass calculated using the instantaneous upper mass velocity. When the remaining work capability equals or exceeds the present energy of the upper mass the controller stores in memory the instantaneous value of the scaled acceleration (wing-gear interface force) for use as the impact limit force and activates the servovalve control loop. The controller attempts to maintain this force by removal or addition of hydraulic fluid from or to the oleo-pneumatic shock strut lower chamber. Feedback from the accelerometer provides the controller with a means of determining the difference between the present and the desired force. The slope of the accelerometer output is also used for rate feedback in the control laws, so that if the force is not at the proper level but is tending to return to it on its own, the magnitude of the servo command would be reduced by some amount. Likewise, force trends away from the desired level provoke servo commands larger than would be generated if using force difference alone in the control laws. When the upper mass energy has been dissipated and the sink velocity is nearly zero, the controller linearly transitions the impact limit force to a value of zero for rollout control. During rollout and taxi the controller maintains the wing-gear interface force within a designed tolerance (deadband of ±1750 lbf (±7.8 kN) for these tests) about the static normal force. After control initiation at touchdown, the controller continuously operates with a long-time constant (5 seconds) control to return the gear stroke to the designed static equilibrium position.

EXPERIMENTAL INVESTIGATION

Landing simulation tests (passive and active) with the nose gear from a F-106B fighter interceptor airplane (fig. 3) were conducted at the NASA Langley Research Center to demonstrate the feasibility and the potential of the active gear for reducing ground loads transmitted to the airframe. The vertical drop tests simulated touchdown impact with and without lift.

Drop Tests

A photograph of the test apparatus for conducting the vertical drop tests of the nose gear is shown in figure 4. Additional details of the gear and apparatus are shown in figure 5. Using the drop test apparatus, the nose gear was dropped vertically with simulated lift at 4.5 fps (1.37 m/s) in both the passive and active modes. A 1-g lift simulation was obtained by using crushable aluminum honeycomb to stop the drop carriage (upper mass) vertical acceleration. The chosen test condition is representative of the airplane being derotated at a high pitch rate. A second test of the gear was also conducted at a vertical speed of 2.5 fps (0.76 m/s) without lift. Without lift applied, vertical speeds higher than about 2.5 fps (0.76 m/s) would cause the gear to bottom out. Such a drop test is representative of losing pitch control during derotation.

A comparison of the measured upper mass acceleration for the active versus passive gear without lift is shown in figure 6. Significant events such as drop carriage release, free fall, tire impact, and control activation are indicated in the figure. A 47% decrease in upper mass acceleration was obtained with the active control gear. The decrease in acceleration translates to a 47% decrease in the amplitude of forces transmitted to the airframe. For the 2.5 fps (0.76 m/s) vertical drop without lift, the passive gear stroke shown in figure 7 nearly bottomed out; consequently, the active gear stroke was essentially the same as for the passive gear case. Upper mass acceleration data for a 4.5 fps (1.37 m/s) drop with lift are shown in figure 8. A 36% decrease in the transmitted force was obtained with the active gear. As shown in figure 9, there was a 10% increase in the strut stroke associated with the active control.

CONCLUDING REMARKS

A potential method for improving the operational characteristics of aircraft on the ground by the application of active-control technology to the landing gears to reduce ground loads applied to the airframe has been investigated. An experimental program was conducted on a series-hydraulic active-control nose landing gear from a F-106B fighter interceptor aircraft involving both passive and active control modes. Results of the investigation show: (a) That such a concept can be achieved through modification of existing hardware, and (b) that the concept is effective in significantly reducing the loads transmitted by the gear to the airframe during landing and ground operations.

REFERENCES

1. Wignot, Jack E.; Durup, Paul C.; and Gamon, Max A.: Design Formulation and Analysis of an Active Landing Gear. Volume I, Analysis. AFFDL-TR 71-80, Vol. I, U.S. Air Force, August 1971. (Available from DDC as AD 887 127L.)

2. Bender E. K.; Berkman, E. F.; and Bieber, M.: A Feasibility Study of Active Landing Gear. AFFDL-TR-70-126, Air Force, July 1971. (Available from DDC as AD 887 451L.)

3. McGehee, John R.; and Dreher, Robert C.: Experimental Investigation of Active Loads Control for Aircraft Landing Gear. NASA TP-2042, 1982.

4. Morris, David L.: Active Landing Gear Response Testing. ADWAL-TM-82-177-FIEM, U.S. Air Force, April 1982.

5. McGehee, John R.; and Morris, David L.: active Control Landing Gear for Ground Load Alleviation. AGARD-CP-384, pp. 18-1 through 18-12, March 1985.

6. Morris, David L.: F-4 Active Control Landing Gear Dynamic Response Testing. AFWAL-TR-85-3005, Air Force, August 1985. (Available from DDC as AD-B096481L.)

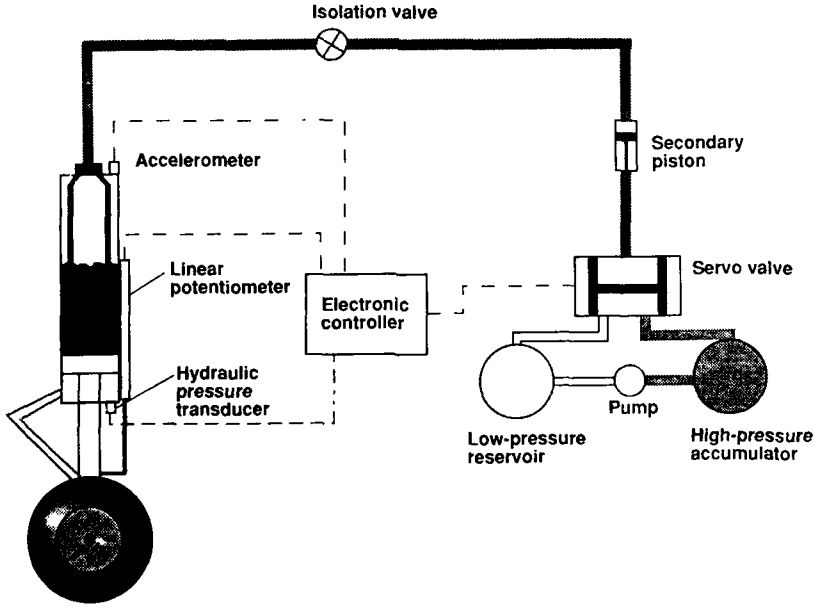

Figure 1. Schematic of series-hydraulic active control landing gear.

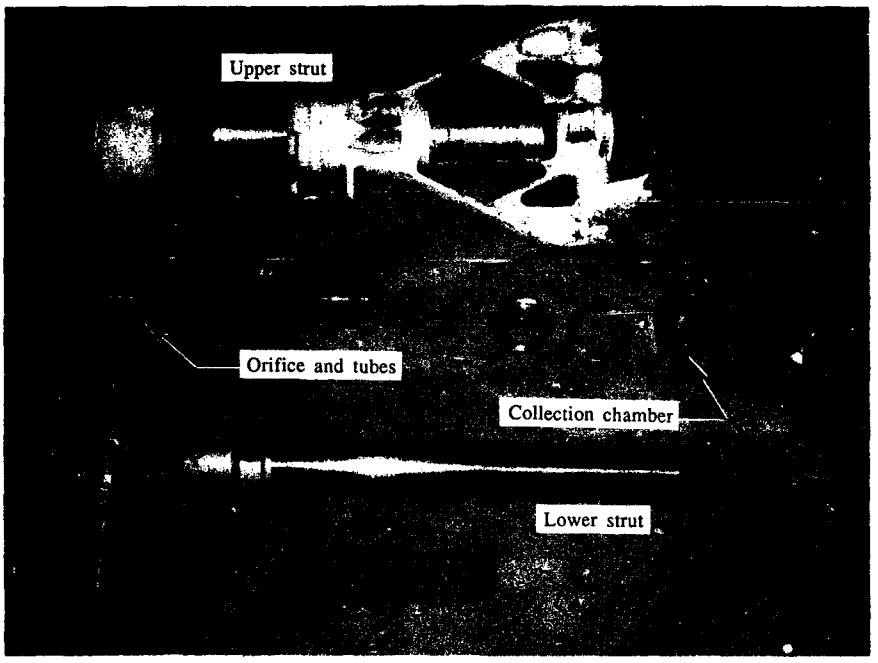

Figure 2. Disassembled, modified F-106B nose gear.

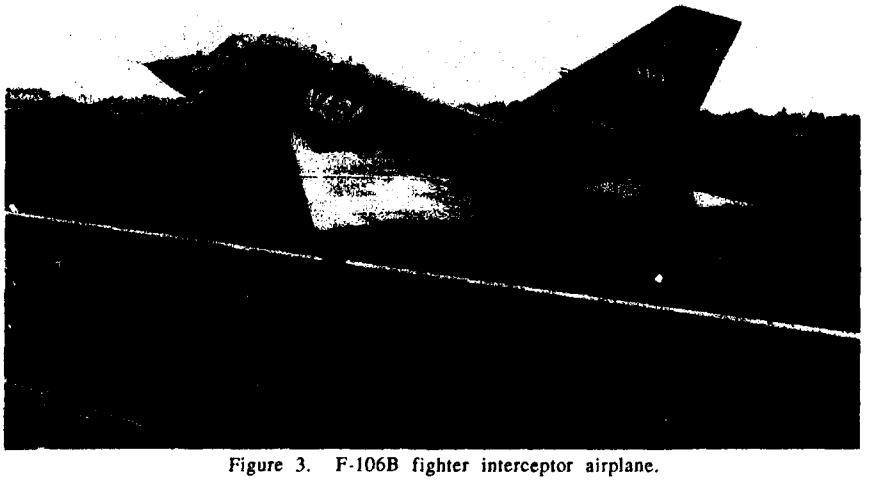

Figure 3. F-106B fighter interceptor airplane.

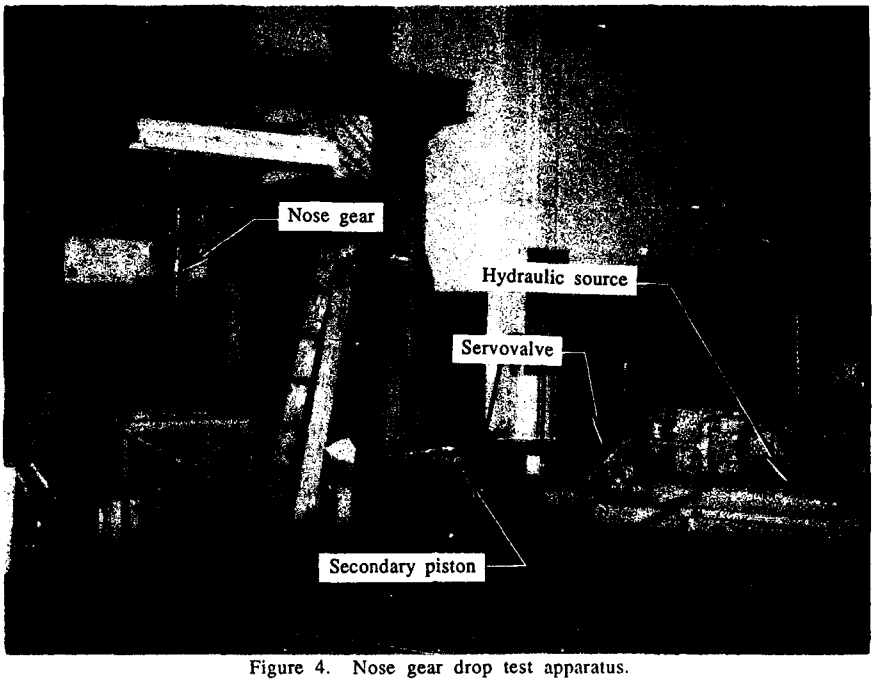

Figure 4. Nose gear drop test apparatus.

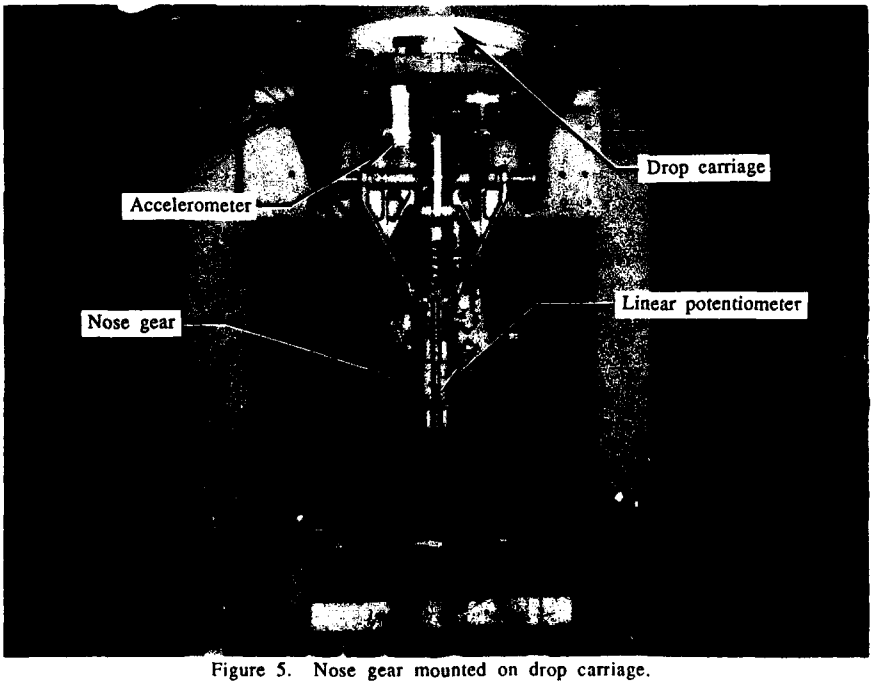

Figure 5. Nose gear mounted on drop carriage.

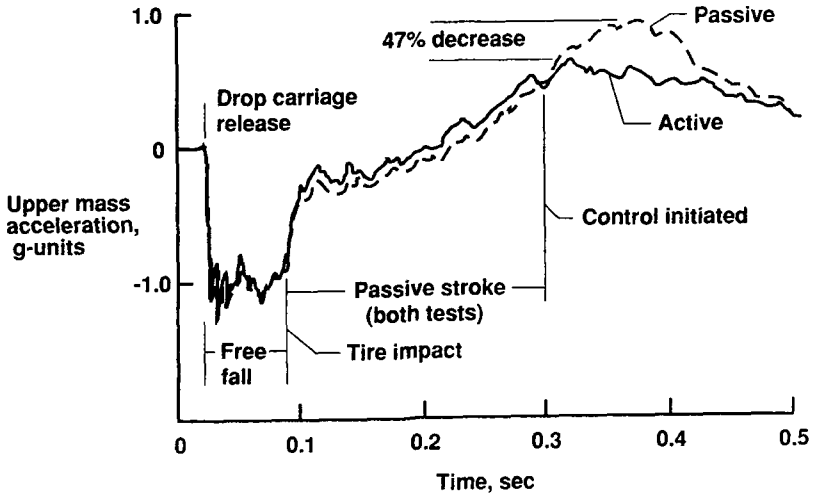

Figure 6. Comparisen of passive and active control accelerations for vertical drop of nose gear at 2.5 ft/sec (0.76 m/sec) without lift.

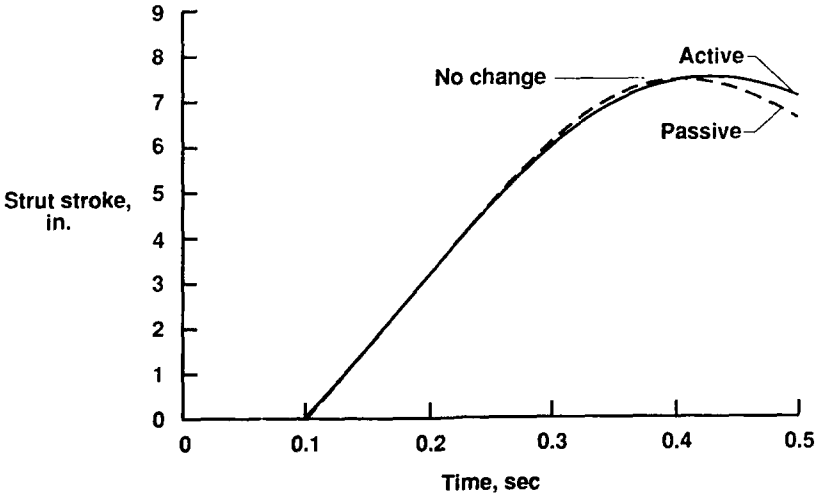

Figure 7. Comparison of passive and active control strut stroke for vertical drop of nose gear at 2.5 ft/sec (0.76 m/sec) without lift.

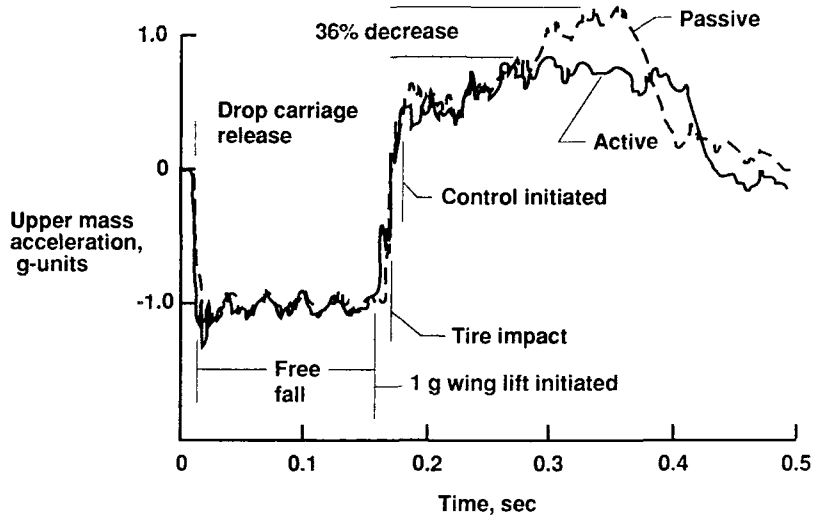

Figure 8. Comparison of passive and active control accelerations for vertical drop of nose gear at 4.5 ft/sec (1.37 m/sec) with lift.

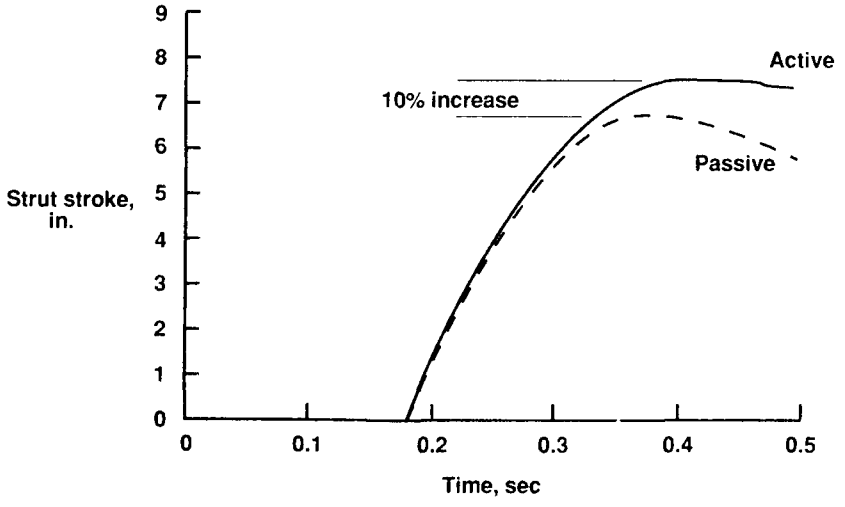

Figure 9. Comparison of passive and active control strut stroke for vertical drop of nose gear at 4.5 ft/sec (1.37 m/sec) with lift.

ACTIVELY DAMPED LANDING GEAR SYSTEM

by

Dr-Ing. Raymond Freymann
Division Chief, Structural Dynamics and Acoustics
BMW AG – EW-5
Postfach 40 02 40
8000 München 40
Germany

Abstract

An active control undercarriage for the alleviation of aircraft landing gear and structural loads during operation on rough runway surfaces is described. For quantitative determination of the improvements obtained with an active control undercarriage compared with conventional landing gear systems, aircraft taxiing is realistically simulated by means of a laboratory test set-up especially designed for this kind of testing.

1. Introduction

Since many years the NATO countries have been concentrating on the problem of how to improve the capabilities of aircraft to operate from damaged/repaired runways. The background and the goal of the thus related work is to guarantee the readiness of aircraft even in the event of an airfield attack.

The many investigations performed have indicated that among others a considerable effort has to be placed in the development of advanced landing gear systems for improvement of the aircraft structural dynamic response behavior when taxiing on rough runway surfaces. With regard to the landing gear system this especially implies to prevent the bottoming of the struts when encountering a series of discrete obstacles located at worst spacing conditions [1]. It has repeatedly been shown - by tests [2] and analyses [1] - that the dynamic landing gear and aircraft structural loads encountered during realistic taxi phases on damaged/repaired runways can significantly exceed the specified landing impact loads [3,4,5], thus becoming the most critical ultimate or fatigue landing gear design loads.

With regard to a satisfactory performance of aircraft in the case of rough runway conditions, it is of primary importance to design an aircraft which can meet both the landing impact and rough field operational requirements. Despite the partly conflicting landing gear design criteria resulting from the touchdown and taxi load cases, it will always be possible to reach a compromise when laying out the undercarriage. However, the (passive) landing gear construction obtained in this way cannot be regarded as a minimum weight or size design. This disadvantage can be avoided by fitting the undercarriage with an active control system. An active control undercarriage can, to a large extent, adapt a (conventional) landing gear system to the rough field conditions without modifying its touchdown impact characteristics. Starting from a conventional layout of a landing gear system, i.e. a passive undercarriage design considering the touchdown impact as the most critical design load case, it will be shown below, the extent to which the dynamic landing gear and consequently the aircraft structural loads encountered during aircraft taxi on rough runway surfaces can be reduced by the implementation of active control systems. Thereby special focus is pointed on the alleviation of the aircraft landing gear and structural loads when taxiing on a minimum operating strip [6] of a runway scattered with repairs of a significant height, e. g. a series of AM-2 mats [7], located at worst spacing conditions.

Finally it must be explicitly mentioned that this paper does not concentrate on the task to reduce landing gear loads at touchdown by making use of the "almost unlimited" possibilities offered by active control systems.

The basis of the work described in this paper has been elaborated by the author at the DLR-Institute of Aeroelasticity in Göttingen (Germany) as well as at the Air Force Flight Dynamics Laboratory at Wright-Patterson Air Force Base in Dayton (Ohio) and has already been partly published in Refs. [8,9,10].

2. Aircraft Dynamic Response to Runway Roughness

This chapter is intended to give the reader a clear understanding of the formation of the dynamic response of aircraft taxiing on rough runway surfaces. It is not the intention of the author to present here quantitative results from (complicated) dynamic response analyses performed in the time domain on a nonlinear multi degree-of-freedom rigid body/flexible aircraft structural system running over a runway surface with a random shaped roughness profile. Detailed investigations with regard to the handling of this problem have been described in [1] and [9]. But, as was shown in [11], quite simple analytical considerations carried out on a linear one degree-of-freedom oscillator can shed light on the special dynamic response problem we have to deal with here.

Thus, according to this simple mathematical model, the basic mathematical considerations denoted below are based on the following assumptions:

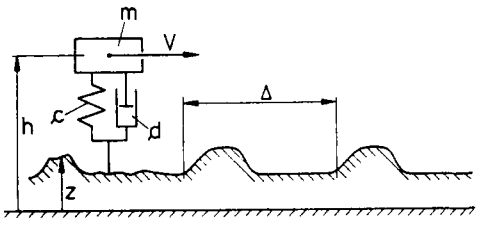

Fig. 1: One degree-of-freedom oscillator taxiing on a rough runway surface

a) The aircraft motion is restricted to its rigid body heave degree-of-freedom which is idealized by the linear single degree-of-freedom oscillator depicted in Figure 1.

b) The stiffness of the (main) landing gear system with its nonlinear polytropic characteristic is linearized in the static working point.

c) The nonlinear damping force, originally being a quadratic function of the velocity of the landing gear elongation, is assumed to be of viscous nature.

d) The stiffness characteristic of the tire is neglected in the calculations. This simplification is tolerable in so far that we are primarily focussing here on the low frequency range related to the aircraft rigid body motion where the dynamic structural behavior of the tires is of minor importance.

In the time domain the equation of motion of the oscillator can be formulated as follows:

$$(1) \qquad m\ddot{h}(t) + d\dot{h}(t) + ch(t) = d\dot{z}(t) + cz(t) \quad .$$

In Equation (1), m is the oscillator mass, d the viscous damping and c the stiffness

of the landing gear strut; h(t), $\dot{h}(t)$, $\ddot{h}(t)$ designate the vertical displacement of the oscillator mass, its velocity or acceleration, respectively; z(t), $\dot{z}(t)$ characterize the runway roughness and its derivative with respect to time t. As shown in [11], this equation can be used as a basis for calculating the (acceleration) response of the oscillator when encountering successive discrete runway disturbances. The most interesting result from these investigations consists in the definition of a factor, the so-called "bump multiplier" M_Δ, which is defined as follows:

$$(2) \qquad M_\Delta = \sqrt{1 + E_\Delta^2 + 2 E_\Delta C_\Delta}$$

with

$$(3) \qquad E_\Delta = e^{-\zeta \omega_\Delta^*} ,$$

$$(4) \qquad C_\Delta = \cos \omega_\Delta^* \sqrt{1 - \zeta^2} ,$$

$$(5) \qquad \omega_\Delta^* = \omega_0 \cdot \Delta / V ,$$

Δ being the bump spacing according to Figure 1, V the aircraft taxi speed, ζ the damping ratio (relative to the critical damping value $\zeta_c = 1$) and ω_0 the natural circular eigenfrequency of the oscillator system. The bump multiplier defines the extent to which a second discrete disturbance amplifies or attenuates the maximum dynamic response of the oscillator to the first disturbance. Equation (2) is valid under the assumption that the two successive disturbances are of a similar shape.

Experimental investigations *[2,12] have shown that the definition of a bump multiplier* is significant in that a conventional landing gear, primarily designed to absorb the aircraft kinetic energy at touchdown, can pass discrete single obstacles with a significant roughness amplitude at all taxi speeds. But the tests also revealed that the aircraft, due to bottoming of the landing gear struts, could not traverse a series of successive discrete obstacles at well-defined "critical" speeds, even in the case that the roughness level was rather small.

Figure 2 depicts the bump multiplier M_Δ as a function of the reduced frequency parameter ω_Δ^*. The plot indicates that, in the case of a second discrete disturbance, we obtain a maximum response in the translatory degree-of-freedom of the oscillator of interest when this disturbance is located at a critical spacing

$$(6) \qquad \Delta = 2k\pi \frac{V}{\omega_0} , \quad (k = 1,2,3,\ldots)$$

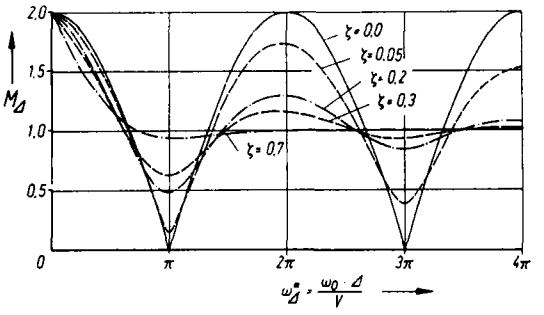

Fig. 2: The bump multiplier for equal obstacles

from the first obstacle. Minimum response occurs if the spacing is

$$(7) \qquad \Delta = (2k - 1)\pi \frac{V}{\omega_0} , \quad (k = 1,2,3,\ldots) .$$

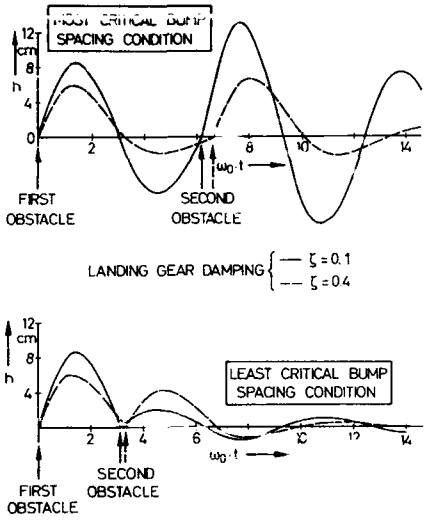

Fig. 3: Calculated dynamic response of the one d.o.f. oscillator to two successive runway obstacles

Furthermore it is obvious that a high damping of the oscillator system can considerably reduce the high values of the bump multiplier in the range of $\omega_\Delta^* = 2k\pi$. To further illustrate this dynamic response/obstacle spacing interrelation, Figure 3 depicts the dynamic response h in the time domain of the oscillator to two successive runway obstacles at the most and the least critical spacing. Worst spacing conditions are characterized by the fact that the oscillator hits the second obstacle when its upward speed $\dot{h}(t)$ reaches its maximum. On the other hand least critical conditions occur when the second bump is hit at a moment of the greatest downward speed of the oscillator. Due to the higher damping value, the decay per unit time of the oscillator dynamic response is more significant. This entails that, in the case of worst spacing conditions, the (initial) upward speed of a highly damped oscillator is smaller than in the case of a system with low damping when encountering the second obstacle and consequently its maximum dynamic response (to the second obstacle) will be lowered.

Application of the results obtained from the example of the one degree-of-freedom oscillator to the example of a complete aircraft structure, which generalized equations of motion are denoted in [9], now leads to the following statements:

When an aircraft is operating on rough surfaces,

1. a high dynamic response in its (rigid body) degrees-of-freedom must be expected when the runway roughness exhibits major obstacles which - in connection with the eigenfrequencies of the various eigenmodes and a range of defined taxi speeds - are located at critical spacings Δ as defined by Equation (6),

2. the dynamic response in the various eigenmodes can be lessened by a higher damping of the undercarriage.

Operating aircraft on unprepared runway surfaces entails that we do not have any influence on the distribution (e.g. critical or non-critical spacing) of major obstacles. Thus, according to the definition of the bump multiplier, the only parameter we can influence to improve the operational capabilities of aircraft on rough runway surfaces is the damping of the undercarriage.

3. Contradictory Requirements for the Design of Undercarriage

As mentioned in the foregoing chapter, a high damping of the landing gear system is beneficial to the taxi capabilities of aircraft when operating on rough runway/unprepared surfaces. High damping values, however, are adverse to a satisfactory design of the landing gear with regard to the touchdown impact. Because the touchdown phase is of extremely short duration, the landing gear loading, due to the damping forces

$$(8)\quad F_d(t) = d \cdot \dot{h}(t) \quad ,$$

can reach extreme values in the case of a (too) large damping factor d. This also applies to the case when the aircraft, operating in its taxi mode, hits a high amplitude obstacle which has a sharp shoulder, hence inducing a high roughness velocity $\dot{z}(t)$ (see Eq.(1)). Due to this fact the damping of landing gear systems must be kept small at least in the compression phase of the shock absorber. To provide, despite this requirement, a landing gear with good energy dissipation characteristics, the practical design of an undercarriage is achieved so that its damping characteristics vary during the compression and recoil phases. Real landing gear systems feature a ratio of about 20 to 30 between their recoil and compression damping factors d_{RECOIL} and d_{COMP}.

Bearing in mind the different curves for the bump multiplier, depicted in Figure 2, it is obvious that this small value of d_{COMP} is highly adverse to the dynamic response behavior of aircraft during tough runway operations. In order to realize both good touchdown and rough runway perfomance of aircraft undercarriage, a landing gear system must be designed which features low damping characteristics in the compression phase with regard to the touchdown impact and the encounter of single high amplitude (short wave) obstacles with a sharp shoulder, and, in accordance with the bump mulitplier, high damping characteristics with regard to the aircraft's taxi capabilities over multiple (long wave) obstacles.

The next chapter will show the extent to which both of these requirements can be fulfilled by the implementation of active-controlled systems into the undercarriage.

4. Active-Controlled Landing Gear

Figure 4 shows two different designs of landing gear systems. On the left-hand side a sketch of a conventional (passive) one-stage oleo-pneumatic shock absorber is depicted. The right-hand side gives a schematic view of an active-controlled landing gear. Fitting the strut with an electrohydraulic servovalve, hydraulically connected to the aircraft oil pressure and return pipes, allows hydraulic oil to be added to or removed from the (upper) strut chamber located between the pneumatic volume and the damping valve. This sytem allows arbitrary forces to be produced in the landing gear strut by feeding the electrohydraulic servovalve with a well-defined electric set-point signal.

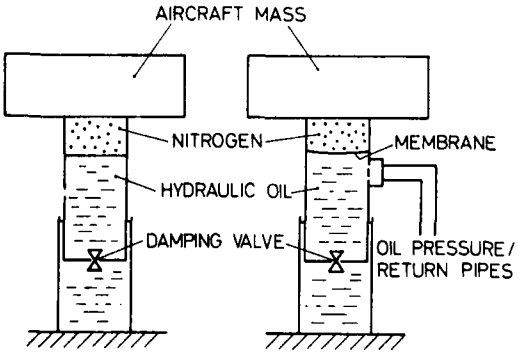

Fig. 4: Passive and active one-stage landing gear system designs

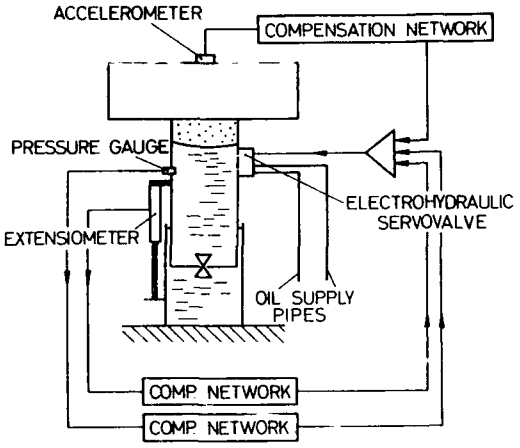

Fig. 5: Active control landing gear system layout

In order to create damping forces in the active shock absorber, the system must be operated in a closed control loop, as depicted for instance in Figure 5 in the case of the one degree-of-freedom oscillator. Thereby an accelerometer detects the dynamic motion of the (aircraft) mass. The electric signal is then fed through a compensation network to the electrohydraulic servovalve which hydraulically activates the landing gear strut. The compensation network can be considered correctly adjusted with regard to the creation of damping forces if the additional internal strut forces produced are in phase with the velocity of the (aircraft) mass on top of the active shock absorber.

Operation of the landing gear in a closed-loop control system allows a very selective damping control to be achieved. In order not to increase the transient (short wave) landing gear loads at touchdown and upon encountering sharp-edged, high-amplitude obstacles, which are characterized by a broad band amplitude spectrum, a low-pass filtering element is included in the compensation network. This precaution guarantees that the dynamic response of the aircraft in the higher frequency range is not fed back to the servovalve and thus not affected by the active control system. To reduce the maximum values of the bump multiplier, extensive damping must be achieved in the (long wave) frequency band adjacent to the rigid body heave frequency of the one degree-of-freedom oscillator. By the implementation of a band-pass filtering element into the compensation network, a pronounced control can be realized in this frequency range. Moreover the characteristics of this element allow any long term (sensor) zeroing errors in the control loop to be suppressed.

Up to this point the active control system for alleviation of the landing gear loads has been described. The operation of the active shock absorber, however, requires the implementation of two additional loops with regard to the static control of the landing gear working point. This reference point is characterized by the following two parameters: the reference elongation of and the reference pressure in the strut. These reference values refer to the static landing gear state with the (oscillator) mass resting on top of the strut. Typical values for real landing gear are in the range of 50 bar for the pressure and 0,2 m for the elongation, if the fully collapsed strut position is considered to be the state of zero-elongation.

The two loops for achievement of the static landing gear control are depicted in Figure 5. A low-pass filtering element with a very low cut-off frequency ($f_c < 0.5$ Hz) is included in both of the loops. This element is required to avoid any feedback from the static control loops in the higher frequency range, which is intolerable since it would cause an enormous stiffening of the strut (as in the case of servocontrolled actuator systems [13]). Furthermore it is of primary importance to provide the strut positioning control loop with a priority on the pressure feedback loop. This entails that, during the take-off-phase, the landing gear will remain in a position adjacent to its reference elongation, even in the case where the landing gear loading is significantly reduced by the aircraft lifting forces.

Having explained the basic functioning of an active-controlled landing gear by means of the example of the one degree-of-freedom oscillator shown in Figure 5, we can now concentrate on the more complicated system consisting of the entire aircraft resting on its undercarriage. Figure 6 shows the way in which the overall rigid body dynamic response behavior of aircraft operating on rough surfaces can be controlled and thus improved by a feedback of the aircraft vertical, pitch and roll motions or of the corresponding velocities or accelerations. Aircraft pitch control is achieved by a feedback of the pitch motion to the active-controlled nose landing gear. The rigid body heave control is realized by an in-phase activation of the active-controlled main landing gear struts, using the aircraft CG heave motion as a feedback control signal. Roll control is achieved by a feedback of the aircraft roll motion, the signal of which, fed through the compensation network, activates the main landing gear struts by phase-opposed signals. As in the case of the one degree-of-freedom system, the layout of the entire compensation network can be considered satisfactory, when the **additional dynamic forces** produced by the various feedback control loops in the struts of the undercarriage **are in phase with the velocities of the respective aircraft motions** they are intended to control.

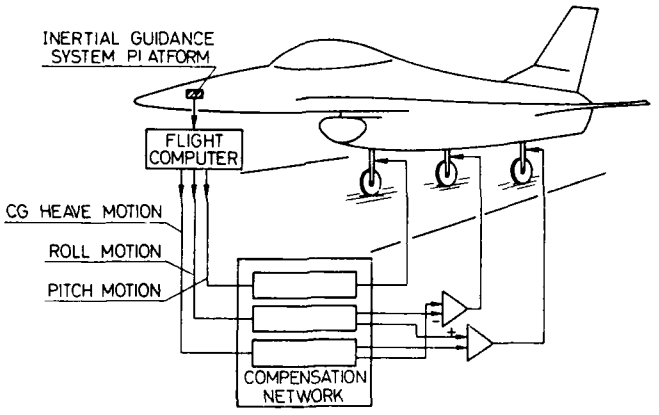

Fig. 6: Load alleviation system acting on the aircraft undercarriage

The feedback loops, as depicted in Figure 6, were drawn based on the assumption that no major coupling exists between the rigid body heave and pitch modes. This applies to aircraft loading configurations with a CG location "just" in front of the main undercarriage. In the case that this criterion is not fulfilled it would be beneficial to the layout of the control system that the resulting structural coupling effects be accounted for by an additional feedback of the pitch motion to the main undercarriage and of the heave motion to the nose landing gear.

5. Analytical Investigations

To determine the possibilities and limitations in connection with equipping aircraft with an active-controlled undercarriage, extensive analytical investigations were per-

formed on a defined configuration of the advanced European Fighter Aircraft (EFA). The calculations considered the coupled heave and pitch degrees-of-freedom (Figure 7) of the longitudinal aircraft motion and were taking into account the nonlinear behavior of the (two-stage) landing gear system by means of linearization techniques [14].

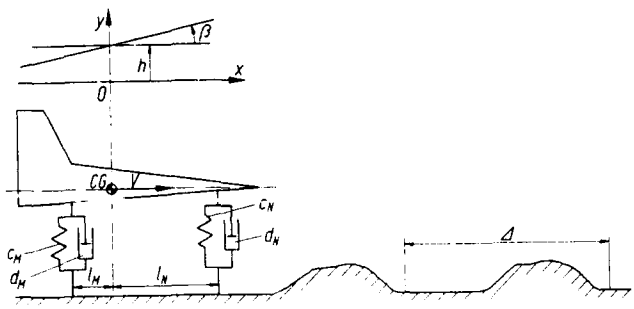

Fig. 7: Mathematical model for determination of the aircraft dynamic response to runway roughness

With regard to the bump multiplier, the results indicated a reduction in the range of 41% for the aircraft pitch motion and of 37% for the aircraft heave motion. A further result is indicated in Figure 8, which depicts the dynamic response of the aircraft pitch and heave motions to a harmonic vertical excitation at its nose and main gear wheels, respectively. The plotted curves clearly indicate the higher damping of the undercarriage in the active-controlled mode, which considerably reduces the peak response in the eigenfrequency neighborhood of the aircraft pitch and heave degrees of freedom.

These very satisfactory results were obtained at rather small flow rates of the hydraulic oil supply. To actively control the entire undercarriage, only a flow rate in the range of 10 l/min was required. It has to be mentioned, however, that the oil supply flow rate is quite dependent on the basic (conventional) design of the undercarriage considered.

Further investigations concentrated on the stability behavior of the active-controlled landing gear system. Nyquist plots, as shown for instance in Figure 9, were calculated to detect eventual instabilities of the active control system. But all of the calculated open loop frequency response "circles" were nicely located at the right hand side of the complex s-plane, thus indicating no stability problems [15].

6. Experimental Investigations

The results obtained from the analytical investigations, some of which were presented in the foregoing chapter, were so promising as to encourage further research in this area. The decision was made to construct a laboratory test setup for simulation of the dynamic (rigid body) behavior of aircraft when operating on rough surfaces. To demonstrate the efficiency of active-controlled landing gear, tests should be run in a conventional (passive) as well as in an active-controlled landing gear configuration. The following sections give a description of the test setup and of the results obtained with it.

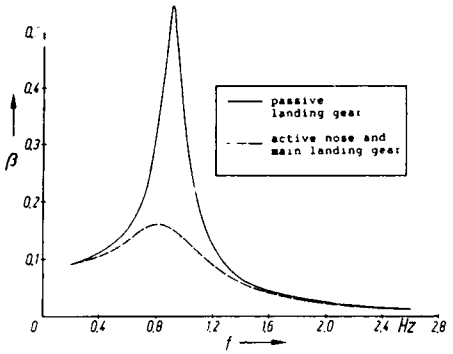

Pitch angle - Vertical excitation at the nose landing gear

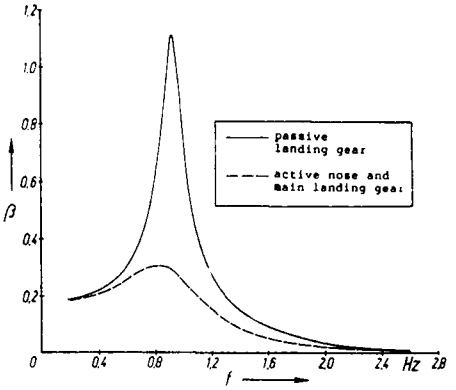

Pitch angle - Vertical excitation at the main landing gear

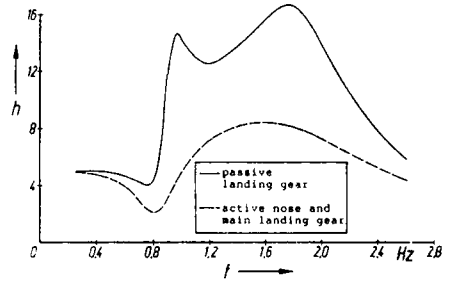

C.G. vertical displacement-Vertical excitation at the nose landing gear

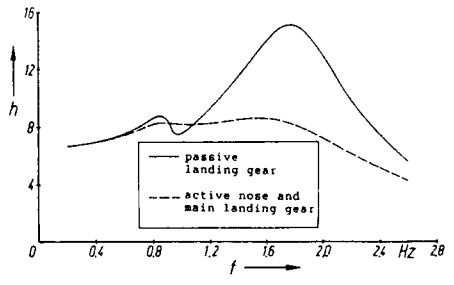

C.G. vertical displacement-Vertical excitation at the main landing gear

Fig. 8: Calculated frequency response plots

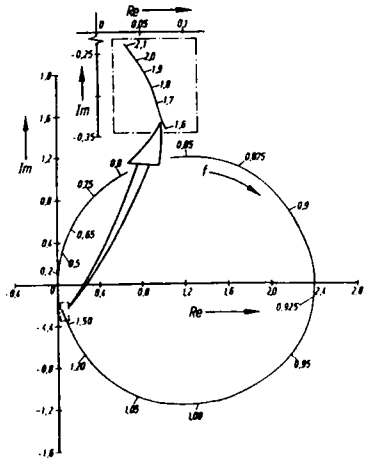

Nose landing gear control loop

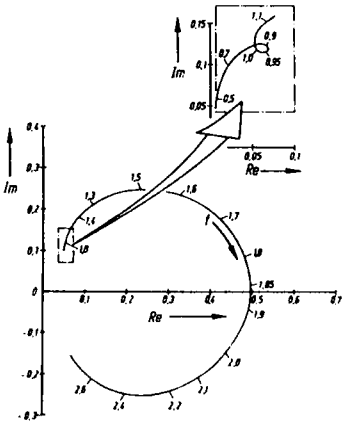

Main landing gear control loop

Fig. 9: Nyquist stability plots

6.1 Test Setup

The aim of the experimental investigations was to demonstrate the improvement in the rough field operational capabilities of aircraft equipped with an active-controlled instead of conventional undercarriage. Due to the smaller size of nose landing gear, it was decided to perform all experimental investigations on an actual sized passive and active nose landing gear system. The test setup is shown in Figures 10 and 11. A beam-shaped structure, idealizing the front part of an aircraft fuselage, is pitching around a pivot point, considered as the (fixed) attachment point of the main undercarriage. On the other end of the beam structure, a modified hydraulic cylinder acts as a nose landing gear shock absorber. A solid rubber element, simulating the nose wheel tire stiffness is fixed to the free end of the cylinder piston rod. The "tire" is placed on top of a platform connected to the piston rod of a hydraulic shaker. This system allows arbitrary rough runway profiles to be simulated by feeding defined electric set value signals to the shaker control system. For the simulation of (different) aircraft inertia properties, a set of masses is fixed to the beam-shaped (fuselage) structure. All hydraulic elements, such as damping and back-pressure valves, which are integrated inside the strut of the real landing gear, are mounted here outside the cylinder on a steel plate and are connected to its upper and lower oil chambers by large-size hydraulic steel tubes. The orifice cross sections of the recoil and compression damping factors are variable, thus allowing the recoil and compression damping factors to be independently adjusted to defined values. The compressed nitrogen volume, forming the stiffness of the shock absorber, is realized by means of a commercially available high-pressure gas reservoir with a well-defined volume.

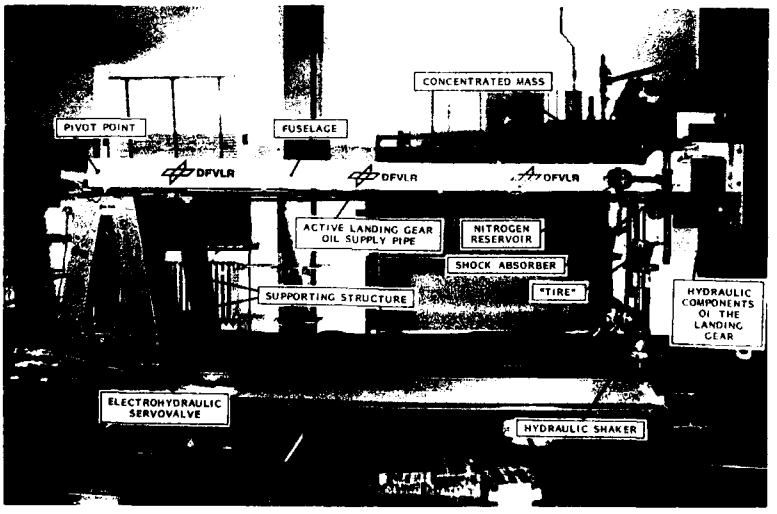

Fig. 10: Laboratory test set-up for rough field testing

As shown in Figure 11, two sensors, an extensiometer for measuring the positon of the landing gear piston in the strut and a gauge to determine the pressure in the upper oil chamber are used for the static control of the landing gear working point. As a feedback to the dynamic load alleviation control system various sensor signals, detecting either the pitch rate or the pitch acceleration, are available.

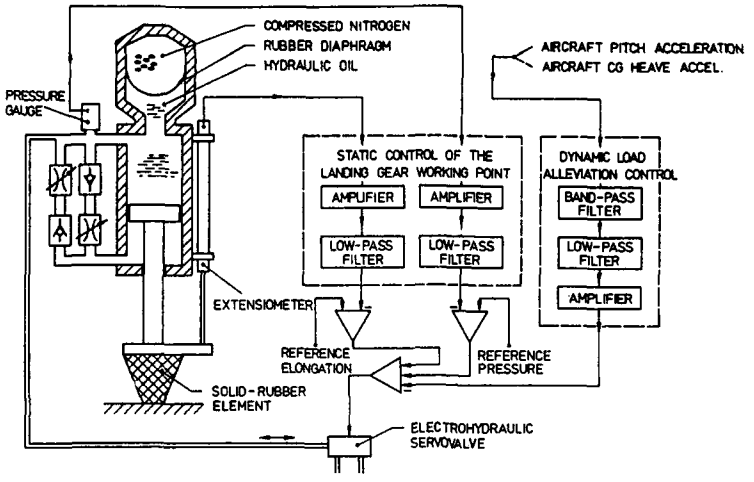

Fig. 11: Sketch of the active control landing gear system investigated

To simulate various supply oil flow rates, a manually adjustable flow rate limiting valve is implemented into the pressure oil supply pipe, allowing the flow rate to be varied between 0 and 25 l/min. Furthermore a mechanical spring system is used to simulate aircraft lifting forces during high-speed taxi phases. This simple mechanism allows the landing gear behavior to be determined in the case of a quasi-steady change of its loading forces, e.g. during take off. Finally it has to be mentioned that the test setup is designed to allow determination of the characteristics of conventional passive landing gear when shutting off the oil pressure and return pipes.

6.2 Test Results

The defining data of the investigated test setup configuration are as follows:

- Dead mass of 1000 kg on top of the landing gear,
- Static landing gear reference point characterized by a strut elongation of 0.2 m and a pressure of 50 bar.

To detect the influence of the supply oil flow rate on the performance of the dynamic load alleviation control system, tests were performed at flow rates of 15 and 25 l/min.

A first test consisted of determining the frequency response of the landing gear transfer function relating the strut pressure in the upper oil chamber to a (harmonic) electric set point signal fed to the electrohydraulic servovalve. The test was performed in a locked strut configuration, thus not allowing any displacement between the shock

absorber cylinder and its piston. The results revealed that, in the entire frequency band of interest ranging from 0 to 5 Hz, the pressure signal is delayed by a phase angle of 90° relative to the servovalve input signal. The reason for this delay is that an appreciable volume of hydraulic oil has to be inserted into the upper oil chamber of the landing gear in order to compress the nitrogen enclosed in the reservoir, before a significant pressure is built up. It is of primary importance to realize and understand this "effect" which is in contrast to the dynamic behavior of servocontrolled actuator systems, the (differential) pressure/servovalve input frequeny response of which exhibits smaller phase lag characteristics in the low frequency range [13].

It is obvious that the 90° phase lag angle between the shock absorber pressure and the servovalve input signal must be taken into account when designing the compensation network of the load alleviation control system. Thus, to produce dynamic damping forces in the strut, it is required that the transfer function of this control system exhibits a phase lead angle of 180° at the eigenfrequency of the rigid body mode to be controlled in the case of a displacement feedback or a 90° phase lead angle in the case of a velocity feedback or a 0° phase angle in the case of an acceleration feedback of the rigid body motion in question. This entails that, if we consider a displacement or velocity feedback, we have to include correspondingly two or one (first-order) differentiating elements into the compensation network. The simplest compensation network, as depicted in Figure 10, can be realized by means of an acceleration feedback of the aircraft rigid body motion. During the tests the three different feedback types described above were investigated. In combination with well-adapted compensation networks their overall performance could be considered equivalent.

To demonstrate the improved operational capabilities of aircraft equipped with active-controlled landing gear on rough runway surfaces, three different types of rough runway surface profiles, being either of sinusoidal or random shape or scattered with discrete obstacles were investigated. Some of the results obtained are presented in the following subsections.

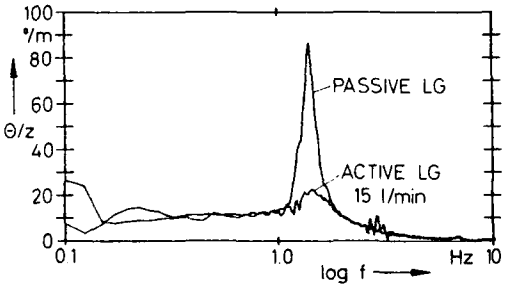

Fig. 12: Measured frequency response of the transfer function relating the aircraft pitch angle to the shaker platform displacement

6.2.1 Frequency Response Tests

In the first test the landing gear system was excited by the shaker platform according to a repeated swept sine function in the frequency range from 0.2 to 10 Hz. The shaker platform displacement z as well as the "aircraft" pitch angle θ around the pivoting point were recorded and analyzed. Tests were performed in both the passive and active landing gear configurations. The obtained frequency responses of the transfer function between the two signals are depicted in Figure 12. The measured curves, which are in full agreement with the calculated dynamic response of Figure 8, clearly indicate the increased damping in the case of the active-controlled landing gear in the vicinity of the pitch eigenfrequency.

6.2.2 Rough Runway Tests

Detailed experimental investigations concentrated on the dynamic behavior of aircraft taxiing on runways with a randomly shaped roughness. For the excitation of the landing gear a random-type displacement of the hydraulic excitation cylinder, with a power spectral density (PSD) as depicted in Figure 13, was considered. The spectrum is realistic with regard to the simulation of rough runway surfaces in that it assumes the long-wave uneveness of the taxi track to be of higher amplitude than the short-wave irregularities.

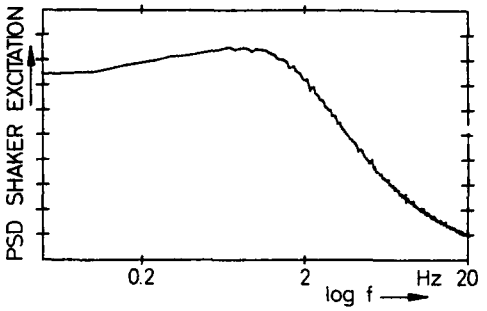

Fig. 13: Power spectrum of the runway roughness

The tests were performed at a high amplitude level of the excitation, ranging between ± 0.05 m. As a result, Figure 14 depicts the power spectra of the dynamic shock absorber force resulting form this type of excitation for both the passive and active landing gear configurations. The improved behavior of the active-controlled shock absorber is indicated by the significant reduction in the peak load level of the response spectrum, leading to a reduction of 42% in the root mean square (RMS) value of the strut force. The improved dynamic response behavior of active-controlled landing gear is also demonstrated by the time plots of Figure 15.

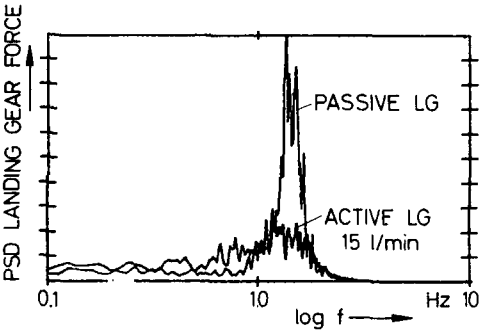

Fig. 14: Measured spectra of the dynamic landing gear force for random type runway roughness

6.2.3 Discrete Obstacle Tests

Final testing of the landing gear system was related to the simulation of aircraft taxi over a series of AM-2 mat repair profiles. A typical sequence of investigated obstacles, consisting out of 3 successive AM-2 mats, is depicted in Figure 16. To determine the aircraft landing gear dynamic response in the entire range of reduced frequencies of interest with regard to the first maximum of the pump multiplier at $\omega_\Delta^* = 2\pi$ (Figure 2), the simulated taxi speed was incrementally varied between 10 and 80 m/s.

The time plots obtained in the case of the worst condition (most critical taxi speed for the given obstacle spacing) are depicted in Figure 17. The plots indicate a significant allevation of the landing gear loads when the control system is activated. Another interesting result is obtained when drawing a plot of the maximum landing gear load, encountered at any location during the full traverse of a sequence of discrete obstacles,

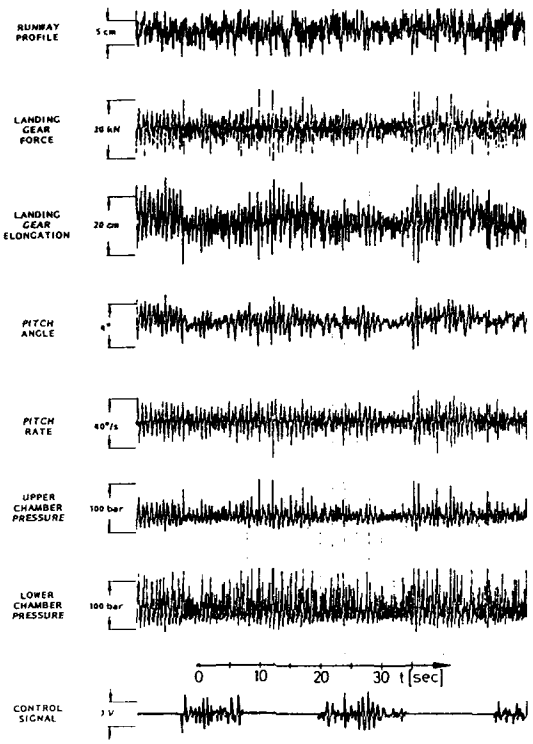

Fig. 15: Measured time plots of the major parameters during the taxi simulation with random type roughness

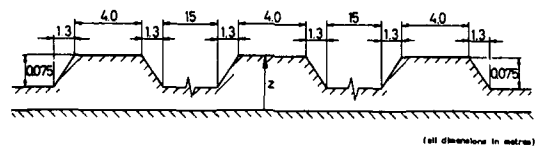

Fig. 16: Investigated obstacle with a profile of 3 successive AM-2 mats

as a function of the (constant) taxi speed. The experimentally determined results in the case of a triple AM-2 mat profile with a height of 0.075 m are depicted in Figure 18. It can be seen that the peak load level is reduced by 33% or 50% for the active-controlled landing gear in the case of an oil supply flow rate of 15 or 25 l/min. Figure 18 depicts moreover the maximum load levels for the testing cases

- triple AM-2 mat profile with a height of 0.10 m,
- double AM-2 mat profile with a height of 0.075 m.

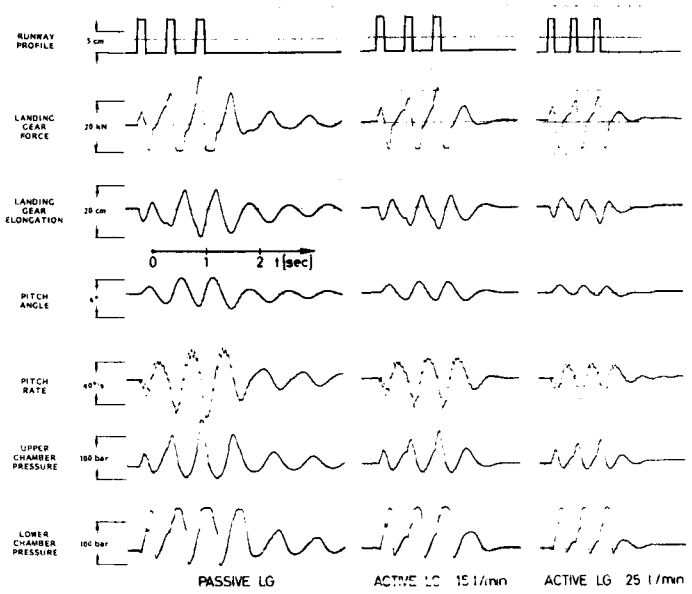

Fig. 17: Measured time plots of the major parameters while crossing a triple AM-2 mat profile in the case of worst spacing conditions

It is interesting to note that the loads produced in the active strut are only identical at very high taxi speeds to the loads in a conventional undercarriage. This fact indicates that the active-controlled landing gear system, as presented here, neither alleviates nor increases the loads induced by short-wavelength obstacles or at touchdown. With regard to the discrete bump testing it has to be mentioned that the simulation of a taxi run over 30 (!) successive AM-2 mat profiles, with a height of 0.075 m and placed at worst spacing conditions, could be achieved without collapsing the actively damped landing gear.

All of the results in the three subsections above clearly indicate that a considerable reduction in the landing gear (peak) loads and consequently in the aircraft structural loading during rough runway operations can be obtained by the implementation of active control systems in the undercarriage.

7. Further Active Control Considerations

Once the undercarriage is "made active" a variety of additional advantages can be expected from such a landing gear design. Above all the two "static" control loops (Figure 11) can be used for further control purposes as illustrated below.

First, the reference pressure could be easily adjusted in accordance with a function of the aircraft inertia parameters. This would allow the undercarriage to be adapted to any aircraft loading configuration and would thus improve its overall landing, take-off and taxi performance by modifying its pneumatic spring characteristics.

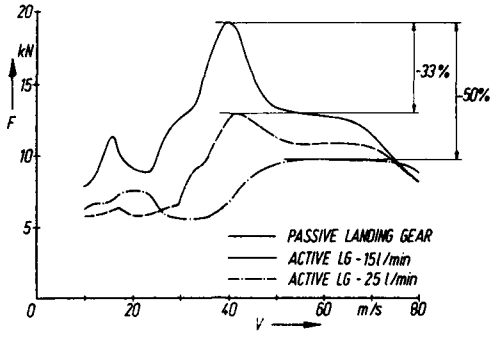

Triple AM-2 mat - 0.075 m in height

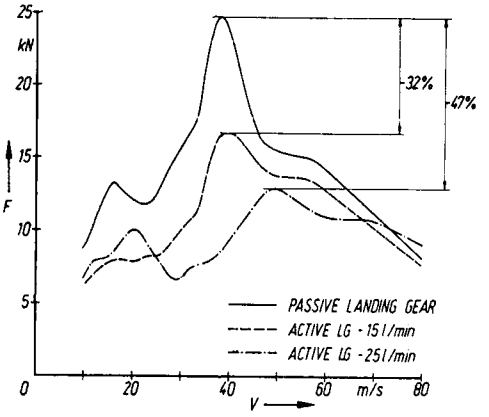

Triple AM-2 mat - 0.100 m in height

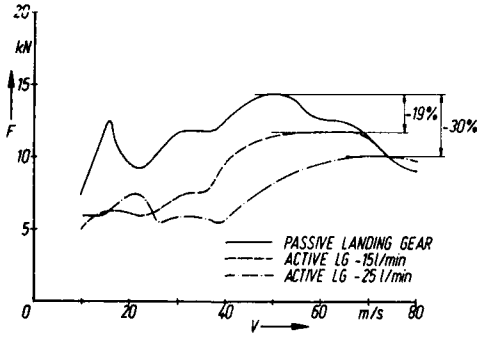

Double AM-2 mat - 0.075 m in height

Fig. 18: Peak landing gear load level as a function of the taxi speed determined during a run over succesive AM-2 mat profiles

Second, the lift produced on the aircraft lifting surfaces, when operating in its high speed take-off phase, could be significantly increased by elongating the nose landing gear strut which entails a higher angle of attack of the entire aircraft. Such a system would require the reference elongation value setting (of the nose landing gear) to be changed in a transient form at a well-defined taxi speed during the take-off phase. Rough estimations have indicated that, due to this type of control, the take-off distance for fighter aircraft with a high power-to-weight ratio could be reduced by about 100 m, which is in the range of 25% of the normal take-off distance.

Third, the storage space inside the aircraft structure of an active-controlled undercarriage could be reduced if the oil volume in the shock absorber were partially removed before the retraction of the landing gear system.

Moreover the simple principle of active damping, as outlined here in detail for the case of the aircraft rigid body modes, could certainly be applied to achieve damping control of defined "critical" aircraft flexible modes. A typical example could be the control of the wing bending and/or torsional eigenmodes or of the fuselage vertical bending mode in order to prevent the structural damage of wing pylon, outer wing or fuselage front structures when operating the aircraft on damaged runways [16]. In this case it would be beneficial to use several accelerometers, distributed on the wing tips and/or at the fuselage nose, to generate convenient feedback signals to the landing gear system control loops [17].

These reflections clearly indicate at least some of the many advantages to be attributed to an active-controlled landing gear design. The question as to the extent to which the various systems can and should be realized addresses above all problems related to the reliability and the extent of damage in the case of a failure inherent to the various active systems under consideration.

8. Conclusion

The design of an active-controlled landing gear system was described. The layout of the control system was designed to provide the active undercarriage with improved damping characteristics in the frequency range related to the aircraft rigid body degrees-of-freedom. This entails the alleviation of the landing gear and aircraft structural loads due to long wave obstacles without influencing the dynamic response, in comparison to a conventional landing gear design, to short wave impacts occurring at touchdown or upon encountering sharp high-amplitude obstacles.

Moreover a detailed description of a test setup for the simulation of aircraft operation on rough runway surfaces was given. It was experimentally demonstrated that an active-controlled undercarriage can significantly reduce the landing gear and consequently the aircraft structural loads during aircraft taxi on unprepared rough runway surfaces. For instance, the RMS-value of the dynamic landing gear forces could be lowered by 42%, in comparison to passive landing gear, in the case of aircraft operation on surfaces with a randomly shaped roughness profile. Simulation of taxi tests over a runway profile with three successive discrete obstacles (AM-2 mat profiles) yielded a reduction of 50% in the peak landing gear loads in the case of worst spacing conditions.

The aim of this paper was to realistically demonstrate, in a laboratory test, the possibilities offered by the implementation of active control systems to aircraft undercarriage and to give a quantitative estimate of the improvements obtainable with such systems. Further work will still be required for the achievement of a practical design of a real active-controlled undercarriage and its control system, especially with regard to failure and reliability questions.

9. References

[1] GERARDI, A.G.
Status of Computer Simulations of USAF Aircraft and Alternative Simulation Technique
AGARD-CP-326, Ref. 11, 1982

[2] JOHNSON, W.P.
Comparison for the A-7D Aircraft Dynamic Response Using Experimental and Analytical Methods
AFWAL-TR-86-3084 (1986)

[3] Airplane Strength and Rigidity, Landplane Landing and Ground Handling Loads
MIL-A-8862 (ASG), May 1960

[4] Airplane Strength and Rigidity, Ground Loads for Navy Procured Airplanes
MIL-A-8863, July 1974

[5] Résistance des Avions
AIR 2004 E, March 1979

[6] STRICKLAND, W.S.; CALDWELL, L.R.
Minimum Operating Strip Selection Procedure
AGARD-CP-326, Ref. 1, 1982

[7] CALDWELL, L.R.; GERARDI, A.G.; BOROWSKI, R.
Runway Surface Roughness
AGARD R-685, Ref. 1, 1979

[8] FREYMANN, R.; JOHNSON, W.P.
Simulation of Aircraft Taxi Testing on the AGILE Shaker Test Facility
DGLR-Bericht 85-02, pp. 468-476, 1985
Second Int. Symp. on Aeroelasticity and Structural Dynamics,
Aachen (Germany), April 1-3, 1985

[9] FREYMANN, R.
An Experimental-Analytical Routine for the Dynamic Qualification of Aircraft Operating on Rough Runway Surfaces
AGARD-R-739, Ref. 2, 1985

[10] FREYMANN, R.
An Active Control Landing Gear for the Alleviation of Aircraft Taxi Ground Loads
Zeitschrift für Flugwissenschaften und Weltraumforschung (ZFW), Band 11, Heft 2 (1987), pp. 97-105

[11] OLSEN, J.J.
Interpretation in Terms of the Response of a One Degree-of-Freedom Oscillator to Two Successive Disturbances
AGARD-R-739, Ref. 1,1985

[12] FREYMANN, R.
Frequency Response Tests Performed on a YF-16 Aircraft Using the AGILE Test Facility
AFWAL-TM-84-205 FIBEB (1984)

[13] FREYMANN, R.
Nonlinear Aeroelastic Analyses Taking into Account Active Control Systems
AGARD-R-698, Ref.2, 1981

[14] FREYMANN, R.
Linearization Techniques
AFWAL-TM-84-229-FiBEB (1984)

[15] DORF, R.C.
Modern Control Systems, 2nd Ed., Reading
Addison-Wesley 1976

[16] HOLPP, J.E.
The HAVE Bounce Program
AGARD-CP-326, Ref. 8, 1982

[17] FREYMANN, R.
Interactions Between an Aircraft Structure and Active Control Systems
Journal of Guidance, Control and Dynamics, Vol 10, No.5, pp. 447-452 (1987)

ASSESSMENT OF THE APPLICATION OF THE WORKING GROUP 22 STANDARD BUMP' CONCEPT TO A CURRENT MILITARY AIRCRAFT

by
E.F. Wild (Mrs)
B.R. Morris
SAC Technology Ltd
Marlborough House
Churchfield Road
Walton-on-Thames
Surrey
KT12 2TJ
United Kingdom

A.E. Dudman
Assistant Chief Aerodynamicist (Dynamics Engineering)
Design Office No.8
British Aerospace Plc (Civil Aircraft Division)
Filton
Bristol
BS99 7AR
United Kingdom

SUMMARY

The application of standardised runway repair obstacles (SRO) for design purposes and post-design capability determinations was a basic outcome of SMP Working Group 22 deliberations.

The WG 22 standardised shapes have been the basis of clearance work for a current military aircraft. To verify the adequacy of the SRO profile for this work the response to real repair profiles, obtained from practice repairs, has been related to the response to the SRO. Some comments on the SRO as a representation of real repairs and on some undesirable features of real repair profiles are presented.

1. INTRODUCTION

Military aircraft clearance over crater-damaged runways is to be determined from the interpretation of clearance information which is based on the aircraft capability over the Standard Repair Obstacle, (SRO). This standardised repair shape was formalised by the AGARD SMP Working Group 22 as a profile that may best represent the repairs that would be encountered in a repaired runway situation. Reference 1 gives details of the Group's findings.

The clearance information, as requested by the UK MOD, will be provided in the form of contour plots. These plots define safe speeds and spacings for crossing double repairs and are based on the calculations of the aircraft response to a specific height of SRO.

In order to establish the adequacy of the SRO as a representation of real repairs a study was made to study the response of a military aircraft to a large number of real repair profiles. This work included a comparison between the aircraft response to real repairs and to the SRO, and the determination of the severity of the real repairs compared to the SRO response by use of the 'Equivalent Obstacle' concept. In addition, and of primary importance to the UK, it would be possible from this study to determine an adequate height to set the SRO for calculation of the contour plots such that they would cover the inevitable variability of the aircraft's response due to the very different real repair profiles.

The objectives of this document are firstly to consider the adequacy of the SRO profile shape as a representation of real repairs with respect to the aircraft response, and hence the accuracy of the contour clearance procedure in the real repair situation. Secondly to consider the Equivalent Obstacle concept as a useful measure of the severity of the real repairs compared to the SRO.

To illustrate the discussion the response calculations of the heavy weight takeoff configuration of the military aircraft are presented. This case models the aircraft accelerating for takeoff from a specified initial speed. The BAe mathematical model of this configuration has been validated against test data.

1.1. Format of the Document

To introduce this discussion the aircraft response to single and double SRO in time-history and contour plot format is outlined first. This is then followed by a

detailed comparison between the aircraft response to three real repairs and the SRO response. A discussion on the adequacy of SRO contour plots to cover the real repair variability is then presented.

The 'Equivalent Obstacle' concept, and its inherent assumptions, are outlined as a way of overcoming the infinite variability of the real repair profiles, and hence aircraft response, and to provide a basis for determining the required magnitude of the SRO for the contour plotting.

2. REPAIR OBSTACLES

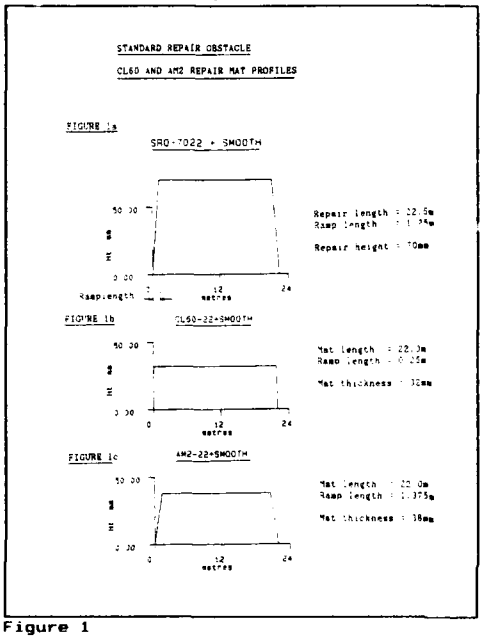

Figure 1

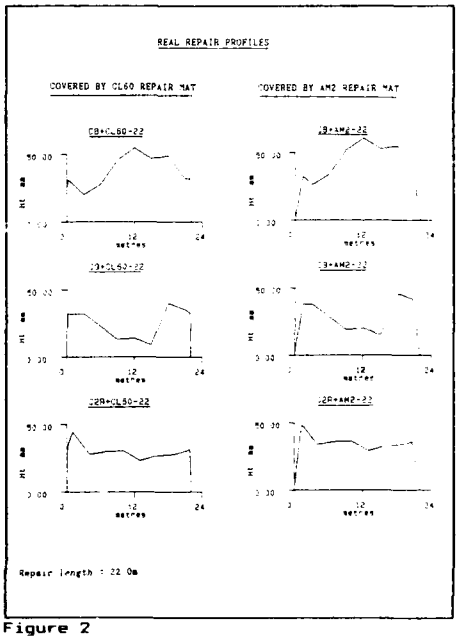

Figure 2

2.1. Standard Repair Obstacles, SRO

The 70mm profile is illustrated in Figure 1a. The maximum height of 70mm, 52mm or 38mm is achieved in 1.25m. The trailing edge has the same slope as the repair leading edge and total length, including the two ramps is 22.5m.

2.2. CL60 and AM2 Repair Mats

The profiles of the CL60 and AM2 repair mats are illustrated in Figures 1b and 1c respectively. The CL60 mat has thickness 32mm and a ramp length 0.25m and the AM2 is of thickness 38mm with a ramp length of 1.375m. For this modelling the total length of the mats including the two ramps is 22m.

2.3. UK Crater Repairs

For this paper three crater repairs have been chosen from a set of greater than 66, UK surveyed profiles, of length 22m.

Having analysed the response of the aircraft to many repairs, BAe found that it was possible to categorise the responses into three broad groups. Humped repairs formed one group and repairs with a deep central dip another. The third was formed of repairs which were of complex or of relatively flat profile (similar to the SRO). The crater C8 was selected to represent a skewed humped repair, C9 to represent a repair with a central dip and C2R a repair most similar to the SRO shape. C2R has, however, some crater in-fill at the leading edge which adds to the height and steepness of the rise on to the repair.

The following assumptions have been made when the craters are covered by the repair mats:

- The runway surface is considered to be completely smooth ahead of and beyond the repair

- The repair mat, including the end ramps follows the surface of the repair profile exactly. Direct addition of the two heights gives the full repair profile.

Figure 2 illustrates the three repairs covered by the CL60 mat and beside for comparison the repairs covered by the AM2 mat. For the BAe modelling the repair mat was fitted exactly over the crater in-fill and therefore the rise onto the repair is distorted by the underlying fill.

3. RESPONSE TO THE 22.5M STANDARD REPAIR OBSTACLES

3.1. As Single Obstacles

The response to the SRO of height 70mm and length 22.5m is shown for the nose and main gears on Figures 3-4 for initial speeds of 20,40,50,60,70m/s at nose gear encounter with the obstacle leading edge.

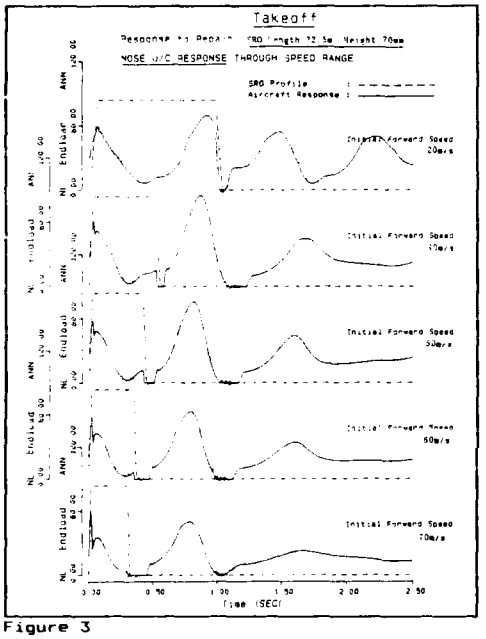

Figure 3

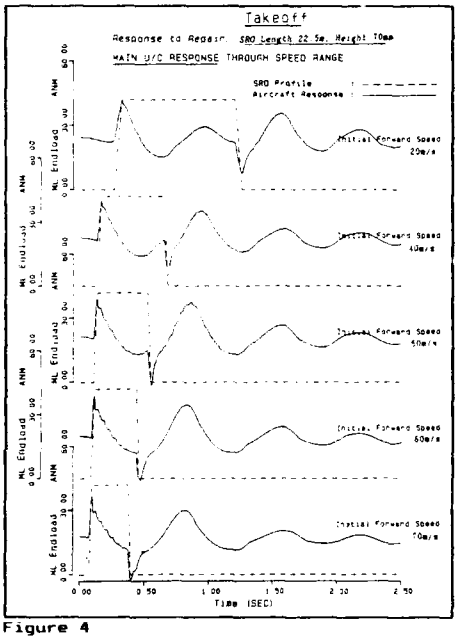

Figure 4

Considering the nose gear first it is seen that for the lowest speed illustrated the aircraft is sufficiently slow for the second peak to occur towards the repair trailing edge and this is then the highest peak. For speeds above this, the first post-mat peak is the maximum and remains so up to 60m/s while for speeds of 70m/s and higher the maximum occurs during the rise onto the repair. Tuning in pitch over this repair occurs at approximately 40m/s as indicated in Figure 5 where the maximum Percentage Available Increment, PAI which occurs throughout each time history is plotted against speed, for the three SRO heights 70mm,52mm and 38mm. The lowest responses occur either side of the peak at speeds of 30 and 60m/s.

PAI is defined as the percentage of the available increment used ie.

$$PAI = \frac{(MAXIMUM\ LOAD - QS)}{(REFERENCE\ LOAD - QS)} * 100\%$$

where QS is the quasi-steady value for that quantity.

The main gear response maxima occur during the rise onto the repair for every speed, although the first post-mat peak is not insignificant for any speed up to 70m/s. These maximum loads do drop slightly as speed, and therefore aerodynamic relief, increases. Figure 6 illustrates this, showing maximum PAI against initial repair encounter speed.

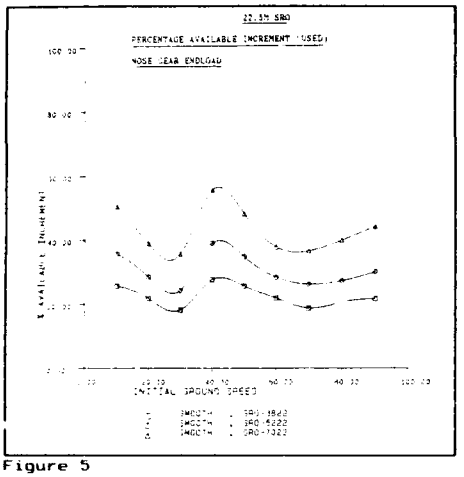

Figure 5

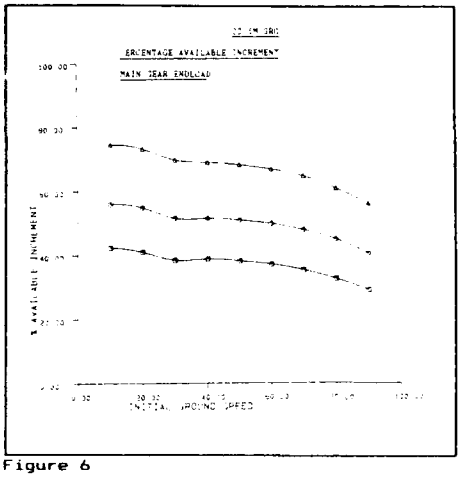

Figure 6

3.2. As Double Obstacles

Response work has been carried out to determine the aircraft capability over double SRD. This capability over doubles is presented in the form of contour plots of PAI against nose wheel encounter speed at the leading edge of the first repair and repair spacing. Repair spacing in this paper, to be consistent with some others, denotes the distance from the trailing edge of the first repair to the leading edge of the second, ie. the gap between the repairs rather than the more appropriate distance for tuning of leading edge to leading edge. The maximum PAI at each speed/spacing combination on this grid is calculated and the 80,90 and 100% PAI contours mapped. This method of defining the clearance gives an indication of the sensitivity of the response at the critical speeds and spacings and makes use of the phasing off the repair to define the maximum allowable clearance.

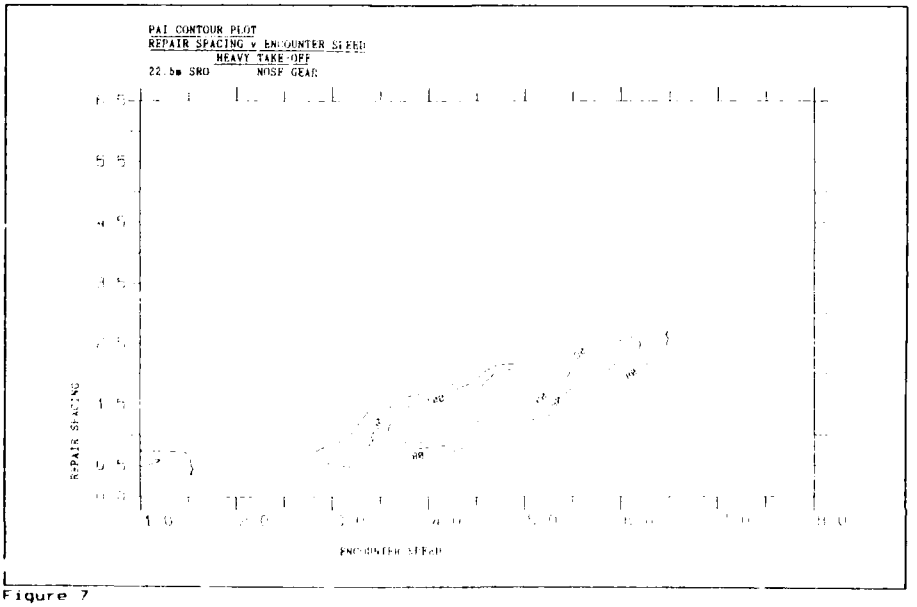

Figure 7

Figures 7-8 show the contour plots calculated for this configuration over the 22.5m SRO for the nose and main gears respectively. The nose gear shows one critical area over the range of tuning speeds 40-50m/s; this lobe being formed from loads caused at encounter with the leading edge of the second repair when placed in the region of the first post-mat peak from the first repair.

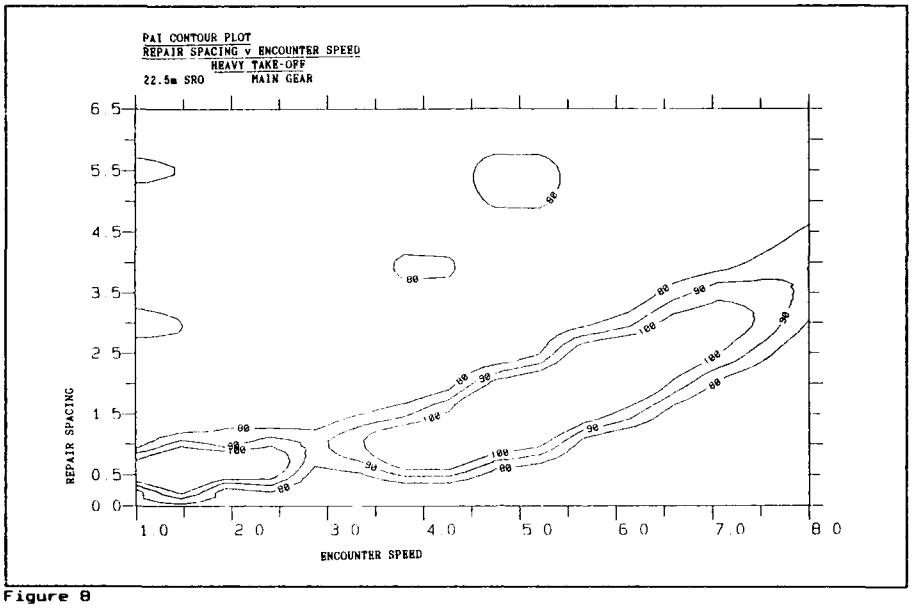

Figure 8

The main gear contours show critical zones when the second repair is placed in the region of the first post mat peak except at speeds close to 30m/s. In addition, areas of some significance, 80%PAI, occur due to the combination of the second post-mat peak and the leading edge of the second repair but only where the second peak after the first repair is sufficiently large.

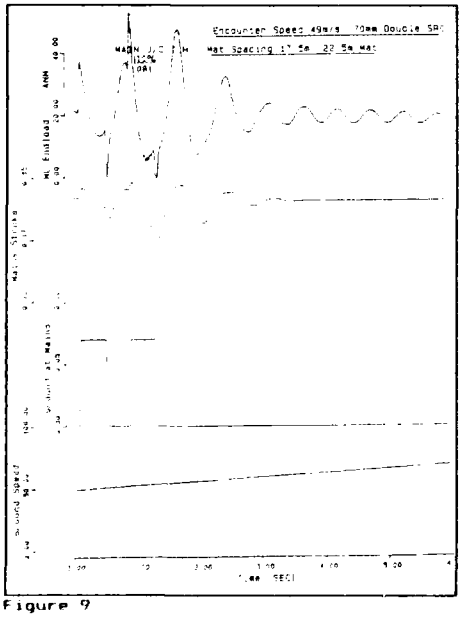

Figure 9

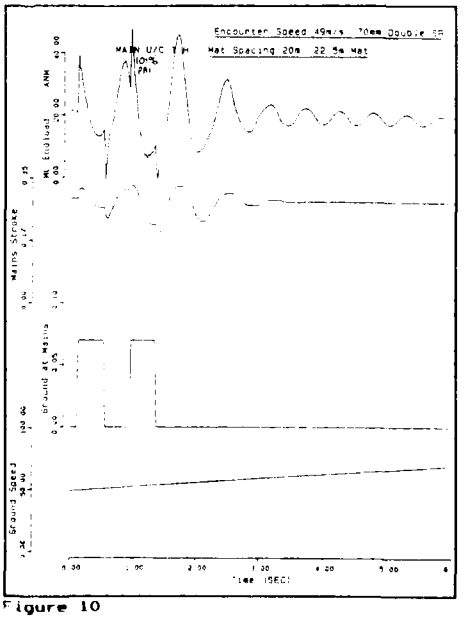

Figure 10

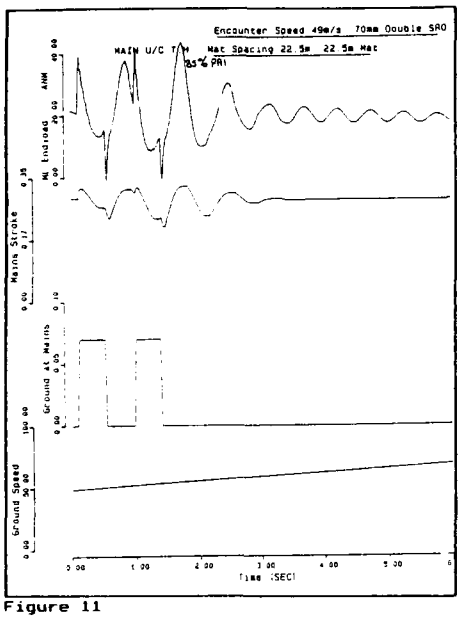

Figure 11

Figures 9-11 show the main gear response for an initial speed of 49m/s with increasing spacings of 17.5m, 20.0m to 22.5m. These illustrate the development of the maximum loads as spacing is increased, while leaving the major unacceptable zone by its upper edge. The maximum load, caused at encounter of the leading edge of the second repair during the first overswing from the first repair, falls as spacing is increased until encounter occurs far enough into the following trough to allow the post-mat peak off the second repair to be the maximum.

4. RESPONSE TO UK CL60 AND UK AM2 COVERED CRATERS

If the contour approach using SRO is to be used as a guide to the aircraft clearance over double repairs then, when translated to the real repair situation, the SRO must show a response similar in both phasing and magnitude to the real repairs.

Similar phasing is essential to ensure that accuracy in spacing definition for leading edge and post-mat loads is achieved. Magnitudes of the loads, at repair leading and trailing edges, from response to the chosen height of SRO must be similar, or just envelope, the loads from real repairs. Too high a level of SRO would result in an unnecessarily restrictive clearance.

A comparison of the magnitudes and phasing between the chosen real repairs C8, C9 and C2R, and the 70mm SRO, are given below.

4.1. CL60 Covered Crater Repairs

Figures 12-13 show the response to C8 the high, late-skewed repair at speeds 20,30,50 and 60m/s. Figures 14-15 show the equivalent plots at leading edge ramp speeds of 20,40,50,60m/s, for C9, the repair with the central dip, and Figures 16-17, C2R the fairly flat repair with the crater in-fill, which adds to the height and steepness of the leading edge ramp.

4.1.1. Nose Gear Post-Mat Loads

The form of humped repair, illustrated by C8, is dominated by the fundamental component of shape but, as it is skewed, the pitch response tunes at a lower speed than that due to an SRO of equal length. Hence, for the nose gear, highest post-mat loads occur at 30m/s over this repair, giving a PAI of only 2.4% less than the SRO, with a lag in the peak load equivalent to 1.9m. At 50m/s the first post-mat peak resulting from response to C8 is lower than the SRO first post-mat peak by 18.3%PAI. This gives, for C8, an equivalent SRO height of only 44mm. The greatest mismatch in phasing occurs at 20m/s with a lead equivalent to 4.3m, however the SRO response is 5.6%PAI greater.

The form of dipped repair, represented by C9, tunes as if the repair consists of a pair of shorter repairs. Hence, for the nose gear, highest post-mat loads occur at 20m/s and C9 shows exceedence over the SRO of 2.9% PAI at 20m/s with a lag equivalent to 1.2m. Through the rest of the speed range (greater than 30m/s) all post-mat loads from C9 are low compared with the SRO, for example at 50m/s C9 produces post-mat loads equivalent to an SRO of height 33mm.

The form of repair most similar to an SRO is represented by C2R. The only deviation in similarity to the SRO is a small section of crater in-fill which adds to the height and steepness of the leading edge ramp. However, post-mat loads show no significant tuning but otherwise the response to the SRO is similar, although of lower magnitude

throughout the speed range. Post mat loads give equivalent loads to a SRO of height 31mm at 50m/s.

Thus, at speeds at which the real repairs tune and the SRO not, ie. 20m/s for repairs with deep central dip, and 30m/s for skewed humped repairs exceedence of the 70mm SRO post-mat loads will be possible. At speeds where the SRO tunes and these repairs do not, the 70mm SRO causes considerably higher loads.

Real repair loads at the second post-mat peak are lower than the SRO loads. Loads closest to the SRO loads in magnitude occur in response to C8 at the low speed end 20-30m/s with a PAI difference of only 3.8% at 20m/s.

4.1.2. Nose Gear Leading Edge Loads

Due to the steepness of the CL60 repair mat leading edge ramp loads occurring during the rise onto CL60 repairs are, in general, the maxima of the time history from speeds as low as 20-30m/s regardless of the detail shape of the repair. Exceptions do occur, for example C8 at the tuning speed of 50m/s, due to the relatively high drop off the repair and low rise onto the repair so that the post-mat peak becomes greater.

Comparison with the equivalent SRO leading edge loads shows magnitudes of the CL60 repairs at the lower speeds 10-30m/s, which are lower than the 70mm SRO, even for the repair C2R. From speeds of greater than 30m/s the magnitude of these leading edge loads is approximately equal to, and may exceed, those due to the 70mm SRO. This indicates that a rise of nominally 32mm over 0.25m (CL60 ramp) gives rise to loads that can equal a rise of 70mm over 1.25m (SRO ramp). In the case of C2R, where crater fill augments the rise these loads will exceed the SRO. An increase in PAI of 5.1% is measured for C2R at 50m/s, this being equivalent to an SRO of 79mm at the leading edge.

In addition, C2R has leading edge loads which are of equal magnitude to the SRO post-mat loads at 60m/s.

The phasing of the nose gear leading edge loads over the CL60 repairs show a lead equivalent to 1.3m due to the sharper rise and effect of crater-fill at this point.

4.1.3. Main Gear Loads

Main gear loads resulting from crossing real repairs shows a similar form to the response as for crossing the SRO. The highest loads throughout the time history occur during the rise onto the repair.

Post-mat loads for real repairs may match and exceed those due to SRO at tuning speeds. C8 shows exceedence of the first post-mat peak of the SRO at 30m/s by 2.7% PAI (equivalent SRO of 72mm) with a lead equivalent to 2.7m and the second post-mat peak by 2.9% PAI (equivalent SRO of 72mm) with a lead of 2.7m. For speeds greater than the tuning speeds of the real repairs the SRO post-mat loads exceed those due to the real repairs, for example C8 at 50m/s shows a PAI of 28.7% less than the SRO and is equivalent to an SRO of 43mm.

The leading edge loads for real repairs are always less than the SRO loads and are equivalent to an SRO of 48mm for C2R at 50m/s; this considered to be the worst repair of the three for leading edge response.

Phasing of real repairs compared with SRO at the leading edge shows a lead equivalent to one metre.

4.1.4. A Modification to the CL60 Repair Mat Leading Edge

To illustrate the detrimental effect of the CL60 leading edge C2R was covered by a CL60 repair mat (32mm thick) with a leading edge ramp of 1.25m, as of the SRO, placed clear of the crater in-fill, and the response calculated at 50m/s. Figures 18-19 illustrate this for the nose and main gear loads respectively. The response is compared with the response to a CL60 mat only and to C2R covered by the nominal CL60 mat (ramp modified by crater in-fill). At this speed the CL60 mat alone gives nose gear leading edge loads equal to the 70mm SRO and therefore C2R must exceed. The modified CL60 ramp shows loads far lower, implying that a far less restrictive clearance level would be possible by:

1. Ensuring that the mat ramps lie outside the crater-fill.

2. Modifying the CL60 leading edge to be less severe and more similar to the SRO ramp.

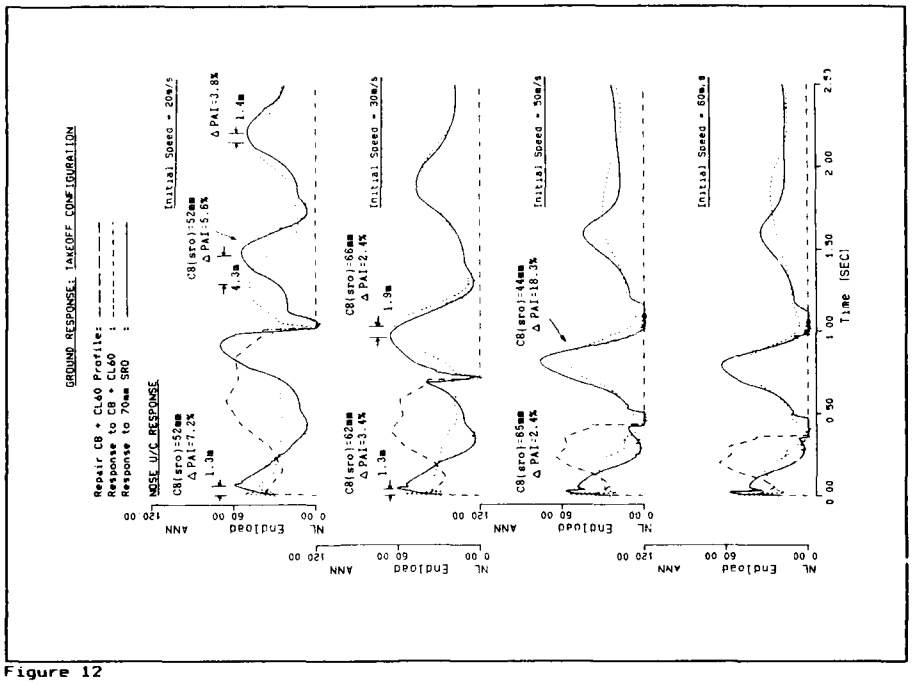

Figure 12

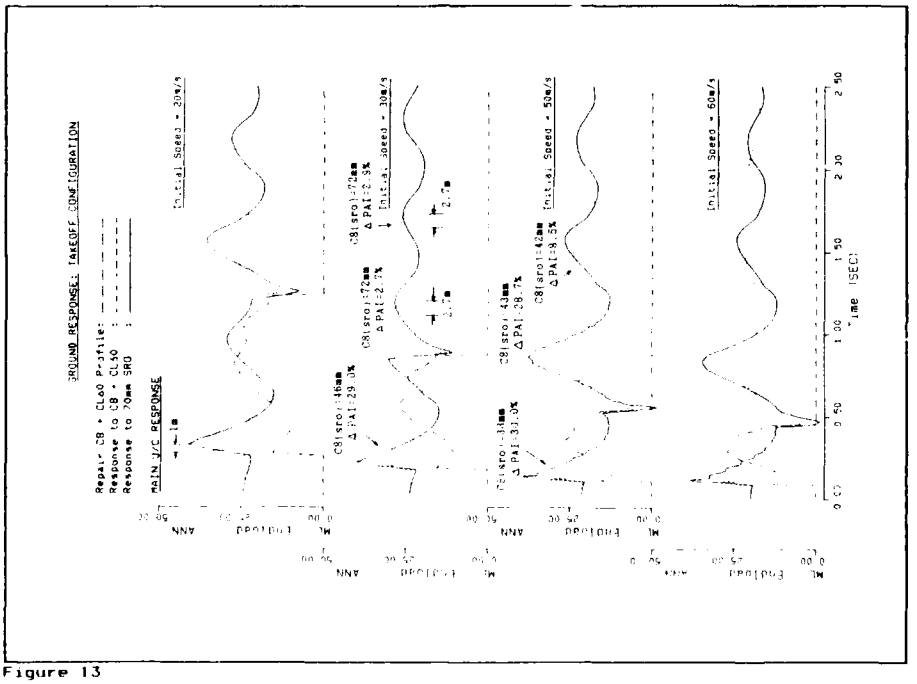

Figure 13

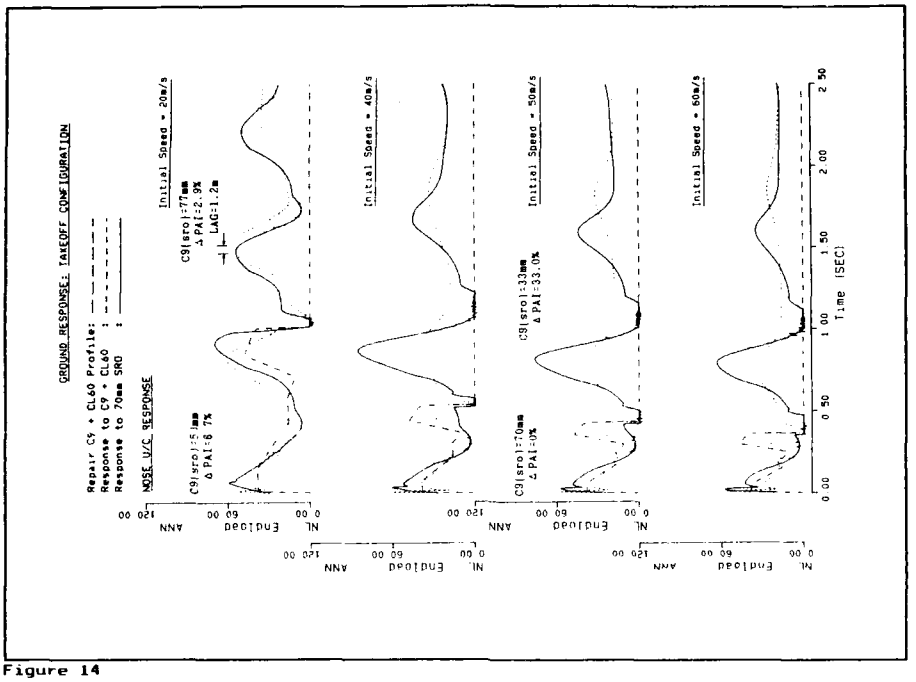

Figure 14

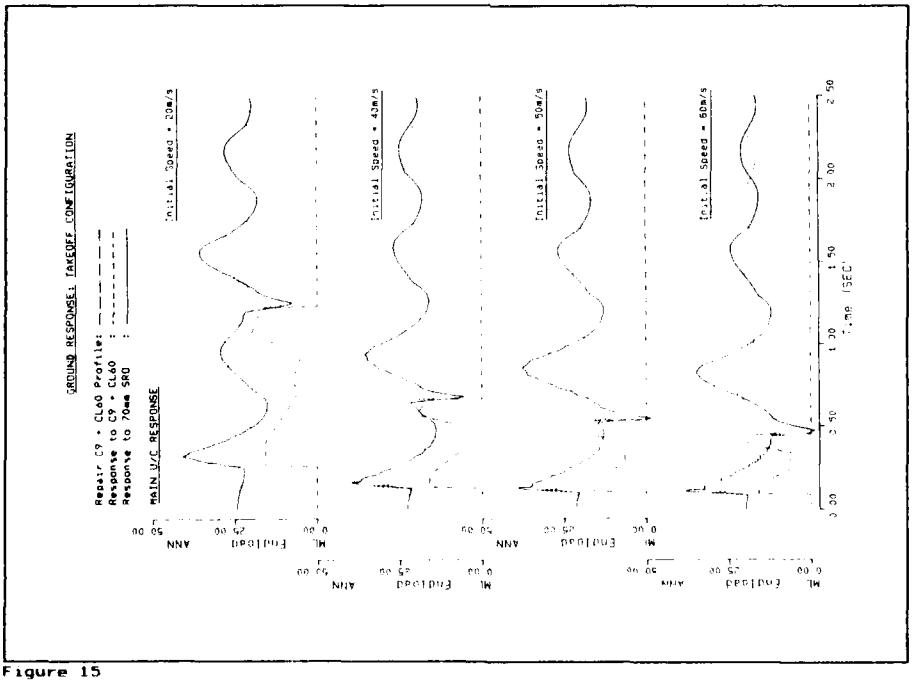

Figure 15

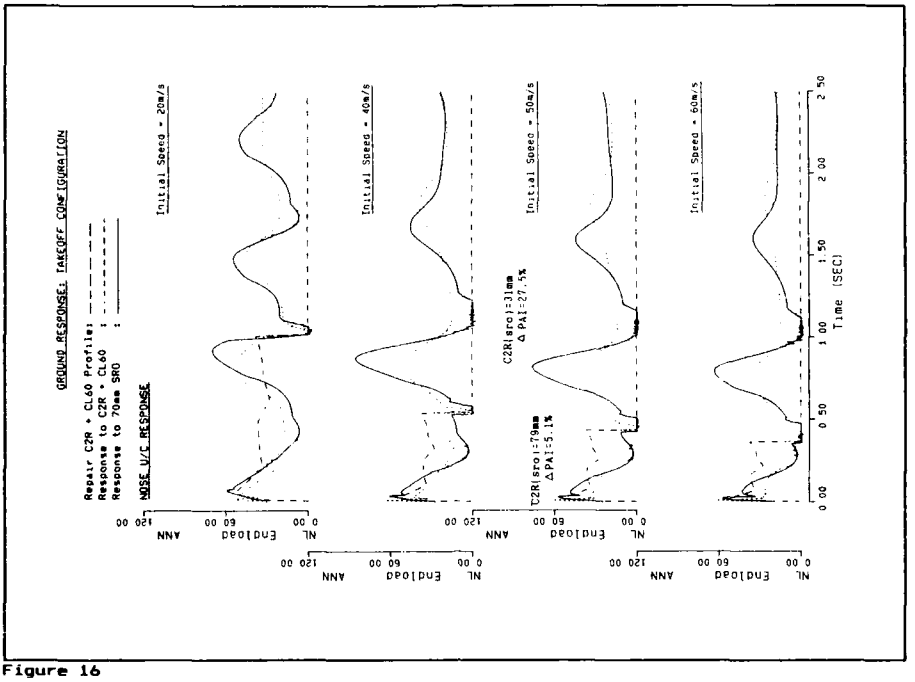

Figure 16

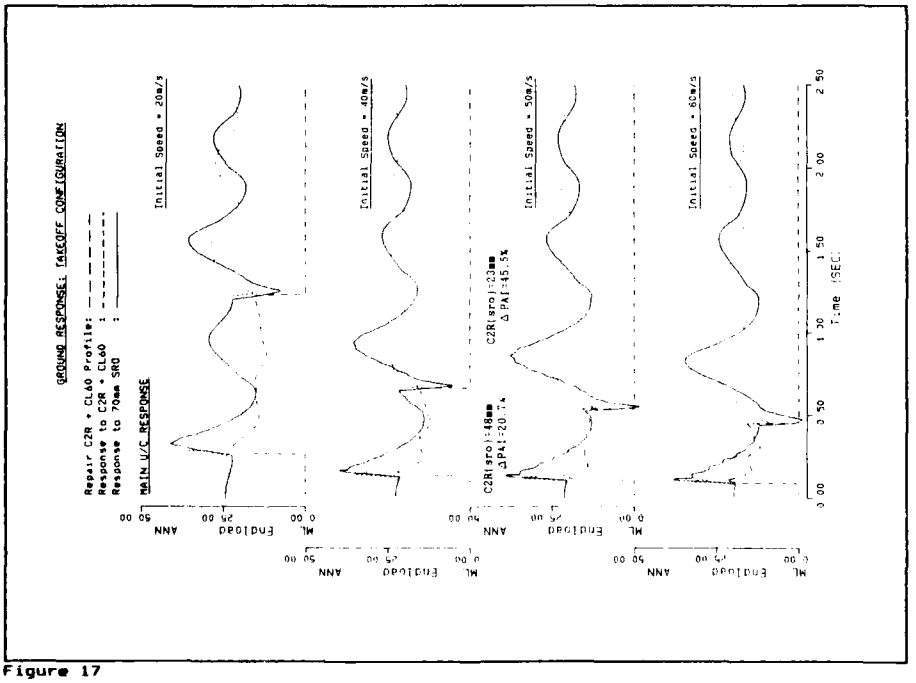

Figure 17

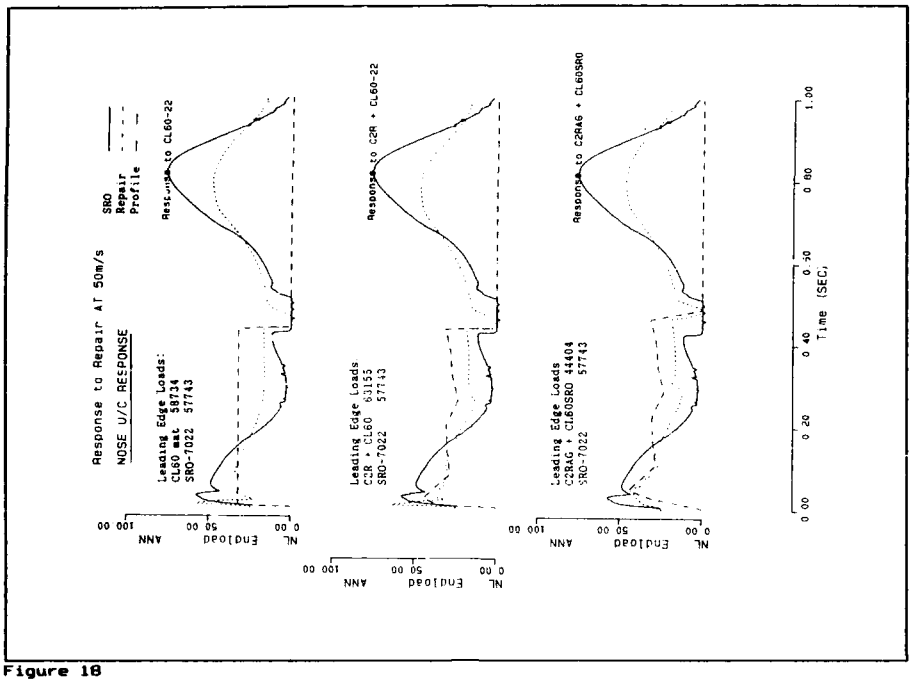

Figure 18

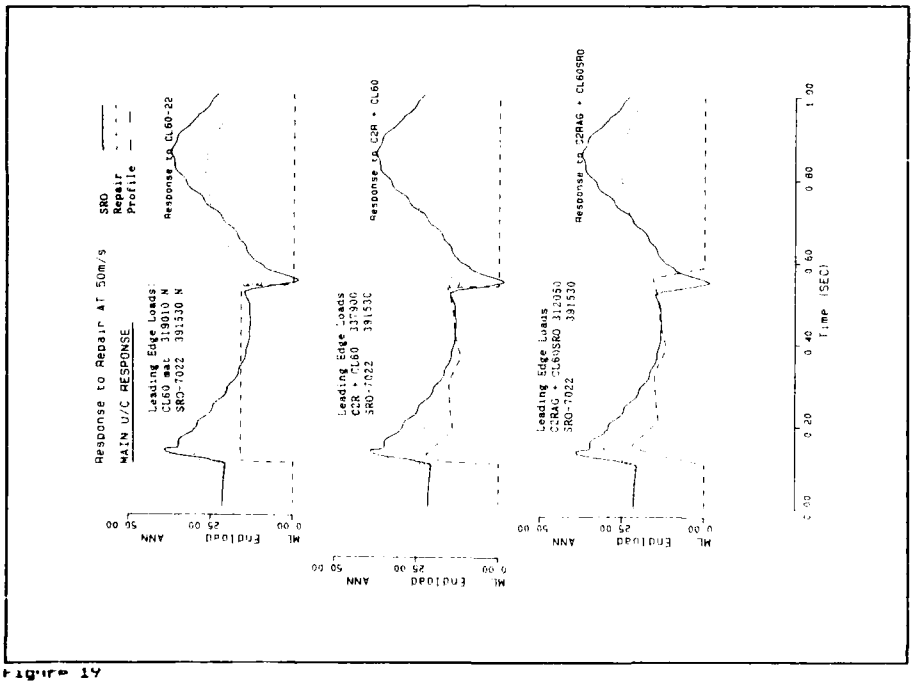

Figure 19

4.2. AM2 Covered Crater Repairs

The response for both nose and main gears are shown in Figures 20-21 for C8 covered by the AM2 mat, Figures 22-23 for C9 and Figures 24-25 for C2R.

4.2.1. Nose Gear Post-Mat Loads

Comments on the tuning characteristics stated for the CL60 repairs apply to the AM2 repairs. At speeds at which the real repairs tune and the SRO not, exceedence of the 70mm SRO post-mat loads will be possible. C8 shows a slight exceedence at 30m/s of 0.1%PAI with a lag equivalent to 1.9m and C9 at 20m/s shows an exceedence of 2.3%PAI with a lag of one metre and giving an equivalent SRO height at this point of 75mm . At speeds where the SRO tunes and these repairs do not, the 70mm SRO causes considerably higher loads. C8 causes the greatest loads at these speeds which at 50m/s are equivalent to an SRO of 49.6mm.

Phasing off the repairs is variable. the maximum difference for these repairs being for C8 at 20m/s showing a lead equivalent to 4.1m.

4.2.2. Nose Gear Leading Edge Loads

The leading edge ramp of the AM2 repair mat is less steep than the SRO, namely, 38mm rise in 1.375m. Leading edge loads are far less severe accordingly. For example, at the speed of 50m/s, C2R only reaches an equivalent SRO at this point of 45mm.

The phasing of the nose gear leading edge loads over the AM2 repairs show no significant difference.

4.2.3. Main Gear Loads

Post-mat loads for AM2 real repairs match those due to SRO at speeds where tuning to the SRO is low, and for the repairs similar to C8 loads may exceed the SRO at the repair tuning speeds. For example, C8 post-mat loads just exceed at 30m/s for both the first and second post-mat peaks, by 2.9%PAI at the first and 3.6%PAI at the second. The lag is equivalent to 2.6m. Main gear leading edge loads for C2R, the repair considered to be the most detrimental at this point, gives an equivalent SRO of 47.9mm at 20m/s and 47.5mm at 50m/s.

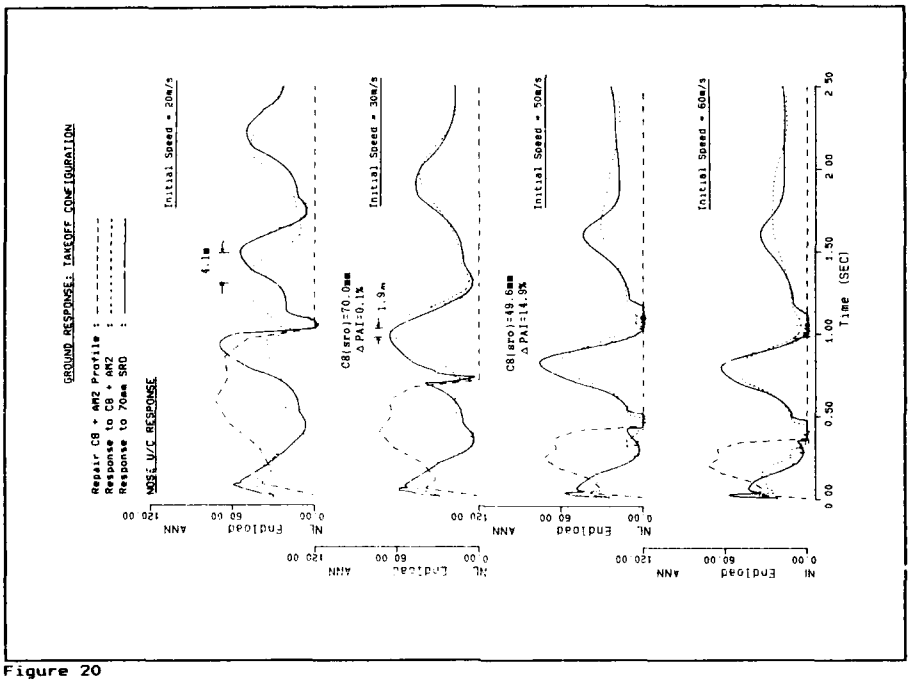

Figure 20

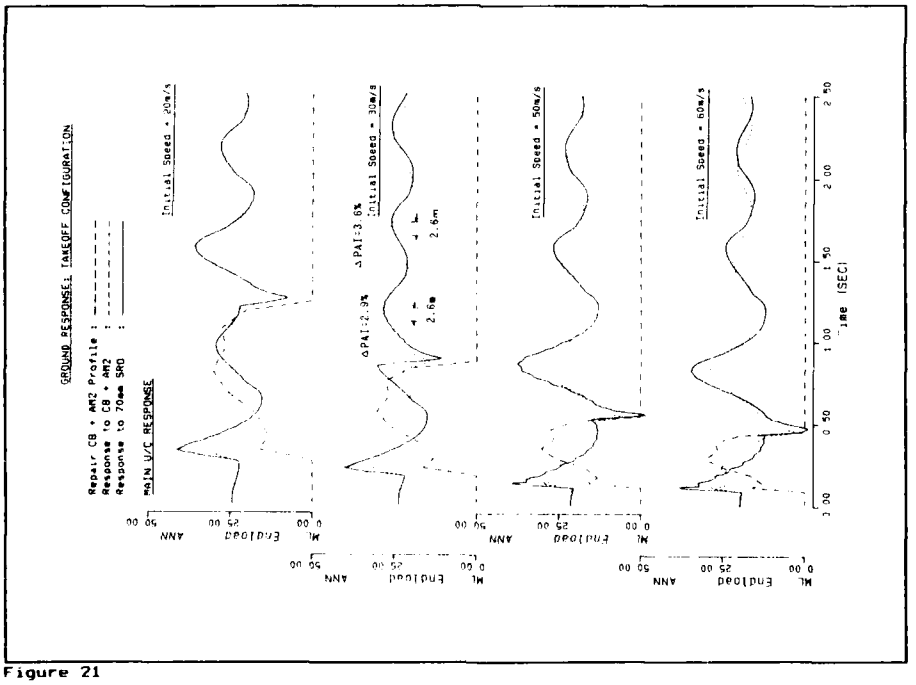

Figure 21

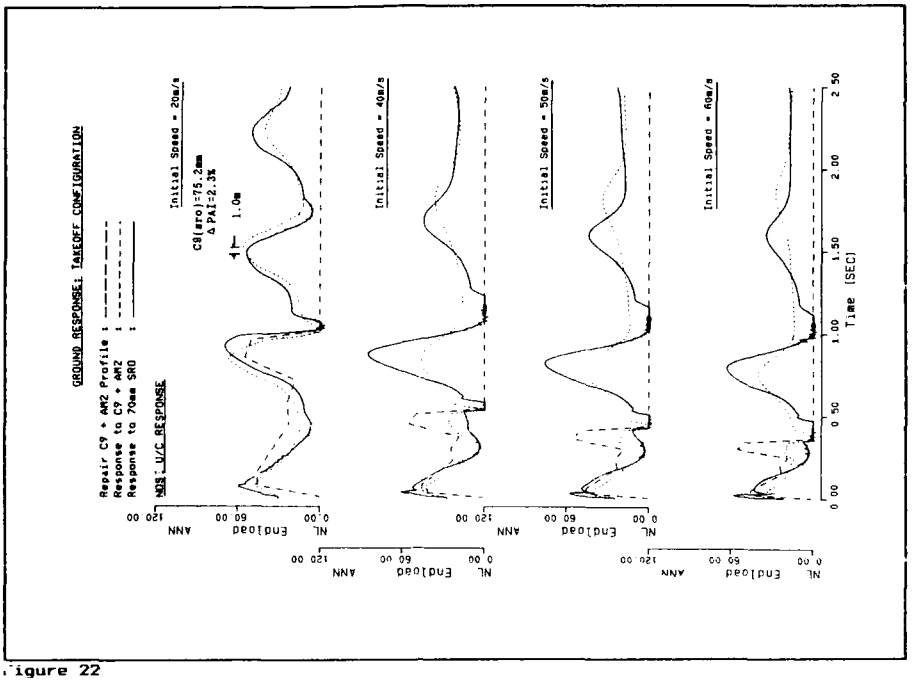

Figure 22

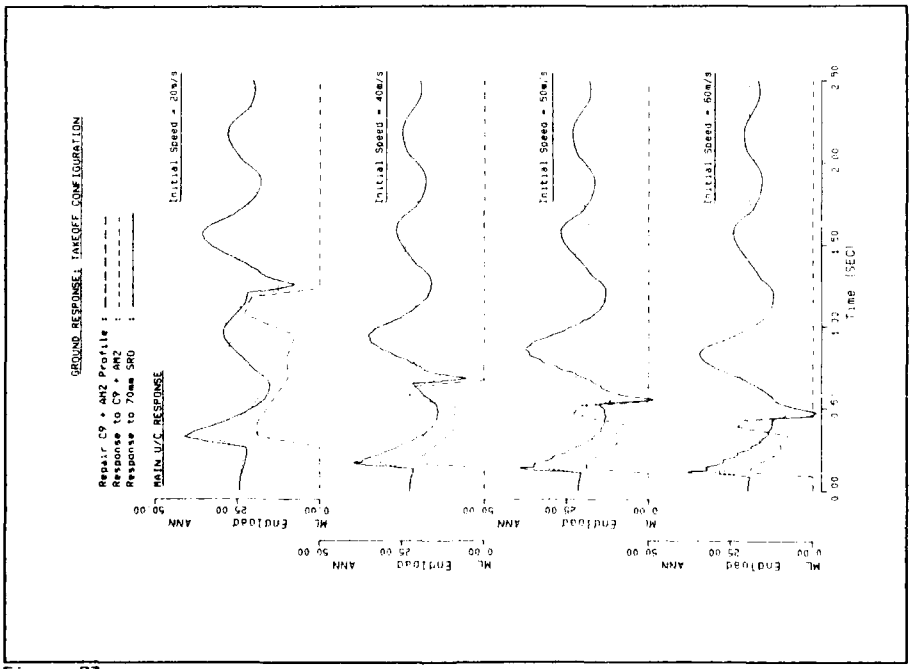

Figure 23

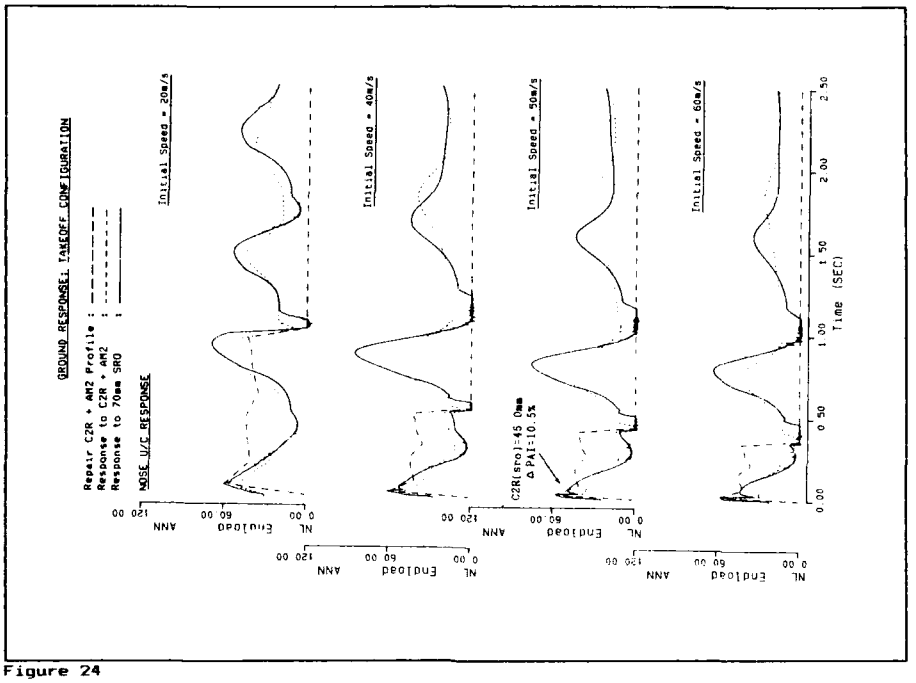

Figure 24

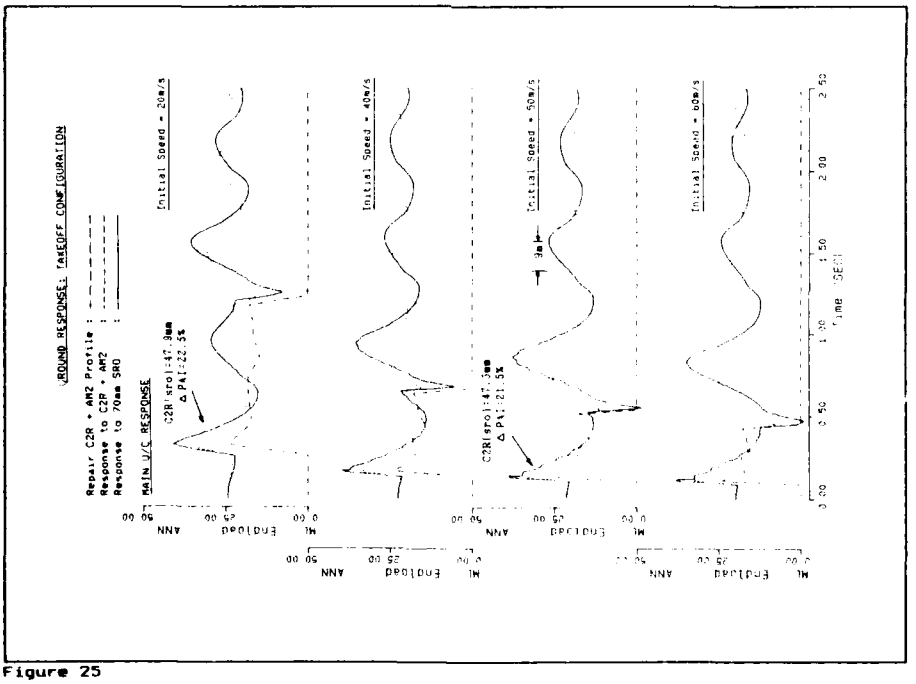

Figure 25

5. THE SRO AS A REPRESENTATION OF REAL REPAIRS

The peak-to-peak comparison of the SRO and real repair responses certainly emphasises the difficulty in trying to select a profile shape which gives a response for both nose and main gear that is similar to, and envelopes, the responses to real repairs. The infinite variability of real repair shapes, even though constrained within a repair-build specification, can lead to a range of responses that cannot be matched accurately by one shape alone.

Two major problems are evident. The first is the effect of the crater in-fill to the repair shape. Whatever the resulting shape of the crater in-fill, be it humped or dipped, the overall effect on the aircraft response is to cause the tuning speeds over that repair to be lower than that over the Standard Repair Obstacle because real repairs will always be effectively shorter than SRO. Tuning occurs strongly at 50m/s over the 22.5m SRO profile and not at the 20-30m/s as for 22m real repairs. Also, due to the differing effective lengths post-mat phasing, especially at the low speed end, will vary. A modification to the flat SRO would be indeterminable, but an adjustment to the length to ensure tuning occurs at speeds more relevant to the real repairs would alleviate the problem.

The second problem lies with the use of repair mats which have leading edge ramps which differ significantly from that of the SRO. The CL60 mat with a rise of 32mm in 0.25m causes loads at the leading edge ramp that are greater than those occurring during the rise onto the SRO at 50m/s. So, in the case of the crater in-fill of a real repair augmenting the repair mat leading edge, as with C2R, the SRO leading edge loads can only be exceeded further. SRO leading edge loads match more successfully to AM2 covered repairs as the ramps are more similar. As previously stated there is the possibility of reducing this leading edge problem by firstly ensuring that the repair mat ramps are set sufficiently away from the crater in-fill so that the in-fill does not augment the mat ramp and secondly serious reconsideration of the CL60 ramp design.

The differences for the CL60 repairs are illustrated in Figures 26-27. An envelope of the maximum PAI resulting from the aircraft response to the full set of CL60 covered repairs analysed by BAe is overplotted against the SRO PAI maxima (reference Figures 5-6). The aircraft response to the real repairs can create nose gear loads which are equal to those resulting from crossing the 70mm SRO. The exceedence of the SRO response at 60m/s actually results from the response to C2R. This is due to the aircraft response at the leading edge exceeding the response to the SRO at both the leading edge ramp and post-mat. The main gear shows a similar trend for both the real repairs and the SRO because the response maxima for both generally occur during the rise onto the repair.

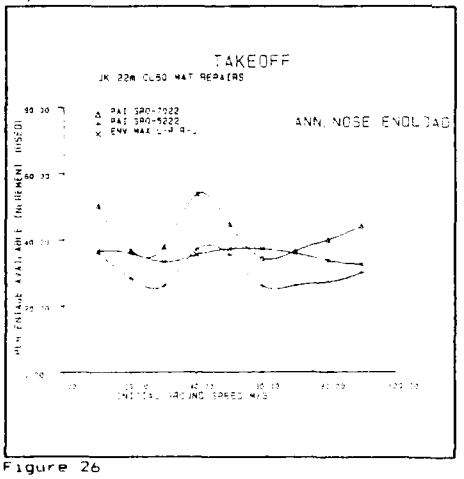

Figure 26

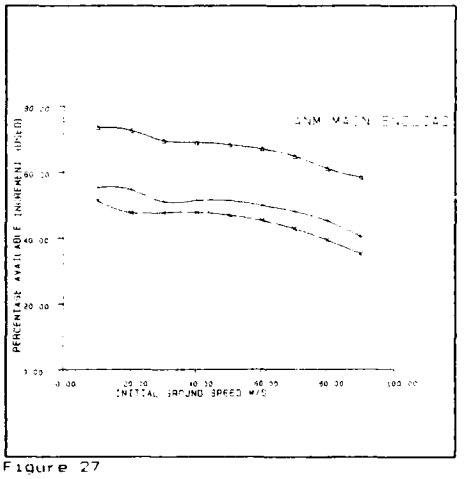

Figure 27

Figures 28-29 show the equivalent plots for the AM2 covered repairs. AM2 repairs show no problems at the 60m/s region and similar to the CL60 repairs at the 30m/s region.

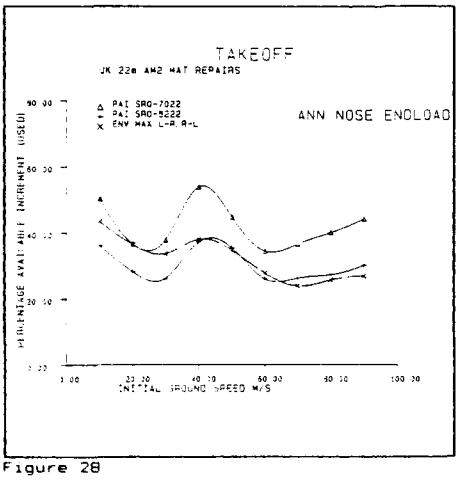

Figure 28

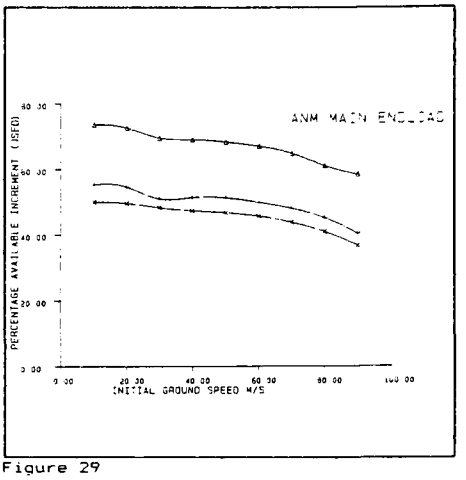

Figure 29

6. IMPLICATIONS FOR THE USE OF THE SRO CONTOURS

On the basis of the comparison of the calculated responses to the three real repairs and to the SRO it is evident that the SRO based contour plots are not ideal. The height of the SRO to be used must evidently be a compromise.

At the low speed end, speeds of 30m/s and less, there are problems with both phasing and magnitude. Post mat loads off real repairs for both nose and main gear give reason to use the 70mm level. Leading edge loads which are equivalent to SRO of less than 70mm at these speeds will give allowance for the inevitable occurrence of post-mat loads equivalent to an SRO of greater than 70mm. An increase in the 90% contour to encompass the 30m/s region, and use of the 90% contour for speeds up to 35m/s, which although cautious, may cover the problems caused by phasing in this region.

For speeds higher than 30m/s the three real repair responses do not exceed post-mat loads which are equivalent to 50mm SRO for both nose and main gear. Leading edge loads for the nose gear over this speed range cause loads equivalent to an SRO of 45mm for the nose and 48mm for the main if the repair is covered by an AM2 mat and 79mm for the nose and 48mm for the main if covered by a CL60 mat. Thus, at these speeds, for a pair of AM2 repairs the 70mm SRO provides unnecessary restrictions on the aircraft. If contours for a 50mm SRO were to be plotted the lobe on the nose gear contour would probably not be there and the main gear lobe would be greatly reduced over this speed range. In addition, no account need be taken of the areas of significance defined for the second post-mat peak since they become further below criticality.

If a pair of CL60 repairs is to be represented at these speeds the leading edge loads give justification for using the clearance based on the 70mm SRO for the nose gear. However, due to the lower post repair loads some over-representation of the severity may still exist.

The above arguments suggest the possibility that two levels of contour plots could be used for the aircraft at this configuration in order to produce a clearance that is not excessively restrictive. The first set would be at 70mm and would be provided to cover speeds of up to 30m/s or possibly 40m/s for some contingency for both nose and main gear. Modification to the plots may be considered to cover the low speed end variances in magnitude and phasing. The second set would be provided for both nose and main gear at the 50mm SRO level to cover combinations of AM2 covered repairs at the high speed end. If no modification to the CL60 repair leading edge is foreseeable then the higher level of contour would have to be applied over the full speed range for the nose gear.

Also when considering interpretation of the contours, some allowance should be made for the following aspects adding to the aircraft loads:

- Runway roughness.
- Repair quality after trafficking.
- Repair quality in a wartime condition.
- Repair asymmetry.

7. THE EQUIVALENT OBSTACLE HEIGHT, EO

7.1. General

BAe studied the response of the military aircraft to a large number of real repair profiles in order to determine the aircraft's capability. Landing and takeoff configurations were analysed. For this work a more simplistic approach had to be adopted in order to reduce the quantity of work that would have been involved in producing a clearance by a peak to peak analysis such as has been used above to illustrate the detail differences between the responses. The Equivalent Obstacle concept had been envisaged by the AGARD WG22 as a possible means of assessing this capability and it was decided that this should be applied to the military aircraft clearance.

The 'Equivalent Obstacle', EO of a real repair is defined to be the height an SRO has to be in order to give the same maximum load as that resulting from the response to the real repair. To determine this height the maximum loads from real repairs are compared to maximum loads from the response to the SRO of heights 70, 52 and 38mm regardless of the point on or off the repair at which the maximums occurred. Figure 30 illustrates the calculation of EO for the repair CB covered by the CL60 mat. In this case this method gives a reasonable estimate for the main gear but is misleading for the nose gear. The nose gear EO results from a comparison of real repair leading edge loads and SRO post-mat loads. Thus nose gear based EO must be considered with care.

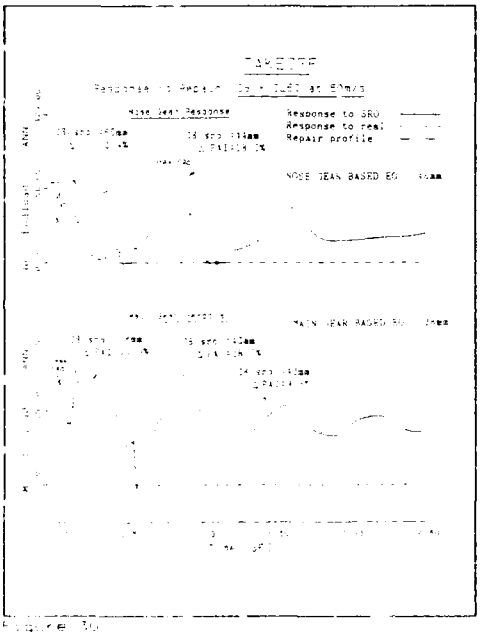

Figure 30

The analysis for this configuration showed both nose and main gear based EO of UK AM2 repairs of no greater than 70mm throughout the speed range. CL60 repairs do show some exceedence of the 70mm level for nose gear based EO at 80m/s.

7.2. The EO of Single Repairs

If the repair may be considered to be a single repair then this evaluation of EO gives a good estimate of the repair's severity provide the responses are similar. Of course, for single repairs, provided limit loads are not reached within a certain level (say 10% allowance for inherent runway roughness), then the actual value of EO for a single repair is not of any special value.

However, the value of EO has an application in the multiple repair situation.

7.3. The EO Concept Extended to a Double Repair Situation

Having established the EO for the single repairs, a level which reasonably encompassed all these values could be determined. This level would be the height at which the SRO would be set for the response plots; based on UK repairs, this has been provisionally set at the 70mm level. This, provided the EO of a real repair is less than 70mm the assumption was postulated that multiples of real repairs with EO of less than 70mm would not exceed multiples of SRO at 70mm. A possible assumption, provided of course that real repair response remains below that of the 70mm SRO at the major peaks throughout the time history and there is sufficient spacing in the phasing at the critical points.

The peak-to-peak matching of the responses of C8, C9 and C2R show that this is not always the case and that exceedences of the 70mm SRO response do occur at certain locations through the time history although the EO calculated for the repairs as singles at these speeds would be less than 70mm. However, it has been shown that, although there may be post mat exceedence of the 70mm SRO response it is unlikely to be followed by a leading edge response equivalent to 70mm SRO that indeed phases sufficiently accurately to cause a transgression into the region bounded by the 100%PAI contour.

A better estimate of EO would be to consider the leading edge ramp loads and the post mat load first and second peaks and calculate an EO at each of these points throughout the speed range and select the most pessimistic. Small phasing differences would be ignored. However this would involve a great deal of work that would not be fully justified considering the variances in the real-life situation.

8. CONCLUSIONS

SRO as a Representation of Real Repairs:

- The SRO shape is not an ideal representation of the real repairs.

  The differing effective lengths of the real repairs compared with the SRO causes tuning at different speeds and hence magnitude and phasing of the post-mat response is dissimilar.

  The differing leading edge ramp on the CL60 repair mat, and to a lesser extent the AM2 repair mat, compared to that for the SRO causes dissimilar responses in both magnitude and phasing during the rise onto the repair.

- Modification to the SRO flat topped shape would be indeterminable.

  However a useful change would be to shorten the SRO length to one that would produce aircraft tuning at more similar speeds to the real repairs. Repairs to smaller craters could need to be matched to even shorter SRO.

- In order to make the response to the real repairs as similar as possible to the SRO it is advisable if possible to avoid both excessive sag at the repair centre and overfilling the repair so as to cause a large hump.

  In addition, ensure that the repair mat ramps are fixed clear of the crater repair to avoid detrimental addition to the rise onto the repair.

UK Clearance Procedure

- The current SRO profile, when set at a height that reasonably encompasses the real repair loads throughout the speed range will lead to a clearance definition which will be adequate at some speeds and overly restrictive for others.

Equivalent Obstacle Concept:

- The peak-to-peak analysis to obtain equivalent SRO at the critical points of the response over a repair would lead to a more accurate theoretical estimate of the severity of the repairs compared with the EO calculation. The excessive work demanded by this technique in order to achieve the additional accuracy is not worth the effort considering all the variability in the real-life situation.

  The Equivalent Obstacle values gives an estimate of the severity of the repair and when considered with care will be sufficiently accurate to provide an estimate for the height of SRO for the UK clearance procedure.

- Modification to the CL60 leading edge ramp to one more similar to that on the SRO would broaden the allowable clearance for this configuration by allowing a lower level of SRO to be used for the contour plots over a substantial speed range.

9. REFERENCES

1. AGARD SMP WG22 Report
   Aircraft Operation on Repaired Runways
   Draft Report September 1989

SUMMARY OF THE FINAL DISCUSSION

by

D.Chaumette*
Dassault-Aviation — France
Specialist Meeting Chairman

It became evident during the Meeting that landing gear are a prime concern because they are the number two system causing major airframe failure. But in most cases the origin of failure is fatigue, often in combination with corrosion. In this respect selection of proper alloys with efficient corrosion protection coatings is very important.

Purely static failures (by exceeding ultimate strength of landing gear) seem to be very seldom, excluding some "rogue" cases beyond any design possibility.

Speaking about regulations, existing military regulations are US MIL Specs 8862A, 8863A and 87221A, and the French AIR 2004 D and E. The MIL Specs are outdated, not well understood and rarely used. The French AIR 2004 E is in use, but may also need improvement in the landing loads section. Concerning statics design cases, there are some divergences between both sets of regulations, this being particularly noteworthy for the landing cases of carrier airplanes.

Resolving or explaining such differences could be profitable to the NATO community.

As mentioned above, fatigue of landing gear structure is not properly accounted for in landing gear design.

It was generally agreed that a *design guide* based primarily on statistically compiled operational data is needed by the industry.

It was proposed that an AGARD working group be formed to:

a) Examine which part of the existing MIL Specs requires revision.

b) Build a ground loads statistical data base from existing and future measured data.

c) Create a "life spectrum(s)" for landing gear so that a realistic fatigue life can be incorporated as a landing gear design factor. This spectrum would be based on the measured data from step b.

d) Examine the usefulness of an "ASIP" type structural integrity tracking program, for landing gear that would be suitable for international adoption.

In the field of computer codes several papers presented extremely impressive computations, including the response of the complete structure, taking into account non linearities typical of landing gears. What remains to be done are more comparisons with actual measured cases. Also problems may remain for such effects as gas-oil thermodynamics or friction forces in oleo struts.

The question of the use of bomb-damaged runways was the subject of several papers. The tentative conclusions are the following:

- Landing gears of older design were optimized only for the landing impact cases. Examples were given that modifications to the oleo struts absorbers may provide lots of improvements for the use of damaged runways; this still using passive systems.
- To respond to a more severe requirement a solution may be to use active systems. There was no clear consensus on the use of active systems, with several concepts ranging between "adaptative damping" and completely piloted oleo struts.
- Questions on issues such as complexity, reliability and oil flow rates are not resolved. And the last point is that up to now severe requirements concerning bomb-damaged runway operations were never introduced in new airplane specs, so such a system is not necessary.

* With the participation taken by J.Gerardi (US) during the discussion

RESUME DE LA DISCUSSION FINALE

par

D.Chaumette*
Dassault-Aviation — France
Président du Specialists Meeting

Il a été évident dans le Meeting que les atterrisseurs sont un souci important car ils sont en deuxième place pour les systemes causant des ruptures majeures de structures d'avion.

Mais dans la plupart des cas l'origine de la rupture est la fatigue, souvent en combinaison avec la corrosion. Sur ce point, la sélection d'alliages appropriées et de revêtements protecteurs efficaces sont très importants.

Les ruptures purement statiques (c'est à dire par dépassement de la charge extrême de l'atterrisseur) semblent être quasi-inexistants, si l'on exclut les cas tellement hors norme qu'il serait irréaliste de vouloir les couvrir dans la conception.

Parlant de règlements, les spécifications militaires existantes sont les US MILS SPECS 8862A, 8863A et 87221A et les normes françaises AIR 2004 D et E. Les MIL SPECS sont démodées, pas très bien comprises et rarement utilisées. La AIR 2004 E est utilisée, mais pourrait aussi nécessiter des améliorations dans sa partie charges d'atterrissage.

En ce qui concerne les cas de dimensionnement statiques il y a quelques divergences entre les deux groupes de règlements, ceci étant particulièrement net pour les cas d'atterrissage sur porte-avions. Réduire ou expliquer de telles différences pourrait être profitable aux pays de l'OTAN.

Comme indiqué plus haut, la fatigue des atterrisseurs n'est pas suffisamment prise en compte lors de leur conception.

Il a été généralement admis qu'un guide de conception, basé principalement sur une compilation statistique de résultats en opération, est un besoin pour l'industrie.

Il a été proposé de former un working group AGARD pour:

a) Examiner quelles parties des MILS Specs nécessitent une révision.

b) Bâtir une base de données de statistiques de charges au sol à partir de données mesurées existantes ou futures.

c) Créer un ou des spectres de chargement pour les atterrisseurs de façon à ce qu'une vie en fatigue réaliste soit intégrée dans la conception. Ce spectre serait basé sur les données mesurées du point b.

d) Examiner l'utilité d'un programme de type "ASIP" de surveillance de l'intégrité structurale des atterrisseurs qui pourrait être adopté internationalement.

Dans le domaine des programmes de calcul plusieurs papiers ont présenté des calculs très impressionnants, incluant la reponse de la structure complète et prenant en compte les non linéarités typiques des atterrisseurs. Ce qui reste à faire est plus de comparaisons avec des mesures de cas nuls. Aussi des problèmes peuvent subsister, liés à des effets tels que les thermodynamiques gaz-huile ou les forces de friction dans les amortisseurs.

La question de l'utilisation de pistes endommagées par bombes a été l'objet de plusieurs papiers.

Une tentative de conclusion pourrait être:

- Les atterrisseurs de conception plus ancienne étaient opimisés seulement pour le cas d'impact à l'atterrissage. On a montré par des exemples que des modifications du dessin des amortisseurs pourraient apporter des améliorations importantes pour l'utilisation de pistes endommagées. Ceci en utilisant toujours des systèmes passifs.
- Pour répondre à des exigences plus sévères, une solution pourrait être l'utilisation de systèmes actifs.

  Il n'y a pas eu de consensus clair sur l'utilisation de systèmes actifs, avec plusieurs concepts allant de l'amortissement adaptatif au systeme hydraulique complètement piloté.

  Des questions sur des sujets tels que la complexité, la fiabilité et les débits d'huile nécessaires ne sont pas résolues.

  Et le dernier point est que à ce jour des exigences sévères concernant l'utilisation à partir de pistes endommagées par bombes n'ont jamais été introduites dans les spécifications d'avions nouveaux, ce qui ne rend pas necessaire ce type de système.

---

* Avec l'aide des notes prises par T.Gerardi (US) pendant la discussion.

REPORT DOCUMENTATION PAGE

1. Recipient's Reference	2. Originator's Reference	3. Further Reference	4. Security Classification of Document
	AGARD-CP-484	ISBN 92-835-0611-1	UNCLASSIFIED

5. Originator Advisory Group for Aerospace Research and Development
North Atlantic Treaty Organization
7 rue Ancelle, 92200 Neuilly sur Seine, France

6. Title LANDING GEAR DESIGN LOADS

7. Presented at the 71st Meeting of the AGARD Structures and Materials Panel, held in Povoa de Varzim, Portugal on 8th to 12th October 1990.

8. Author(s)/Editor(s)	9. Date
Various	June 1991
10. Author's/Editor's Address	**11. Pages**
Various	284

12. Distribution Statement This document is distributed in accordance with AGARD policies and regulations, which are outlined on the back covers of all AGARD publications.

13. Keywords/Descriptors

Landing gear
Design loads
Design analysis

14. Abstract

This publication reports the papers presented to a Specialists' Meeting organised by the Structures and Materials Panel and held at its Fall 1990 Meeting.

The Specialists' Meeting provided a forum for the exchange of experiences between the NATO nations with the aim of advancing landing gear design criteria and methods of landing gear analysis. The Meeting reviewed existing design practices and specifications, considered the various methods for load measurement and data analysis and formulated guidelines for future design procedures.

AGARD Conference Proceedings No.484 Advisory Group for Aerospace Research and Development, NATO LANDING GEAR DESIGN LOADS Published June 1991 284 pages This publication reports the papers presented to a Specialists' Meeting organised by the Structures and Materials Panel and held at its Fall 1990 Meeting. The Specialists' Meeting provided a forum for the exchange of experiences between the NATO nations with the aim of advancing landing gear design criteria and methods of landing gear analysis. The Meeting reviewed existing design practices and specifications, considered P.T.O.	AGARD-CP-484 Landing gear Design loads Design analysis	AGARD Conference Proceedings No.484 Advisory Group for Aerospace Research and Development, NATO LANDING GEAR DESIGN LOADS Published June 1991 284 pages This publication reports the papers presented to a Specialists' Meeting organised by the Structures and Materials Panel and held at its Fall 1990 Meeting. The Specialists' Meeting provided a forum for the exchange of experiences between the NATO nations with the aim of advancing landing gear design criteria and methods of landing gear analysis. The Meeting reviewed existing design practices and specifications, considered P.T.O.	AGARD-CP-484 Landing gear Design loads Design analysis
AGARD Conference Proceedings No.484 Advisory Group for Aerospace Research and Development, NATO LANDING GEAR DESIGN LOADS Published June 1991 284 pages This publication reports the papers presented to a Specialists' Meeting organised by the Structures and Materials Panel and held at its Fall 1990 Meeting. The Specialists' Meeting provided a forum for the exchange of experiences between the NATO nations with the aim of advancing landing gear design criteria and methods of landing gear analysis. The Meeting reviewed existing design practices and specifications, considered P.T.O.	AGARD-CP-484 Landing gear Design loads Design analysis	AGARD Conference Proceedings No.484 Advisory Group for Aerospace Research and Development, NATO LANDING GEAR DESIGN LOADS Published June 1991 284 pages This publication reports the papers presented to a Specialists' Meeting organised by the Structures and Materials Panel and held at its Fall 1990 Meeting. The Specialists' Meeting provided a forum for the exchange of experiences between the NATO nations with the aim of advancing landing gear design criteria and methods of landing gear analysis. The Meeting reviewed existing design practices and specifications, considered P.T.O.	AGARD-CP-484 Landing gear Design loads Design analysis

the various methods for load measurement and data analysis and formulated guidelines for future design procedures. ISBN 92-835-0611-1	the various methods for load measurement and data analysis and formulated guidelines for future design procedures. ISBN 92-835-0611-1
the various methods for load measurement and data analysis and formulated guidelines for future design procedures. ISBN 92-835-0611-1	the various methods for load measurement and data analysis and formulated guidelines for future design procedures. ISBN 92-835-0611-1

AGARD

NATO OTAN

7 RUE ANCELLE · 92200 NEUILLY-SUR-SEINE

FRANCE

Téléphone (1)47.38.57.00 · Télex 610 176
Télécopie (1)47.38.57.99

DIFFUSION DES PUBLICATIONS
AGARD NON CLASSIFIEES

L'AGARD ne détient pas de stocks de ses publications, dans un but de distribution générale à l'adresse ci-dessus. La diffusion initiale des publications de l'AGARD est effectuée auprès des pays membres de cette organisation par l'intermédiaire des Centres Nationaux de Distribution suivants. A l'exception des Etats-Unis, ces centres disposent parfois d'exemplaires additionnels; dans les cas contraire, on peut se procurer ces exemplaires sous forme de microfiches ou de microcopies auprès des Agences de Vente dont la liste suite.

CENTRES DE DIFFUSION NATIONAUX

ALLEMAGNE
Fachinformationszentrum,
Karlsruhe
D-7514 Eggenstein-Leopoldshafen 2

BELGIQUE
Coordonnateur AGARD-VSL
Etat-Major de la Force Aerienne
Quartier Reine Elisabeth
Rue d'Evere, 1140 Bruxelles

CANADA
Directeur du Service des Renseignements Scientifiques
Ministère de la Defense Nationale
Ottawa, Ontario K1A 0K2

DANEMARK
Danish Defence Research Board
Ved Idraetsparken 4
2100 Copenhagen Ø

ESPAGNE
INTA (AGARD Publications)
Pintor Rosales 34
28008 Madrid

ETATS-UNIS
National Aeronautics and Space Administration
Langley Research Center
M/S 180
Hampton, Virginia 23665

FRANCE
O.N.E.R.A. (Direction)
29, Avenue de la Division Leclerc
92320, Châtillon sous Bagneux

GRECE
Hellenic Air Force
Air War College
Scientific and Technical Library
Dekelia Air Force Base
Dekelia, Athens TGA 1010

ISLANDE
Director of Aviation
c/o Flugrad
Reykjavik

ITALIE
Aeronautica Militaire
Ufficio del Delegato Nazionale all'AGARD
3 Piazzale Adenauer
00144 Roma/EUR

LUXEMBOURG
Voir Belgique

NORVEGE
Norwegian Defence Research Establishment
Attn: Biblioteket
P.O. Box 25
N-2007 Kjeller

PAYS-BAS
Netherlands Delegation to AGARD
National Aerospace Laboratory NLR
Kluyverweg 1
2629 HS Delft

PORTUGAL
Portuguese National Coordinator to AGARD
Gabinete de Estudos e Programas
CLAFA
Base de Alfragide
Alfragide
2700 Amadora

ROYAUME UNI
Defence Research Information Centre
Kentigern House
65 Brown Street
Glasgow G2 8EX

TURQUIE
Milli Savunma Başkanliği (MSB)
ARGE Daire Başkanliği (ARGE)
Ankara

LE CENTRE NATIONAL DE DISTRIBUTION DES ETATS-UNIS (NASA) NE DETIENT PAS DE STOCKS DES PUBLICATIONS AGARD ET LES DEMANDES D'EXEMPLAIRES DOIVENT ETRE ADRESSEES DIRECTEMENT AU SERVICE NATIONAL TECHNIQUE DE L'INFORMATION (NTIS) DONT L'ADRESSE SUIT.

AGENCES DE VENTE

National Technical Information Service
(NTIS)
5285 Port Royal Road
Springfield, Virginia 22161
Etats-Unis

ESA/Information Retrieval Service
European Space Agency
10, rue Mario Nikis
75015 Paris
France

The British Library
Document Supply Division
Boston Spa, Wetherby
West Yorkshire LS23 7BQ
Royaume Uni

Les demandes de microfiches ou de photocopies de documents AGARD (y compris les demandes faites auprès du NTIS) doivent comporter la dénomination AGARD, ainsi que le numéro de série de l'AGARD (par exemple AGARD-AG-315). Des informations analogues, telles que le titre et la date de publication sont souhaitables. Veuiller noter qu'il y a lieu de spécifier AGARD-R-nnn et AGARD-AR-nnn lors de la commande de rapports AGARD et des rapports consultatifs AGARD respectivement. Des références bibliographiques complètes ainsi que des résumés des publications AGARD figurent dans les journaux suivants:

Scientifique and Technical Aerospace Reports (STAR)
publié par le NASA Scientific and Technical
Information Division
NASA Headquarters (NTT)
Washington D.C. 20546
Etats-Unis

Government Reports Announcements and Index (GRA&I)
publié par le National Technical Information Service
Springfield
Virginia 22161
Etats-Unis

(accessible également en mode interactif dans la base de données bibliographiques en ligne du NTIS, et sur CD-ROM)

Imprimé par Specialised Printing Services Limited
40 Chigwell Lane, Loughton, Essex IG10 3TZ